

# **Design and Implementation of MEMS Biomechanical Sensors for Real-Life Measurements of Gait Parameters**

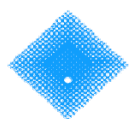
A THESIS

SUBMITTED IN FULFILMENT OF THE REQUIREMENTS FOR THE DEGREE OF  
DOCTOR OF PHILOSOPHY

**YUFRIDIN WAHAB**

2009

**School of Engineering & Science**  
**Faculty of Health, Engineering and Science**  
Victoria University, Australia



**VICTORIA  
UNIVERSITY**

**A NEW  
SCHOOL OF  
THOUGHT**

***To my beloved parents Khalijah Shariff and Wahab Ahmad,***

***my wonderful wife Azizah Abdullah,***

***and....***

***my lovely daughters,***

***Nurulizzah and Nuraqila.***

## ABSTRACT

As the health industry enters the new millennium, fast changing demographics are compelling health service delivery systems to make dramatic changes in their diagnostic delivery infrastructure. A reducing ratio of servicing professionals to the population, an increasing percentage of the elderly group and surging lifestyle related diseases are also driving the need for more real world measurement of key health indicators. These needs will grow further as new remote real-time e-health applications become more feasible and pervasive. Sensor embedded mobile health diagnostic systems with wireless technology compatibilities are the solution to accommodate the growing need for the next generation of highly reliable, efficient, in situ, cheap and more importantly, practical devices for use in real life activities.

Obviously, these 'dream' systems can only be materialized by adoption of the already practically proven microelectronics and micro-electro-mechanical system technologies. These technologies are said to bring a number of significant improvements into next generation biomedical instrumentations, including miniaturization, low power consumption, full integration of system capability and also low cost of production. Miniaturization is a great advantage as it means the devices or systems should require only small volumes of space. With low power consumption, only small batteries might be needed as a power supply, or even energy scavenging can be enough to power them, if not a combination of these. As full system integration on a single silicon chip is also possible, signal processing and computation can be performed on the same silicon piece with greatly improved overall system performance. Most interestingly, the low per-unit cost is what business and consumers are looking for in every product and this has been an undeniable trend. In addition, technologically, it also offers numerous materials that are not only

excellent mechanically for sensing and actuation, but also biologically compatible. Undoubtedly, these MEMS based devices are promising tools for outdoor ambulatory measurement and monitoring.

Foot clearance above the ground during walking is an important clinical and rehabilitation gait analysis parameter. Current bulky and laboratory environment based instruments are not suitable for measurement in the natural environment such as in the outdoors. This research analyses three promising distance measurement techniques (capacitive, electric field and ultrasound) that may be suitable for MEMS realization of foot clearance measurement. The study suggests that ultrasound-based technique is very suitable for this application and thus a model is proposed in this research. The ultrasonic transducer model is suitable for MEMS realization using the increasingly popular Capacitive Micromachined Ultrasonic Transducer technology. The Capacitive micromachined ultrasound transducer is recently becoming the focus of many researchers due to its high performance, in terms of electromechanical coupling factor, bandwidth, mechanical impedance and sensitivity. An investigation into the capability of MEMS technology in the design and analysis of ultrasonic transducer is reported. The work includes an investigation into design process, modeling and simulation. Analysis was performed on the produced transducer to investigate several key performances such as pull-in voltage, resonance frequency, electromechanical coupling factor, deflection and the resulting capacitance change.

To further complement the foot based health diagnostic system, another key parameter, pressure, is also taken into focus. As a matter of fact, in our modern living era, pressure sensing is one of the most performed measurements to enhance quality of life, encompassing a variety of specific applications. Measurement of

interface pressure between the foot and shoe underpins a number of important applications in quality of life and health monitoring. Abnormal pressure may indicate instability in gait and risk of ulceration development, especially in diabetic foot as well as many other biomedical diagnostic applications. As the current foot pressure sensors in the market exhibit many limitations, a new sensor design based on the more promising MEMS technology is therefore explored. As such, this thesis reports the requirement studies, design, silicon development, analysis and optimization of a MEMS pressure sensor for foot pressure measurement. The silicon implemented pressure sensor had a high linearity output with a pressure span approaching 3 MPa. This characteristic indicates excellent potential for a wide spectrum of biomechanical activities. Recently, the sensor had successfully been fabricated using the highly proven technology offered by Infineon Technologies SensorNor AS.

Experimental work clearly reveals that a high linearity measurement of pressure is achievable using the fabricated sensors. The sensors also demonstrated good signal magnitudes for efficient diagnosing of health conditions. Finally, a new pressure measurement system has been developed to reliably and securely characterize the sensors.

The research is proven to show that silicon based MEMS sensors are fulfilling the requirements of next generation biomedical sensor implementation.

## DECLARATION OF ORIGINALITY

“I, Yufridin Wahab, declare that the PhD thesis entitled **Design and Implementation of MEMS Biomechanical Sensors for Real Life Measurements of Gait Parameters** is no more than 100,000 words in length including quotes and exclusive of tables, figures, appendices, bibliography, references and footnotes. This thesis contains no material that has been submitted previously, in whole or in part, for the award of any other academic degree or diploma. Except where otherwise indicated, this thesis is my own work”.

---

Signature

---

Date

## ACKNOWLEDGEMENT

First and foremost, I would like to express my deep and sincere gratitude to my supervisor, Associate Professor Dr Aladin Zayegh, of Faculty of Health, Engineering and Science. His breadth of knowledge, enthusiasm and dedication have been of great value for me. His understanding, encouraging and personal guidance have provided a very strong basis for the present thesis. I am also deeply grateful to my co-supervisor, Associate Professor Dr Rezaul K. Begg, Centre of Ageing, Rehabilitation, Exercises and Sport Science (CARES) for his detailed and constructive comments, and for his influential support throughout this work.

I wish to express my warm and sincere thanks to Dr Daniel Lapadatu of Infineon Technology SensoNor AS, who is always ready to answer my questions about the foundry process and design rules. Also, my warm and sincere thanks are dedicated to Mr Donald Ermel, Mr Abdulrahman Hadbah and Mr Taky Chan of Victoria University who are always ready to share their technical skills and help me with the laboratory settings.

I owe my loving thanks to my mother, Khalijah Shariff, my wife Azizah Abdullah, my two daughters, Nurulizzah and Nuraqila. Without their sacrifice, encouragement and understanding, it would have been impossible for me to finish this work timely.

My precious times in Melbourne are made even more meaningful and memorable, thank you to all my supportive friends in CTME, School of Engineering and Science and others, especially Mohd Tafir, Yuhanis and Nahar.

Last, but not least, the scholarship award by University Malaysia Perlis, Ministry of Higher Education, Malaysia is also gratefully acknowledged.

## LIST OF ABBREVIATIONS

<b>3D</b>	Three dimensional
<b>AC</b>	alternating current
<b>ADL</b>	activity of daily living
<b>Al<sub>2</sub>O<sub>3</sub></b>	aluminum oxide
<b>CMOS</b>	Complementary Metal Oxide Semiconductor
<b>CMUT</b>	Capacitive micromachined ultrasonic transducer
<b>COP</b>	centre of pressure
<b>CS</b>	capacitive sensing
<b>dB</b>	decibel
<b>DC</b>	direct current
<b>EFS</b>	electric field sensing
<b>FEA</b>	Finite Element Analysis
<b>FSO</b>	full span output
<b>FS</b>	full scale
<b>GDS</b>	Graphic Data System
<b>GRF</b>	ground reaction force
<b>MEMS</b>	Micro-Electro Mechanical Systems
<b>MFC</b>	Minimum foot clearance
<b>MPW</b>	Multi project wafer
<b>MinZ</b>	minimum z coordinate of a structure
<b>N-EPI</b>	N type epitaxial layer
<b>N-WELL</b>	N material doped well
<b>PDMS</b>	Polydimethylsiloxane

---

<b>PMUT</b>	piezoelectric micromachined ultrasonic transducer
<b>PNL</b>	pressure non-linearity
<b>PVDF</b>	Polyvinylidene Fluoride
<b>PZR</b>	Piezoresistor
<b>PZT</b>	Lead Zirconate Titanate
<b>SNR</b>	signal to noise ratio
<b>SoC</b>	System on Chip
<b>SONAR</b>	Sound Navigation and Ranging
<b>TOF</b>	time of flight
<b>US</b>	ultrasonic sensing
<b>Vpp</b>	volts peak to peak
<b>WHO</b>	World Health Organization
<b>SEM</b>	Scanning Electron Microscope

# TABLE OF CONTENTS

ABSTRACT	ii
DECLARATION OF ORIGINALITY	v
ACKNOWLEDGEMENTS	vi
LIST OF ABBREVIATIONS	vii
LIST OF FIGURES	xii
LIST OF TABLES	xxi
LIST OF PUBLICATIONS	xxiii
<b>CHAPTER 1 THESIS OVERVIEW</b>	
1.1 Introduction	1
1.2 Motivation	5
1.3 Research Methodology	6
1.4 Summary of Contributions	9
1.5 Thesis Organization	11
<b>CHAPTER 2 LITERATURE REVIEW</b>	
2.0 Chapter Overview	12
2.1 Trends in Human Motion Measurement	12
2.2 The Foot Plantar Pressure Measurement	16
2.3 The Foot Clearance Measurement	31
2.4 MEMS Technology for Gait Measurement	43
2.5 Chapter Summary	60
<b>CHAPTER 3 FOOT CLEARANCE SENSOR ON SILICON</b>	
3.0 List of Refereed Publications Produced	61
3.1 Chapter Overview	62
3.2 Selection and Analysis of Clearance Sensing Technique	63

3.3	Selection of Ultrasound MEMS Mechanism and Fabrication	82
3.4	Design Specification of CMUT	84
3.5	CMUT Mathematical Modeling	85
3.6	CMUT Process Modeling and Simulation	93
3.7	CMUT FEA Design Modeling and Simulation	96
3.8	Chapter Summary and Discussion	103

## **CHAPTER 4 FOOT PRESSURE SENSOR ON SILICON**

4.0	List of Refereed Publications Produced	106
4.1	Chapter Overview	107
4.2	Design Specification	108
4.3	Fabrication Options and Requirement	110
4.4	Sensor Design – Mathematical Modelling and Simulation	111
4.5	Sensor Design – Silicon Modelling and Simulation	123
4.6	Sensor Design – FEA Modelling and Simulation	130
4.7	Sensor Design – System Modelling and Simulation	135
4.8	Sensor Design – System Optimization and Simulation	139
4.9	Sensor Design – Overall Results	145
4.10	Sensor Design – Silicon Implementation	147
4.11	Chapter Summary and Discussion	153

## **CHAPTER 5 PRESSURE SENSOR PACKAGING AND TESTING**

5.0	List of Refereed Publications Produced	154
5.1	Chapter Overview	155
5.2	Sensor Interconnection	156
5.3	GDS II with Level 0 Packaging	157
5.4	Level 1 Packaging for Testing	162
5.5	Electrical Testing Set-up Design and Result	165
5.6	Mechanical Testing Set-up Design and Result	167
5.7	Chapter Summary and Discussion	177

**CHAPTER 6 CONCLUSION AND RECOMMENDATION**

6.1	Chapter Overview	179
6.2	Summary of Achievements	180
6.3	Recommendation for Future Work	184

<b>REFERENCES</b>	<b>185</b>
-------------------	------------

**APPENDICES**

<b>A – CoventorWare™ Datasheets</b>
<b>B – Infineon Tech. (MultiMEMS) Project Report</b>
<b>C – Infineon Tech. (MultiMEMS) Fabrication Report</b>
<b>D – Certificate of Calibration</b>
<b>E – Risk Management Assessment Approval</b>

## LIST OF FIGURES

- Figure 1.1:** *Definitions of two gait parameters required in quantifying health risks, human locomotion and stability.* **2**
- Figure 2.1:** *The occurrence of falls among the elderly, (Left) places where falls occur and (Right) the activities performed during falls (Berg et al., 1997).* **14**
- Figure 2.2:** *The recently proposed patient monitoring system that includes human movement monitoring (Jovanov et.al, 2005).* **16**
- Figure 2.3:** *A visual representation of qualitative foot plantar pressure changes during gait.* **17**
- Figure 2.4:** *(Left) The GaitRite mat (Bontrager, 1998), (Middle) Optical Pedabograph (Mothiram, 2002), (Right) Graph of vertical GRF during stance phase of gait cycle and the path of the COP (Rodgers, 1988).* **19**
- Figure 2.5:** *(Left) The Gaitshoe proposed in MIT (Morris, 2004; Bamberg et al., 2008), (Middle) The instrumented shoe for GRF determination (Liedtke et.al, 2007) and (Right) SmartShoe (Kong & Tomizuka, 2008).* **21**
- Figure 2.6:** *(Far Left) Bio-foot ® insole with 64 piezoelectric pressure sensors (Martinez-Nova et al., 2007), (Middle Left) the SIMS insole with 32 pressure sensors (Zhang et al., 2004), (Middle) the Parotec insole layout (Chesnin, Selby-Silverstein & Besser, 2000), (Middle Right) the instrumented shoe sole (Faivre et.al, 2004) and (Far Right) the SmartShoe sole (Kong & Tomizuka, 2008).* **21**
- Figure 2.7 :** *(Left) Hysteresis cause by loading and unloading of a pressure sensor is usually measured at the 50% pressure range and is expressed as percentage of full-scale (FS) (Beeby, 2004, pg 119). (Right) Negligible hysteresis of a MEMS based pressure sensor (Lee et al., 2001).* **25**

<b>Figure 2.8 :</b> <i>(Left) The definition of nonlinearity (Chiou &amp; Chen, 2008) and (Right) the nonlinearity of the F-scan insole (Luo, Berglund &amp; An, 1998).</i>	<b>25</b>
<b>Figure 2.9:</b> <i>The effect of sensor (squares) sizing and placement (Urry, 1999).</i>	<b>27</b>
<b>Figure 2.10:</b> <i>Examples of erroneous readings due to sensor creep of the Pedar insoles (Arndt, 2003).</i>	<b>28</b>
<b>Figure 2.11:</b> <i>The factors that lead to foot ulceration among diabetics (Boulton, 2004).</i>	<b>29</b>
<b>Figure 2.12:</b> <i>Bony prominence, plantar pressure and foot ulcer (Endemir et.al,2005).</i>	<b>30</b>
<b>Figure 2.13:</b> <i>Relationship between plantar thickness, pressure, time/repetition and plantar injury among the diabetes patients (van Schie, 2005).</i>	<b>30</b>
<b>Figure 2.14:</b> <i>(Left) Foot trajectory during gait detailing the vertical displacement of foot for one gait cycle showing MFC during mid swing. (Right) The markers on the shoe (Begg et.al, 2007).</i>	<b>33</b>
<b>Figure 2.15:</b> <i>(Left) A foot clearance measurement during stair decent using passive markers (Hamel et al.,2005). (Right) Passive markers (Bontrager, 1998).</i>	<b>33</b>
<b>Figure 2.16:</b> <i>Electric field distance sensor electrode attached to the Gaitshoe outsole for foot clearance measurement (Morris, 2004).</i>	<b>34</b>
<b>Figure 2.17:</b> <i>A capacitive sensor considered here (Luo, 1996), (a) the fringing capacitance, (b) the top view of the sensor, and (c) the side view.</i>	<b>37</b>
<b>Figure 2.18:</b> <i>The working principle of electric field sensing for height determination (Morris, 2004).</i>	<b>38</b>
<b>Figure 2.19:</b> <i>The pocket sized Polaroid Sx-70 Sonar OneStep Land camera with the first mobile ultrasound distance measurement.</i>	<b>40</b>

- Figure 2. 20:** (Right) A 40 kHz Ultrasonic car height measurement for  $0^{\circ}\text{C}$ - $40^{\circ}\text{C}$  operating temperature, 0.1m-0.6m range and better than 1mm resolution (Carullo & Parvis, 2001), (Left) Ultrasound sensor is used by robot to measure height ( $y_{sens}$ ) with resolution of 0.3 mm (Kajita & Tani, 1996). **41**
- Figure 2.21:** A direct ultrasound ranging system in gait analysis (Weir, 1997). **41**
- Figure 2.22:** A simple time of flight concept (Ohya, Ohno & Yuta, 1996). **42**
- Figure 2.23:** (Right) Surface micromachining and (Left) Bulk micromachining (Judy, 2001). **47**
- Figure 2.24:** A coin and MEMS pressure sensors with the smallest one having dimensions of  $175 \times 700 \times 1000 \mu\text{m}^2$  (Judy, 2001). **48**
- Figure 2.25:** (Left) A tripple layered surface micromachined capacitive pressure sensor crossection (Zhou, Huang & Qin, 2005). (Right) A non-linear capacitive pressure sensor output (De Bruyker, 1998). **49**
- Figure 2.26:** (Left) A crossectional view of a bulk micromachined piezoresistive pressure sensor using PDMS as membrane (Lee & Choi, 2008). (Right) A linear piezoresistive pressure sensor output (De Bruyker, 1998). **51**
- Figure 2.27:** A Piezoresistive MEMS pressure sensor in action: (Top) the insole of a Robot at University California, Berkeley (Wheeler et al., 2006), (Bottom-Right) The Parotec hydrocell insole (Chesnin, Selby-Silverstein & Besser, 2000), and (Bottom-Left & Middle) a biomechanical pressure sensor (Lee et al., 2001). **51**
- Figure 2.28 :** As reported in the referenced literature (Luo, 1996), (a) and (b) shows the top view of possible electrode arrangements, and (c) the top view of a micro-fabricated and tested sensor, (d) another MEMS capacitive proximity sensor able to measure up to 10 cm using the method similar to the Luo's design (Lee, Chang & Yoon, 2006). **54**
- Figure 2.29:** The working principle of electric field sensing for height determination using the effect of capacitance variation induced by height changes (Morris, 2004). **55**

<b>Figure 2.30:</b> <i>A complete system of ultrasound sensing system with a 1 mm<sup>2</sup> MEMS membrane (Kuratli &amp; Huang,2000).</i>	<b>56</b>
<b>Figure 2.31:</b> <i>(Left) The crossection of a pMUT (Wang et.al, 2005) and (Right) a CMUT (Oralkan et.al,2002).</i>	<b>57</b>
<b>Figure 2.32:</b> <i>A possible implementation using two points sensing.</i>	<b>59</b>
<b>Figure 3.1:</b> <i>The distribution of MFC in one report (Begg et al.,2007)</i>	<b>64</b>
<b>Figure 3.2:</b> <i>Capacitive Sensor showing the fringing effect, the top view of the sensor is on the right while the side view is on the left. (Luo, 1996)</i>	<b>67</b>
<b>Figure 3.3:</b> <i>Two of the best Matlab simulation result for the capacitive sensor.</i>	<b>67</b>
<b>Figure 3.4:</b> <i>The working principle of electric field sensing for height determination using the effect of capacitance variation induced by height changes (Morris, 2004).</i>	<b>70</b>
<b>Figure 3.5:</b> <i>The working principle of E-field focusing using Shield Electrode (Driven Electrode), (Left) without Driven Electrode and (Right) with the Driven Electrode.</i>	<b>70</b>
<b>Figure 3.6:</b> <i>The Matlab simulation result for electrode area A from 1 mm<sup>2</sup> to 1 cm<sup>2</sup>.</i>	<b>71</b>
<b>Figure 3.7:</b> <i>The distance that the signal travels is equivalent to double the actual distance/clearance between a transmitting/receiving transducers and the target surface (Massa, 1999; Bilgin, 2003).</i>	<b>73</b>
<b>Figure 3.8:</b> <i>Pulse length and wavelength of a five cycles signal (Wells, 1968).</i>	<b>75</b>
<b>Figure 3.9:</b> <i>The speed of sound in air for different temperatures (Bohn, 1988).</i>	<b>76</b>
<b>Figure 3.10:</b> <i>Transmission and echo signal for a tof system (Magori &amp; Walker, 1987)</i>	<b>76</b>

- Figure 3.11:** *Measured ultrasound signal attenuation and the maximum distance measurable for each signal frequency based on the conventional piezoelectric technology (Yano, Tone & Fukumoto,1987). The two 'x' marks in the graph indicates the current maximum ultrasound measurement range based on CMUT technology (Ergun et al.,2006).* **79**
- Figure 3.12:** *The total ultrasound attenuation for various measurement distance and frequencies. The actual distance measured is half of each figure.* **79**
- Figure 3.13:** *Approximation of best ultrasound frequency for distance of 30 cm from simulation which is about 1.05 MHz. The horizontal dotted line touches the y axis at ~120dB point. Even though the target distance is just 5 cm, this long range measurement capability may enable application in more human activities (Wahab et al., 2008; Wahab et al.,2007).* **80**
- Figure 3.14:** *A cross-sectional view of a CMUT ( Adapted from Ergun, Yaralioglu & Khuri-Yakub,2003).* **86**
- Figure 3.15:** *The lumped electromechanical model for CMUT.* **86**
- Figure 3.16 :** *A possible implementation using two points sensing.* **90**
- Figure 3.17:** *The simplified process sequence.* **94**
- Figure 3.18:** *The process sequence in the fabrication modeling.* **95**
- Figure 3.19:** *The 3D model produced by the Solid Modeler module.* **95**
- Figure 3.20:** *The crossectional view of the CMUT.* **96**

<b>Figure 3.21:</b> <i>The meshed membrane's side-view showing the top electrode on top and bottom electrode at the bottom. The substrate is hidden for clarity.</i>	<b>97</b>
<b>Figure 3.22:</b> <i>The meshed membrane's top-view showing the meshed top electrode on top of the membrane. The yellow square is the substrate.</i>	<b>98</b>
<b>Figure 3.23:</b> <i>The mode 1 result of modal analysis.</i>	<b>100</b>
<b>Figure 3.24:</b> <i>The deflection and pull-in voltage.</i>	<b>101</b>
<b>Figure 3.25:</b> <i>The deflection of membrane at pull-in voltage.</i>	<b>101</b>
<b>Figure 3.26:</b> <i>The layout of the CMUT.</i>	<b>102</b>
<b>Figure 4.1:</b> <i>A conceptual design of a MEMS pressure sensor in a cross-sectional view.</i>	<b>109</b>
<b>Figure 4.2:</b> <i>Transversal and longitudinal stresses acting on a piezoresistor with respect to the current flow direction <math>\mathbf{J}</math> (Zamali &amp; Talghader, 2006).</i>	<b>112</b>
<b>Figure 4.3:</b> <i>The Pressure versus Membrane Deflection of thick membranes.</i>	<b>117</b>
<b>Figure 4.4:</b> <i>The Pressure versus Membrane Deflection of thin membranes.</i>	<b>118</b>
<b>Figure 4.5:</b> <i>The convergence of stress and dimensional relationships for (Top) 3.1 <math>\mu\text{m}</math> and (Bottom) 23.1 <math>\mu\text{m}</math> membrane in MPa unit.</i>	<b>119</b>
<b>Figure 4.6:</b> <i>A simple layout for the membrane design to model the minimum size requirement.</i>	<b>122</b>
<b>Figure 4.7:</b> <i>The simplified process sequence showing conceptually how the device is formed.</i>	<b>124</b>

<b>Figure 4.8:</b> <i>The simplified process sequence as extracted from the CoventorWare™ process design tool.</i>	<b>124</b>
<b>Figure 4.9:</b> <i>A cross-sectional view of the key mechanical parts of the sensor structure with definition of various structural dimension parameters.</i>	<b>127</b>
<b>Figure 4.10:</b> <i>A layout for the realization of a membrane and its silicon frame.</i>	<b>128</b>
<b>Figure 4.11:</b> <i>The yield of silicon process simulation. (Top Left) The square (pink coloured) membrane surface that receives the applied pressure, (Top Right) another view from the other side of the membrane, and (Bottom) is the device cross-section showing various layers.</i>	<b>129</b>
<b>Figure 4.12:</b> <i>(a) The partitioning frame view of the developed model. (b)(c) The 3D view with partitioning lines (d) The partitioned 3D model with some segments are made invisible to enable better appreciation of the various layers and segment shapes.</i>	<b>131</b>
<b>Figure 4.13:</b> <i>3D model and its mesh. In actual design, all four corners of the model are symmetrical.</i>	<b>132</b>
<b>Figure 4.14:</b> <i>Mises Stress on the (Top) 278 <math>\mu\text{m}</math> (Middle) 200 <math>\mu\text{m}</math> and (Bottom) 100 <math>\mu\text{m}</math> pressure sensor membranes.</i>	<b>134</b>
<b>Figure 4.15:</b> <i>The system level simulation representation.</i>	<b>135</b>
<b>Figure 4.16:</b> <i>A resistive Wheatstone bridge circuit (Karki, 1999).</i>	<b>137</b>
<b>Figure 4.17:</b> <i>A highly linear output voltage vs pressure relationship. The relationship between the applied pressure and output voltage of the (Top) 100 <math>\mu\text{m}</math>, (Bottom) 200 and 278 <math>\mu\text{m}</math> membranes.</i>	<b>138</b>
<b>Figure 4.18:</b> <i>The parameters involved in the optimization. (Top) A top view of an enlarged membrane zone. (Bottom) The cross-section of the sensor for reference.</i>	<b>140</b>
<b>Figure 4.19:</b> <i>Output voltage against Offset_x parameter.</i>	<b>143</b>
<b>Figure 4.20:</b> <i>Output voltage against Offset_x parameter.</i>	<b>144</b>

<b>Figure 4.21:</b> <i>Output voltage against piezoresistor length.</i>	<b>144</b>
<b>Figure 4.22:</b> <i>Output voltage against piezoresistor length.</i>	<b>145</b>
<b>Figure 4.23:</b> <i>Graphs showing plots of output voltage versus pressure for (Top) 200 <math>\mu\text{m}</math>, (Middle) 278 <math>\mu\text{m}</math> and (Bottom) 100 <math>\mu\text{m}</math> pressure sensors.</i>	<b>146</b>
<b>Figure 4.24:</b> <i>Layouts of the three sensors.(Top) 100 <math>\mu\text{m}</math> pressure sensor, (Middle) 120 <math>\mu\text{m}</math> pressure sensor and (Bottom) 278 <math>\mu\text{m}</math> pressure sensor.</i>	<b>152</b>
<b>Figure 5.1:</b> <i>The silicon die frame, sensor to pads interconnections and the Level 0 Package definitions all included in this foundry compatible GDS II tape-out file.</i>	<b>158</b>
<b>Figure 5.2:</b> <i>(Top) A glass waferbonded Level 0 Packaged chip from Infineon Technology SensoNor as (Kronendorfer &amp; Kim, 2007), and (Bottom) the dimensional description (Infineon, 2007).</i>	<b>159</b>
<b>Figure 5.3:</b> <i>The produced dice from the foundry. The left die exposes the designed holes. Pads for outside connections are shown on the right one.</i>	<b>160</b>
<b>Figure 5.4:</b> <i>The almost similar pressure sensor in an open package (Kronendorfer, 2004).</i>	<b>163</b>
<b>Figure 5.5:</b> <i>The packaged die for device level testing.</i>	<b>164</b>
<b>Figure 5.6:</b> <i>The electrical testing.</i>	<b>165</b>
<b>Figure 5.7:</b> <i>The designed printed circuit board to reduce the size of the overall circuit and improve the electrical interconnection to the pressure sensor. The design is based on Altium Designer Winter 09 Evaluation Package.</i>	<b>168</b>

- 
- Figure 5.8:** *The completed veroboard for the integrated three pressure sensors.* **168**
- Figure 5.9:** *Pressure chamber with all other required components attached to the main cylinder (A), an end cap (B), the stand (C) and a pressure gauge (D) attached to the other end cap.* **169**
- Figure 5.10:** *Pressure sensor veroboard attached to one of the end cap. The end cap is clamped to a stand. Visible is the bottom side of the veroboard.* **171**
- Figure 5.11:** *The complete mechanical testing set-up.* **172**
- Figure 5.12:** *The amplifier circuit design and its veroboard implementation.* **173**
- Figure 5.13:** *The graphs produced from the recorded experimental pressure and output voltage relationship. The voltages are not amplified.* **176**

## LIST OF TABLES

<b>TABLE 2.1</b> IN-SHOE PRESSURE SENSORS IN THE MARKET	22
<b>TABLE 2.2</b> SILICON VS STEEL AND OTHER COMMON MEMS MATERIALS	45
<b>TABLE 2.3</b> MPW PROCESS TECHNOLOGY COMPARISON	47
<b>TABLE 2.4</b> COMPARISON OF THE THREE TECHNIQUES	58
<b>TABLE 3.1</b> SIMULATION RESULTS FOR $R_2 = 1$ cm	68
<b>TABLE 3.2</b> COMPARISON OF THE THREE TECHNIQUES	81
<b>TABLE 3.3</b> COMPARISON OF PMUT AND CMUT (Pappalardo et al.,2008)	83
<b>TABLE 3.4</b> DESIGN EXAMPLES USING (24) AND COMPARISON WITH MEASUREMENTS IN RELEVANT LITERATURE	93
<b>TABLE 3.5</b> VOLTAGE(IN V), DISPLACEMENT( $\mu$ m) AND CAPACITANCE(pF)	100
<b>TABLE 4.1</b> VALUES OF EM COEFFICIENTS	112
<b>TABLE 4.2</b> FOUNDRY SPECIFIED MAXIMUM SIZE FOR SQUARE MEMBRANES	115
<b>TABLE 4.3</b> PARAMETERS OF SELECTED SQUARE SENSORS DESIGN	115
<b>TABLE 4.4</b> MIMIMUM MEMBRANE SIDE LENGTHS	121

---

<b>TABLE 4.5</b> THE MAXIMUM VON MISES STRESS	133
<b>TABLE 4.6</b> THE ELECTRICAL PART DESIGN SHAPES AND PARAMETERS	148
<b>TABLE 4.7</b> THE PIEZORESISTANCE VALUES	151
<b>TABLE 5.1</b> THE PADS DESCRIPTIONS	161
<b>TABLE 5.2</b> THE SUPPLY VOLTAGE RANGE AND RESISTANCE (CALCULATION)	165
<b>TABLE 5.3</b> RESISTOR VARIATION	167
<b>TABLE 5.4</b> PHYSICAL DIMENSION OF THE STAINLESS STEEL PRESSURE CHAMBER	171
<b>TABLE 5.5</b> RISK MANAGEMENT	174
<b>TABLE 5.6</b> PRESSURE SENSOR RESPONSE TO PRESSURE	175

## LIST OF PUBLICATIONS

1. Wahab, Y, Zayegh, A., Begg, R.K. and Veljanovski, R., 2008. 'A model for the measurement of foot-to-ground clearance and potential realization of micro-electro-mechanical systems', **AMSE Journal: Modelling, Measurement and Control C**, vol. 69, no. 1, pp. 59-74. ISSN 12595977.
2. Wahab, Y, Zayegh, A., Begg, R.K. and Veljanovski, R., 2007. 'Analysis of foot to ground clearance measurement techniques for MEMS realization', in **Proceedings of the IEEE International Conference on Computer and Information Technology (ICCIT 2007)**, 27-29 December, Dhaka Bangladesh, pp. 413-417. ISBN 978-1-4244-1550-2.
3. Wahab, Y, Zayegh, A., Begg, R.K. and Veljanovski, R., 2007. 'CMUT For Human And Humanoid Locomotion Mesurement', in **Proceedings of Int. Con. on Robotics, Vision, Information and Signal Processing 2007**, Universiti Sains Malaysia, Penang, Malaysia, 28-30 November, pp. 359-364. ISBN 978-983-43178-1-2.
4. Wahab, Y., Zayegh, A., Veljanovski, R. and Begg, R.K., 2008. 'Micro-sensor for foot pressure measurement, in **Proceedings of TENCON 2008. IEEE Region 10 Conference**, pp.1-5, 19-21 November, Hyderabad, India. ISBN 978-1-4244-2408-5.
5. Y. Wahab, A. Zayegh, R. Begg and R. Veljanovski, 2008. 'Sensitivity optimization of a foot plantar pressure micro-sensor', in **Proceedings of IEEE International Conference on Microelectronics, Sharjah, UAE**. pp. 104-107, 14-17 December. ISBN 1-4244-2370-5.
6. Y. Wahab, A. Zayegh, R. Begg and R. Veljanovski, 2008. 'Modeling and Simulation of Micro-Electro-Mechanical System Pressure Sensor for Biomechanical Application', in **Proceedings of Int. Conf. Modeling and Simulation (MS 2008)**, pp. 49-54, 18-20 November, Jordan. ISBN 978 995 786 430 9.
7. Wahab, Y., Zayegh, A., Veljanovski, R. and Begg, R.K., 2008. 'Design of MEMS biomedical pressure sensor for gait analysis', in **Proceedings of IEEE International Conference on Semiconductor Electronics**, 2008, pp.166-169, 25-27 November. Johor Bahru, Malaysia. ISBN 978-1-4244-3873-0.

8. Wahab, Y., Zayegh, A., Begg, R.K. and Sauli, Z., 2009. 'Testing of MEMS Biomedical Pressure Sensor for Gait Analysis', in *Proceedings of IEEE Regional Symposium on Microelectronics*, August 10-12, Kota Bharu, Malaysia. ISBN 978-967-5048-55-5.
9. Wahab, Y., Zayegh, A. and Begg, R.K., 2009. 'Comparison and Silicon Realization of Custom Designed MEMS Biomedical Pressure Sensors', submitted to the **21<sup>st</sup> IEEE International Conference on Microelectronics**, 19-22 December, Marrakech, Morocco.
10. Wahab, Y., Zayegh, A. and Begg, R.K., 2009. *Silicon Implementation of Micro Pressure Sensor*, submitted to the **5<sup>th</sup> IEEE International Conference on Intelligent Sensors, Sensor Networks and Information Processing (ISSNIP 2009)**, 7-10 December, Melbourne, Australia.

## Thesis Overview

## CHAPTER

# 1

- 1.1 Introduction
- 1.2 Motivation
- 1.3 Research Methodology
- 1.4 Summary of Contributions
- 1.5 Thesis Organization

### 1.1 Introduction

Gait analysis is the study of lower limb movement patterns and involves the identification of gait events and the measurements of kinetics and kinematics parameters. These include for example, toe-off, landing, stance, swing, displacement, speed, acceleration, force, pressure and the pressure-time-integral. Gait analysis is a very important procedure in assessing and improving many quality of life indicators. In sports, gait analysis can be used to improve athlete's performance and injury prevention. For patients, such as those suffering from diabetes, gait analysis can be used to screen for development of foot ulceration thus preventing them. In term of gait stability, gait analysis is proven to be very helpful in assessing and improving balance among the elderly, patients with diabetes or peripheral neuropathy and many other sicknesses. Gait analysis is also widely used in rehabilitation.

The occurrence of fall is becoming more of a significant health threat recently. This is due to the fact that the worldwide phenomenon of growing population of the elderly is continuously observed in many developed and developing countries. It is estimated that the world's elderly citizen will reach 2 billion in 2050 from current figure of 670 million. To make matters worse, the total number of the world's diabetic sufferers is increasing from 171 million in

2000 to 366 million in 2030, with an obvious trend of surging proportion for the above 65 years group.

In order to further understand the situation that leads to the health hazard, many research groups around the world are seriously looking into the matter. Recently, it is reported that foot plantar pressure can be used to assess gait stability and risk of fall. In addition, foot clearance above ground/floor during gait is also reported to be related to the occurrence of fall among the elderly. This is especially true when the foot is swaying on the air, or also called swing phase. Notably, pressure is measured when the foot is already touching the ground, which is known as stance phase, while clearance is measured during mid-swing to heel strike. These terms and various other terms of gait analysis are visually described in Figure 1.1. If both pressure and clearance parameters of gait analysis are used together in an integrated manner, a better way of fall prediction and prevention can be produced.

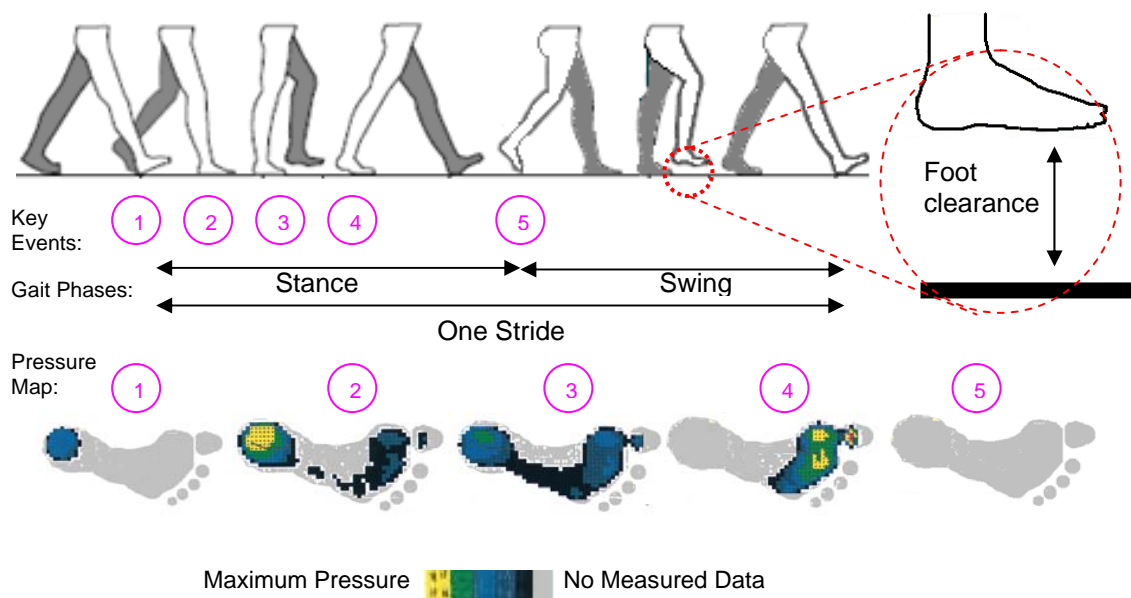


**Figure 1.1:** Definitions of two gait parameters required in quantifying health risks, human locomotion and stability.

In addition to assessing balance, the measurement of foot plantar pressure and foot clearance are also useful in many other gait assessments. This foot pressure measurement has wide applications, for example in screening for high risk diabetic foot ulceration, design of orthotics for diabetes mellitus and peripheral neuropathy, footwear design, sports injury prevention in athletes, study of the development of gait among the children plus many more. It also can be used to identify gait events such as heel strike, toe off, the timing of swing, stance, stride, the double support phase and also cadence. If stride length is known, the horizontal speed and acceleration can also be determined. On the other hand, the foot clearance measurement can also be useful in determining the vertical component of gait kinematics such as maximum vertical displacement, vertical velocity and its acceleration.

At current, the health system is still lacking. While the ratio of medical professional to patients is reducing, such measurements are still mostly conducted in exclusive research facilities, rehabilitation laboratories or hospitals. For example, the use of gait mats, force sensing platforms, motion analysis systems with efficient computer processing and ultrasonic ranging system are used for indoor analysis. Despite their efficiency and reliability, these state-of-the-art measurement systems are still using the bulky old fashioned technology. Considering the global trend of increasing elderly and diabetic population, a major paradigm shift is therefore highly required. As a solution, the advances in the instrumentation technology should be explored and used to its fullest capability. The aim is to enable the measurement to be performed in the patient's real environment with the revolutionary e-health connectivity and supporting pervasive healthcare concept.

While e-health system demands internet application for better management and implementation of healthcare provision, pervasive healthcare promotes wireless interconnection between monitoring devices. In this case, sensors that are part of body sensor network can be used. These sensors should not interfere with the actual movement itself so that the readings are representative of the actual tasks performed. This demands that the devices be small, lightweight and easily attached to the shoes or feet. One possible way of satisfying such exclusive demands is, of course, through the application of the fast developing micro-electro-mechanical system (MEMS) technology. This relatively new but promising instrumentation technology provides a great opportunity to further advance the intended gait measurement system.

This technology is proven to be capable of shrinking the device size, integrating sensors and actuators with their processing and controlling circuitry and lowering the power consumption of the overall system. The fusion of its technology is now covering wide applications across a multitude of disciplines from medical to military and spaces from in-vitro of human body organs to the infinity of aerospace. The great achievement has been due to cheap and easy integration of microelectronic signal processing circuits and MEMS technologies. Thus, the potential of these technologies should be explored in the design of newer generation of gait analysis instruments to ensure greater progress of the gait analysis application with significant impact to society. Therefore, in this thesis, the exploration and realization of micro-sensors for the measurement of gait parameters using MEMS technology is explained.

## 1.2 Motivation

As roughly mentioned in the previous section, the current status of the development of untethered in-shoe gait stability measurement devices is still lacking behind the reality of technology achievement. In this subsection, the motivation for this research is described. Specifically, with respect to their measurand, the current devices are not fully optimized in many aspects.

### **Foot Clearance:**

- Not suitable for real world or outdoor measurement.
- Not cost effective
- Not enabling efficient signal processing
- Not fully integratable for better reliability and long lasting use

### **Foot Plantar Pressure:**

- Not providing the required pressure range for diabetic related application
- Not supporting efficient signal processing
- Exhibits hysteresis and other weaknesses.

Most interestingly, despite the proven track records, there is no reported innovation that targets gait analysis parameters of clearance and plantar pressure concurrently based on MEMS as yet.

### 1.3 Research Methodology

This section elaborates on the steps and tools used during throughout the research duration to accomplish the research target. In general, the use of CoventorWare 2006 as an integrated tool for Micro-electro-mechanical design is involved. In addition, mathematical modelling tool, namely Matlab 2007 and the spreadsheet tool Microsoft Excel 2003 is also used when required. As the target measurements involves two different physical quantities, namely distance and pressure, this subsection is divided into two parts of easy elaboration. The first part, which is 1.3.1 is devoted to foot clearance measurement device while 1.3.2 caters for the pressure measurement device.

#### 1.3.1 Foot Clearance Measurement Device

The steps involved in the research for this device's design and analysis are enlisted below:

##### 1.3.1.1 *Study of foot clearance pattern during gait and the current status*

This step involves searching and digesting the knowledge presented in the related publications. It is found that the vertical displacement of foot during swing, or other words, foot clearance, is found to be about maximum at 30 cm. Depending on the length of the lower limb of an individual, the risk of fall is increased if the downward movement of the foot before touching the ground/floor is not stable, especially at about 1 cm to 2 cm above the ground/floor.

### 1.3.1.2 *Analysis of the available clearance measurement techniques*

This step requires the study and analysis of various suitable measurement of distance/displacement or also termed ranging. It also involves the study of the current related practice in gait analysis. Currently, no direct measurement of foot clearance is performed. Instead, the clearance is determined through complex calculation and computer processing of acceleration data or recorded video. For that reason, three suitable techniques for direct determination of foot clearance are identified and analysed. They are capacitive distance sensing, electric field sensing and ultrasonic ranging.

### 1.3.1.3 *Identification and modelling of the chosen suitable technique*

Once the analysis of the three techniques are producing results, the more suitable technique is then chosen. This is done by comparing all the three analysis results and also studying their silicon realization capability based on literature.

### 1.3.1.4 *Study of possible silicon implementation*

The chosen technique is then modelled in various possible silicon realizations. There are many silicon sensing and actuation techniques that can be applied to the intended ultrasonic transducer, namely piezoelectric technique, electrothermal. However, there is one which is more practical for implementation which is capacitive. Then, several possibly suitable silicon micromachining technology are studied and compared. Aspects considered includes cost and integrated circuit integration capability.

### 1.3.1.5 *Design, Modelling and Characterization of the device*

The device is then designed using silicon micromachining, modelled in three dimensional and then characterized using finite element analysis technique.

## 1.3.2 Foot Plantar Pressure Measurement Device

The steps involved in the research for this device's design and analysis are:

### 1.3.2.1 *Study of foot plantar pressure pattern and the current status*

Literature review on the above subject is carried out to understand the real need of the pressure measuring device, covering all possible gait application. The current status is then compared with the actual needs to identify the gap.

### 1.3.2.2 *Analysis of the available measurement techniques*

Various pressure sensing techniques are considered by analysing their strengths and weaknesses. It is found that piezoelectric, capacitive and piezoresistive are the three major sensing techniques, with each of them can be further divided into many material specific individual techniques.

### 1.3.2.3 *Study of possible silicon implementation*

The technique that is proven to be more suitable is then analysed for silicon realization. Several silicon micromachining technologies are considered based on the available design space and cost.

#### 1.3.2.4 *Design, Modelling and Characterization*

Once a suitable technology is identified, the design and three dimensional modelling is performed. The finite element analysis is used to optimize and characterize the sensor under development.

#### 1.3.2.5 *Physical device realization*

Physical realization of the device is implemented using the chosen silicon technology. This step includes laying out the device design, checking its foundry design rule compatibility and creating its GDS II file format.

#### 1.3.2.6 *Packaging and Testing*

The fabricated devices are packaged, wired on PCB and attached to a specially designed pressure chamber for laboratory characterization.

### **1.4 Originality of the Thesis**

This research will contribute to the knowledge in silicon sensor implementation for foot clearance and foot plantar pressure measurements as it addresses major issues in realization of efficient, reliable and practical devices. The research is one of the pioneering attempts in introducing, designing, finalizing, realizing and characterizing the sensors for gait analysis. This research will contribute to knowledge in the following specific areas:

#### *1.4.1 The Development of Device Specification for Clearance Measurement*

For the first time, the requirements that a sensor should satisfy in order to be able to measure foot clearance is identified. Following this, a list of foot clearance sensor specification is proposed.

#### *1.4.2 Comparative Study of Techniques*

A proper comparative study of techniques of measuring foot clearance is performed analytically. The analysis results are evaluated in terms of key capabilities such as detectable range, linearity of signal and MEMS readiness and thus a suitable technique for foot clearance measurement suitable for silicon realization is identified and reported.

#### *1.4.3 Development and Characterization of Foot Clearance Device Model*

A methodology for realizing silicon MEMS model for ultrasound sensor that is theoretically capable of performing foot clearance measurement is proposed. A sensor is also developed and characterized.

#### *1.4.4 The Development of Device Specification for Pressure Measurement*

By considering the more challenging applications, the foot plantar pressure sensing requirements are identified and a list of pressure sensor specifications for measuring foot plantar pressure is proposed.

#### *1.4.5 Development and Characterization of Pressure Sensor Model*

A methodology for realization of silicon MEMS pressure sensor model optimized for gait analysis is proposed.

#### *1.4.6 Fabrication and Testing of the Physical Pressure Sensor*

A methodology for transferring the silicon MEMS pressure sensor model onto physical silicon via foundry service is proposed. The fabricated sensors are then tested to verify the methodology.

### **1.5 Thesis Organization**

The literature review for foot clearance measurement and foot plantar pressure measurement are explained in Chapter 2. The mathematical modelling, design, characterization, analysis and implementation of the proposed foot clearance measurement are mentioned in Chapter 3. The following chapter, Chapter 4 is devoted to the mathematical modelling, design, optimization, analysis and implementation of the proposed foot plantar pressure measurement sensor. Chapter 5 elaborates on the efforts towards physical realization of the foot plantar pressure measuring device which include the laying out of the design, the foundry rule violation checking and the preparation of the foundry compatible design representation format file for submission. In addition, Chapter 5 provides the fabricated foot plantar pressure sensor wirebonding, packaging, testing set-up development, laboratory testing implementation, its results and also technical discussions on the matter. Conclusion and further research recommendations are provided in Chapter 6.

## Literature Review

## CHAPTER

# 2

- 2.0 Chapter Overview*
- 2.1 Trends in Human Motion Measurement*
- 2.2 The Foot Plantar Pressure Measurement*
- 2.3 The Foot Clearance Measurement*
- 2.4 MEMS Technology for Gait Measurement*
- 2.5 Chapter Summary*

### **2.0 Chapter Overview**

This chapter elaborates mostly on the current progress of foot pressure measurement and also foot clearance measurement as available in the literature and the market and also highlights the surging need for new generation of such sensors. A discussion on the contribution and potential of MEMS technology in biomechanical and gait analysis is also included. As such, it is divided into four main sections. The first section is devoted to a short overview on trends of human motion measurement. Next is the section for a review of foot plantar pressure measurement. Then, a section for foot clearance measurement follows. A section dedicated for MEMS technology and its potential comes next. Lastly, the chapter summary highlights the need for new generation sensors based on the more technologically advanced MEMS platform that enables real-life measurement of foot clearance and foot plantar pressure.

### **2.1 Trends in Human Motion Measurement**

Gait is simply defined as a style of walking (Curran, 2005). Gait analysis is the study of lower limb movement patterns and involves the measurements of kinetics and kinematics parameters. These include, for example gait events and

phases such as toe-off, landing, stance, swing, double support, and kinematics such as foot displacement, speed, acceleration, and kinetics such as force, pressure and the pressure-time-integral (Rodgers, 1988). The understanding of normal gait principles is the basis for understanding the pathologic and compensatory gait deficits. Normal gait for human being is bipedal in nature that distinguishes human from other primates but is often taken for granted until something goes wrong (Curran, 2005). It is achieved by use of the lower limbs that comprise of foot as one of the key parts. The foot is a complex structure that is made of 26 bones, 33 joints and more than 300 soft-tissue structures (Curran, 2005). As the terminal structure in the human kinetic chain, it performs the pivotal roles of dissipator for compressive, tensile and shear forces while performing rotational motions during stance. In other words, from a podiatrics point of view, foot functions as a shock absorber, a mobile adapter and finally a rigid lever (Curran, 2005). Nowadays, the need for the measurement of human motion parameters is getting higher due to the increase in the number of fields requiring it, especially numerous medical specializations (Simon, 2004), activity of daily living (ADL) assesment and sports (Billing et al.,2006; Aminian & Najafi, 2004). In medical field, the use of gait analysis encompasses the tests for central nervous disorders, locomotor disorders, rheumatology, orthopedics, endocrinology and neurology (Simon, 2004). At present, the measurement is mostly performed in specialized facilities such as hospital or laboratories (Best & Begg, 2006). These facilities require very high setting up cost (Simon, 2004). Despite the high cost, it is argued that the performed measurement is not accurate or a

true representative of the actual daily activities of the subject as it is claimed to only gauge a person's potential walking ability at a given time (Simon, 2004). In fact, the facilities also limit the space usable for the measurement. It is claimed that the most inconvenient aspects of these systems is the fact that the subject must walk in a closed and restrained space (Aminian & Najafi, 2004). The expanding use of gait analysis is catalyzed by the fact that it is able to evaluate walking "out-of-the lab" where most of the daily living activities are performed (Simon, 2004). As an example, it can be seen in Figure 2.1, that the locations where falls occur are 77 % outside of the house (Berg et al.,1997). Even though the recent instruments does not measure the gait in real living condition, the trends is moving towards that direction. In addition to their competitive price, user friendliness, miniaturized for portability, capability of efficiently recording and processing larger number of parameters in less time and space are among the required traits of such devices (Simon, 2004). Obviously, these 'dream' system can only be materialized by adoption of the already practically proven microelectronics and micro-electro-mechanical system technologies.

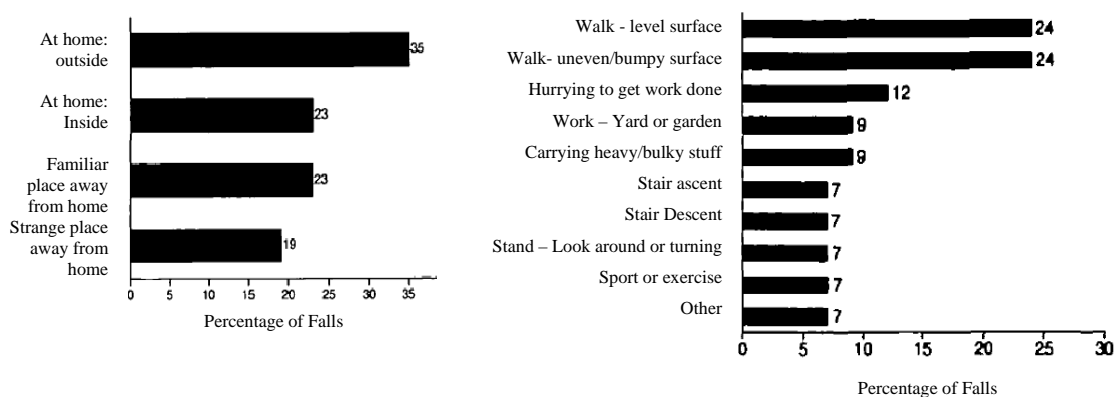


**Figure 2.1:** The occurrence of falls among the elderly, (Left) places where falls occur and (Right) the activities performed during falls (Berg et al., 1997).

These technologies are said to bring over a number of significant improvements into biomedical instrumentation realization which includes miniaturization, low power consumption, full integration of system and also low cost of production (Bryzek et al., 2006; Jovanov et al., 2005; Hierold,2003). Miniaturization is a great advantage as it means the devices or systems should require only small volume of space. With low power consumption, only small batteries might be needed as power supply, or maybe even energy scavenging can be enough to power them up, if not a combination of them. As full system integration on single silicon chip is also possible, the signal processing and computation can be performed on the same silicon piece with greatly improved overall system performance. Most interestingly, the low per-unit cost is what business and consumers are looking for in every product and have been an undeniable trend (Grace, 1991). In addition, technologically, it also offers numerous materials that not only excellent mechanically for sensing and actuation (Bryzek et al.,2006), they are also biologically compatible (Kotzar et al.,2002). Undoubtedly, these MEMS based devices are the promising tools for outdoor ambulatory measurement and monitoring (Aminian & Najafi, 2004). These new breed of health monitoring and diagnostic devices will enable the realization of a more technologically advanced patient and health monitoring system, similar to the one proposed recently in the literature as depicted in Figure 2.2 (Jovanov et al., 2005). More interestingly, biomedical application is considered as one of the key new frontiers of MEMS based device development in the future with the worth of billions of dollars (Ko, 2007; Kotzar et al.,2002).

In short, with the integration of elegant engineering, advanced instrumentation technology and continuous development in computing propels the art and science of human movement analysis beyond its basic description towards a more prominent role in surgery decision making, orthosis design, rehabilitation, ergonomics and sports (Curran, 2005).

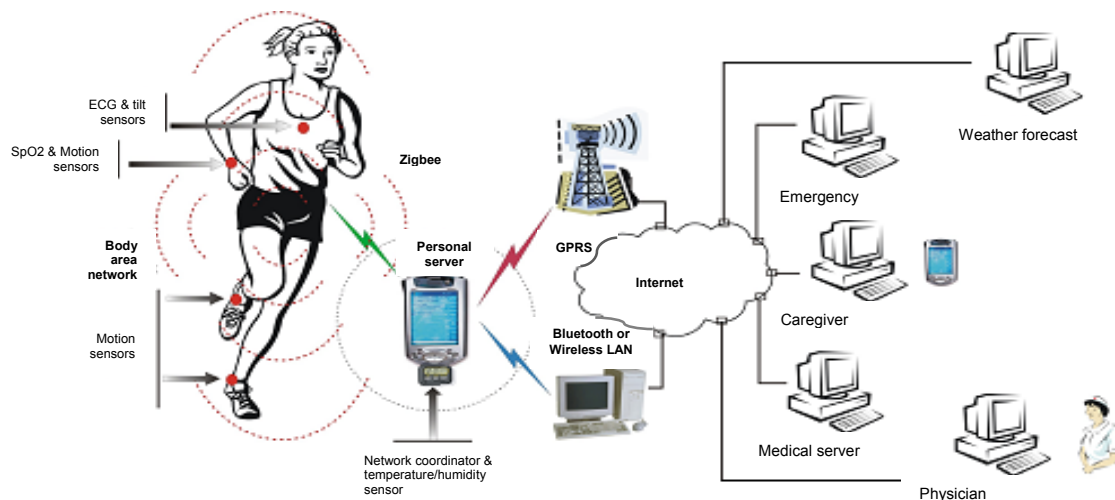


**Figure 2.2:** *The newly proposed patient monitoring system that includes human movement monitoring (Jovanov et al., 2005).*

## 2.2 The Foot Plantar Pressure Measurement

This section is divided into four subsections, namely Overview of Foot Plantar Pressure Measurement, In-Shoe Sensors, The Application Requirements and lastly the Section Summary. As the name implies, the first section discusses the general idea and the current implementation of foot plantar pressure measurement. The second section highlights the currently available in shoe sensors in the market and their weaknesses. The third subsection discusses the required characteristics or specifications of a high performance foot plantar pressure sensor. The last part summarizes the section.

### 2.2.1 Overview of Foot Plantar Pressure Applications

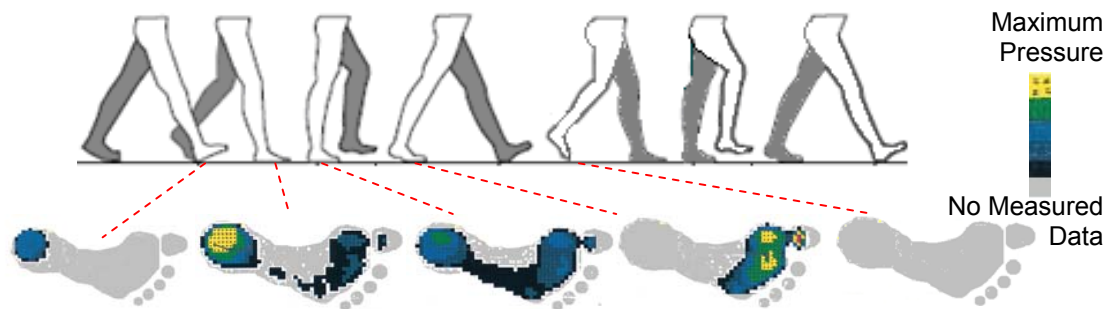


**Figure 2.3:** *Right foot plantar pressure changes during gait. The foot plantar pressure during stance phase is measured using many methods and tools.*

Figure 2.3 depicts foot plantar pressure pattern during gait. The foot is the key limb in human movement. Without foot, a person's mobility is significantly reduced. As a result, the activities of daily living are limited and quality of life is dropped. One way of determining the foot health is by examining the foot plantar pressure. In fact, the interface pressure between foot plantar surface and shoe soles is among the key parameters frequently measured in biomechanical research. This parameter is widely used in various applications, for example, screening for high risk diabetic foot ulceration, design of orthotics for pressure redistribution of diabetes mellitus and peripheral neuropathy patients, design of footwear (Mueller,1999), improvement of balance (Santarmou et al.,2006; Bamberg et al., 2006), sports injury prevention in athletes (Gefen, 2002). For example, foot ulceration due to diabetes related excessive foot plantar pressure is estimated to cause over \$1 billion per year worth of medical expenses in the United States alone (Mackey & Davis,2006). Diabetes is now considered an epidemic and the number of patients is expected to increase from 171 million in 2000 to 366 million in 2030 (Wild et al., 2004).

Apart from that, the growth of the percentage of world elderly population is also demanding foot plantar pressure measurement. The gait instability in the elderly community may lead to fall and fall itself costs billions of dollars annually (Best & Begg, 2006). Therefore, foot plantar pressure information is now used for improvement of balance among the elderly. In addition, foot ulcer among the elderly is also alarming and the risk is increased by Alzheimer's disease, congestive heart failure, chronic obstructive pulmonary disease, cerebral vascular accident, diabetes mellitus, deep venous thrombosis, hip fracture, hip surgery, limb paralysis, lower limb oedema, malignancy, malnutrition, osteoporosis, Parkinson's disease, rheumatoid arthritis, and urinary tract infections (Margolis et al., 2003). Another example is the foot deformities due to rheumatoid arthritis (RA). It is estimated that 2.1 million people will be diagnosed with RA in the United States in 2020 (Lawrence et al., 1998), and up to 97% of them exhibits foot related problems (Coughlin, 2003). It is therefore critical to ensure the availability of an accurate and efficient technique of measuring this pressure.

### **2.2.2 Common Foot Plantar Pressure Measurement Methods**

As the foot plantar pressure develops only during the stance phase of gait, it is helpful to see how the pressure changes in a chronological manner in relation to the body weight (BW) value. Figure 2.4 shows the relationship between stages of stance, the ground reaction force (GRF) changes and the path of centre of pressure (COP), which is represented by series of instantaneous centroids of GRF during walking (Rodgers, 1988). As mentioned earlier, balance can be assessed by the use of foot plantar force values and deriving the path of COP.

When the foot plantar touches the ground, the GRF that is exerted on the foot plantar is absorbed by the foot soft tissues. Pressure is defined as force per unit area. Therefore, the pressure values at any place under the foot plantar skin can be determined by the use of force sensing platform. As the sensing area is known, the sensed value is an average pressure for that area.

Traditionally, the foot plantar pressure measurement is performed in the specialized settings such as laboratories, hospitals or other clinical premises (Best & Begg, 2006). This includes various gait analysis systems such as foot plantar pressure platforms and foot plantar pressure mats. Due to their sizes and the number of equipments required, these measurement systems require specialized settings, as can be seen in Figure 2.4 . As the depicted pressure measuring systems measure barefoot pressure, the results are obviously not representing real dynamics of foot-shoe interactions. Due to these two obvious limitations, a more natural way of measuring pressure is highly required. For that reason, in-shoe pressure measurement devices are more suitable for use in natural living environment.

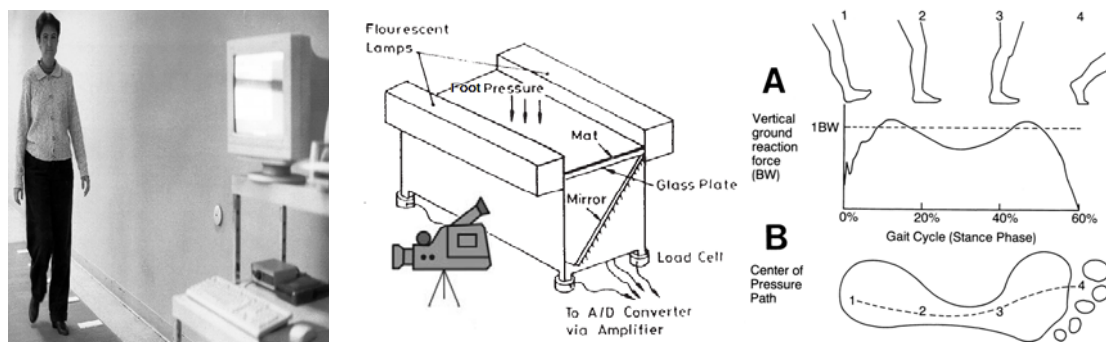


**Figure 2.4:** (Left) *The GaitRite mat (Bontrager, 1998)*, (Middle) *Optical Pedobarograph (Patil,Charanya & Prabhu,2002)*, (Right) *Graph of vertical GRF during stance phase of gait cycle and the path of the COP (Rodgers, 1988)*.

### 2.2.3 In-Shoe Sensors

Nowadays, a number of foot-shoe pressure sensors are available in the market and many are mentioned in (Urry,1999). These sensors are made of many different types of material, using different types of manufacturing technologies, made in different sizes, characterized by unique specifications and are operated based on various measurement techniques.

The materials include flexible polymeric layers, dielectrics and also electrical conductors. Some materials used in the sensor development limit the sensor's performance thus creating many issues such as hysteresis, repeatability, accuracy and creep as highlighted in (Lee et al.,2001; Wheeler et al., 2006). Slow response time is among the highlighted weaknesses too (Wheeler et al., 2006). In short, there are obviously many limitations of the currently available sensors in the market as discussed in detail and compiled in the literature (Hsiao, Guan & Weatherly, 2002). Many of the sensors are made as arrays of similarly sized sensor elements. Size of individual sensor affects the efficiency of the measurement system (Urry,1999). Basically, there are two categories of in-shoe sensors available, the research ones and the commercial ones. Examples of sensor integrated shoes are shown in Figure 2.5 which include GaitShoe (Morris, 2004; Bamberg et al, 2008), Smartshoe (Kong & Tomizuka, 2008) and another instrumented (Liedtke et al., 2007). There are also other related works (Abu-Faraj et al.,1997 ; Tanwar, Nguyen & Stergiou, 2007). Figure 2.6 presents some of the available instrumented insoles. In terms of measurement technique, commonly used techniques are resistive, capacitive,

ink-based and others. Each of the techniques offers unique sensitivity and other signal properties. Table 2.1 shows some of the portable in-shoe applicable sensors currently available in the market with their key characteristics. A number of companies produce and markets various brands of foot plantar pressure measurement devices too. Among them are FSA, Tekscan, Novel and Paromed. Unluckily, the currently available commercial sensors such as from FSA, Tekscan and Novel exhibit many performance limitations as they are made of sheets of polymer or elastomer. The resulting issues include repeatability, hysteresis, creep and non-linearity of the sensor output (Lee et al.,2001). In addition to the above weaknesses, some sensors (e.g., manufactured by Parotec) have a relatively large sensor size that may significantly underestimate the pressure, if the arguments in (Urry,1999) is considered. In fact, this view is supported by another report too (Sarah, Carol & Sharon, 1999).

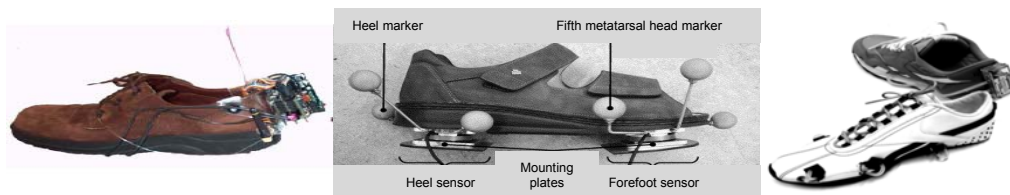


**Figure 2.5:** (Left) *The Gaitshoe proposed in MIT (Morris, 2004; Bamberg et al.,2008)*, (Middle) *The instrumented shoe for GRF determination (Liedtke et al., 2007)* and (Right) *SmartShoe (Kong & Tomizuka, 2008)*.

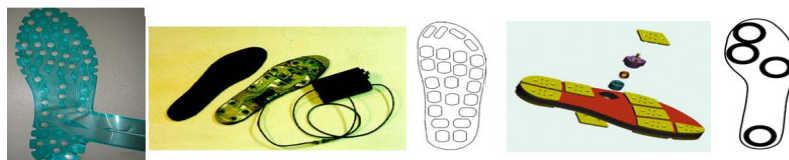


**Figure 2.6:** (Far Left) *Bio-foot ® insole with 64 piezoelectric pressure sensors (Martinez-Nova et al.,2007)*, (Middle Left) *the SIMS insole with 32 pressure sensors (Zhang et al.,2004)*, (Middle) *the Parotec insole layout (Chesnin, Selby-Silverstein & Besser, 2000)*, (Middle Right) *the instrumented shoe sole (Faivre et al., 2004)* and (Far Right) *the SmartShoe sole (Kong & Tomizuka, 2008)*.

TABLE 2.1: IN-SHOE PRESSURE SENSORS IN THE MARKET

	<b>FSA</b>	<b>Tekscan</b>	<b>Novel</b>	<b>Parotec</b>
<b>Sensor size</b>	7.94 mm X 12.7 mm ~1cm <sup>2</sup> (2mm thick) #	0.15 mm thick@, (4 sensors/cm)	(1.9 mm thick) **	~4cm <sup>2</sup> (hydrocell) +
<b>Number of sensors</b>	128 (in-shoe) #	4 sensors/cm, 960@ (insole)	99 (insole) **	24 (insole) ++
<b>Range (kPa)</b>	206 #	1034 @	600 to ~1300 **	~625 from bench testing (62.5Ncm <sup>-2</sup> ) ++
<b>Frequency (Hz)</b>	Not available	500 @	Not available	100 basic and 250 sport ++
<b>Hysteresis</b>	Not available	21% ≈	<7% **	0.05% at 20 Ncm <sup>-2</sup> ++
<b>Among obvious limitations</b>	Pressure range, sensing area	Pressure range, linearity, repeatability	Pressure range, linearity, repeatability	Sensing area

# (Vista Medical Ltd., n.d. ; Vuillerme et al., 2007 )

+ (Carol, Sarah &amp; Shannon, 1999)

++ (Chesnin, Selby-Silverstein &amp; Besser, 2000)

@ (Tekscan Inc., n.d.).

\*\* (Novel GmbH, n.d.).

≈ (Urry, 1999).

## 2.2.4 The Application Requirement

In performing any measurement, the measuring device must be optimized for that specific application, or else, the observed readings might possibly not accurate. Therefore, a very careful and detail analysis of the specific application requirement must be thoroughly considered before any measurement is performed. For foot plantar pressure measurement, the requirement includes surface area, thickness, pressure range, sensor placement, packaging, operating temperature, sampling frequency, hysteresis and sensitivity.

### 2.2.4.1 The Target Implementation Requirement

Nowadays, real-time and in-situ measurement of natural parameters is becoming an unavoidable trend. To catch-up with the fast changing and very demanding trend, also, as gait analysis is about measurement of uninterrupted real parameters, it is very important that the measurement is performed in the real environment. In fact, the effect of daily activities on our health is clearly understood (Urry,1999). This means the sensor should be very mobile, un-tethered, can be placed in the shoe sole and also can measure effectively in the targeted environment. The detailed requirements are as follows:

*i.) Very Mobile*

To make a sensor very mobile, it must be very light and of small overall size (Morris, 2004; Bamberg et al., 2008; Tanwar, Nguyen & Stergiou, 2007). There is no specific mass as suggested by the literature but a shoe mounted device of mass of 300 g or less is previously reported to be suitable.

*ii.) Limited cabling*

It should exhibit low power consumption so that energy from a small battery is sufficient to power it up for collecting and recording the required data for analysis. This is to ensure comfortable and natural gait is uninterrupted (Tanwar, Nguyen & Stergiou, 2007).

*iii.) Shoe Placement*

To place it in the shoe sole, the sensor system must be thin, flexible (Lee et al.,2001) and light (Morris, 2004). It is reported that a shoe

attachment of mass 300 g or less does not affect gait (Morris, 2004; Bamberg et al.,2008).

*iv.) Low cost*

The sensor needs to be low cost to make it affordable to more people (Tanwar, Nguyen & Stergiou, 2007).

#### **2.2.4.2 Common Gait Analysis and Plantar Pressure Sensor Requirements**

Any devices that are to be used in gait analysis must fulfill the requirements such as those explained in detail in (Lee et al.,2001; Urry,1999; Morris, 2004; Bamberg et al.,2008). The required key specifications for a pressure sensor in terms of sensor performance include linearity, hysteresis, temperature sensitivity, sensing size and pressure range.

*i.) Hysteresis*

Hysteresis can be determined by observing the output signal when the sensor is being loaded and unloaded. When the applied pressure is increased by loading the sensor or decreased by unloading of the sensor, two different responses may be observed as can be seen in Figure 2.7. It is related to the performance of the sensor as it indicates the accuracy of the readings. Sensors with low hysteresis are preferred.

*ii.) Linearity*

The response of the sensor to the applied pressure, if plotted, will show the linearity figure of merit. It is a measure of 'how straight the

plotted line is'. Linearity indicates how simple or complicated the signal processing circuitry will be. Highly linear response requires very simple signal processing circuitry, and vice versa. Therefore, it is highly preferred to have a linear pressure sensor. For example, pressure nonlinearity (PNL) is represented by PNL in Figure 2.8.

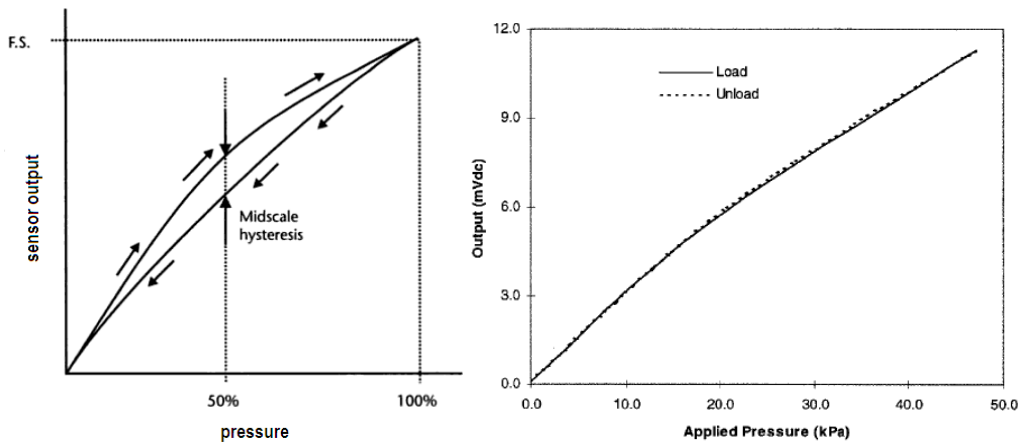


**Figure 2.7 :** (Left) Hysteresis cause by loading and unloading of a pressure sensor is usually measured at the 50% pressure range and is expressed as percentage of full-scale (FS)(Beeby et al.,2004, pg. 119). (Right) Negligible hysteresis of a MEMS based pressure sensor (Lee et al.,2001).

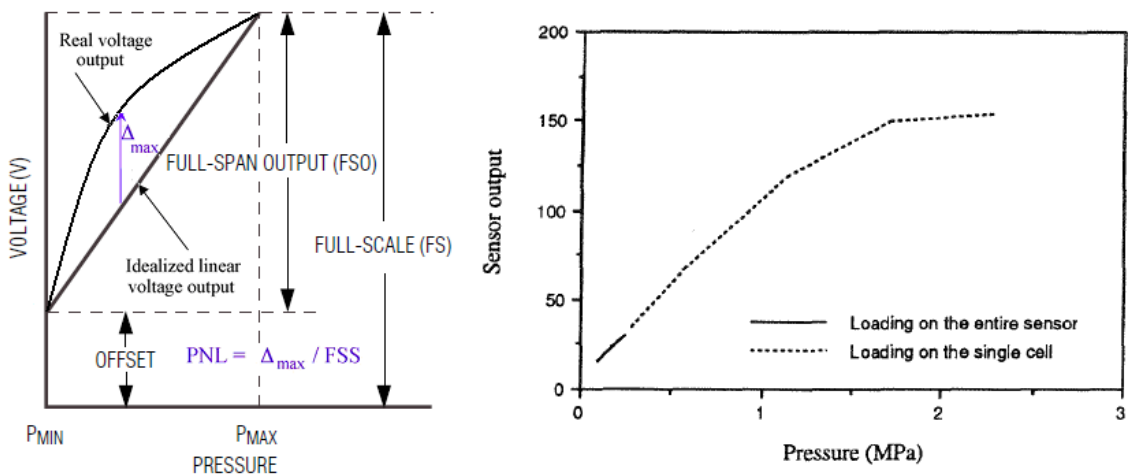


**Figure 2.8 :** (Left) The definition of nonlinearity (Chiou & Chen, 2008) and (Right) the nonlinearity of the F-scan insole (Luo, Berglund & An, 1998).

*iii.) Temperature Sensitivity*

Sensors may produce different pressure readings as the ambient temperature changes. This may be due to the materials that are parts of the sensor body, as different materials responses differently to temperature change. A sensor with low temperature sensitivity in the 20°C to 37°C range is preferred (Lee et al.,2001).

*iv.) Pressure Range*

The range of pressure that the sensor can measure is the key specification for a pressure sensor. As different application requires different operating pressure, an application specific sensor development is normally adopted in the design. Maximum pressure is the upper extreme limit that the pressure sensor can measure, and vice versa. As a note, burst pressure is the maximum pressure that the sensor can withstand before breakage, as opposed to maximum pressure value. Foot plantar pressure values of close to 1900 kPa is reported in the literature (Cavanagh, Ulbrecht & Caputo, 2000). In fact, extreme pressure of up to 3 MPa is previously reported (Urry,1999). One of the foot plantar pressure sensor design considers 3 MPa as the burst pressure value (Patel et al.,1989). For consideration, when a healthy normal person of 75 kg body weight is standing on the forefoot on one of his feet, if the pressure is evenly distributed, the interfacial pressure for every 31.2 mm<sup>2</sup> foot plantar area is close to 2.3 MPa (Luo, Berglund & An, 1998).

v.) *Sensing Area of the Sensor and Its Placement*

Size and placement of sensor are also critical. Figure 2.9 explains this. As large sized sensor may underestimate the peak pressure, it is suggested that sensor size of 5mm X 5mm should be used, whereas sensors smaller than this must be designed as array sensors. Based on the explanation in the literature, it is found that higher resolution measurement is considered more accurate (Urry,1999), Therefore, by arranging micro sized sensors as a dense array sensor, the resolution and accuracy can be better.

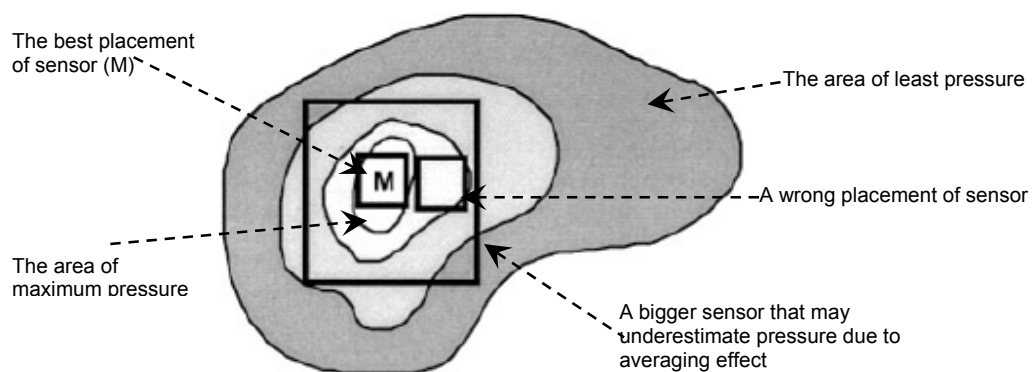


**Figure 2.9:** *The effect of sensor (squares) sizing and placement (Urry, 1999).*

vi.) *Operating Frequency*

In terms of frequency of operation, it is suggested that sensors that are capable of sampling at least 200 Hz must be designed to be useful in measuring pressure accurately of all the regions under foot (Urry,1999).

vii.) *Creep and Repeatability*

Creep is the deformation of material under elevated temperature and static stress. It directly relates to the time dependent permanent deformation of materials when subjected to a constant load or stress (Jia & Madou,2006), as in Figure 2.10. Low creep sensors are one of the key requirement in foot pressure measurement. Repeatability refers to the ability to produce reliable result even after long period of time (Lee et al.,2001). High cyclic loads may cause deformation or fatigue (Jia & Madou,2006). Repeatability problem can be eliminated if the sensor exhibits no creep or deformation over repetitive or high cyclic loads.

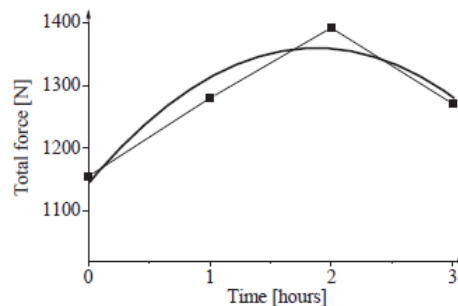


**Figure 2.10:** *Examples of erroneous readings due to sensor creep of the Pedar insoles (Arndt, 2003).*

### 2.2.4.3 Diabetic Requirement

In diabetic application, no reports highlight any required additional features other than pressure range. For this reason, the maximum pressure measurable is the only key determining factor. Pressure readings as high as 1900 kPa is reported in the literature (Cavanagh, Ulbrecht & Caputo, 2000). This is obviously a very

demanding requirement, as compared to the maximum pressure as obtained in normal people. The pressure ranges of the currently available sensors are very limited. As an example, most of the diabetic sufferers are off the scale as the upper measuring limit of the Emed SF device is approximately 1250 kPa only (Cavanagh, Ulbrecht & Caputo, 2000). Another worrying fact is that, another famous foot plantar pressure product, the F-scan insole, is reported to produce linear pressure reading only up to 1700 kPa (Luo, Berglund & An, 1998). In addition to the above mentioned requirements, a report on diabetic ulceration highlighted that patients measured with foot pressure of  $\sim 875$  kPa or  $87.5 \text{ Ncm}^{-2}$  may be susceptible to ulceration (Lavery et al., 2003). The development of foot plantar ulcer can be visualized as in the Figure 2.11. Many factors that lead to ulceration are shown. An example of foot ulceration is shown in Figure 2.12.

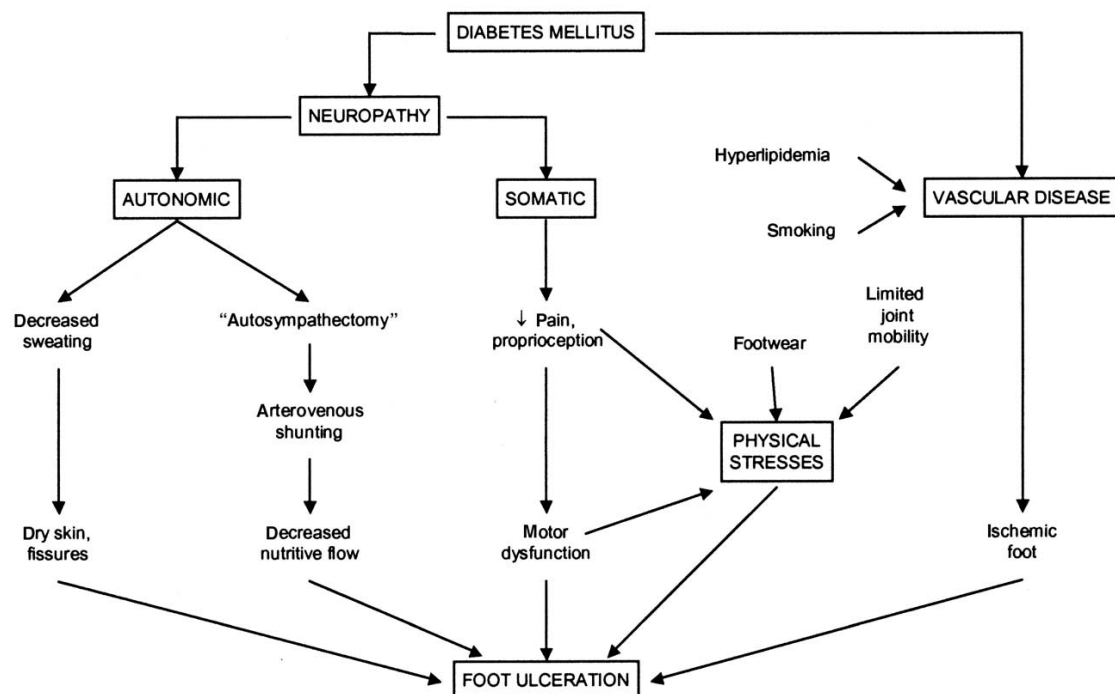


**Figure 2.11:** The factors that lead to foot ulceration among diabetics (Boulton, 2004).

In another report, it is stated that there are three mechanisms that account for the occurrence of ulceration generating pressure (van Schie, 2005). They are: increased duration of exposure to pressures, increased magnitude of pressures and also increased frequency or repetition of exposure to pressure. The relationships between pressure and plantar thickness and also pressure-repetition and injury are shown in Figure 2.13.

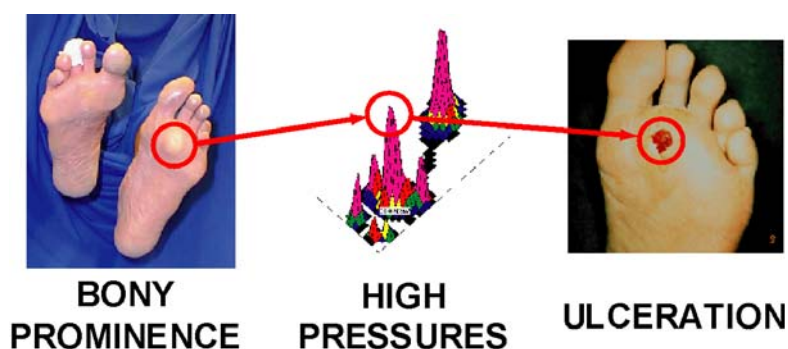


**Figure 2.12:** *Bony prominence, plantar pressure and foot ulcer (Erdemir et al.,2005).*

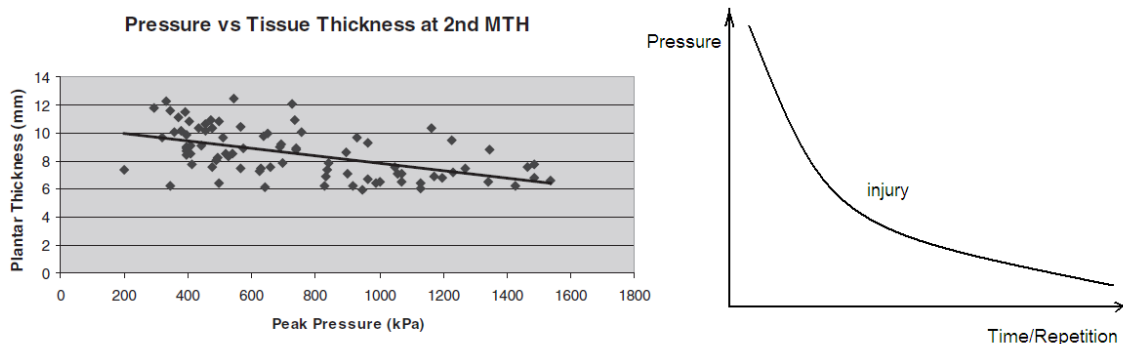


**Figure 2.13:** *Relationship between plantar thickness, pressure, time/repetition and plantar injury among the diabetes patients (van Schie, 2005).*

Another very important finding from the literature is the fact that for the measurement of foot plantar pressure among the diabetic sufferers, high resolution measurement is required (Urry, 1999).

### **2.2.5 Section Summary**

It is obvious that the need for lower cost in-shoe based pressure sensing devices due to the changing demographics of the world population. Unluckily, the currently available in-shoe sensors are not fully supporting the actual application due to their documented limitations such as limited pressure range, inappropriate sensing area size, hysteresis, linearity, creep and repeatability. Considering all the above requirements and the current limitations, it is obvious that there is a need for an improved design of in-shoe foot plantar pressure measurement device to satisfy the requirements. The great potentials of MEMS technology, which are already proven in other applications, should be explored to achieve this target.

### **2.3 The Foot Clearance Measurement**

This section is divided into four subsections, namely Overview of Foot Clearance Measurement, Shoe Integrated Foot Clearance Measurement, The Foot Clearance Measurement Requirements, Distance Measurement Techniques and lastly the Section Summary. The first subsection discusses the need for foot clearance measurement and its current implementation. The second subsection highlights the currently available shoe integrated foot clearance sensor and its weaknesses. The third subsection covers the discussion on the actual requirements. An introduction to three potentially MEMS compatible distance measurement techniques are given in the fourth subsection. The last part suggests the solution to the current limitations.

### 2.3.1 Overview of Foot Clearance Measurement

Gait related healthcare cost continues to increase globally partly due to the surge in occurrence of falls among the elderly population. As higher and higher percentage of the world population, including Australia, is made up of the elderly, more and more occurrence of falls is expected each year. In Australia alone, a total of about \$3 billion is reported to be spent as a result of the falls-related injuries in 1999 (Best & Begg, 2006). Among the important gait parameters that directly influence the risk of fall among the elderly is foot clearance. It is the spatial parameter of the foot during the swing phase of the gait cycle representing the distance of shoe sole above the ground. In a recent study involving the analysis of the tripping and falls risks among the elderly individuals during walking (Begg et al., 2007; Best & Begg, 2006; Winter, 1992), it is found that the movement of the foot during mid-swing phase is the most critical event that can initiate the possibility of trip-related fall. This highly important parameter is called minimum foot clearance (MFC). The pattern of foot clearance during gait is depicted in Figure 2.14 where MFC of below 5 cm and foot trajectory of up to about 17 cm is shown (Begg et al., 2007). Unluckily, the current practice in measuring foot clearance mostly requires laboratory settings with the use of reflective or active markers, as shown in Figure 2.14 and 2.15, one or more video cameras, thread-mill or suitable floor and computer software running on suitable computers (Best & Begg, 2006). This type of foot clearance measurement may not be representative of real life ADL based measurement in natural settings (Lai et al., 2008), such as at home or outdoor. Problems such as marker slippage

may also occur even during laboratory measurement (Best & Begg, 2006). A more advanced technique is by the use of accelerometers, however, the required calculation that involves double integration of acceleration data yields erratic results due to the effect of drift and errors (Aminian & Najafi, 2004; Lai et al., 2008). The sensing of MFC using accelerometer based measurement on surfaces that are uneven, bumpy or during stair descend or ascend is obviously problematic as it is not directly measuring clearance but rather calculate it using acceleration data.

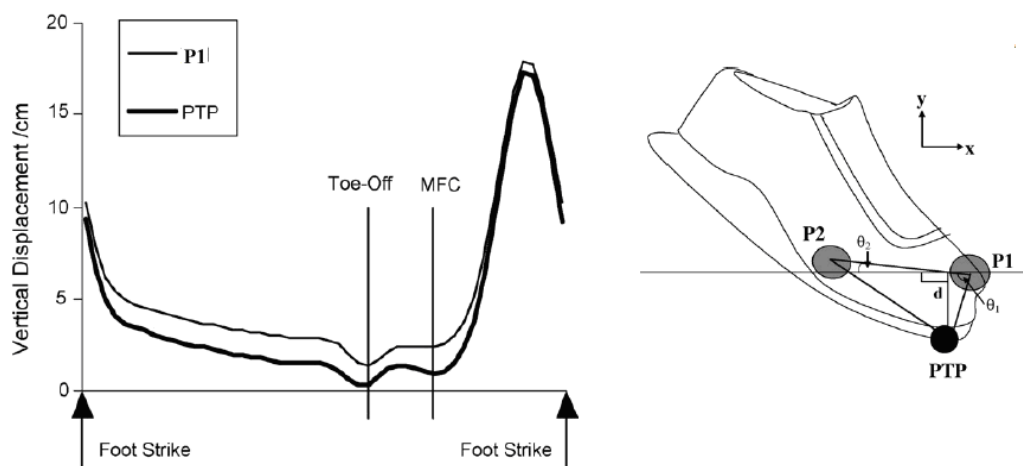


**Figure 2.14:** (Left) Foot trajectory during gait detailing the vertical displacement of foot for one gait cycle showing MFC during mid swing. (Right) The markers on the shoe (Begg et al., 2007).

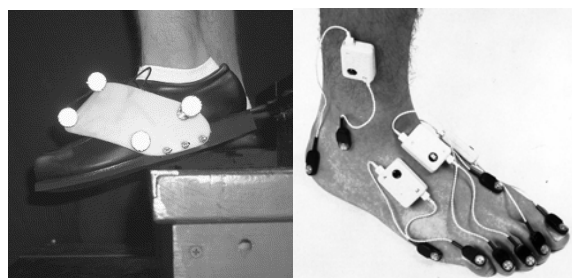


**Figure 2.15:** (Left) A foot clearance measurement during stair decent using passive markers (Hamel et al., 2005). (Right) Passive markers (Bontrager, 1998).

As current state-of-the-art instruments are mostly requiring exclusive research, clinical or rehabilitation laboratories settings, plus the fact that they are limited in simulating the real world activities of an individual (Best & Begg, 2006; Lai et al., 2008), an in-shoe approach is undoubtedly a better option of implementation.

### 2.3.2 Shoe Integrated Foot Clearance Measurement

At current, foot clearance measurement is performed in the laboratories or other clinical settings that use markers, video recorders and other bulky equipments. Only markers are placed on the shoes. Other calculation based measurements, but shoe integrated, are actually accelerometer based system (Aminian & Najafi, 2004; Lai et al., 2008). A shoe integrated direct foot clearance measurement system is the mostly unexplored topic in gait analysis and bio-mechanic research. So far, only one design of shoe integrated direct foot clearance measurement system is reported in the literature (Morris, 2004; Bamberg et.at,2008). It is as shown in Figure 2.16.



**Figure 2.16:** *Electric field distance sensor electrode attached to the Gaitshoe outsole for foot clearance measurement (Morris, 2004).*

Unluckily, the design exhibits several key drawbacks such as follows:

- low height or clearance measurement range of just up to 5 cm
- the requirement for minimum 5 layers of electrodes and insulators increases the total thickness of the insole
- the placement of the conductive electrodes beneath the shoe sole exposes the large area electrode to environmental elements such as water or other materials that may reduce the efficiency and repeatability of the system output

Due to the obvious limitations, newer systems based on more mobile technology are highly required. As discussed earlier, MEMS offer many great opportunities to close the gap between current requirements and their solutions. Possibility of developing MEMS based devices for clearance measurement is therefore considered. For that reason, various distance measurement techniques need to be analysed and their MEMS applicability needs to be identified. This requires that a better understanding of the requirements of this particular measurement is gained. The knowledge is then compared with the actual strengths and weaknesses of MEMS technology to formulate probably the most suitable and efficient implementation.

### **2.3.3 The Foot Clearance Measurement Requirement**

In order to enable a thorough and effective study, it is crucial that the measurement and monitoring devices are brought into the real environment where the activities are performed.

This means, the ability to be attached to the subject's own shoes is the key requirement. Other general requirements for gait analysis are that the device must not affect movement, un-tethered and capable of measuring parameters for both feet (Wahab, et al., 2007a, 2007b, 2008; Morris, 2004). This means that the device should be as small and as light as possible. A measurement range of close to 20 cm is preferable considering maximum toe clearance. However, our current laboratory research suggests minimum foot clearance during the swing phase of walking to be within 3 cm above the walking surface (Begg et al., 2007).

A portable system attached to the lower limb having a mass of 300 g or less has been reported to not affect the normal gait (Morris, 2004). For monolithic CMOS integration, only compatible materials and processes must be used. MEMS device normally fabricated of the size range between 1  $\mu\text{m}$  and 1 cm (Liu, 2006). Considering a 120 steps per minute of adult walking, the sampling rate of 75 Hz, or every 13.4 ms suits well for this application (Morris, 2004). It is reported that the toe clearance above walking surface or ground is minimum around 1.4-1.6 cm during normal walking and around 1.7-2.1 cm during fast walking. On the other hand, the maximum clearance during normal walking is around 5.7-6.9 cm while during fast walking, it is about 6.3-7.8 cm (Eible et al., 1991).

### **2.3.4 Distance Measurement Techniques**

#### **2.3.4.1 Capacitive Sensing (CS)**

Capacitive sensing devices are based on fringing effect (Chen & Luo, 1998; Luo, 1996). The referenced article includes many detailed analysis of the use of the

capacitive sensor for measurement of distance. If a target is placed in the nearby environment, it will influence the sensed capacitance between the dual plate sensor. Figure 2.17 exhibits the working principle where  $d$  is the distance,  $E_1$  and  $E_2$  are the electrodes,  $S$  the electrode separation and  $R_1$  and  $R_2$  are the radius of  $E_1$  and  $E_2$  respectively. The total capacitance sensed by both electrodes will vary with distance variation between the sensor and the target. The advantages of this technique are capability of sensing almost every material, high resolution, mature capacitive based processing and suitability for silicon micromachining. It was claimed that the sensor can detect up to few centimeters.

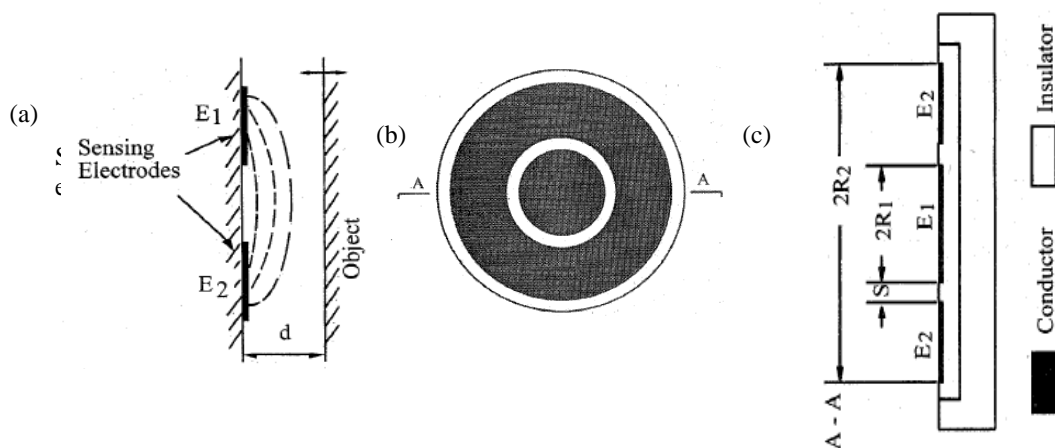


**Figure 2.17:** A capacitive sensor considered here (Luo, 1996), (a) the fringing capacitance, (b) the top view of the sensor, and (c) the side view.

#### 2.3.4.2 Electric Field Sensing (EFS)

The electric field sensing technique developed at the MIT Media Laboratory is proven to be successful in various applications such as gait analysis, entertainment, home automation, automotive etc. In general terms of sensing technique, this technique is basically another type of capacitive sensing. Interestingly, even though the Luo's article on capacitive sensing explains all

capacitive sensing types in clear manner, this unique technique is not mentioned at all in his paper. Therefore, this technique is a unique technique. More interestingly, there is a microchip produced by Motorola to support the technique (Morris, 2004), indirectly indicating its capability and commercial value. However, the chip is not fabricated with integrated sensor electrodes so as to enable more flexibility to application designers. Application may cover multitude of fields encompassing consumer electronics and automotive applications. An implementation of this technique in gait analysis is also reported in the literature (Morris, 2004; Bamberg et al., 2008). The working principle is shown in Figure 2.18.

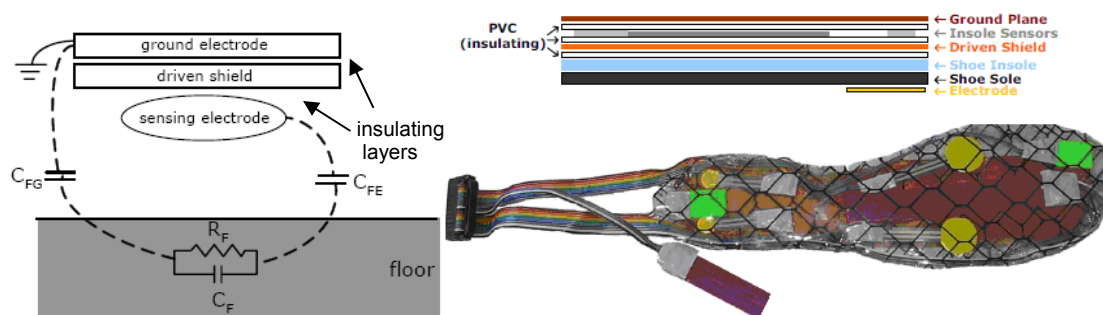


**Figure 2.18:** *The working principle of electric field sensing for height determination (Morris, 2004).*

This technique involves electric field sensing between two plates of a capacitor, namely the sensing plate or sensing electrode, and the ground plate or ground electrode. The sensing electrode is connected to the signal transmitting circuitry to generate an electrical field from a sinusoidal AC signal. On the other hand, the ground electrode is connected to the ground of the circuitry. The floor, as the target of which its distance from the sensing plate is to be measured, contributes to the change in capacitance reading. The change is sensed by the

sensing electrode. As the distance between the floor and sensing electrode is varied, the measured capacitance is also varied. Even though this technique is quite simple, it is highly capable of producing quality data for distance measurement. Despite its simplicity and high accuracy, its use is limited by the sensing electrode size requirement. This fact agrees well with the published design guideline (Sieh & Steffen, 2006).

#### 2.3.4.3 *Ultrasonic Sensing (US)*

Initially, ultrasound is used for tracking the seabed following the Titanic disaster in 1912 from which it then developed into what is called today as Sound Navigation and Ranging (SONAR) (Smith & Schoenwald, 1984). The application of ultrasound for distance measurement is basically the same with the underwater SONAR, the only difference is the speed of measurement. The speed of ultrasound in air is around  $345 \text{ ms}^{-1}$ . A number of system level and transducer level design for ultrasonic range measurement realization are reported in the literature such as in automotive and robotic applications (Carullo & Parvis, 2001; Song, Chen & Huang, 2004; Kajita & Tani, 1997). Examples of ultrasonic technique used are such as robotic obstacle avoidance (Bank, 2002), robot height above ground (Kajita & Tani, 1997), car reverse parking assistance (Turner & Austin, 2000), car height above road surface determination (Carullo & Parvis, 2001). It is also used in other assistive technology for the disabled such as assistance for the blind (Ando, 2003) and wheelchair (Simpson et al., 2004; Dutta & Fernie, 2005). Ultrasonic sensing is among the mostly used techniques in biomedical fields, inclusive of several laboratory measurements of gait (Wahab et

al., 2008; Begg et al., 2007; Sabatini & Colla, 1998; Weir & Childress, 1997; Abulaffio, Gelernter & Pillar, 1996). Other biomedical applications include therapy, 3D imaging and arterial diameter determination and other biomedical uses (Ling et al., 2007; Coleman et al., 2004). The interest in ultrasound technique is increasing due to its non-ionising or non-electromagnetic characteristic (Smith & Schoenwald, 1984). It is thus a safer method as compared to the ionising ones. Interestingly, it is said that the widespread use of ultrasound for distance measurement is sparked by the famous pocket-sized Polaroid camera developed in the late 1970s as shown in the Figure 2.19. This very portable technology relies on a 5 V battery to produce up to 400 V of pulse-train signal for the excitation of the camera's capacitive ultrasound transducer during auto-focus operation (MacIsaac & Hamaalinen, 2002). With this technology, the camera is able to sense an object 11 m away. Polaroid produces similar ultrasound ranging system for the market and thus enabled development of other ultrasound distance measurement systems for various applications by other companies. It is becoming the precursor for development of ultrasonic ranging systems (Smith & Schoenwald, 1984) and is then considered as one of the enabling technology of the 90's (Grace, 1991).



**Figure 2.19:** *The pocket sized Polaroid Sx-70 Sonar OneStep Land camera with the first mobile ultrasound distance measurement.*

It is also said that ultrasound signals are used as most of surfaces and objects are good reflectors of ultrasound (Turner & Austin, 2000). Two applications that successfully measure height above ground surface in real outdoor environments are as shown in the Figure 2.20. The figure proves that it is highly probable that ultrasound based system is capable of measuring foot clearance above ground. In addition, Figures 21 shows ultrasound application in the measurement of distance travelled during gait.

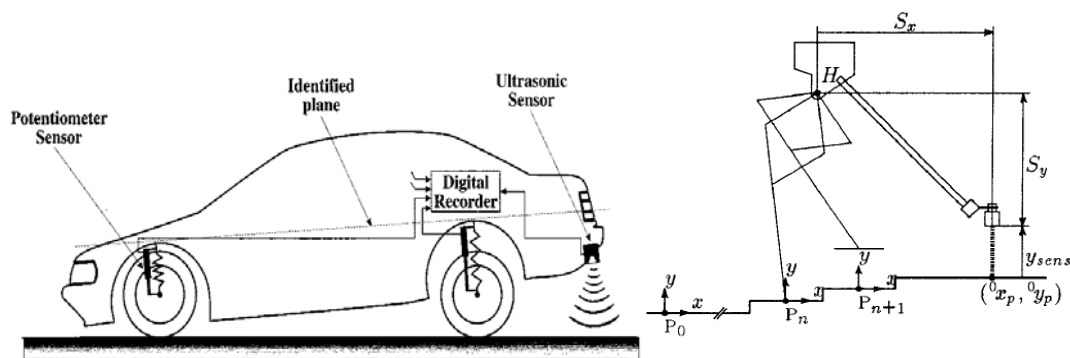


**Figure 2.20:** (Right) A 40 kHz Ultrasonic car height measurement for  $0^{\circ}\text{C}$ - $40^{\circ}\text{C}$  operating temperature, 0.1m-0.6m range and better than 1mm resolution (Carullo & Parvis, 2001), (Left) Ultrasonic sensor is used by robot to measure height ( $y_{sens}$ ) with resolution of 0.3 mm (Kajita & Tani, 1997).



**Figure 2.21:** A direct ultrasound ranging system in gait analysis (Weir, 1997).

Considering that ultrasound ranging systems are already bearing fruit in mobile ranging application, height above ground application and other gait analysis applications with good distance range, it is therefore a very promising

technology for the target application. Several techniques of distance measurement for ultrasound ranging system were proposed in the literature. These include time-of-flight ( $t_{of}$ ), continuous wave phase-shift method, and also combination of  $t_{of}$  and phase (Gueuning et al., 1997). For example, in using  $t_{of}$  method as shown in Figure 2.22, after an ultrasound signal is transmitted by a transmitting transducer (transmitter), the distance,  $l$ , can be calculated based on the time  $t$ , taken by the ultrasound echo to return to the receiver.

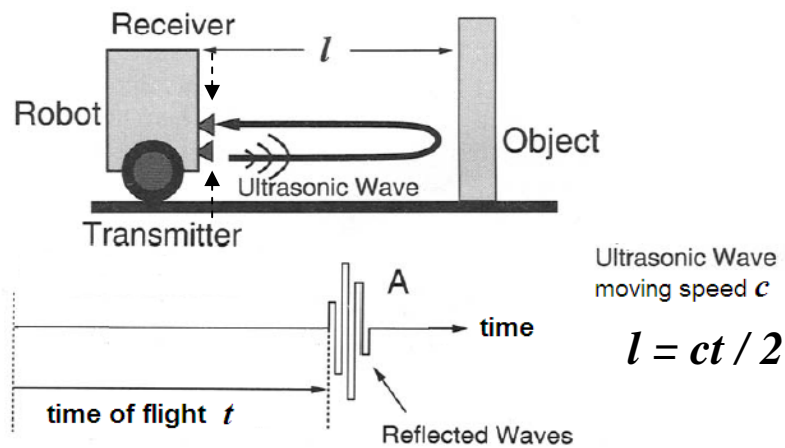


**Figure 2.22:** A simple time of flight concept (Ohya, Ohno & Yuta, 1996).

It is generally understood that increasing ultrasound frequency improves detection resolution (Coleman et al., 2004; Yano, Tone & Fukumoto, 1987) and reduces dead zone length (Bruinsma et al., 2006). However, the high attenuation in air which increases with frequency is a great challenge (Magori, 1994; Yano, Tone & Fukumoto, 1987). It is reported that 1 MHz signal can theoretically measure distance up to 20 cm (Yano, Tone & Fukumoto, 1987), while 2 MHz

signal can measure up to few centimeters (Noble et al.,1995). Recently, very high frequency ultrasonic transducers are reported for various high resolution biomedical applications. A more detail discussion on this technology is provided in the next section of the chapter.

### **2.3.5 Section Summary**

From the extensive reference in the literature, it is finally obvious that a direct measurement of foot clearance is highly needed. Unluckily, the instrumentation technology is not paying enough attention to this need for unknown reason. The need for it is increasing due to the changing global population demography. Therefore, this research is trying to close the obviously expanding gap. Three suitable distance measurement techniques are identified for consideration. Each of the technique has its own strength and weaknesses. Therefore, further analysis on the mentioned techniques is warranted. Next, consideration is going to take into account the limitation and strength of MEMS. In this regard, the applicability of the three techniques will again be evaluated after adaptation to suit MEMS technology requirement is made on them.

## **2.4 MEMS Technology for Gait Measurement**

MEMS technology offers a number of significant advantages in the instrumentation design and development field, as extensively discussed in many available literatures (Bryzek et al.,2006). Among the main reasons why MEMS technology is becoming the focus platform for instrumentation design nowadays

are its capability of incorporating CMOS processing circuits onto the same die. This capability significantly improves system performance. For further elaboration, this section is further divided into four categories, namely overview of MEMS material, overview of process technology, overview of MEMS pressure sensing and finally overview of MEMS ultrasonic actuation.

#### **2.4.1 Overview of MEMS Material**

Silicon as a mechanical material has long been studied and the material characteristics documentations for it have long been published. Silicon is a very promising material in micro-scale sized. These proven facts further boost the exploration activities around silicon based MEMS device realization. Key properties that are important in selection of MEMS materials are such as Yield Strength, Mechanical Hysteresis and Fatigue Failure. Yield Strength is the point when the material starts to exhibit plasticity, which means, it will elongate un-proportionally the same way a plastic material reacts under external force. This is true in many materials such as steel. In contrast, silicon is a perfect elastic material so that it exhibits a linear or proportional stress-strain relationship. In fact, it yields catastrophically when stress of more than its Yield (or Fracture) Strength figure is applied (Jia & Madou,2006). Silicon exhibits almost double the Yield Strength as compared to Steel. In addition, perfect elasticity also indicates another great advantage of silicon in sensing performance as it means no Mechanical Hysteresis. As silicon is not exhibiting deformation, it is very insensitive to fatigue and creep (Jia & Madou,2006). Therefore, in terms of

Mechanical Hysteresis and Fatigue Failure, silicon is showing significant advantages as none of both characteristic being exhibited (Bryzek et al.,2006). Comparing silicon with other MEMS materials, again silicon is reported to lead in pressure sensing performance as shown in Table 2.2.

TABLE 2.2: SILICON VS STEEL AND OTHER COMMON MEMS MATERIALS

Materials	Fracture Strength (MPa)
Silicon	7000 (Bryzek et al.,2006)
Silicon Nitride	1000 (Spearing, 2000)
Aluminium	300 (Spearing, 2000)
Silicon Carbide (Si-C)	2000 (Spearing, 2000)

#### 2.4.2 Overview of Fabrication Process Technology

In fabricating MEMS devices, two methodologies are involved, they are surface micromachining and bulk micromachining. Next, the discussion on these two different approaches is first given before they are being compared.

##### *i.) Bulk Micromachining*

This process technology is relatively mature. In bulk micromachining, the substrate material of typically single-crystal silicon is patterned and shaped into functional components. These include high-precision complex three-dimensional shapes, such as V-grooves, channels, pyramidal pits, membranes, vias and nozzles. The formations of structures are made possible by the use of predictable anisotropic etching. Therefore, in bulk micromachining, silicon substrate does not simply act as a rigid mechanical base, but rather the key functioning structure of the device itself (Judy, 2001).

Diaphragm or membrane based pressure sensors based on this technology using silicon are already reported beginning 1962. This technology involves the use of mostly pools of liquid chemicals as processing mechanism. Even though the set-up is quite similar to the one use in integrated circuit fabrication, the implementation is slightly different in the sense that high aspect ratio structures are involved for MEMS. Aspect ratio is a term representing the ratio between the height and width of a structure. Basically, in this process, the three dimensional device is formed by etching the bulk crystalline and non-crystalline layers. A fabrication facility that offers cheap multi-project wafer (MPW) for prototyping is the one owned by Infineon Technology SensoNor AS in Norway. This facility is famous for its Tyre Pressure Measurement System or TPMS based on bulk micromachining. The device can be made integrated with any Complementary Metal Oxide Semiconductor (CMOS) circuits by use of post-processing technique. Figure 2.23 gives a basic flow as an example.

*ii.) Surface Micromachining*

As opposed to the etching of the bulk, this process uses layer by layer deposition, patterning and etching starting from the substrate surface up to the topmost layer. An important step is the removal of sacrificial layers to make the realization of mechanical structures possible. Each layer has a typical height limit of between 1-100  $\mu\text{m}$  (Judy, 2001). Dry etching is used instead of the wet ones. This process technology is suitable for CMOS integration too. An example of a basic flow is given in Figure 2.23.

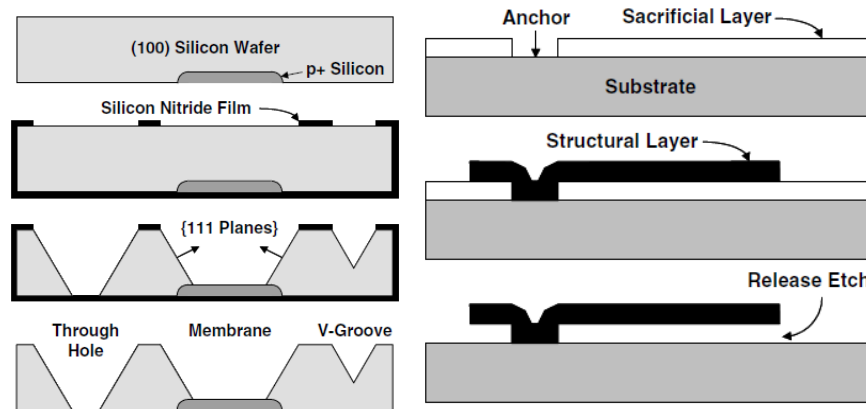


**Figure 2.23:** (Right) Surface micromachining and (Left) Bulk micromachining (Judy, 2001).

### iii.) Comparison of Process Technologies

Each of these two technologies has its own strength and weaknesses that can be compared. As an example and for the sake of simplicity, only two MPW process technologies are sampled and compared in Table 2.3. Also, the comparison only involves key figure of merits such as price, process technology and sensing techniques. Considering all factors, the Infineon's offer is more competitive.

TABLE 2.3 : MPW PROCESS TECHNOLOGY COMPARISON

<b>Particulars</b>	<b>Bulk Micromachining</b> (Infineon Technologies SensoNor AS, n.d.)	<b>Surface Micromachining</b> (MEMSCAP Inc., n.d.)
<b>Company name</b>	Infineon Technology SensoNor SA	Memscap Inc.
<b>Cost</b>	1000 € ≈ AUD 1900	US\$ 3700 ≈ AUD 5300
<b>Sensing Techniques</b>	Silicon diaphragm with piezoresistive elements	Thin film diaphragm with capacitive or piezoresistive sensing
<b>CMOS compatibility</b>	Yes	Yes

### 2.4.3 Overview of MEMS Pressure Sensing

Literature has shown that pressure sensing using MEMS is very widely used. To discuss this matter in a more organized way, this subsection is further divided into two parts, namely MEMS Pressure Sensing Techniques and MEMS Biomechanical Pressure Sensor Requirement.

#### 2.4.3.1 MEMS Pressure Sensing Techniques

There are a number of pressure sensing techniques currently implemented in pressure sensors. The most pervasive ones are those relying on membrane deflection. Two mostly used techniques are membrane based piezoresistive and capacitive ones (DeHennis & Chae, 2008). Pressure sensing are divided into several categories, namely absolute pressure, differential pressure or gage pressure. If the measured pressure is measured relative to vacuum, it is categorized as an absolute pressure one. This overview covers only the absolute pressure measurement technique. The size of pressure sensors varies and as a comparison, Figure 2.24 shows various pressure sensors besides a coin.

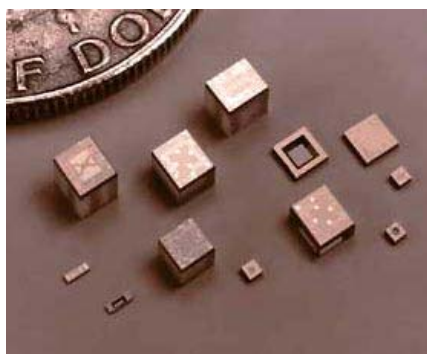


**Figure 2.24:** A coin and MEMS pressure sensors with the smallest one having dimensions of  $175 \times 700 \times 1000 \mu\text{m}^2$  (Judy, 2001).

i). *Capacitive Sensing*

Since 1970s, various designs of capacitive pressure sensor are reported in the literature. Two plates or electrodes separated by an insulating or dielectric layer are basically what it takes to create a capacitive sensing mechanism in MEMS. One of the electrode is normally attached to the deflectable insulator membrane while the other electrode is placed beneath a vacuum cavity, as shown in Figure 2.25. When pressure is applied on the membrane, it deflects according to the pressure magnitude. The increase in membrane deflection causes capacitance increase in a nonlinear way. Based on the literature, it is obvious that the capacitive pressure sensor output is nonlinear, if compared to the piezoresistive one (De Bruyker, 1998).

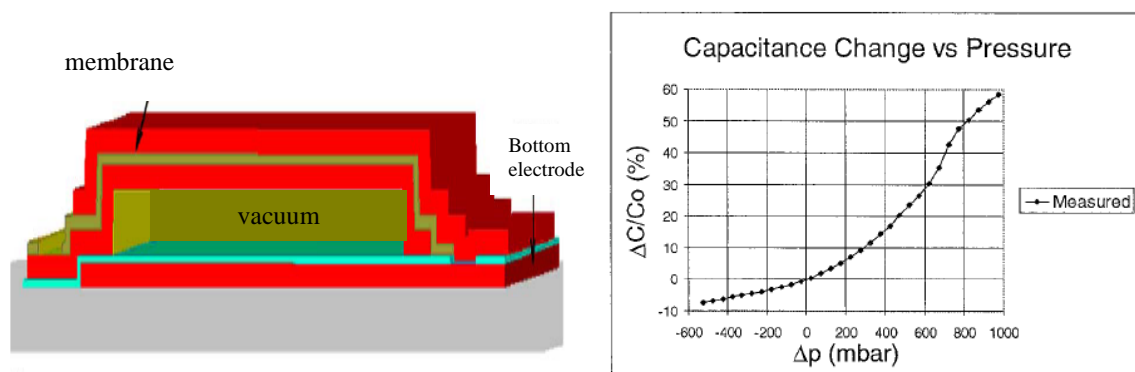


**Figure 2.25:** (Left) A tripple layered surface micromachined capacitive pressure sensor crosssection (Zhou, Huang & Qin, 2005). (Right) A non-linear capacitive pressure sensor output (De Bruyker, 1998).

ii) *Piezoresistive Sensing*

Smith (1954) reported the historic discovery of piezoresistive effect in doped semiconductor. Following the discovery, research and development on silicon based piezoresistive sensor initiates the era of MEMS technology (Bryzek et

al.,2006). This technique is therefore a very mature technique and sits among the earliest techniques identified as a promising technique in the realization of MEMS microscale devices (DeHennis & Chae, 2008). This technique requires the use of piezoresistors that are buried or infused into the deflectable membrane. The pressure is converted into a electrical signal by the use of resistance change phenomena due to the stress or strain of the piezoresistors. The stress or strain causes electrical signal fluctuations in two ways, one way is by structural deformation induced resistance variations, and the other way is by the quantum-physical phenomena induced resistivity variations (DeHennis & Chae, 2008). A wheatstone bridge structure based on two pairs of piezoresistors are commonly used. Due to their location on the membrane, the piezoresistors are named either longitudinal resistors or transversal resistors. Physically, a longitudinal one elongates as the membrane deflects, while the transversal one widens. Each pair makes up one branch of the bridge. In different branch of the bridge, the serial arrangement of longitudinal and transversal piezoresistors is alternated. As varying pressure is applied onto the membrane surface, the branch voltage of each of the branch differs accordingly and this differential voltage signal is then amplified as the sensor output signal. For absolute pressure measurement, the membrane is required to cover a vacuum cavity. Overall, piezoresistive based sensing is still the leading MEMS based technique in terms of commercial products domination (Bryzek et al.,2006). An example of a MEMS piezoresistive pressure sensor and an example of an output is shown in Figure 2.26. Piezoresistive pressure sensors are attracting attention of many insole designers

and biomechanical researchers lately. For an example, recently, an exoskeleton robot designed in the University of California, Berkeley, is reportedly to use MEMS piezoresistive pressure sensor array in its insole as shown in Figure 2.27 (Wheeler et al., 2006). Other examples that involve MEMS piezoresistive pressure sensors are such as the Parotec Insole and the Motorola MEMS based design (Chesnin, Selby-Silverstein & Besser, 2000; Lee et al., 2001).

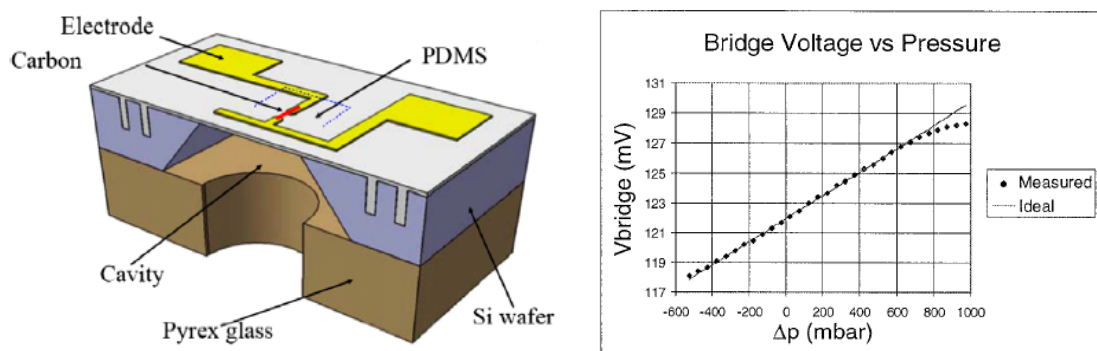


**Figure 2.26:** (Left) A cross-sectional view of a bulk micromachined piezoresistive pressure sensor using PDMS as membrane (Lee & Choi, 2008). (Right) A linear piezoresistive pressure sensor output (De Bruyker, 1998).

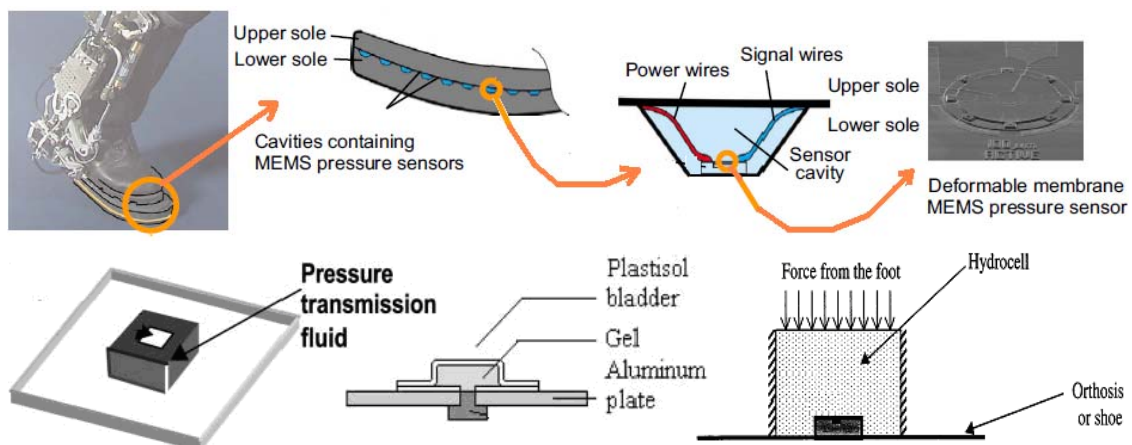


**Figure 2.27:** A Piezoresistive MEMS pressure sensor in action: (Top) the insole of a Robot at University California, Berkeley (Wheeler et al., 2006), (Bottom-Right) The Parotec hydrocell insole (Chesnin, Selby-Silverstein & Besser, 2000), and (Bottom-Left & Middle) a biomechanical pressure sensor (Lee et al., 2001).

### **2.4.3.2 MEMS Biomechanical Pressure Sensor Requirement**

For pressure measurement, MEMS based designs are undoubtedly the mostly used devices in the world today. It encompasses high technology applications inclusive of aerospace, biomedical, marine, manufacturing, robotics and automotive. In all of the mentioned applications, the exact placement of the sensors determines the specific set of requirements or specifications that the particular sensor should comply or exhibit. This includes sensor material selection, sensing technique or mechanism selection and also packaging material selection. Similarly, foot plantar pressure measurement sensor must be designed in a way that enables an effective operation of the sensor when it is placed at the target location. This requires that the materials to be used, especially the packaging materials, be biologically suitable and complies with the established standard, rules or regulation as published by the relevant authorities.

In a research presented in (Lee et al.,2001) an analysis of a new package design for a silicon based pressure sensor is explained. The proposed package is proven to enable silicon MEMS pressure sensor to be used in foot plantar pressure measurement efficiently. The sensing technique and mechanism should be suitable with the soft foot plantar tissue loading. As foot plantar measurement requires certain sensing mechanism size which is relatively small as compared to the overall plantar area, an array arrangement for sensors should be more suitable. Therefore, a less complex signal processing is another requirement. MEMS materials to be used in the sensor itself should offer good sensing capability in the confined space of shoe insole.

#### **2.4.4 Overview of Micromachined/MEMS Distance Measurement**

This subsection is divided into two parts, namely Micromachining/MEMS and Distance Sensing and MEMS Foot Clearance Sensing Requirement. The first part is more into the current achievement of MEMS distance sensing divided into the three identified techniques. The second part is dedicated to the requirement of MEMS foot clearance measurement.

##### **2.4.4.1 Micromachining/MEMS and Distance Sensing**

In evaluating suitability of an identified distance measurement method for MEMS realization, a closer look into each of the techniques is necessary. This includes the structural requirement, the operational requirement and the material requirement. Next, the discussion is divided into three segments corresponding to the three individual techniques.

###### *i) Capacitive Distance Measurement*

A silicon micromachined capacitive distance and proximity sensing devices have been reported in the literature (Luo, 1996). They are based on two electrodes sensing structure and use fringing capacitance effect to determine the range value. However, there is no mechanical part involved as they are basically planar structures without any physical movement. The electrodes are made of deposited chrome that is later patterned using photolithography and etch to form two separate electrodes. Due to its micromachining capability, it is therefore suitable for CMOS circuit integration. This is an innovative sensing technique where the

strength of MEMS technology is creatively used to reduce the device vertical dimension so that the originally required ground screen is no longer needed. A more recent attempt of realizing this technology in MEMS is reported to successfully measure distance of 10 cm (Lee, Chang & Yoon,2006). Figure 2.28 shows examples of electrode shapes and a cross-section of a more recent design. With already proven as MEMS capable, further analysis is warranted.

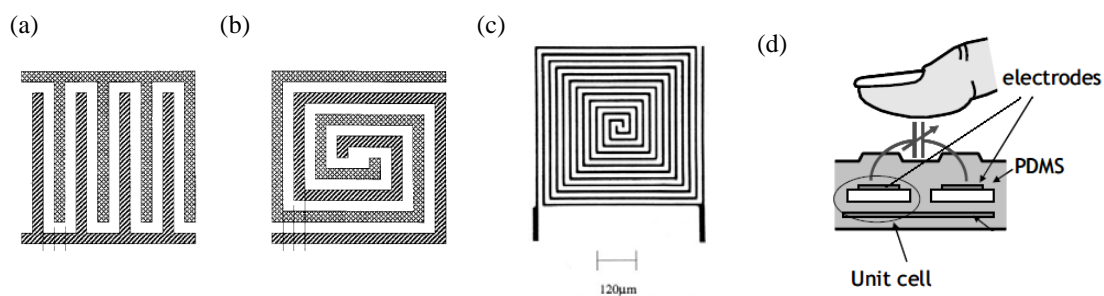


**Figure 2.28** : As reported in the referenced literature (Luo, 1996), (a) and (b) shows the top view of possible electrode arrangements, and (c) the top view of a micro-fabricated and tested sensor, (d) another MEMS capacitive proximity sensor able to measure up to 10 cm using the method similar to the Luo's design (Lee, Chang & Yoon,2006).

#### ii) Electric Field Distance Measurement

Another method of sensing distance is by use of electrical field. In general terms of sensing technique, this technique is basically another type of capacitive sensing, however, it is different in many ways within its implementation. It is unique in the sense that it uses three electrodes that are aligned like a sandwich, with insulators separating the adjacent electrodes. The arrangement of electrodes from top in sequence are Ground Electrode, Drive Electrode (Driven Shield) and Sensing Electrode, as shown in Figure 2.29. However, this technique has never been reported in micromachined form. From application point of view,

this technique has been reported as useful for foot clearance during gait application. In terms of MEMS capability, the sandwich structure of conductive and dielectric layers and their patterning is undoubtedly possible. One possible limitation is the electrode size which requires further analysis.

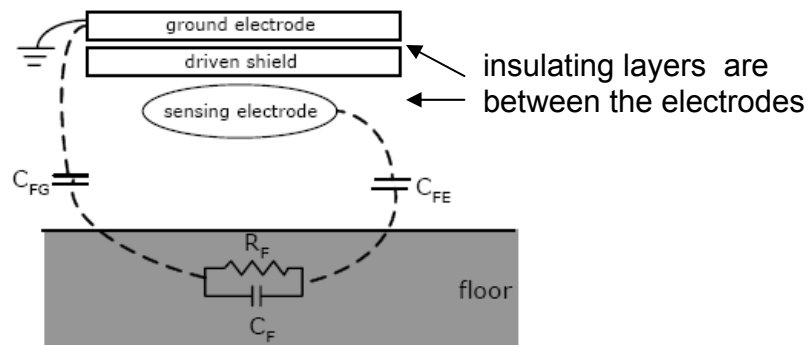


**Figure 2.29:** The working principle of electric field sensing for height determination using the effect of capacitance variation induced by height changes (Morris, 2004).

### iii) Ultrasound Distance Measurement

Another method that has been reported for distance sensing is ultrasound distance sensing. Literature has shown that MEMS technology is applicable for this technique. Ultrasound generation and sensing in MEMS is not a very new topic. However, the application is growing especially in the biomedical field. MEMS based ultrasound sensing is better in the sense that they are relatively smaller in size and tend to be cheaper (Kuratli & Huang, 1998).

So far, many researchers have reported MEMS based ultrasonic transducers which enable low cost integration with integrated circuit signal processing for various applications (Ergun, Yaralioglu & Khuri-Yakub, 2003; Kuratli & Huang, 2000; Jin, Ladabaum & Khuri-Yakub, 1998; Yaralioglu et al., 2003). It is claimed that the transmission and reception of 11 MHz ultrasound

signal in air is first demonstrated by CMUT technology (Spoliansky, Ladabaum & Khuri-Yakub, 1996). It is also claimed that CMUT is suitable for air application due to its low membrane acoustic impedance, which is attributed to by its thin nature. A number of MEMS based system level and transducer level design for ultrasonic range measurement realization are reported in the literature (Yamashita et al.,2005; Yaralioglu et al.,2003; Kuratli & Huang,2000). One of them is shown in Figure 2.30. However, they exhibit low resolution sensing and long dead-zone characteristic due to the relatively low ultrasound frequencies used. So far, all the reported MEMS ultrasonic ranging sensors are not optimized for the measurement of foot clearance. Ultrasound signal can be produced and sensed using a number of methods. This includes piezoelectric, magnetostrictive and capacitive (Ergun, Yaralioglu and Khuri-Yakub, 2003). Thermal actuation is also practiced (Kuratli & Huang,2000). Two mostly used ultrasound transduction technique using MEMS technology are piezoelectric and capacitive techniques.

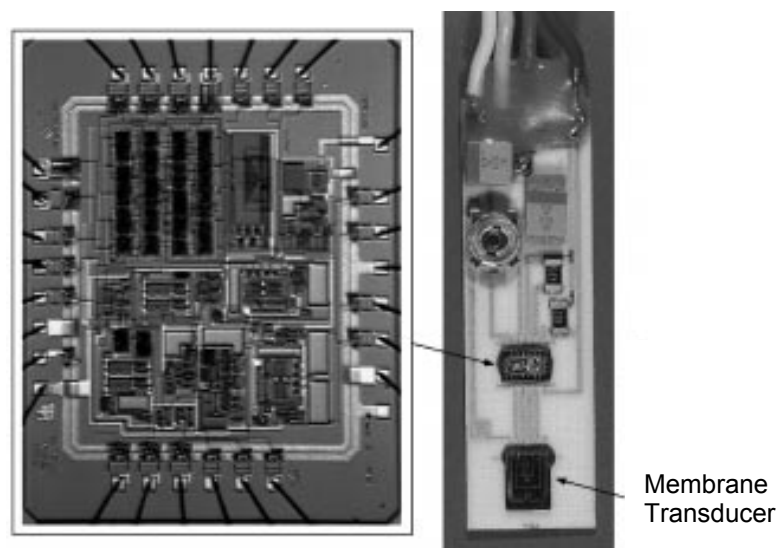


**Figure 2.30:** A complete system of ultrasound sensing system with a 1 mm<sup>2</sup> MEMS membrane (Kuratli & Huang,2000).



that capacitive micromachined ultrasonic transducer or CMUT is better for CMOS integration, leading to reduced costs through batch processing, improved scalability (Ergun, Yaralioglu & Khuri-Yakub,2003) and improved signal processing performance. As recent system development targets CMOS technology due to its superiority in almost all the aspects considered, capacitive sensing is obviously a better candidate. Previously, it is reported that the theoretical dynamic range that can be achieved by CMUT is 130 dB (Jin, Ladabaum & Khuri-Yakub,1998). In another report, an in air pitch-catch experiment using CMUT exhibits a 16dB SNR of ultrasonic signal detection (without averaging) (Yaralioglu et al.,2003). From this discussion, it is obvious that CMUT is a better technology for implementation.

*iv) Comparison of the three techniques*

Based on the published reports collected from the literature, the comparison of the three techniques is shown in the Table 2.4.

TABLE 2.4: COMPARISON OF THE THREE TECHNIQUES

<b>Key observation</b>	<b>Capacitive</b>	<b>Electric Field</b>	<b>Ultrasound</b>
<b>sensing range at the reported sensor size</b>	few hundred $\mu\text{m}$ @ few hundred $\mu\text{m}^2$ sized electrodes (Luo, 1996)	>5 cm @ 25 $\text{cm}^2$ (Morris, 2004)	11 cm @ 1 $\text{mm}^2$ diameter (Kuratli & Huang,2000)
<b>previously reported as MEMS/micromachined</b>	Yes (Luo, 1996)	No	Yes (Kuratli & Huang, 2000; Yaralioglu, 2003)
<b>ever used in foot clearance measurement</b>	No	Yes (Morris, 2004)	No

A method that offers more advantages in key aspects such as performance, signal processing, miniaturization, cost and manufacturability is obviously a better candidate and will be selected after further analysis.

#### 2.4.4.2 MEMS Foot Clearance Sensing Requirement

MEMS based devices are relatively small and thin as compared to shoe sole or outsole. Placement of MEMS distance sensor in the shoe sole should not interfere with the normal foot biomechanical activities. However, due to the fact that the foot is tilted during walking and other specific activities, it is required that sensing at both two ends of the shoe is performed. In literature, this is already implemented (Morris, 2004). For example, while walking, the foot plantar is normally not perfectly horizontal alignment with the pathway surface. In other possible occasion during gait, the toes need to be raised to avoid some obstacles. Therefore, inserting a pair of sensing or measuring units to the shoe is a better option. This is shown in the Figure 2.32.



**Figure 2.32 :** *A possible implementation using two points sensing.*

### **2.4.5 Section Summary**

The capability of current MEMS technology is discussed. In addition, the requirements of the named measurements are also explained. Considering the factors affecting the measurement and what MEMS can offer for its implementation, few points of action can be decided. For foot plantar pressure measurement, silicon piezoresistive technology is a better choice due to its simple processing circuitry requirement which makes array or matrix arrangement less complex and also due to its low processing price. For distance measurement, further analysis will be performed to ensure proper selection of sensing technique is made based on practicality of MEMS realization.

## **2.5 Chapter summary**

Following the trend in biomedical instrumentation, its actual requirement and the current status of technology achievement, undoubtedly, MEMS technology is the best platform to be adopted for the next generation gait analysis instrumentation. Considering the global phenomena of surging aging and diabetes mellitus affected citizens, the need for measurement systems that can effectively quantify foot plantar pressure and foot trajectory during activities of daily living is becoming very obvious. After long literature review about the state-of-the-art of such sensors, it is obvious that there is need for better sensors to satisfy the requirement of foot clearance measurement and foot plantar pressure measurement. For that reasons, the promising MEMS technology will be explored to design and possibly materialize the better sensors.

## Foot Clearance Sensor on Silicon

## CHAPTER

# 3

- 3.0 *List of Refereed Publications Produced*
- 3.1 *Chapter Overview*
- 3.2 *Selection and Analysis of Clearance Sensing Technique*
- 3.3 *Selection of Ultrasound MEMS Mechanism and Fabrication*
- 3.4 *Design Specification of CMUT*
- 3.5 *CMUT Mathematical Modeling*
- 3.6 *CMUT Process Modeling and Simulation*
- 3.7 *CMUT FEA Design Modeling and Simulation*
- 3.8 *Chapter Summary and Discussion*

### 3.0 List of Refereed Publications Produced From This Chapter

1. Wahab, Y, Zayegh, A., Begg, R.K. and Veljanovski, R., 2008. 'A model for the measurement of foot-to-ground clearance and potential realization of micro-electro-mechanical systems', **AMSE Journal: Modelling, Measurement and Control C**, vol. 69, no. 1, pp. 59-74. ISSN 12595977.
2. Wahab, Y, Zayegh, A., Begg, R.K. and Veljanovski, R., 2007. 'Analysis of foot to ground clearance measurement techniques for MEMS realization', in **Proceedings of the IEEE International Conference on Computer and Information Technology (ICCIT 2007)**, 27-29 December, Dhaka Bangladesh, pp. 413-417. ISBN 978-1-4244-1550-2.
3. Wahab, Y, Zayegh, A., Begg, R.K. and Veljanovski, R., 2007. 'CMUT For Human And Humanoid Locomotion Mesurement', in **Proceedings of Int. Con. on Robotics, Vision, Information and Signal Processing 2007**, Universiti Sains Malaysia, Penang, Malaysia, 28-30 November, pp. 359-364. ISBN 978-983-43178-1-2.

### 3.1 Chapter Overview

As discussed in the previous chapter, the monitoring of foot clearance during gait and while performing other related activities is crucial in preventing falls, especially among the fast growing elderly population. While the current conventional measurement devices that are in use are not capable of performing the task in an efficient way, a new instrument is obviously in dire need. To ensure that the foot clearance is measured effectively, the new device must fulfill these basic requirements which include small size, very light, unobtrusive, can be integrated with signal processing and memory and also very low power. For that reason, MEMS technology is the best platform for implementation as it exhibits all the required traits as mentioned. To achieve the target, this research explores the possibility of realizing such measurement using MEMS compatible foot clearance sensing technique. However, there are several questions that require answering and a number of milestones that need to be achieved for the real implementation to be successful. In this chapter, the actual work and its milestones, challenges and the chosen solutions are presented and discussed in detail.

In discussing and presenting the actual work on foot clearance measurement aspect, the chapter is divided into nine sections inclusive of this chapter overview. As their names imply, each of the section presents and discusses specifically the relevant aspects according to the given names, which are : List of Refereed Publications Produced, Selection and Analysis of Clearance Sensing Technique, Selection of Ultrasound Fabrication and Mechanism, Design Specification of CMUT, CMUT Mathematical Modeling,

CMUT Process Modeling and Simulation, CMUT FEA Modeling and Testing and lastly Chapter Summary and Discussion.

The list of refereed publications resulting from this work is as listed in the previous section. One of the main work of the research, which is the selection of the most suitable and practical distance sensing technique for MEMS realization is covered in the third section. After the selection process is made as explained in that section, the work then concentrated on ultrasound based sensing and its MEMS realization, as covered in the rest of the chapter.

### **3.2 Selection and Analysis of Clearance Sensing Technique**

This section is divided into four subsections. The first three subsections discusses the analysis performed on the three identified distance measurement techniques that may be suitable for foot clearance sensing using MEMS technology. In the last subsection, the comparison of the three techniques to select the most suitable technique for development is presented and it ends with the summary of the section.

Considering many factors, the mandatory distance range to be measured is 6 cm. Even though the minimum foot clearance in normal gait is in the range of 0 to 5 cm, the minimum foot clearance above stairs is 6 cm (Hamel et al.,2005). In avoiding obstacles, it is even reported that clearance of maximum 6.4 cm is required for objects 2.5 cm of height (Ashton-Miller, 1999). Another important consideration is that maximum foot clearance during normal gait is around 17 cm. In performing some other activities such as stair ascending or exercise such as jumping, higher vertical clearance is normal. In

a study about raised surface negotiation during gait, it is reported that for a raised surface of 15 cm, about 11 cm of clearance is observed, and this characteristic is similar to stepping over an obstacle (Begg & Sparrow, 2000). This means that the measurement of foot clearance of close to 30 cm will enable application in more possible activities. For that reason, this work adopts mandatory measurement of 6 cm, with provision of higher range of up to 30 cm, if the performed analysis shows it is technologically possible. The required resolution is high, at least 1 mm. As can be seen in the histogram of MFC during normal gait shown in Figure 3.1, the MFC values varies a lot with possibility of differences in the sub-millimeter range.

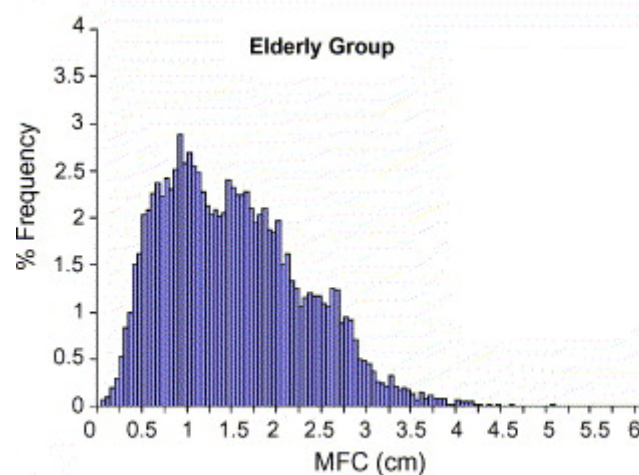


**Figure 3.1:** *The distribution of MFC in one report (Begg et al., 2007)*

The sizing requirement is another key requirement as the maximum size is limited by MEMS size of 1 cm. As the sensing technique is evaluated for the target distance range, the size of its sensing mechanism should comply with this MEMS sizing requirement. Another key consideration is the material required for realization. If the materials required are not suitable for MEMS realization, or not available in any MEMS technology vendor, the

technique is surely not suitable for MEMS realization. However, material substitution with those of MEMS compatible types is always considered too.

As mentioned in Chapter 2 section 2.3.4, the main distance measurement techniques are Capacitive Sensing, Electric Field Sensing and Ultrasound Sensing. In this work, these techniques are critically analyzed through series of extensive simulations on the three techniques. The key investigation is the relationship between the sensed signal strength, measurable distance, sensor size and linearity. Other aspects such as resolution and material requirement are mostly obtained from literature. In short, the key criteria of the selection process are the range of detection, the sizing requirement, the possible resolution, and the sensing material necessary for realization.

### 3.2.1 Analysis of Capacitive Sensing

Based on the Luo's paper (Luo, 1996), the total capacitance sensed by both plates separated by a dielectric will vary with distance variation between the sensor and the target. This is a high resolution measurement technique. The governing equation for fringing capacitance,  $C_f$  as explained in the literature can be determined using the Equation (1).

$$C_f = 4R_1\epsilon_o\epsilon_r(\rho_1 + \rho_s) \sum_{n=1}^{\infty} \frac{I_1(n\rho_1)}{I_1(n\rho_2)} \times \{I_1(n\rho_2)K_1[n(\rho_1 + \rho_s)] - I_1[n(\rho_1 + \rho_s)]K_1(n\rho_2)\} \quad (1)$$

where  $\rho_1$ ,  $\rho_2$  and  $\rho_s$  are  $\rho_1 = \frac{\pi R_1}{d}$ ,  $\rho_2 = \frac{\pi R_2}{d}$  and  $\rho_s = \frac{\pi S}{d}$ . Here,  $\epsilon_o$  is  $8.854E^{-12}$

and  $\epsilon_r$  is the relative permittivity of air,  $I_1$  and  $K_1$  are the modified Bessel

functions of the first and the second kind and  $R_1$ ,  $R_2$  and  $S$  are defined in Figure 3.2. For reasonable time and accuracy, summation variable,  $n$  is taken as 10, similar to the referenced work. Based on the simulation, it is found that the signal is very weak if small sized sensors are used. Figure 3.3 shows two simulation results using Matlab for determining the relationship between fringing capacitance reading, distance at two different set of sensor dimension values of  $R_1$ ,  $R_2$  and  $S$ . As shown in Figure 3.3, the size of the sensor needs to be in the centimeter range to obtain good sensing coverage up to 30 cm distance.

For measurement of about 20 cm range,  $R_2$  of about 5 cm should be used, while for 30 cm,  $R_2$  should be around 50 cm. An important observation from the plots is that, increasing  $R_2$  causes the measurable range to increase but with lower sensitivity, and vice versa. Even though the sensitivity is controllable by use of different plate separation sizes,  $S$ , the required size for distance measurement of 30 cm is at least about 50 cm radius which would not be suitable for MEMS realization. Similarly, for measurement of up to 20 cm, a 5 cm radius sensor is required, which is again far beyond MEMS maximum size.

A further study with consideration of MEMS sensor size limit of radius 1 cm is also performed. In executing this task, since the maximum size is determined by  $R_2$ , the radius  $R_2$  is made constant with value of 1 cm. As the sensing performance is increased by manipulating the values of  $R_1$  and separation  $S$ , these two parameters are swept across all possible values within the constraint of  $R_2$  size. Based on the previous results, it is proven that changing the values of the electrode separation  $S$  and radius of the inner

electrode  $R_1$  while  $R_2$  is being fixed is a good way to determine the maximum distance that the sensor can sense.

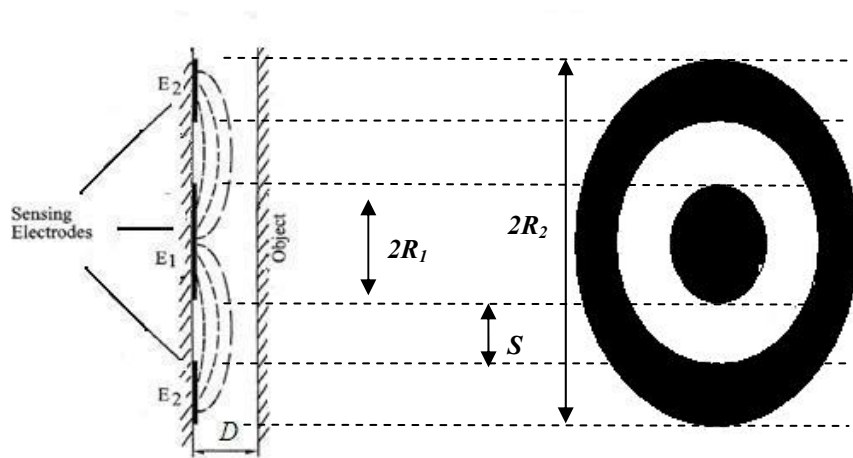


**Figure 3.2:** Capacitive Sensor showing the fringing effect, the top view of the sensor is on the right while the side view is on the left. (Luo, 1996)

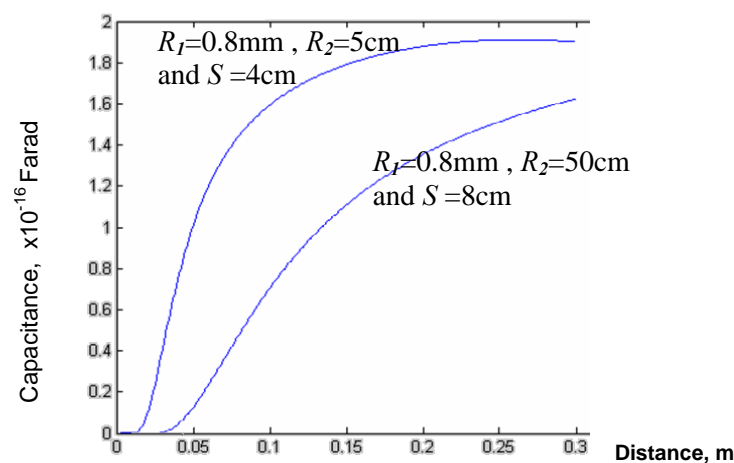


**Figure 3.3:** Two of the best Matlab simulation result for the capacitive sensor.

Table 3.1 depicts values of maximum range detectable with a 1 cm radius sensor.  $C_{max}$  and  $D_{max}$  are the maximum values for capacitance and distance respectively. As expected, by manipulating the values of  $S$  and  $R_1$ , the maximum distance measurable can be increased, as shown in Table 3.1. The increase in electrode separation increases the measurable distance significantly initially. Afterwards, further increase of  $S$  shows very small influence on measurable distance. Even though MEMS offer capability of

producing micrometer sized features, this measurable distance ‘saturation’ characteristic indicates less usefulness of miniaturization towards that range. Obviously however, the capacitance values are significantly very small, which may raise the question of sensing performance such as noise immunity and system signal capturing capability for such a small signal. At  $R_2$  of 1 cm, the sensor area is about 3.14 cm, this is already unjustified for MEMS, but yet the maximum distance is still below the target range.

**TABLE 3.1:** SIMULATION RESULTS FOR  $R_2 = 1$  cm

$R_1$ (m)	$S$ (m)	$C_{max}$ (F)	$D_{max}$ (cm)
8.90E-03	1.00E-03	2.40E-14	2.0
4.90E-03	4.90E-03	5.00E-15	4.8
1.00E-04	8.00E-03	1.55E-17	5.0
1.00E-03	8.50E-03	4.30E-16	5.0
1.00E-04	9.80E-03	8.70E-18	5.1
2.00E-04	9.70E-03	3.50E-18	5.1
3.00E-04	9.60E-03	7.80E-18	5.1
4.00E-04	9.50E-03	1.40E-17	5.2

Overall, it can be clearly seen that the smaller the overall size of the sensor, the smaller the measurable distance is. Again, as can be seen, the application of this type of capacitive sensing is limited due to MEMS sizing limitation. Even though the linearity is good, the range and distance figure of merit is very weak. In term of material requirement, there are many candidate materials offered by MEMS technology and is not at all a problem.

### 3.2.2 Analysis of Electric Field Sensing

Another capacitive sensing that uses different structure is referred to as electric field sensing, following the original report (Morris, 2004; Stewart, n.d.; Sieh & Stefen, 2006). Figure 3.4 shows this high resolution technique in action. One unique characteristic of this technique is the use of driven electrode to help boost sensing performance. Figure 3.5 shows the effect of driven electrode to the sensor performance. Two alternating signals are used, a 5 Vpp 120 kHz sensing electrode signal and its buffered one for the driven electrode. During sensor operation, the driven electrode isolates the sensing electrode from the metal parts such as the ground electrode so that no inter-electrode coupling occurs and that the field is much stronger. As shown in the Figure 3.5, with the use of the driven electrode, the sensing signal, or in another word, the electric field, is more focused towards the target when the driven electrode is placed between the sensing electrode and the ground electrode. Using this technique, the distance between shoe sole and the ground/floor is directly affecting the total of the capacitances between the sensing electrode and ground electrode. This is attributed to the varying capacitance between the floor and the ground ( $C_{FG}$ ) and capacitance between the floor and the sensing electrode ( $C_{FE}$ ). According to the basic capacitor equation (2), using a fixed sensing area size, the total capacitance is inversely proportional to the distance between the sensing electrode and the ground electrode due to fringe capacitance effect. Even though both electrodes are separated by a fixed distance in the shoe, there is no direct path for capacitance between them as the driven electrode blocks this from

happening. Therefore, the capacitance between the sensing and ground electrodes is inversely proportional only to the foot clearance from ground/floor by means of fringing capacitance path outside of the shoe.

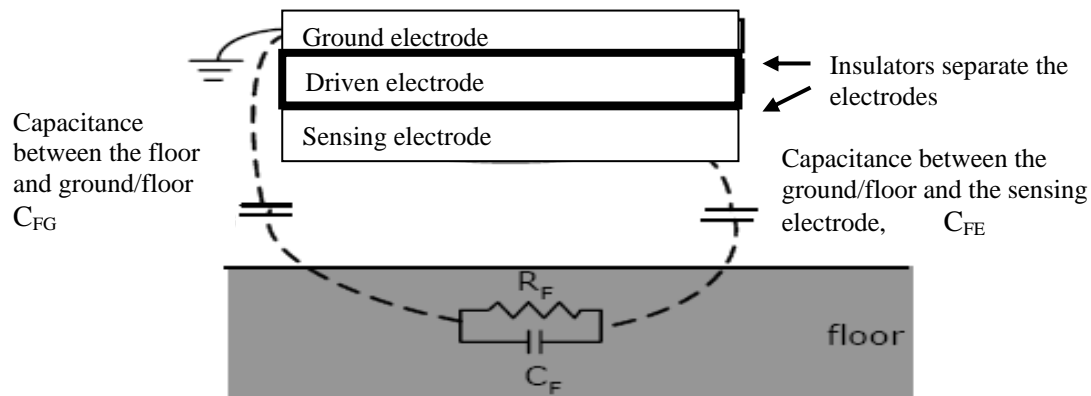


**Figure 3.4:** The working principle of electric field sensing for height determination using the effect of capacitance variation induced by height changes (Morris, 2004, p. 81).

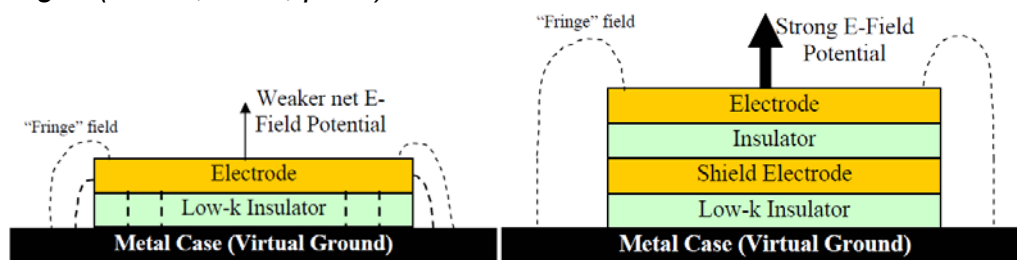


**Figure 3.5:** The working principle of E-field focusing using Shield Electrode (Driven Electrode), (Left) without Driven Electrode and (Right) with the Driven Electrode.

The use of the general equation for capacitance is already sufficient in determining the sizes required for the electrodes. Consider  $\epsilon_0$  as the permittivity of free space,  $\epsilon_r$  is the relative permittivity of air, the measurement reading of capacitance value,  $C$ , with distance,  $D$  and electrode size,  $A$ , is governed by the relationship shown in equation (2) (Freescale, 2006). Considering a maximum distance and sensor size, the simulation produced a graphical representation of the relationship between capacitance values, electrode sizes and the corresponding distances as shown in Figure 3.6.

$$C = \frac{\epsilon_o \epsilon_r A}{D} \dots \quad (2)$$

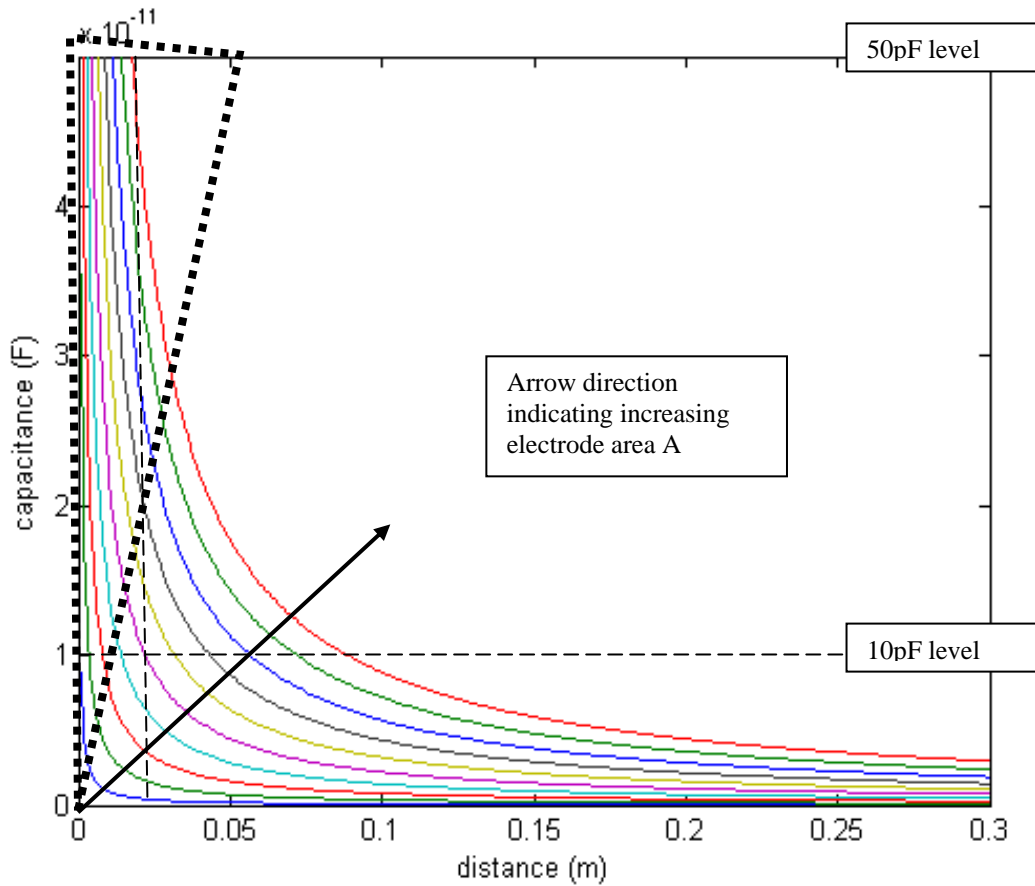


**Figure 3.6.** The Matlab simulation result for electrode area  $A$  from  $1 \text{ mm}^2$  to  $1 \text{ cm}^2$ .

If sensitivity is simply defined by the rate of change of capacitance to distance, which can be represented by the slope of the curves in Figure 3.6, the included triangle can be a helpful guide to determine the most suitable sensor size and the corresponding measurable distance.

Considering the high sensitivity zone, the larger the electrode area, the better the measurable range is. Unluckily, all the outputs regardless of electrode size are very non-linear. This is most probably why a special dedicated signal processing circuitry is required, e.g in-built the Motorola/Freescale MC33794 and MC34940 (Freescale, 2006).

Depending on the signal detection performance, the range may also be limited. For example, by referring to Figure 3.6, considering a close to linear capacitance to distance relationship, a  $1 \text{ cm}^2$  electrode can measure distance of up to around 2 cm only. A brief design guideline on this technique suggests that an electrode size of about  $1 \text{ ft}^2$  ( $\sim 930 \text{ cm}^2$ ) is needed to detect a target 12 inches ( $\sim 30 \text{ cm}$ ) away (Osoinach, 2008; Sieh & Steffen, 2006). Another key drawback of this technique is the limited capacitance range that can be detected which is between 0 to 100 pF, but for a near linear output, the range is between 10 to 100 pF (Zhao et al., 2006). In addition, DeLong & Booth (2004) suggested that for optimum system performance, capacitance range of within 50 pF to 75 pF range only should be used. As shown in Figure 3.6, the theoretical capacitance is barely within the pico-Farad range for distances more than  $\sim 8 \text{ cm}$ . If optimum system performance is a key requirement, the measurable distance will fall to below  $\sim 2 \text{ cm}$  for a  $1 \text{ cm}^2$  electrode. Due to this performance weakness, the Motorola/Freescale chip is no longer suitable, thus a totally new design of signal processing circuitry is becoming a necessity. In term of resolution, it is proven that resolution as high as 0.1 pF is achievable by using a 10-bit analog to digital converter (Zhao et al., 2006).

In short, to obtain a sensor based on this technique that is capable of offering good range to satisfy the basic gait requirement within  $1 \text{ cm}^2$  is not possible. Even though it is a high resolution technique, the highly non-linear output and the need for a new specialized processing circuitry are also among the main concerns. However, in terms of MEMS fabrication, the required sandwich structure is not a problem to materialize.

### 3.2.3 Analysis of Ultrasound Sensing

Assuming a time-of-flight (TOF) technique which is the commonly used technique. The governing equation of speed, distance and time is a linear relationship in equation (3). Linearity is an important advantage as it simplifies the signal processing complexity.

$$t_{of} = \frac{2D}{v_s} \quad (3)$$

The actual distance that the ultrasound signal travels is equivalent to double of the separation or clearance between the transducer and the floor as shown in Figure 3.7. It is as if the receiving transducer/sensor receives the signal from a virtual transmitter located at a distance double the receiver to floor distance (Massa, 1999; Bilgin, 2003). So, the actual distance to be considered is twice the shoe outsole and ground/floor clearance.

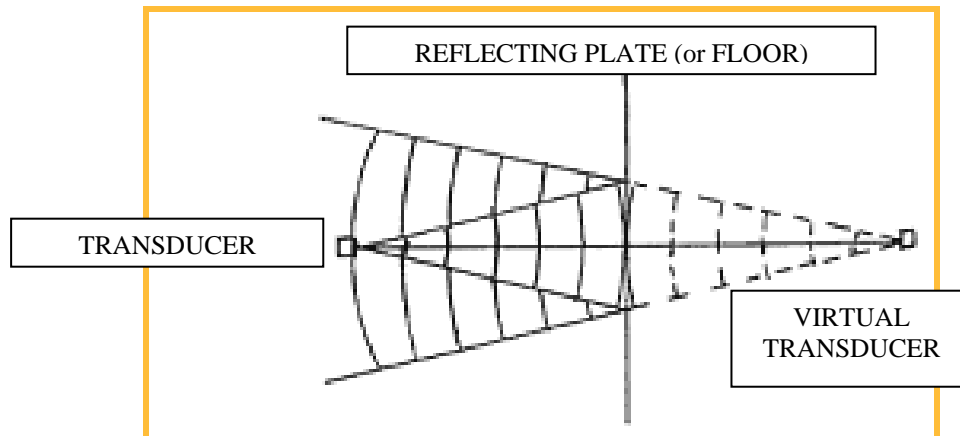


**Figure 3.7:** The distance that the signal travels is equivalent to double the actual distance/clearance between a transmitting/receiving transducers and the target surface (Massa, 1999; Bilgin, 2003).

It is generally understood that increasing ultrasound frequency improves detection resolution (Coleman et al.,2004; Massa, 1999; Magori, 1994, Manthey,Kroemer & Magori,1992), reduces dead zone length

(Bruinsma et al., 2006; Cittadine, 2000; Massa, 1999) and lowers noise susceptibility (Massa, 1999; Manthey, Kroemer & Magori, 1992, Tone & Fukumoto, 1987).

The resolution of measurement will be limited by wavelength due to the fact that ultrasound signal is transmitted in the form of a pulse-train that consists of a few wavelength. Since ultrasound speed is a constant at any given temperature and humidity, increasing the ultrasound frequency alters wavelength directly. This can be clearly seen in (4) where the relationship between ultrasound propagation speed,  $v_s$ , its frequency,  $f$ , and its wavelength,  $\lambda$ , is shown.

$$v_s = f \lambda \quad (4)$$

Maximizing frequency is also effective to reduce the dead-zone if a single sensor/transducer is used for both emission and detection. Dead-zone refers to a relatively short non-measurable range immediately in front of the sensor/transducer/transceiver, if compared to the total measurable range. The dead zone is attributed to the occurrence of time period the transmitting transducer's membrane requires to stop its vibration, or also called ring-down period. It is also affected by the pulse-train length of the transmitted ultrasound signal. For example, if a 1 MHz signal is emitted as a pulse-train of 5 cycles, the pulse length is then 5 times the wavelength, as shown in Figure 3.8. Using Figure 3.9, for temperature of 0°C, the ultrasound speed is approximately 330 m/s, while for 45°C, the speed is about 357 m/s. So, at 0°C, the wavelength is 330  $\mu\text{m}$  and the pulse length is 1.65 mm, while at 45°C, the wavelength is 357  $\mu\text{m}$  and the pulse length is 1.785 mm. Thus, ultrasound signal with shorter wavelength or lesser number of cycles results in shorter

pulse-train length. While a transducer is transmitting a pulse-train, it is not able to detect any echo or reflected signal, this causes the minimum limit of distance detectable, or simply called dead-zone. That is why shorter pulse can reduce dead-zone (Manthey, Kroemer & Magori, 1992). However, dead-zone is usually eliminated by the use of two different transducers, one for transmission and one for reception functions.

Reduction in noise susceptibility is another advantage of using higher frequencies (Massa, 1999; Yano, Tone & Fukumoto, 1987). As attenuation is significantly increased in higher frequencies range, noise is almost eliminated in that range. Cittadine (2000) reported that operations at elevated frequency range of 500 kHz to MHz shift the system away from the noise due to the flow of gaseous liquids, which is typically at 200 kHz. It is even reported that above 500 kHz, noise is not affecting the measurement at all (Yano, Tone & Fukumoto, 1987). Most interestingly, it is highlighted that frequencies above 60 kHz are safe from acoustic noise as the noise is maximum up to around 40 kHz (Manthey, Kroemer & Magori, 1992). In addition, at frequencies above 500 kHz, humidity is no longer a factor that affects air absorption of ultrasound signal (Schindel et al., 1995).

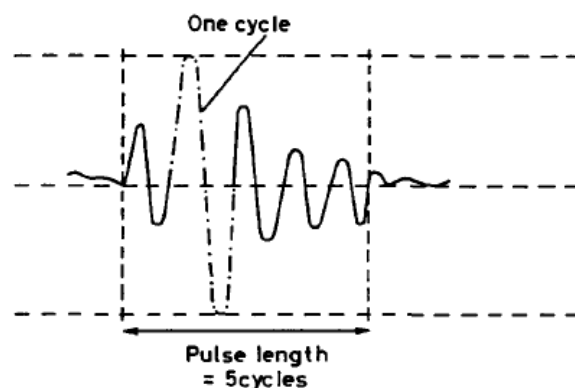


**Figure 3.8:** *Pulse length and wavelength of a five cycles signal (Wells, 1968).*

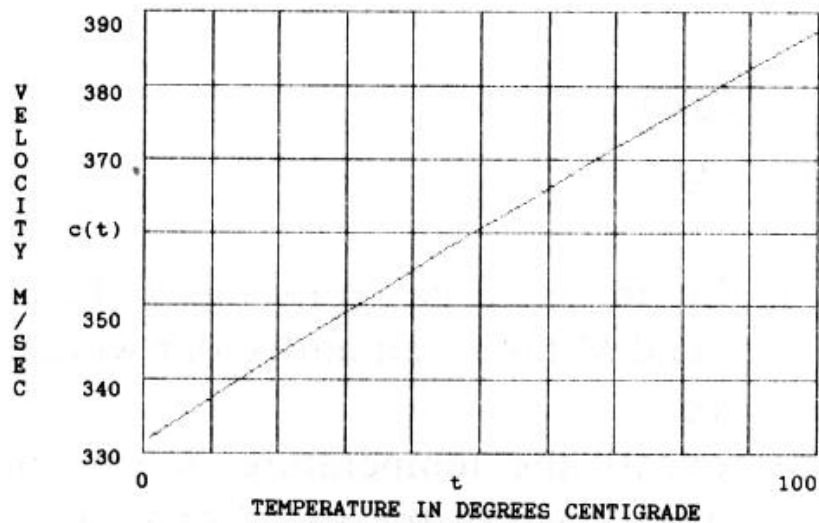


Figure 3.9: The speed of sound in air for different temperatures (Bohn, 1988).

For a time-of-flight (TOF) based ultrasound sensing system, the received signal must be at least of certain threshold amplitude that is called detection threshold. The minimum detection range is the distance in front of the transducer at which the transmit signal touches the detection threshold, as shown in Figure 3.10.

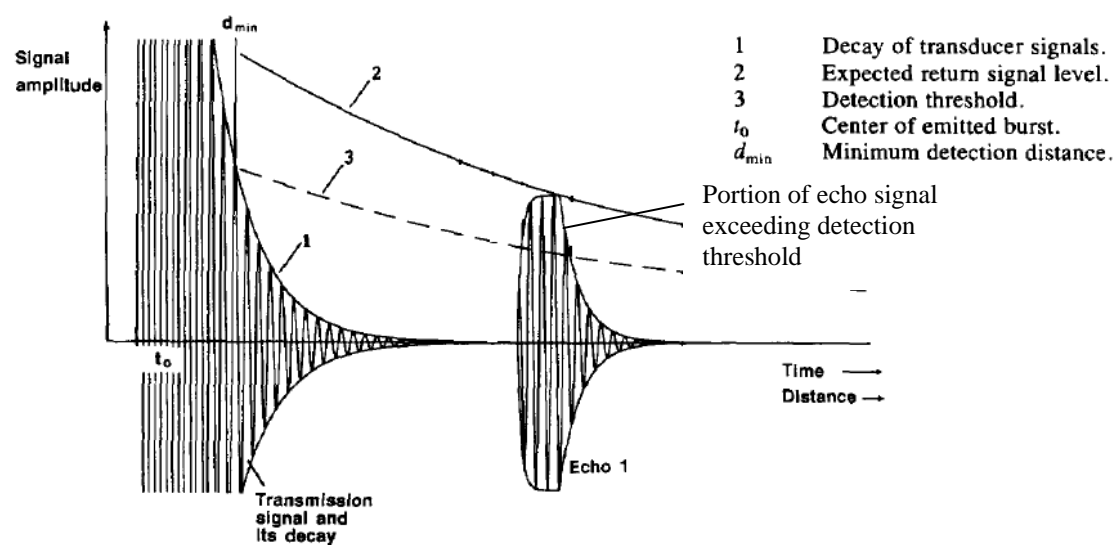


Figure 3.10: Transmission and echo signal for a TOF system (Magori & Walker, 1987)

To examine the applicability of ultrasound technique, the analysis of total signal loss is adopted following the similar technique adopted in the literature (Ladabaum et al, 1998; Yano, Tone & Fukumoto,1987). According to Ladabaum et al. (1998), a pitch-catch system experiment involving a 1 cm<sup>2</sup> CMUT 2.3 MHz ultrasound signal transmitter and a 0.25 cm<sup>2</sup> receiver is capable of achieving a 110 dB dynamic range in air. In the experiment, it is found that 5 dB of loss is due to 0.8 cm air trip, 70 dB loss due to the aluminum slab, 5 dB of loss by electrical impedance mismatch between the transducer and the receiving electronics. A signal with 30 dB signal-to-noise ratio (SNR) is received at the end proving a 110 dB dynamic range.

It is reported that the theoretical dynamic range that can be achieved by CMUT is 130 dB (Jin, Ladabaum & Khuri-Yakub,1998). In another report on an in air pitch-catch experiment using CMUT, a 16 dB SNR of ultrasonic signal (without averaging) is successfully detected (Yaralioglu et al.,2003). However, the high attenuation in air which increases with the square of frequency is a great challenge. The ultrasound attenuation,  $\alpha$ , for each frequency,  $f$ , is discussed in detail by Irwin (1997) . However, the relatively higher measured attenuation data by Yano, Tone & Fukumoto (1987), as shown in Figure 3.11 is used in this thesis.

The work on piezoelectric technology by Yano et al. (1987) also reported that a 1 MHz transducer is theoretically able to sense distance of up to 20 cm. Later in the research, it is experimentally proven to be able to measure distance of 17 cm. In Figure 3.11, the work by Yano et al. (1987) using their piezoelectric transducers for measuring distance in air is included to enable comparison with a more recent result.

In another study, it is reported that a 2 MHz signal can only measure distance up to few centimeters (Noble et al.,1995; Schindel et al., 1995). However, with the recent advancement in CMUT based technology, the use of precision circuitry and setting SNR of 1, maximum distance measurable by 2 MHz and 1 MHz are 24 cm and about 100 cm respectively (Ergun et al.,2006), as also shown in Figure 3.11. It is therefore can be concluded that, undoubtedly, CMUT based ultrasound can measure the required distance for foot clearance monitoring.

To further analyze the ultrasound capability of measuring the required distance in foot clearance application, an analysis based on total air trip attenuation and dynamic range is performed. Based on the measured attenuation data by Yano et al. (1987) as given in Table 3.11, the simulated relationship of total attenuation for various total air trip propagation at several frequencies are presented in Figure 3.12. It is assumed that the floor surface is a perfect flat reflector of ultrasound as in most of the cases (Turner & Austin, 2000), and that the signal is approaching the pathway surface in the normal direction. If the theoretical dynamic range of CMUT of 130 dB is assumed, the total 60 cm air propagation results in traveling loss of just around 114 dB. Neglecting other losses, SNR of 16 dB is achievable. If SNR of 1 is the target, the maximum pitch-catch distance can be measured is obviously should be around 75 cm at 1 MHz. In terms of sampling rate, using ultrasound to obtain a 75 Hz sampling rate is not a problem at all. As the time for a complete signal propagation in a 60 cm trip is 1.8 ms at 0 °C (1.74 ms at 25 °C), ultrasound based measurement can sample the distance almost 7 times more frequent than the target frequency.

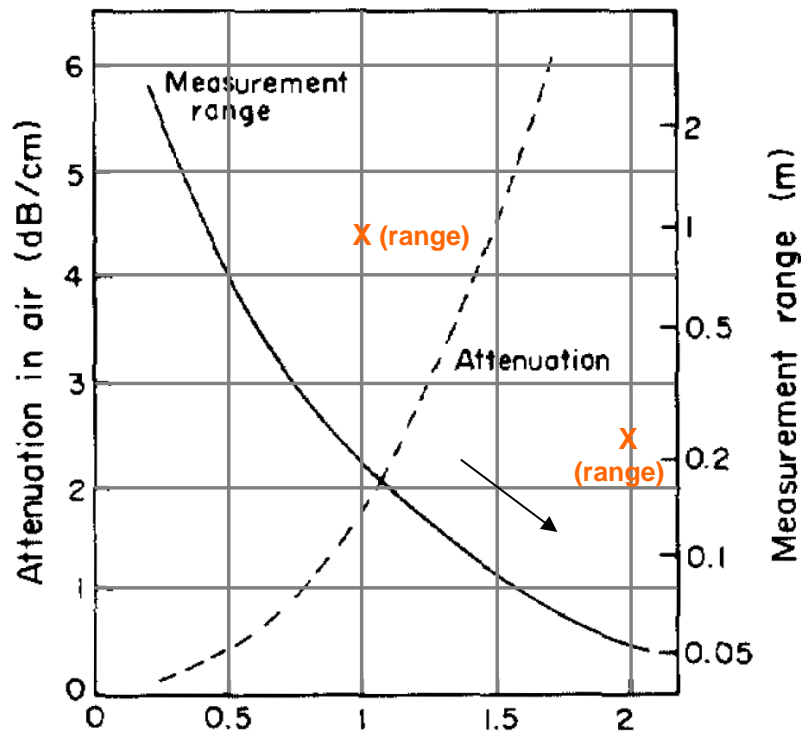


**Figure 3.11:** Measured ultrasound signal attenuation and the maximum distance measurable for each signal frequency based on the conventional piezoelectric technology (Yano, Tone & Fukumoto, 1987). The two 'x' marks in the graph indicates the current maximum ultrasound measurement range based on CMUT technology (Ergun et al., 2006).

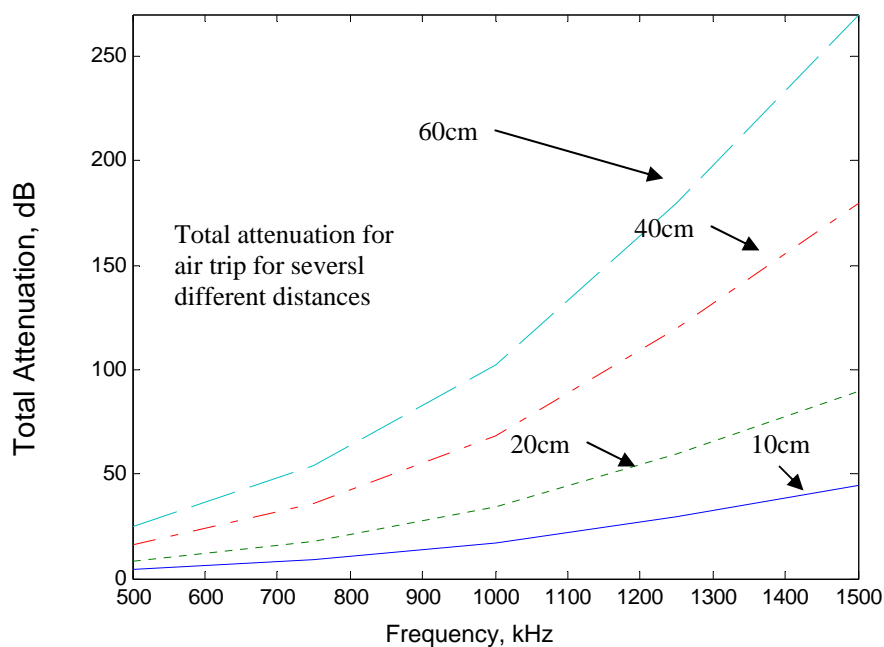


**Figure 3.12:** The total ultrasound attenuation for various measurement distance and frequencies.

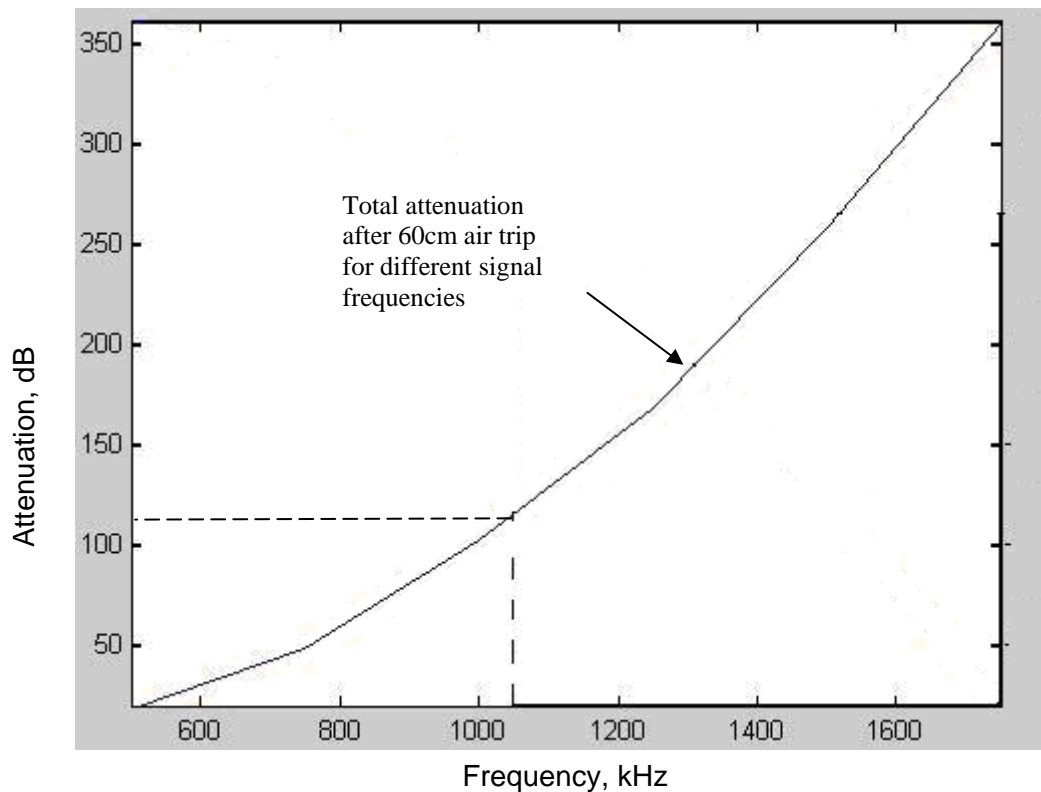


**Figure 3.13:** Approximation of best ultrasound frequency for distance of 30 cm from simulation which is about 1.05 MHz. The horizontal dotted line touches the y axis at ~120dB point. Even though the target distance is just 5 cm, this long range measurement capability may enable application in more human activities (Wahab et al., 2008; Wahab et al., 2007).

It is important to note that low frequency ultrasound is already proven to be able to measure distance of up to the meters range, as also shown in Figures 3.11, 3.12 and 3.13. However, its wavelength limits the minimum distance that the transducer can measure. As the measurement of foot clearance requires the attachment of the ultrasound transducer to the shoe, it is important to reduce the minimum distance as much as possible, and this can be done by choosing the maximum possible ultrasound frequency. By choosing the maximum frequency, the resolution can also be maximized, but by trading the maximum distance measurable.

### 3.2.4 Section Summary and Technique Selection

Results from numerical simulations to evaluate the three distance measurement techniques, which include capacitive sensing, electric field sensing and also ultrasonic sensing are already presented and discussed. Summary of the results showing some important aspects of the three measurement techniques are presented in Table 3.2 for comparison.

TABLE 3.2: COMPARISON OF THE THREE TECHNIQUES

Key observation	CS	EFS	US
sensing range with up to 1 cm <sup>2</sup> sensor area	5 cm @ 1 cm <sup>2</sup>	15 - 20 cm @ 1 cm <sup>2</sup>	11 cm @ 1 mm <sup>2</sup> diameter (Kuratli & Huang,2000) ~25cm @ 1 cm <sup>2</sup> using CMUT (Almqvist et al.,2002) 1 m @ 1 MHz, 0.49 cm <sup>2</sup> and 24 cm @ 2 MHz, 0.49 cm <sup>2</sup> (Ergun et al.,2006)
previously reported as MEMS or micromachined	Yes (Luo, 1996)	No	Yes (Kuratli & Huang, 2000; Yaralioglu, 2003)
ever used in foot clearance measurement	No	Yes (Morris, 2004)	No
signal to distance relationship (linearity)	linear	Non-linear	linear
remarks based on the analysis results in Section 3	Not suitable due to size	Not suitable due to size	Ultrasound of around 1 MHz may offer good resolution and signal strength
Suitability for MEMS, taking range dependent sensor size as limit	Not suitable	Not suitable	suitable

As presented in Table 3.2, the comparison between the three techniques shows that high resolution ultrasound ranging is the best choice due to the fact that it is capable of sensing the distance of up to 30 cm, which is the highest range achieved if MEMS size is the key criteria. If the most recently published experimental work by Ergun et al. (2006) is considered,

there is no doubt that ultrasound is the best choice for implementation. Obviously, the ultrasonic measurement technique is not only suitable for MEMS, it is also theoretically proven to be able to measure the foot clearance during most of gait related activities too. This result indicates that ultrasound is a very promising technique. Considering those facts, ultrasound is thus selected in this work for the design of a foot clearance measurement sensor.

### **3.3 Selection of Ultrasound MEMS Mechanism and Fabrication**

In real implementation of MEMS, the process technology determination is the key consideration. This is so because for each process technology, the sets of materials offered and process implementation are very unique. It is reported that piezoelectric based PMUT technology fabrication is difficult to implement. The limitation is due to the difficulty to produce a thick piezoelectric layer required for producing good PMUT transmitter (Wang et al., 2005). It is also said that PMUT's electromechanical coupling factor figure is very low, of only 6 % (Baborowski, 2005; Muralt, 2005). A good comparison of PMUT and CMUT is given by Pappalardo et al (2008) and is listed in Table 3.3.

For airborne distance detection, such as foot clearance measurement, the measurement device needs to have excellent air matching characteristic. Since CMUT exhibits very low mechanical impedance, which is attributed to by its capability of using very thin membrane, it matches air acoustic impedance very well. In terms of energy transfer efficiency, CMUT is shown to demonstrate electromechanical coupling efficiency as high as 0.8 or 80 percent. Other advantage includes high dynamic range which increases measurable distance. CMUT also exhibits wide bandwidth, high operating

frequencies and also tolerance to humidity, particles and most chemicals too (Ergun et al.,2006). From literature, it is also found that capacitive type of MEMS ultrasound transduction, CMUT is more CMOS compatible (Ergun, Yaralioglu & Khuri-Yakub,2003). The advantages of being CMOS compatible are the fact that the overall system performance is highly enhanced. As most of the microelectronic circuit fabrication is based on CMOS, CMUT is obviously a better choice of MEMS realization. In short, due to so many advantages shown by CMUT, it is therefore a better technology of implementation and thus chosen in this research.

TABLE 3.3: COMPARISON OF PMUT AND CMUT (Pappalardo et al.,2008)

	<b>PMUT</b>	<b>CMUT</b>
<b><i>material</i></b>	Piezoelectric layer needed	Commonly used silicon micromachining and fabrication materials are used
<b><i>maturity</i></b>	Still very new	better
<b><i>process</i></b>	Difficult and time consuming, deposition of crack free PZT layer is difficult, not fully compatible with surface micromachining	Surface micromachining is widely used. Many shows CMOS compatibility
<b><i>performance</i></b>	Not proven yet	Proven
<b><i>characterization</i></b>	Not fully reported yet	Fully studied and reported

Another important consideration in the device realization is the prototyping cost, which is mainly due to sensor micro-fabrication charges. For this research, the fabrication can be performed by use of multi-project-wafer service (MPW). Two commonly used CMUT fabrication service is the Integramplus MPW (Qinetiq Ltd.) and the MUMPs MPW (MEMSCAP)

services as used in several reports (Campbell, 2007; Octavio, 2007; Greve, Wu and Oppenheim, 2006). The MEMSCAP is the cheapest in this regard, priced at USD 4500 (~AUD 5800). Due to the high cost, the custom surface micro-machine processing is developed and used.

### **3.4 Design Specification of CMUT**

The target of this work is to design a sensor for use in a portable gait analysis and fall prevention system. To ensure practicality of the design, an application based design specification is developed considering the application requirements as discussed in Chapter 2. The specifications are:

#### ***Operating Frequency***

The target operating frequency of between 500 kHz and 1 MHz is a good choice. As discussed in the previous section, to eliminate the ultrasound noise, frequencies above 500 kHz is compulsory. On the other hand, frequencies more than 1 MHz may cause significant signal degradation of more than 100 dB. Even though good dynamic range can be realized theoretically, it is better to allow more signal to noise margin (SNR) figure, possibly more up to 30 dB. In the selected frequency range, however, 1 MHz signal may offer higher resolution due to its low wavelength. Nevertheless, if system level algorithm optimization is considered, even low frequency ultrasound can be used to produce sub-millimeter resolutions, as discussed in the preceding section.

### ***Supporting The Required Sampling Frequency***

The sensor should be capable of supporting the required 75 Hz distance sampling frequency. Which means, a distance value must be obtained every 13.3 ms. This is not a problem with ultrasonic technique as, consider the worst case scenario where 30 cm foot clearance is measured (ultrasound speed of  $340 \text{ ms}^{-1}$ ), using equations (3) the TOF is merely 1.765 ms. In this case, about seven distance measurement can be performed every 13.3 ms, which proves the compliance with the requirement.

### ***Foot Clearance Range***

The sensor must be designed to be able to measure foot clearance above ground/floor of at least 5 cm.

### ***Sensor Size***

The sensor should comply with the MEMS requirement of maximum  $1 \text{ cm}^2$  area.

## **3.5 CMUT Mathematical Modeling**

A structural cross-sectional view for CMUT is given in Figure 3.14 while its electromechanical model is depicted in Figure 3.15. To understand the CMUT electromechanical behaviour, it is imperative to firstly analyze the fundamental equation for capacitance and then use it together with the electromechanical model.

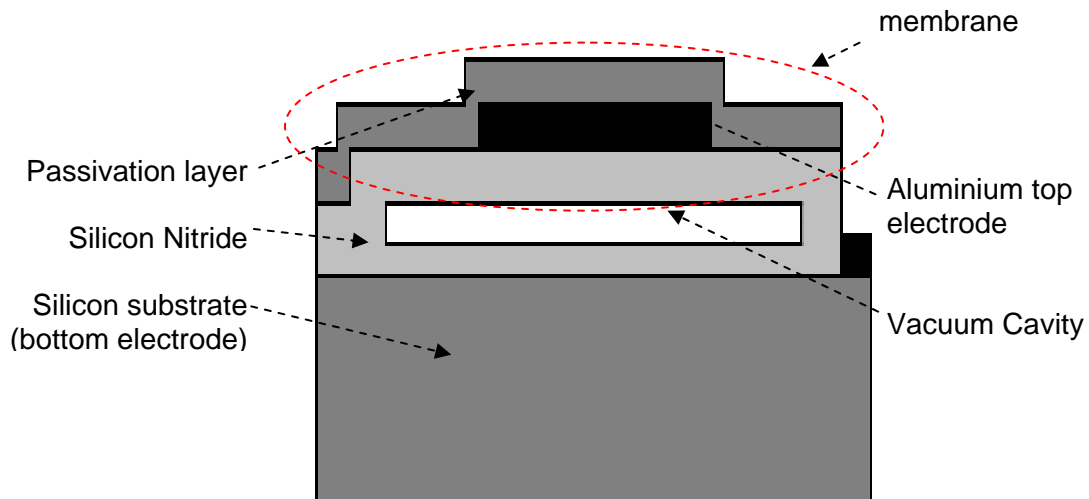


**Figure 3.14:** A cross-sectional view of a CMUT (adapted from Ergun, Yaralioglu & Khuri-Yakub, 2003).

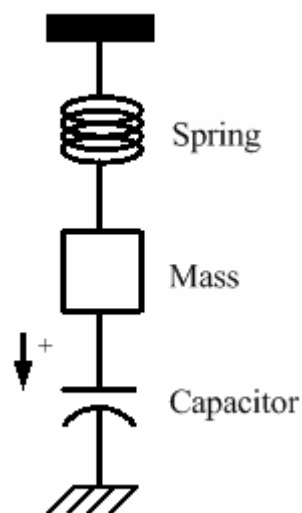


**Figure 3.15:** The lumped electromechanical model for CMUT.

For a parallel plate capacitor with movable top and both plates are of area  $A$ , designed plate separation  $t_g$ , permittivity of  $\epsilon$ , a top plate displacement of magnitude  $x$ , the capacitance can be represented by equation (5). The electrical energy and the electrical force can then be calculated using equations (6) and (7).

$$C = \frac{\varepsilon A}{t_g - x} \quad (5)$$

$$E = \frac{1}{2} CV^2 = \frac{\varepsilon AV^2}{2(t_g - x)} \quad (6)$$

$$F_{ele} = -\frac{dE}{dx} = \frac{\varepsilon AV^2}{2(t_g - x)^2} \quad (7)$$

As shown in Figure 3.15, the three force components are the one acting on the spring, the mass and the capacitor. They are  $F_{spring}$ ,  $F_{mass}$  and  $F_{ele}$ , respectively. In equilibrium, the net forces acting in the system can be equaled to zero as shown in equation (8). Taking  $m$  as the membrane mass,  $k$  as the spring constant of the membrane and  $a$  as the acceleration of the membrane, the spring and mass forces can be represented by equations (9) and (10).

$$F_{spring} + F_{mass} + F_{ele} = 0 \quad (8)$$

$$F_{spring} = -kx \quad (9)$$

$$F_{mass} = ma \quad (10)$$

Inserting the elemental forces into equation (8) and including their time dependencies yields equation (11) and (12) (Yamaner, 2006).

$$-kx(t) + ma(t) + \frac{\varepsilon AV(t)^2}{2(t_g - x(t))^2} = 0 \quad (11)$$

$$-kx(t) + m \frac{dx(t)^2}{dt^2} + \frac{\varepsilon AV(t)^2}{2(t_g - x(t))^2} = 0 \quad (12)$$

However, during static bias, the system is not time dependent, and this can be simplified to only consist of the forces due to the spring and the capacitor. Solving for  $V$  yields equation (13).

$$V = \sqrt{\frac{2kx}{A\varepsilon}}(t_g - x) \quad (13)$$

The differentiation of equation (13) for  $V$  with respect to  $x$  gives only one real root ( $dV/dx = 0$ ) for  $x < t_g$  and  $V$  smaller than the voltage value that causes the membrane deflection to be non-linear. Its solution is given in (14) (Ergun, Yaralioglu & Khuri-Yakub,2003). At this voltage, the membrane is said to collapse, and the bias voltage is called collapse voltage or pull-in voltage.

$$x = \frac{t_g}{3} \quad (14)$$

By rearranging (13) and substituting (14) into it, the collapse voltage mathematical representation is obtained, as shown in (15) (Ergun, Yaralioglu & Khuri-Yakub,2003).

$$V_{col} = \sqrt{\frac{8kt_g^3}{27\epsilon_0 A}} \quad (15)$$

For a circular membrane with radius  $r$ , area  $A$  can be represented as  $\pi r^2$ . Substituting the spring constant  $k$  of (16) into (15) produces (17) (Bozkurt et al.,1999).

$$k = \frac{16\pi Y_0 t_m^3}{(1-\sigma^2)r^2} \quad (16)$$

Here,  $t_m$  is the membrane thickness,  $\sigma$  is the poisson ratio,  $Y_0$  is the young modulus of the membrane material and  $r$  is the membrane radius. The vibration of the membrane due to the exerted force produces ultrasonic signals that propagate in perpendicular direction with the membrane plane, towards the floor or walking path ground. As the biasing DC voltage is increased up to a point referred to as the collapse or pull-in voltage, the mechanical restoring force is becoming overwhelmed by the electrostatic force. Beginning this point, the membrane deflects non-linearly with the

increasing DC bias and the membrane touches the bottom of the gap. This important voltage value is represented by equation (17). Here,  $\varepsilon_0$  is the permittivity of free space,  $8.854 \times 10^{-12}$  F/m.

$$V_{col} = \sqrt{\frac{128 Y_0 t_m^3 t_g^3}{27 \varepsilon_0 (1 - \sigma^2) r^4}} \quad (17)$$

Equation (17) can be used to estimate the collapse voltage of a CMUT. It is important to note that in many cases, the effective gap height, or  $d_{eff}$ , can be further analyzed as the resultant of the combination of the designed gap/cavity height,  $t_g$  and the membrane thickness,  $t_m$ . This more accurate electrode separation value can thus be represented by  $d_{eff}$  as shown in (18).

$$d_{eff} = t_g + \frac{t_m}{\varepsilon_r} \quad (18)$$

In addition to identifying the point where the membrane deflection becomes non-linear, the collapse voltage is also an important indicator for another electro-mechano-acoustical characteristic of the membrane which is called the electromechanical coupling factor,  $k_T$ . As a figure that shows how good the electrical energy is transformed into mechanical and acoustical energy, the coupling factor is a very important parameter of CMUT. This is due to the fact that CMUT exhibits a significantly high coupling factor as compared to the piezoelectric based transducers. This can be calculated using (19) (Ergun, Yaralioglu & Khuri-Yakub, 2003).

$$k_T = \frac{2x}{d_{eff} - x} \quad (19)$$

The reflected signal activates vibration of the receiver transducer and alters the capacitance value of the transducer structure. The readout circuit detects the capacitance change for appropriate processing of distance information. Considering an ultrasonic measurement technique, a system view of the proposed model is shown in Figure 3.16.

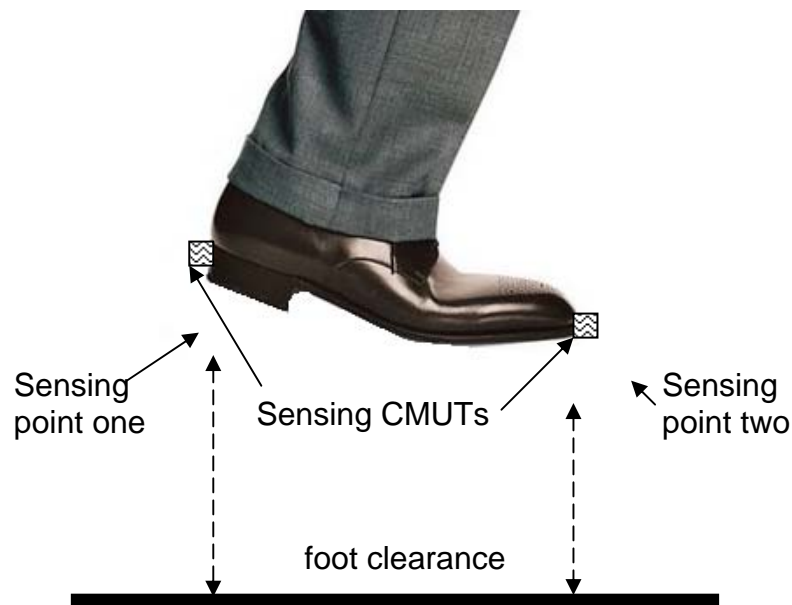


**Figure 3.16 :** *A possible implementation using two points sensing.*

Since a transducer can be operated for as either transmitter or receiver, the use of a single transducer at each point is already adequate for this application. However, for best performance, using two transducers at each point is suggested, one as a transmitter and the other as a receiver. These transducers may be attached to the shoes, one each at the front and back end sides of the shoes. This way the tilting of shoe soles may be calculated while minimum height of the shoe from the floor or ground is easily determined.

High performance CMUT is operated at its membrane resonance frequency (Ergun et al., 2006; Anbalagan & Uma,2006). To obtain a transducer design specification for operation at a certain frequency, a fast and simple approximation is favourable. A mathematical model for a V-grooved backplate is previously reported (Matilla et al,1995). However, as current CMUT is mostly made using CMOS compatible surface micromachining where the structures of deposited layers are planar in shape, the V-grooved model is not applicable here. Modification to the model is thus performed here. Since electrostatic transducer can be modeled as a mass-spring oscillator (Matilla et al,1995), and taking the membrane as the mass and the cavity as the spring, the resonant frequency of a membrane structure is given by (20).

$$f_r = \frac{1}{2\pi} \sqrt{\frac{1}{mC_m}} \quad (20)$$

In (20),  $m$  is the mass of the spring and  $C_m$  is the mechanical compliance of the backplate cavity, which is given by

$$C_m = V / \rho_o v_s^2 A^2 \quad (21)$$

where  $V$  is the cavity volume,  $\rho_o$  is air density,  $v_s$  is sound speed in air and  $A$  is the membrane area. Assuming a sacrificial layer of thickness  $d_g$  is being etched to release a membrane structure of area  $A$ , the resulting cavity volume can then be simply represented by (22).

$$V=A d_g \quad (22)$$

Now consider the membrane material. If  $\rho_m$  is the material's density and  $d_m$  is its thickness, the mass  $m$  can be represented by (23).

$$m=\rho_m d_m A \quad (23)$$

Substituting  $C_m$  and  $m$  into (20) we get (24).

$$f_r = \frac{1}{2\pi} \sqrt{\frac{\rho_o v_s^2}{\rho_m d_m d_g}} \quad (24)$$

Material selection is a crucial step in the design. However, numerous MEMS materials with published physical properties are available for consideration (Liu, 2006). Table 3.4 is produced by applying (24) in some transducer designs using commonly used MEMS materials such as silicon nitride. The membrane design and material selection for the proposed 1.05 MHz CMUT of this work, and comparison with published results in the literature is also included. Table 3.4 shows that the model is in good agreement with other published results. Considering that this modeling is fast and practical to apply, it can be used as the first step to identify suitable CMUT geometry values before proceeding to the detail step of computer simulation. By using the newly derived equation (24), the thickness of a silicon nitride membrane that resonates at 1.05 MHz is identified to be 1.1  $\mu\text{m}$ . Since equation (24) is proven to be acceptably accurate enough when compared to many measured works in the literature, it is hereby proposed as a useful early modelling tool.

TABLE 3.4: DESIGN EXAMPLES USING (24) AND COMPARISON WITH MEASUREMENTS IN RELEVANT LITERATURE.

Membrane Material	Structure dimension	Calculated frequency	Comments
Silicon Nitride,	$d_g=0.5\mu m$ $d_m=0.5\mu m$	2.19 MHz	Comply with calculation in example of (Eccard, Niederer & Fischer,1997)
Silicon Nitride,	$d_g=1.0\mu m$ $d_m=1.0\mu m$	1.11 MHz	In close agreement with result in (Jones et al.,2001)
Silicon Nitride,	$d_g=0.3\mu m$ $d_m=0.2\mu m$	1.6 MHz	About 10% difference with measured in (Ladabaum et al.,1998)
Al <sub>2</sub> O <sub>3</sub>	$d_g=0.75\mu m$ $d_m=0.6\mu m$	4.1 MHz	About 5% difference with measured in (Liu et al.,2004)
Silicon Nitride,	$d_g=1.0\mu m$ $d_m=1.1\mu m$	1.05 MHz	Calculation for the optimized frequency

### 3.6 CMUT Process Modeling and Simulation

All CMUT on silicon design work is performed using the industry standard *Coventorware* tool (see **Appendix A**) (Coventor Inc. , 2006). As nitride layer is used as the membrane structure material, therefore the top and bottom electrode will never be touched during membrane deflection as it vibrates following the AC voltage excitation.

Process for developing the transducer is custom sequenced using the available process libraries in *Coventorware Process Editor* module. The simplified flow is shown in Figure 3.17 and the snapshot from *Coventorware* is shown in Figure 3.18. The sequence starts with a silicon substrate and followed by a nitride deposition of 0.5  $\mu m$ . A conducting polysilicon of 0.5  $\mu m$  is then deposited, patterned to form the bottom plate of 45  $\mu m$  diameter. Following this, the unwanted polysilicon areas are removed by etching.

A temporary  $1\mu\text{m}$  sacrificial boron phosphosilicate glass material is then deposited and patterned. This sacrificial layer is actually used to define the structure that represents the cavity area between the membrane and the bottom electrode. Similarly, the unwanted phosphosilicate areas are then removed by etching. The next step is deposition of the second nitride with thickness of  $1\mu\text{m}$  to form the wall structure and membrane. On top of the membrane, the second electrode of similar diameter is formed by deposition and patterning of aluminium. Practically, the electrodes are four times thinner than the membrane (Bozkurt et al.,1999). So as to increase the bandwidth, the top electrode is made relatively small as compared to total membrane area.

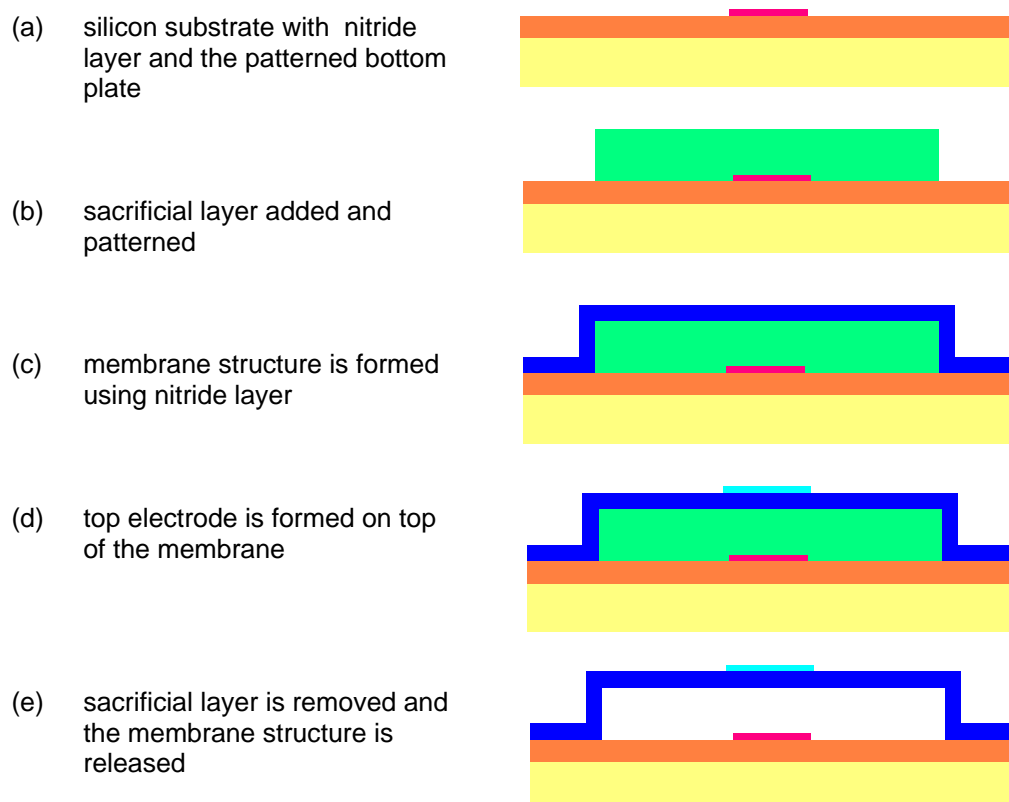


**Figure 3.17:** *The simplified process sequence.*

Number	Step Name	Action	Layer Name	Material Name	Thickness	Mask Name
0	Substrate	Substrate	Substrate	SILICON	20	SubstrateMask
1	Stack Material	Stack Material	nitride	SIN	0.5	
2	terminal1	Stack Material	botplate	POLYSILICON	0.5	
3	botplateshape	Straight Cut				botplate
4	sac	Stack Material	sac	BPSG	1	
5	sacetch	Straight Cut				sacshape
6	wallShell	Conformal Shell	nitridewall	SIN	1	
7	Cutwall	Straight Cut				wallcut
8	toplate	Conformal Shell	toplate	ALUMINUM(FILM)	0.25	
9	toplateshape	Straight Cut				toplateshap
10	sacdelete	Delete		BPSG		
11	sealnitride	Conformal Shell	sealnitride	SIN	1	
12	sealmat	Straight Cut				leavesseal

**Figure 3.18:** The process sequence in the fabrication modeling.

The release of the membrane structure is performed next where all sacrificial material beneath the structural nitride is removed. This is done through an opening at the side of the wall where the sacrificial layer is exposed. A nitride seal is then deposited in low pressure process to seal the hole left by sacrificial removal leaving cavity in near vacuum.

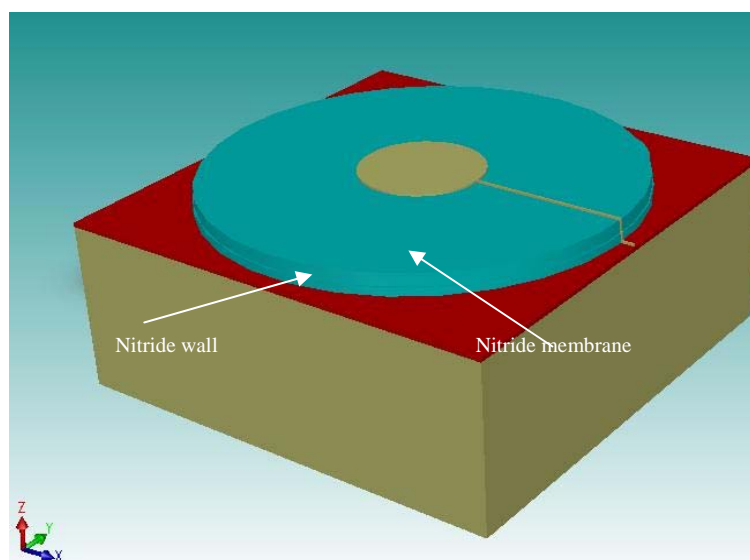


**Figure 3.19:** The 3D model produced by the Solid Modeler module.

Figure 3.19 shows a three dimensional view of the designed transducer in *Coventorware SolidModeler*. The circular blue layer periphery is the Silicon Nitride wall and Silicon Nitride membrane is the planar circular structure on the top. Metal conductor of Aluminium in golden colour on top of the membrane functions as the top electrode. The polysilicon bottom electrode is hidden beneath the membrane structure and the cavity. The membrane is  $1\mu\text{m}$  thick. The gap between the membrane and the bottom electrode is also  $1\mu\text{m}$ . The membrane diameter is  $140\mu\text{m}$ . A crosssectional view of the CMUT is shown in Figure 3.20.

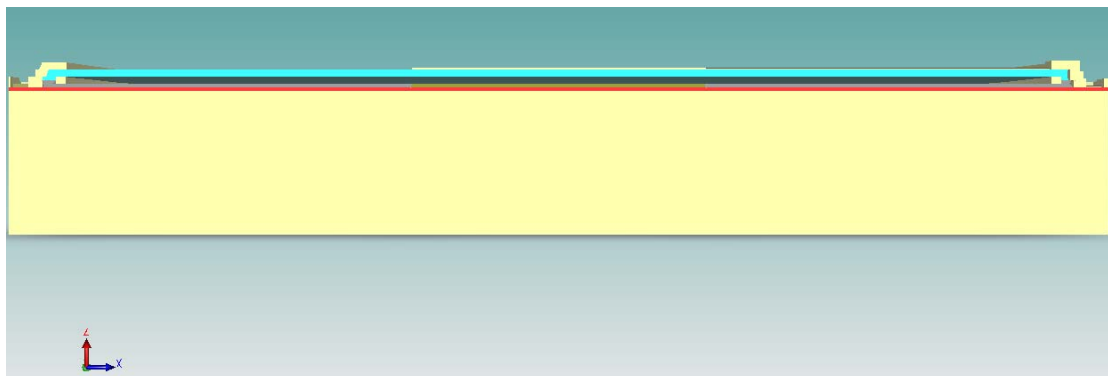


**Figure 3.20:** *The crosssectional view of the CMUT.*

### 3.7 CMUT FEA Design and Testing

The experiments using *Analyzer* involves important setting such as clamping of the membrane edge. This is done by appropriate setting of the relevant boundary conditions.

To accomplish this task, the 3D model is first divided into several parts for appropriate meshing. As shown in Figure 3.21 and Figure 3.22, the circular membrane and the electrodes are meshed for the FEA simulation.

In order to determine the best response frequency of the transducer, a modal analysis is performed. Using the *MemMech* modal analysis in Analyzer, a three dimensional diagram of Figure 3.23 is produced showing mode 1 of the membrane structure. As shown in Figure 3.23, the natural resonance frequency value of about 0.93 MHz, which is close to design prediction using equation (24) is observed. With this frequency, using equation (4), assuming air temperature of 300K, the wavelength,  $\lambda$ , is 0.37 mm. Thus, a spatial resolution higher than 1 mm can be achieved if pulse of one or even two  $\lambda$  is used. Obviously, this is far better than the design target and will enable high resolution foot clearance measurement.

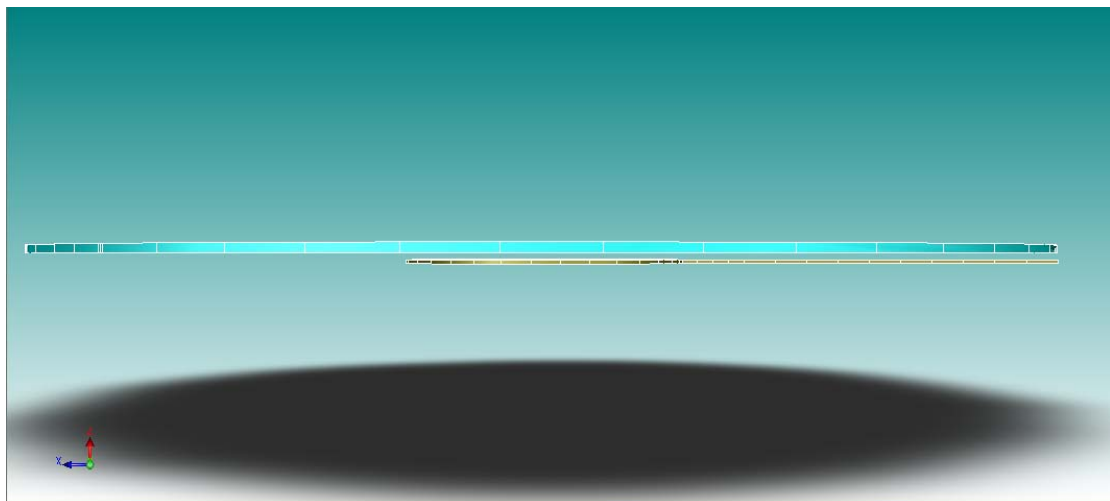


**Figure 3.21:** *The meshed membrane's side-view showing the top electrode on top and bottom electrode at the bottom. The substrate is hidden for clarity.*

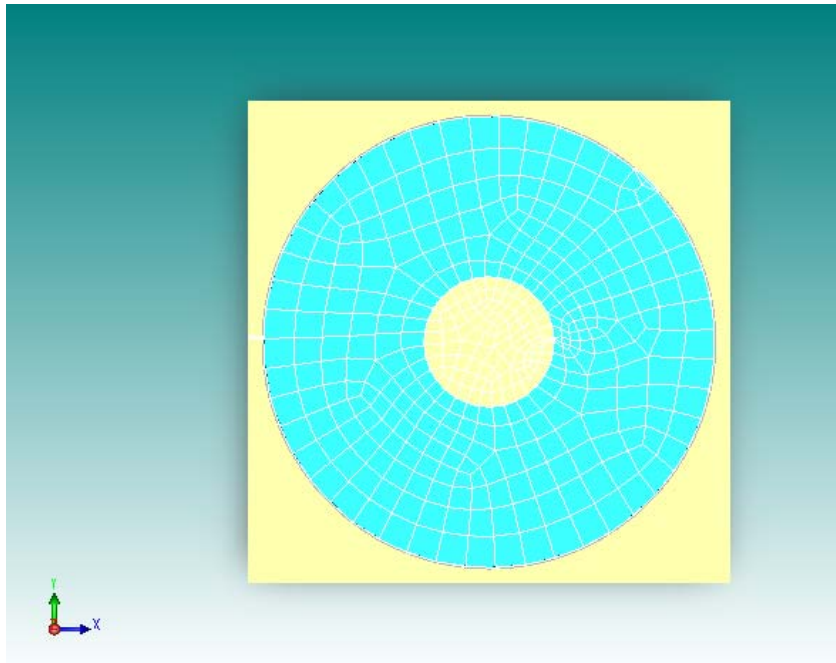


**Figure 3.22:** The meshed membrane's top-view showing the meshed top electrode on top of the membrane. The yellow square is the substrate.

However, as this process is CMOS compatible, more advanced signal processing circuitry for implementing optimization algorithm can be integrated to further enhance the resolution (Schweitzer & Elmer,2005). The pull-in or collapse voltage of the membrane is analyzed using *CoSolve* which involve *MemMech* and *MemElectro* modules. In Figure 3.24, the pull-in voltage is observed to be 104 V. MinZ represents the lowest point of the membrane deflection in micrometers. The high collapse voltage is expected as the ratio of electrode areas to the membrane area is small. The figure also shows how the membrane movement becomes highly nonlinear as the applied voltage between both electrodes is increased close to the pull-in value. At the pull-in voltage, as shown in Table 3.5, the size of deflection increment is at its maximum of 0.025  $\mu\text{m}$  between trajectory step 11 and step 12 for bias

increment of only about 0.3 V. This is true as at pull-in voltage, the mechanical restoring force of the membrane is overwhelmed by the electrostatic force applied to the membrane by the bias voltage. Table 3.5 also shows the resulting transducer capacitance change due to membrane deflection up to step 11. As can be seen in the table, the capacitance value increases with the increase in membrane deflection. Physically, as the membrane deflects more towards the bottom electrode, the effective separation between the electrodes, and thus the capacitor plates separation, decreases. It is thus most probable that the surge in capacitance is caused by the decreasing effective separation distance between both top and bottom electrode.

The effect of applying pull-in voltage to the membrane structure can be visually seen in Figure 3.25 which is an output of *Visualizer*. The top electrode and its connection can also be seen to follow the curvature of membrane deflection shape. In *Visualizer*, the setting is made to graphically exaggerate the deflection by 25 times to enable better appreciation of the phenomenon. As shown, the deflection close to 0.45  $\mu\text{m}$  is achieved during the application of pull-in voltage across the membrane and the cavity.

Another advantage of CMUT is its high electromechanical coupling factor,  $k_T^2$ , which is a measure of CMUT's capability of transforming electrostatic energy to mechanical energy. A value close to 1, meaning a 100% transformation, can be achieved if DC bias of close to pull-in voltage is applied. The electromechanical coupling factor can be calculated based on the values available in Table 3.5. Following the work in (Ergun, Yaralioglu &

Khuri-Yakub,2003), using the previously defined  $d_{eff}$ , which is the effective gap height and  $x$ , the membrane deflection, equation (19) can be used to calculate the electromechanical coupling factor.

TABLE 3.5: VOLTAGE(V), DISPLACEMENT( $\mu\text{m}$ ) AND CAPACITANCE(pF)

step	voltage	Displacement	Displacement_Change	C_bot-elec_top-elec
1	50	6.476171E-02	2.839193E-04	-1.351571E-02
2	60	8.934805E-02	3.277883E-04	-1.374654E-02
3	70	1.214784E-01	8.585602E-04	-1.406E-02
4	80	1.647922E-01	5.770922E-04	-1.426049E-02
5	90	2.253425E-01	7.590205E-04	-1.491939E-02
6	100	3.279423E-01	6.373525E-04	-1.629378E-02
9	1.025E02	3.742323E-01	9.326339E-04	-1.702324E-02
10	1.037E02	4.117945E-01	9.660423E-04	-1.76745E-02
11	1.043E02	4.482004E-01	9.871126E-04	-1.836321E-02
12	1.046E02	4.777755E-01	2.523661E-03	
13	1.045E02	4.740587E-01	1.311779E-03	

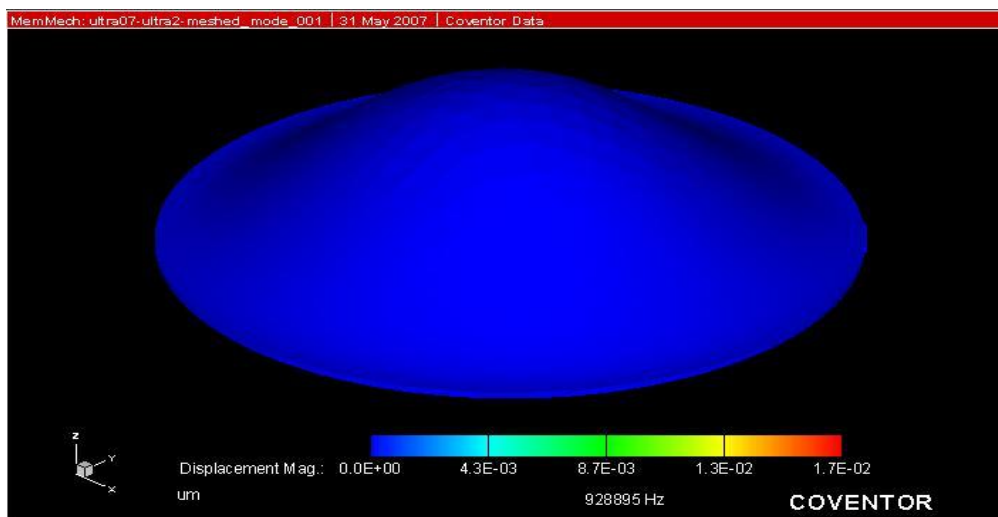
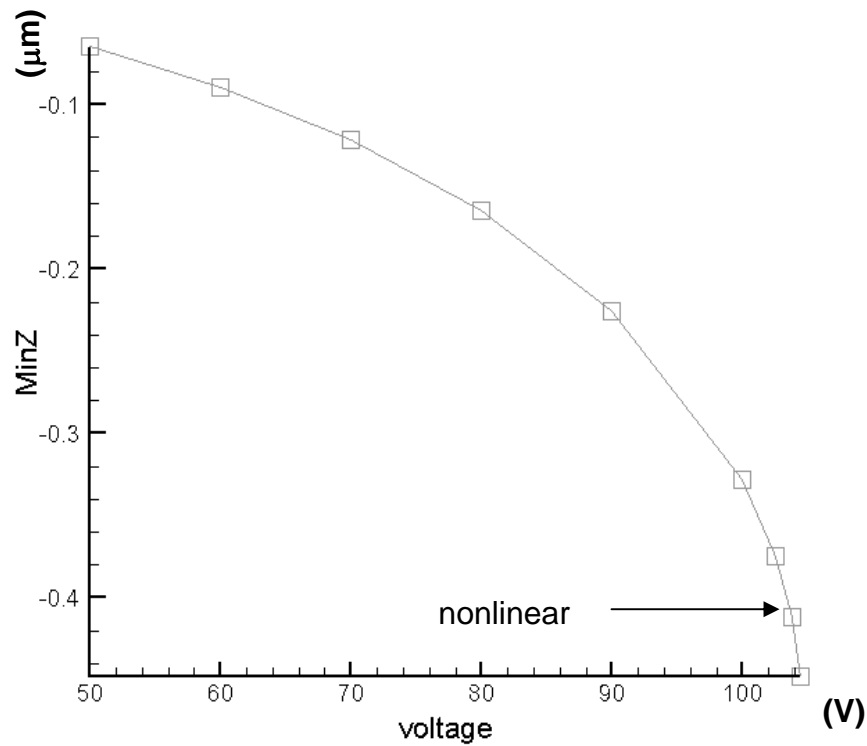
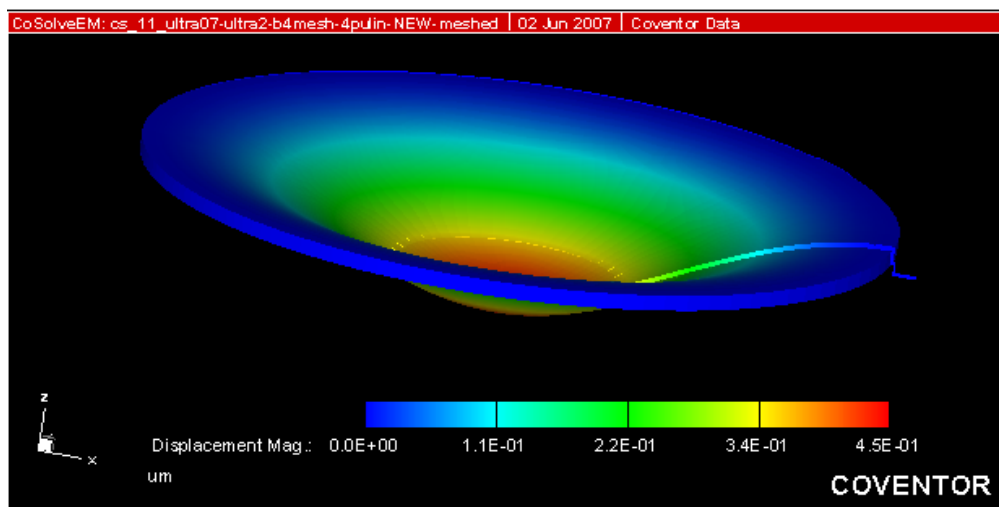


Figure 3.23: The mode 1 result of modal analysis.



**Figure 3.24.** The deflection and pull-in voltage.



**Figure 3.25:** The deflection of membrane at pull-in voltage.

Since DC bias is limited by pull-in voltage, while electromechanical coupling factor is maximum at pull-in, it will be best if the DC bias is chosen to be close but smaller than pull-in voltage for maximum possible signal strength. If 100 V is chosen, the electromechanical coupling factor value

will be 0.815 which is high and is normal to CMUT as reported by many CMUT researchers such as Ergun et al (2006). According to literature, to bias CMUT up to 200 V, the use of a 10 V battery as power supply is already sufficient if CMOS high voltage dc–dc up converter is used together (Chebli & Sawan,2004). Since electromechanical coupling factor is dependent on the bias, the signal strength is also dependent on the bias magnitude. So, for shorter range measurement, the supply voltage is less than 10 V.

Figure 3.26 shows the layout of the CMUT. To produce a more sensitive device, an array of similar CMUT device in Figure 3.26 can be arranged in an array of one dimensional or two dimensional setting with ease. In an array configuration, the total size of the arrayed CMUTs can be few  $\text{cm}^2$  as implemented in many reports, as the main constraint is the individual membrane size (Huang et al, 2003; Noble et al, 2001).

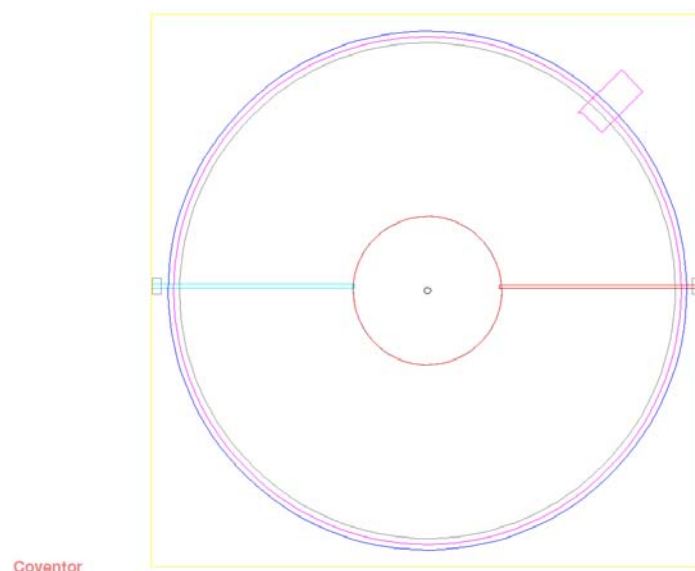


**Figure 3.26:** *The layout of the CMUT.*

In short, the objective of this study, which is to investigate, design and implement CMUT device for measuring foot-to-ground clearance is achieved. An ultrasound transducer capable of transmitting and receiving signal frequency of 0.93 MHz that can theoretically measure up to 30 cm with sub-millimeter range in linear fashion is successfully designed and implemented.

### **3.8 Chapter Summary and Discussion**

Three most suitable distance measurement techniques are studied and presented for consideration towards realization of a MEMS based foot clearance sensing device. They are firstly optimized for MEMS according to the MEMS technology requirement, in aspects such as structural materials and size. They are then evaluated in terms of suitability for foot clearance measurement application by means of maximum distance and linearity simulations.

The requirements for gait analysis application are also presented and used as the guidelines for the selection. The analysis of the simulation results and comparisons with the measured data in literature are also included. Ultrasound-based distance measurement technique is preferred due to its proven practical use in similar other applications and also due to good simulation results in terms of maximum foot clearance that can be measured. In addition, it is also generally showing linear relationship between clearance and TOF signal.

Various ultrasound generation and sensing mechanisms such as piezoelectric and capacitive are studied. The selection of sensing mechanism is based on aspects of fulfilment of gait analysis needs, competitiveness of manufacturing cost and capability for total integration with circuitry for performance and system miniaturization. Among the gait analysis needs include small size, light weight and suitable range. In addition to dependency of sensing range on signal frequency, the measureable range is also dependent on signal strength, so, the right choice of electromechanical coupling factor is important when biasing the CMUT. This characteristic offers an additional flexibility in terms of range and power management.

As a result, a CMOS compatible CMUT realization is chosen and explored. This includes the design requirement and specification, mathematical analysis, computer simulation and finally design implementation of a CMOS compatible CMUT tailored for ultrasonic foot clearance measurement. All results pertaining to various steps are presented and discussed. Some key parameters of the CMUT are also included.

In addition to the many device related advantages inherited from the use of CMUT technology, the system level strengths, such as signal processing, will be further enhanced due to its CMOS compatibility. The literature proves that CMUT dedicated CMOS circuits such as for signal processing is already studied and developed (Wygant et al.,2004). The inclusion of sensors, signal processing and compensation circuitry, memory and wireless communication capability in one chip as an SoC may produce a high performance ultrasonic system (Svilainis & Dumbrava,2005; Schweinzer & Elmer,2005).

In short, the objective of the study which is to explore MEMS applicability for the measurement of foot-to-ground clearance has been achieved and demonstrated. A suitable technique is identified, and as a result, an ultrasonic transducer suitable for foot clearance measurement system is fully designed, modelled, and implemented. The transducer/sensor is optimized for gait analysis application. As it is CMOS compatible, further works on CMOS circuitry will enable system level integration for the realization of an integrated high performance system for foot clearance measurement.

## Foot Pressure Sensor on Silicon

## CHAPTER

# 4

- 4.0 List of Publications Produced From This Chapter
- 4.1 Chapter Overview
- 4.2 Design Specification
- 4.3 Fabrication Options and Requirement
- 4.4 Sensor Design – Mathematical Modelling and Simulation
- 4.5 Sensor Design – Silicon Modelling and Simulation
- 4.6 Sensor Design – FEA Modelling and Simulation
- 4.7 Sensor Design – System Modelling and Simulation
- 4.8 Sensor Design – System Optimization and Simulation
- 4.9 Sensor Design – Overall Results
- 4.10 Sensor Design – Silicon Implementation
- 4.11 Chapter Summary and Discussion

### 4.0 List of Refereed Publications Produced From This Chapter

1. Wahab, Y., Zayegh, A., Veljanovski, R. and Begg, R.K. 2008, 'Micro-sensor for foot pressure measurement,' in **Proceedings of IEEE Region 10 Conference (TENCON 2008)**, IEEE Inc., Hyderabad, India. pp.1-5. ISBN 978-1-4244-2408-5.
2. Wahab, Y., Zayegh, A., Begg, R. and Veljanovski, R. 2008, 'Sensitivity optimization of a foot plantar pressure micro-sensor,' in **Proceedings of IEEE International Conference on Microelectronics (ICM 2008)**, IEEE Inc., Sharjah, UAE. pp. 104-107. ISBN 1-4244-2370-5.
3. Wahab, Y., Zayegh, A., Veljanovski, R. and Begg, R.K. 2008, 'Modeling and Simulation of Micro-Electro-Mechanical System Pressure Sensor for Biomechanical Application,' in **Proceedings of Int. Conf. Modeling and Simulation (MS 2008)**, AMSE, Jordan, pp. 49-54. ISBN 978 995 786 430 9.
4. Wahab, Y., Zayegh, A., Veljanovski, R. and Begg, R.K. 2008, 'Design of MEMS biomedical pressure sensor for gait analysis,' in **Proceedings of IEEE International Conference on Semiconductor Electronics**, IEEE Inc., Johor Bahru, Malaysia, pp.166-169. ISBN 978-1-4244-3873-0.

## 4.1 Chapter Overview

As discussed in Chapter 2, the monitoring of foot plantar pressure during gait and while performing other activities of daily living is crucial in screening for high risk diabetic foot ulceration, design of orthotics for pressure redistribution of diabetes mellitus and peripheral neuropathy patients, design of footwear (Mueller,1999), determination and improvement of balance (Santarmou et al.,2006; Bamberg et al., 2006), sports injury prevention in athletes (Gefen, 2002) etc. While the current conventional measurement devices that are in use are not capable of performing the task in an efficient way, a new instrument is obviously in dire need. To ensure that the foot plantar pressure is measured effectively, the new device must fulfil these basic requirements which include pressure range, optimal size, very light, unobtrusive, low power, and can be integrated with signal processing and also memory. For that reason, MEMS technology is the best platform for implementation as it exhibits all the required traits as mentioned. To achieve the target, this research explores the possibility of realizing such measurement using MEMS compatible foot plantar pressure sensing technique. However, there are several questions that require answering and a number of milestones that need to be achieved for the real implementation to be successful. In this chapter, the actual work and its milestones, challenges and the chosen solutions are presented and discussed in detail.

This chapter encompasses activities towards silicon implementation. The chapter is divided into twelve sections inclusive of this overview. The sections' names, in **bold**, and their respective contents are briefly explained in the next paragraph.

### **List of Refereed Publications Produced From This Chapter**

(previous section), **Chapter Overview** (this section), **Design Specification** is contained with the discussion on the design specification for the pressure sensor, **Fabrication Options and Requirement** discusses fabrication related matters such as foundry selection and cost, **Sensor Design – Mathematical Modelling and Simulation** explains the key components of the sensor, the mathematical model and analysis, **Sensor Design – Silicon Modelling and Simulation** is where the fabrication process on silicon is modelled and the resulting three dimensional silicon model described in detail, **Sensor Design – FEA Modelling and Simulation** is where the discussion on partitioning of the three dimensional silicon model and finite element analysis are performed, **Sensor Design – System Modelling and Simulation** discusses the overall pressure sensing system finite element analysis simulation works and the obtained results, **Sensor Design – System Optimization and Simulation** is where a discussion on a series of sensor system simulation, optimization and results is given, **Sensor Design – Overall Results** presents the overall results, and lastly **Chapter Summary and Discussion** discusses and summarises the achievements of the foot pressure sensor implementation.

## **4.2 Design Specifications**

As discussed in detail in Chapter 2, Section 2.2.3, an uninterrupted measurement of gait parameters can be performed if the sensor in use is flexible, thin, easy to use, cost effective, and finally must ideally be unobtrusive. Performance wise, it should exhibit acceptable linearity, low hysteresis, low creep (drift), low temperature sensitivity for the range of 20°C

to 37°C of operation and repeatability of readings (Lee et al., 2001). MEMS technology is thus the best answer.

As a matter of fact, MEMS sensors are proven to be able to miniaturize many mechanical structures while displaying negligible mechanical hysteresis. In terms of linearity, piezoresistive sensing technique exhibits excellent performance and thus requiring simple signal processing that makes it even more practical. In terms of pressure range, to ensure compatibility with most of gait related measurement as discussed in Section 2.2.3.2 and 2.2.3.3 in Chapter 2, a target of 3000 kPa is adopted here. Dimension wise, it is this research's aim that sensor size of no larger than 5 mm X 5 mm is to be developed. Frequency wise, the sensors should be designed to perform well for operation at 200 Hz or higher (Urry, 1997).

The structure of the sensor is as depicted in Figure 4.1. Sensing piezoresistors are normally connected as Wheatstone bridge elements and can be either buried or placed on the surface of the membrane. The determination and justification of values of the key parameters of the sensor, as shown in Figure 4.1, are explained in detail in the subsequent sections. A piezoresistor's dimensions will normally include values for its width and length while its location is normally at places of high stress within the membrane or near the membrane edges.

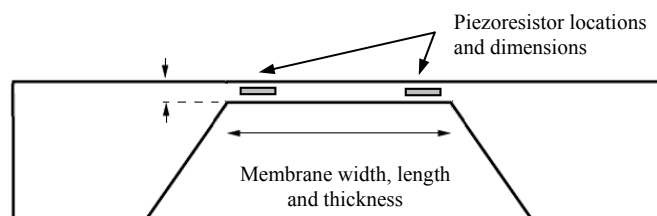


**Figure 4.1:** A conceptual design of a MEMS pressure sensor in a cross-sectional view.

During device operation, the measurand, specifically pressure, pushes the bottom surface of the membrane so that the membrane deflects according to its magnitude. As the membrane is embedded with a Wheatstone Bridge of piezoresistors aligned in such a way that the output voltage vary proportionally with membrane deflection, the relationship of the applied pressure magnitude and its voltage representation can be characterized for use in real measurements.

### 4.3 Fabrication Options and Requirement

The Infineon Technologies SensoNor AS MPW arm, MultiMEMS, is a proven silicon sensor technology company. The MultiMEMS MPW service offers bulk micromachining silicon MEMS technology with infused piezoresistive transduction mechanism. Options of membrane thickness of either 3.1 $\mu\text{m}$  or 23.1 $\mu\text{m}$  are available. The wafers with <100> crystal orientation are used (MultiMEMS, 2007). The design and process modeling and simulations involve the use of MultiMEMS design kit provided through Coventor Inc. as tool vendor. However, individual user organization license is required for use of the process technology in Coventorware<sup>TM</sup> 2006. The process is in-built in the Coventorware<sup>TM</sup> Process Editor module's Foundry Database. Most of the simulations, modelling and concurrent optimization are performed in the Coventorware<sup>TM</sup> Designer, Analyzer and Architect modules. The Infineon Technologies SensoNor AS fabrication technology definition is kept in the Materials Properties Database and Foundry Database of the tool.

## 4.4 Sensor Design – Mathematical Modelling and Simulation

### 4.4.1 Methodology

Firstly, the shape is determined based on the piezo-resistance sensing requirement. Based on literature, square shape membrane is capable of providing high stress areas, as high as 1.64 times as compared to a circular one (Berns et al., 2006). Mathematical modeling is the first major step of the design with an aim of determining the membrane thickness and side length that can perform pressure measuring task for the specified range. The values of its thickness, length and width must allow linear membrane deflection within the pressure range while ensuring no mechanical damage or fracture.

So, it is highly crucial that the effect of membrane thickness and membrane size on the pressure induced membrane deflection and membrane stress is thoroughly studied at the initial stage. As the output of the sensor is highly dependent on the deflection characteristic parameter and resistance change parameter, the output voltage linearity is thus affected by both parameters too. According to the foundry design guidelines (MultiMEMS, 2007), the piezoresistance change and stress relationship is governed by the linear equation given in (1). On the other hand, equations (2) and (3) relate piezoresistor stresses to the applied pressure in small deflection regime (Gong & Lee, 2001). In these equations,  $R$  and  $R_o$  are the piezoresistor's resistance value when external pressure is applied and the piezoresistor's resistance without any applied pressure respectively,  $\Pi_L$  and  $\Pi_T$  are the piezoresistance coefficient for longitudinal and transversal directions

respectively,  $h$  is membrane thickness,  $L$  is membrane edge length,  $e_m$  is the  $m$ -th coefficient as given by Gong & Lee (2001) and listed in Table 4.1,  $\nu$  is Poisson ratio,  $l_p$  is piezoresistor's length,  $\sigma_T$  is the average transversal stress across the piezoresistor and  $\sigma_L$  is the average longitudinal stress along the piezoresistor. The stress components are shown in Figure 4.2.

$$R = R_0(1 + \Pi_L \sigma_L + \Pi_T \sigma_T) \quad (1)$$

$$\sigma_T = \frac{-48}{\pi^4} P \left(\frac{L}{h}\right)^2 \left(\frac{L}{l_p}\right) \sum_{m=1,3,5}^{\infty} \frac{e_m}{m} (-1)^{\frac{m-1}{2}} \sin\left(\frac{m \pi l_p}{2L}\right) \quad (2)$$

$$\sigma_L = \nu \sigma_T \quad (3)$$

TABLE 4. 1. VALUES OF  $E_M$  COEFFICIENTS

PARTICULARS	VALUES
$e_1$	-0.372
$e_3$	0.0379
$e_5$	0.0175

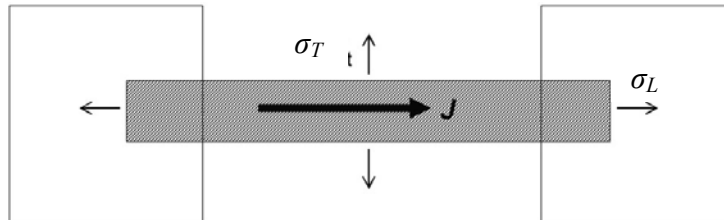


**Figure 4.2:** Transversal and longitudinal stresses acting on a piezoresistor with respect to the current flow direction  $\mathbf{J}$  (Zamali & Talghader, 2006).

The importance of membrane deflection lies on the fact that since the resistance change due to deflection is already linear in nature, the deflection characteristic therefore becomes the sole determining factor for the linearity of the sensor output. It is reported that the magnitude of membrane deflection is linear with the applied pressure when the deflection is still in the small

deflection regime. The membrane is said to operate in this regime as long as the deflection is less than 25 to 50 % of its thickness (Wang et al., 2005, Gong & Lee 2001). For comparison, two equations representing the applied pressure and square membrane deflection are given in equation (4) and (5) (Linlin, Chen & Guangdi, 2006). The former equation is for small deflection regime while the latter represents the large deflection regime. Maier-Schneider, Maibach & Obermeier (1995) also reported large deflection relationship in even more detail, complete with its derivation. As can be seen, the small deflection equation represents a linear relationship, as opposed to the non-linear cubic equation for large deflection. In these equations, in addition to the previously defined symbols,  $\nu$  is Poisson ratio,  $a$  is half of edge length,  $\sigma_0$  is the intrinsic stress of the membrane,  $E$  is the Young's Modulus and  $w_0$  are the maximum deflection of the membrane.

$$P = \left( 3.41 \frac{h \sigma_0}{a^2} + 4.31 \frac{Eh^3}{a^4(1-\nu^2)} \right) w_0 \quad (4)$$

$$P = 3.04 \frac{h \sigma_0}{a^2} w_0 + 1.88 \frac{Eh}{a^4} w_0^3 \quad (5)$$

In addition to the linearity requirement, the mathematical analysis is also important in determining another key design specification, namely maximum pressure measurable. This is due to the fact that the magnitude of total membrane stress determines the maximum pressure value that the membrane may be able to withstand, beyond which the membrane breaks. For that reason, the point of rupture which is also known as Fracture Stress must be taken into account in the determination of suitable membrane dimension. Therefore, the relationship between membrane dimensions and its deflection and stress is extensively analyzed.

Next, the relationship between the applied pressure,  $P$ , and maximum membrane deflection,  $w_0$ , as modeled by equation (6) (Peters et al., 2002), is used to identify the suitable thickness and size. The reason why this equation is used instead of equation (4) and (5) is due to its independence from the small and large deflection regimes definition. In this step, equation (10) is also used as it relates the maximum deflection and the resulting total membrane stress,  $\sigma_{TM}$  so that the maximum pressure the membrane is able to withstand can be identified (Linlin, Chen & Guangdi, 2006). Equation (6) requires a numerical solution and  $N$ ,  $\alpha$  and  $\gamma$  can be calculated using equations (7), (8) and (9).

$$1.935 a^2 P = (234.156 \frac{N}{2} \alpha + 46.988 \frac{D}{4a^2} + 6.671) w_0 - 289.97 \frac{Eh}{8a^2} \gamma w_0^3 \quad (6)$$

$$N = \frac{\sigma_0 h}{1 - \nu} \quad (7)$$

$$\alpha = \frac{(\nu - 17.148)^2}{(71.837 - 4.189\nu)^2} \quad (8)$$

$$\gamma = \frac{(\nu - 17.148)(\nu - 6.236)(\nu + 1.421)}{(71.837 - 4.189)^2 (\nu^2 - 1)} \quad (9)$$

$$\sigma_{TM} = 0.864 \frac{Eh^2}{a^2} \left( \frac{w_0}{h} \right)^2 + 6.5 \frac{Eh^2}{a^2} \left( \frac{w_0}{h} \right) + \sigma_0 \quad (10)$$

The inclusion of intrinsic stress,  $\sigma_0$  is crucial as the silicon material might be exposed to stress inducing processes. Two key limiting stress components are used to identify if a membrane is nearing its point of rupture or not. They are the foundry maximum stress rule (MultiMEMS, 2007) and the theoretical silicon Fracture Stress. If the total stress surpasses these stress points, the structure may be broken, theoretically. However, out of the two key stress

components, the foundry maximum stress rule is quite straight forward. According to MultiMEMS (2007), as long as the design adheres to the conditions as listed in the Table 4.2, the design complies with the foundry stress rule. For that reasons, only designs that comply with the Table 4.2 rules are explored.

TABLE 4. 2. FOUNDRY SPECIFIED MAXIMUM SIZE FOR SQUARE MEMBRANES

PARTICULARS	MEMBRANE WIDTH/LENGTH
THIN MEMBRANE 3.1 $\mu\text{m}$	430 $\mu\text{m}$
THICK MEMBRANE 23.1 $\mu\text{m}$	3480 $\mu\text{m}$

In the mathematical analysis, 12 different membrane designs are studied involving two membrane thicknesses as shown in Table 4.3. For the membrane of the thickness 3.1  $\mu\text{m}$ , the square membrane side lengths of 10  $\mu\text{m}$ , 25  $\mu\text{m}$ , 50  $\mu\text{m}$ , 100  $\mu\text{m}$ , 200  $\mu\text{m}$  and 300  $\mu\text{m}$  are analyzed. The thicker 23.1  $\mu\text{m}$  membranes of side lengths 50  $\mu\text{m}$ , 100  $\mu\text{m}$ , 200  $\mu\text{m}$ , 300  $\mu\text{m}$ , 500  $\mu\text{m}$  and 1000  $\mu\text{m}$  are also included in the analysis.

TABLE 4. 3. PARAMETERS OF SELECTED SQUARE SENSORS DESIGN

SENSOR	P1	P2	P3	P4	P5	P6	P7	P8	P9	P10	P11	P12
SIZE	10	25	50	100	200	300	50	100	200	300	500	1000
THICKNESS	3.1	3.1	3.1	3.1	3.1	3.1	23.1	23.1	23.1	23.1	23.1	23.1

The values for calculation are Young's Modulus,  $E = 152$  GPa, Poison's ratio,  $\nu = 0.3$  and intrinsic stress,  $\sigma_0 = 65$  MPa, taken from (Linlin, Chen & Guangdi, 2006).

#### 4.4.2 Results

##### *Membrane Response to External Pressure*

The mathematical analysis is performed on each of the design. Modeling result observation is focused towards the key membrane response characteristic such as the linearity of deflection and pressure relationship and the applied pressure values when the points of Fracture Stress are reached.

Using the relationship derived by Peters et al.(2002), the deflection profile of the membranes are analyzed covering both small and large deflection regimes. Figure 4.3 and Figure 4.4 shows the pressure and deflection relationship for 23.1  $\mu\text{m}$  and 3.1  $\mu\text{m}$  thick square membranes respectively. As can be seen, the relatively larger membranes exhibit more obvious nonlinearity as compared to the smaller ones. Observing the thickness factor, thinner membrane exhibits higher nonlinearity as compared to thicker ones of similar size. It is obvious that larger sized membranes and thinner membranes are more flexible than the smaller and thicker membranes. This is due to the fact that these structures have less flexural rigidity values, which is a measure of structural stiffness.

Another important observation is that among the thick membranes, membranes smaller than or around 300  $\mu\text{m}$  can be selected for silicon realization. On the other hand, among the thin membrane ones, membranes smaller than or around 50  $\mu\text{m}$  may be suitable for implementation.

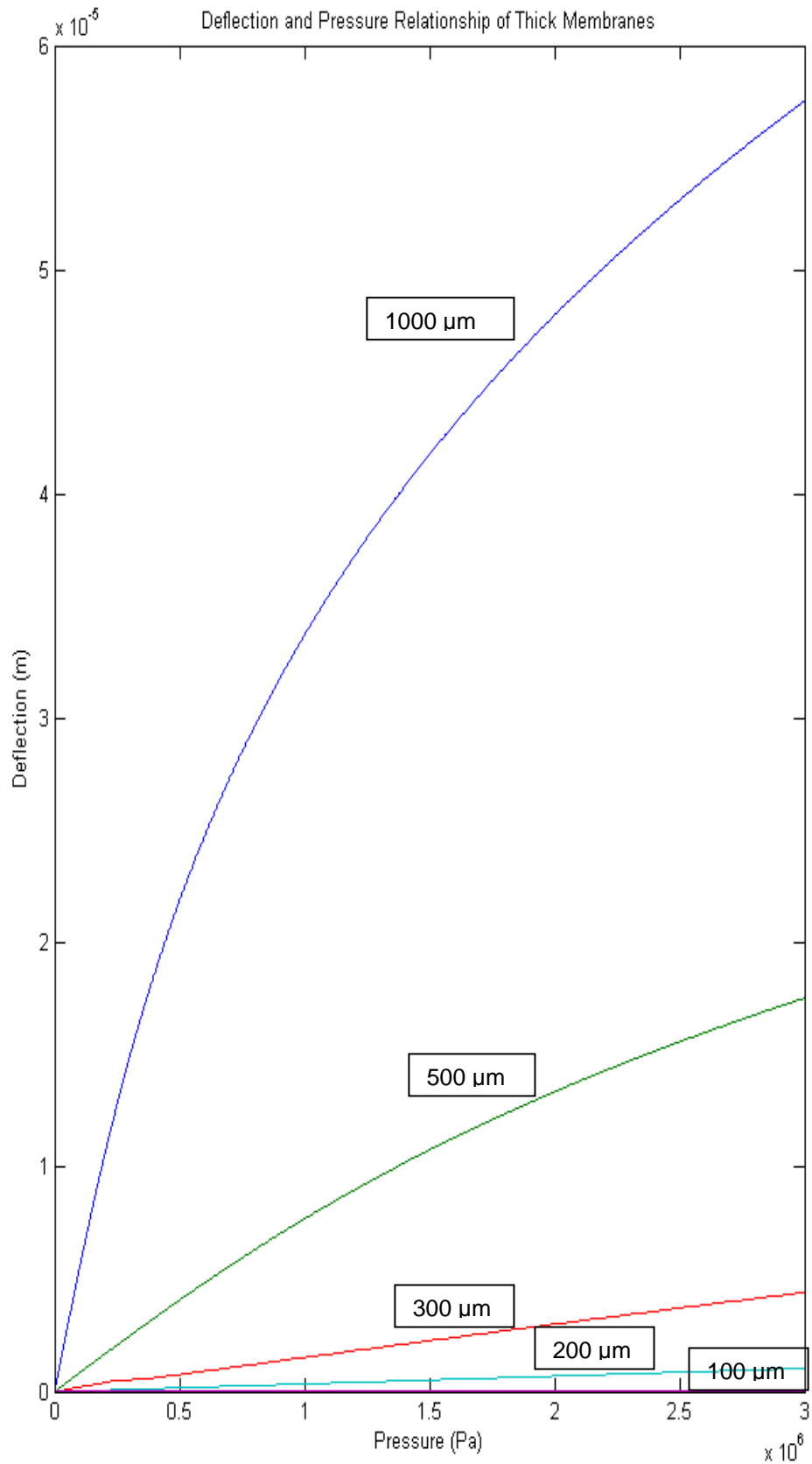


**Figure 4.3:** The Pressure versus Membrane Deflection of thick membranes.

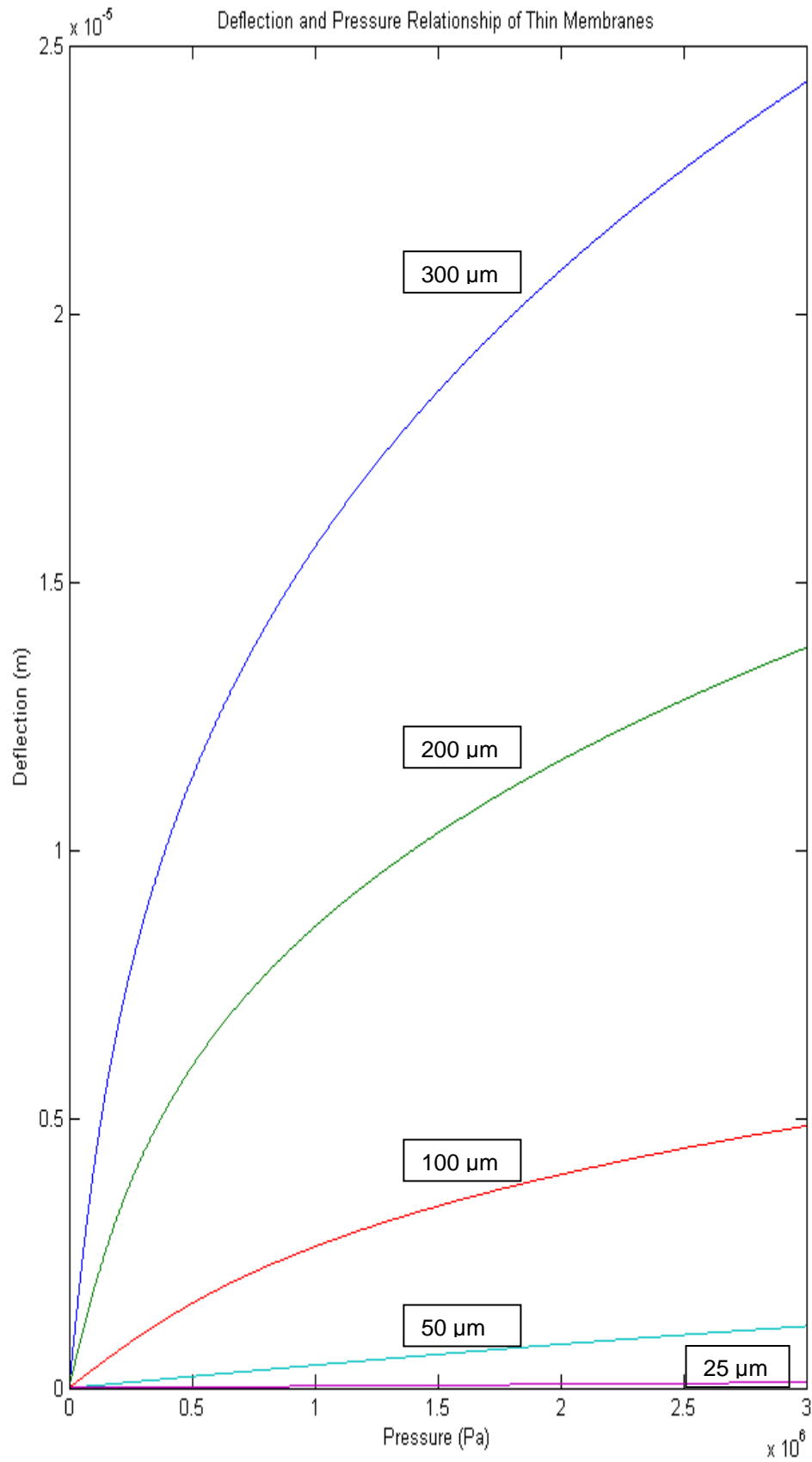


**Figure 4.4:** The Pressure versus Membrane Deflection of thin membranes.

Next, using the stress equation (10) proposed by Linlin, Chen & Guangdi, (2006), stress analysis is performed considering the key material physical characteristic, the fracture stress, and the results are shown in Figure 4.5. It is interesting to see that there is a point where the response to pressure is converged when the square membrane size is increased. As can be seen, it seems that for both thicknesses, the fracture stress is reached at around 3 MPa of applied pressure for larger sized membranes. This mathematical approximation helps in understanding the effect of membrane thickness and size on the pressure sensor capability.

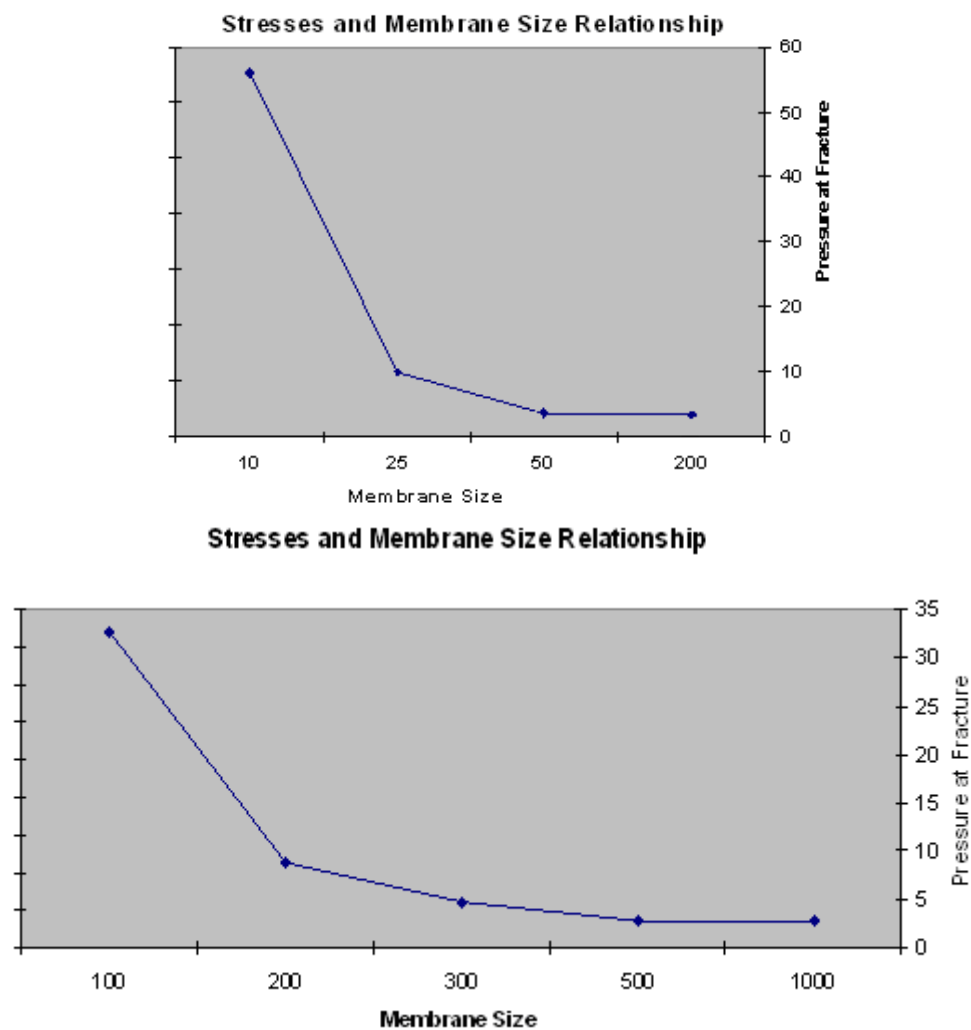


**Figure 4.5:** The convergence of stress and dimensional relationships for (Top) 3.1 μm and (Bottom) 23.1 μm membrane in MPa unit.

### *Overall Mathematical Result*

The use of mathematical model is beneficial in terms of obtaining the basic idea about how the membrane stress is related to dimension. According to the result as shown in Figure 4.5, the thin membrane designs should be made very small as compared to the thicker membrane ones. However, there should be a minimum limit of membrane size, as far as foundry design rules are concerned (MultiMEMS, 2007). However, there is no direct information about minimum membrane size in the literature. To identify this key determining factor, the foundry design rules are analyzed and relevant mathematical model is developed in this research so that it can be better understood and to ensure realization of practically achievable designs.

Using the design features which only use surface piezoresistors and surface conductors, a basic layout is produced to model the foundry rule based membrane minimum size limitation. In Figure 4.6, membrane area is defined by the red square which covers most of the area in the layout. Orange coloured features represent the surface conductors while piezoresistors are indicated by green rectangles. In this design, there are four membrane size determining factors shown, namely, drawn feature minimum width and length,  $L_{MIN}$ , non-contiguous surface conductor minimum separation,  $S_C$ , minimum overlapping of surface conductors and surface resistors,  $C_{CR}$ , and minimum margin between the surface conductor sides and surface resistor sides,  $M_{CR}$ . The arrows in the Figure 4.6 are used to show the locality of the minimum dimension factors. Considering the horizontal axis, the minimum membrane side length,  $SIZE_{HORIZ}$ , should be modeled with equation (11) while the one for vertical axis,  $SIZE_{VERT}$ , is represented by equation (12).

$$SIZE_{HORIZ} = 4L_{MIN} + 3S_C + 4M_{CR} \quad (11)$$

$$SIZE_{VERT} = 4C_{CR} + 3S_C + 2M_{CR} \quad (12)$$

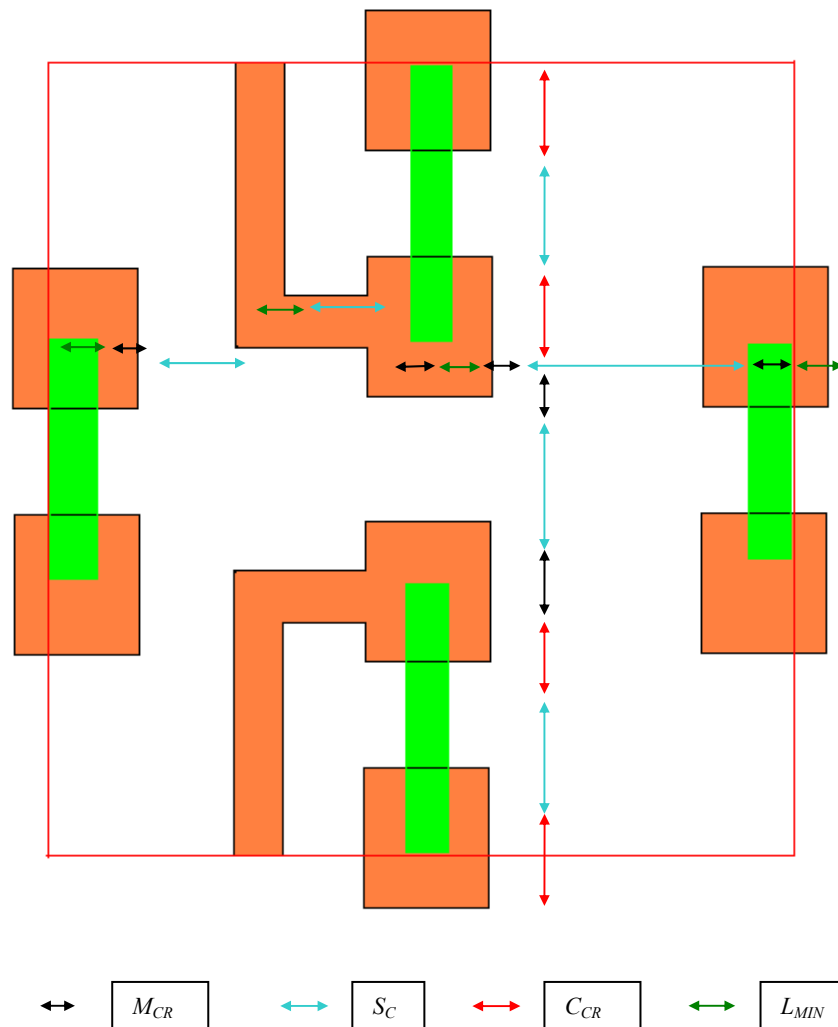
According to the process description (MultiMEMS, 2007),  $L_{MIN} = 4 \mu\text{m}$ ,  $S_C = 6 \mu\text{m}$ ,  $C_{CR} = 5 \mu\text{m}$  and  $M_{CR} = 5 \mu\text{m}$ . Using (11) and (12) together as an approximation tool for determination of the minimum membrane size suitable for fabrication in Infineon Technologies SensoNor AS, Table 4.4 is produced showing the minimum limits of membrane size.

TABLE 4. 4. MIMIMUM MEMBRANE SIDE LENGTHS

PARTICULARS	$SIZE_{HORIZ}$	$SIZE_{VERT}$
MINIMUM SIZE	54 $\mu\text{m}$	48 $\mu\text{m}$

Based on the mathematical modeling and analysis, the theoretically suitable design can be identified which is bound by the foundry rule inferred minimum membrane size. Therefore, it can now be concluded that the membrane design space is practically bounded by the foundry stress rule as shown in Table 4.2 on the maximum side and the foundry design rule as shown in Table 4.4 sets the minimum side. Considering the values given in Table 4.4 and the graph of maximum total stress in Figure 4.5, the thin membrane designs should be avoided. This is due to the fact that the minimum size that a membrane should be designed, according to Table 4.4 is about 50  $\mu\text{m}$ , but unluckily, according to Figure 4.5, for thin membrane designs, the membranes of the size 50  $\mu\text{m}$  or larger may only withstand pressure of up to around 3 MPa. Most of thin membranes of that size range also exhibit membrane deflection non-linearity, as can be seen in Figure 4.4.

Now, considering 3 MPa as the maximum pressure limit, the deflection linearity analysis result of Figure 4.3 and stress withstanding capability analysis result of Figure 4.5, suggests that the thick membranes should be designed at maximum size of around 300  $\mu\text{m}$ . Considering the foundry design rule based minimum membrane size modeling result, the minimum membrane size of around 50  $\mu\text{m}$  must be obeyed. Therefore, the design space for membrane size of the pressure sensors should be limited to be between 50  $\mu\text{m}$  to 300  $\mu\text{m}$ .



**Figure 4.6:** A simple layout for the membrane design to model the minimum size requirement.

## 4.5 Sensor Design – Silicon Modelling and Simulation

### 4.5.1 Methodology

After extensive mathematical analysis, the final designs are then determined which consists of only thick membranes. This is due to their compliance with the physical design requirements as identified in the stated foundry maximum size limits, the derived foundry rule based minimum size limit, deflection linearity modelling result and stress withstanding capability modelling result. Finally, only few membrane sizes are chosen to be modeled in silicon.

These selected designs include the ones using 100  $\mu\text{m}$ , 200  $\mu\text{m}$  and 278  $\mu\text{m}$  membranes. Out of the three sensors, the 100  $\mu\text{m}$  sized sensor is the one that can measure wider pressure range, but with less sensitivity and signal magnitude. Whereas, the 200  $\mu\text{m}$  and 278  $\mu\text{m}$  ones are also designed and simulated for comparison and further studies purposes Silicon modeling involving the use of MultiMEMS processes is implemented in Coventorware™ and the three dimensional models are generated for performance analysis. The simplified process sequence is presented in Figure 4.7 and Figure 4.8.

In using the process steps to model the devices, it is necessary to perform the three model design stages. These stages includes identification of key structural layers required for successful and effective implementation of finite element analysis, layout specifications of the required layers and finally meshing design requirement.

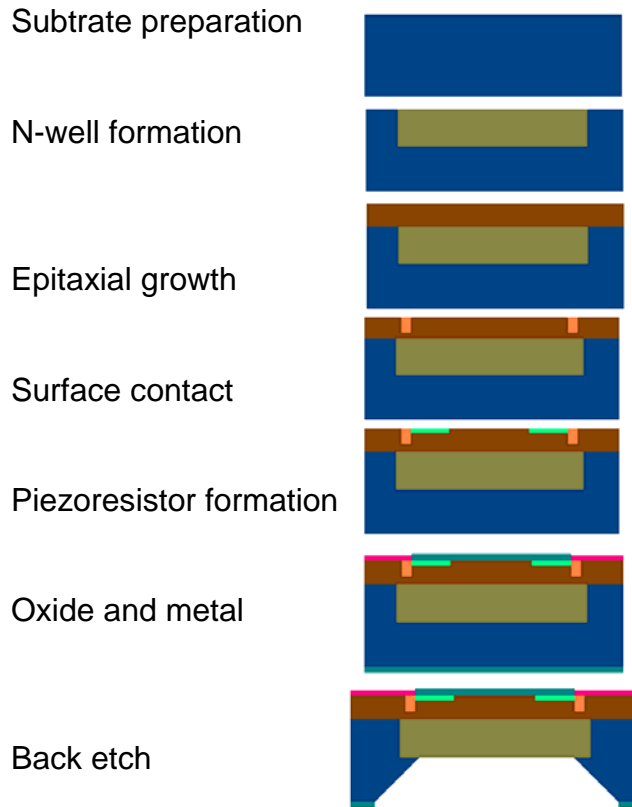


**Figure 4.7:** The simplified process sequence showing conceptually how the device is formed.

Number	Step Name	Action	Layer Name	Material Name	Thickness
0	Substrate	Substrate	Substrate	SILICON_100	399.1
1	Implantation Nwell	Sequence			
1.1	Implantation NWEELL Step 1	Straight Cut			
1.2	Implantation NWEELL Step 2	Planar Fill	Nwell	SILICON_100	0
2	Epitaxial Growth - Part 1	Stack Material	Epi1	SILICON_100	2.3
3	Implantation Buried Resistors	Sequence			
4	Epitaxial Growth - Part 2	Stack Material	Epi2	SILICON_100	0.8
5	Implantation Surface Conductors	Sequence			
5.1	Implantation SUCON Step 1	Straight Cut			
5.2	Implantation SUCON Step 2	Planar Fill	surface_conductor	SURES	0
6	Implantation Surface Resistors	Sequence			
6.1	Implantation SURES Step 1	Straight Cut			
6.2	Implantation SURES Step 2	Planar Fill	surface_resistor	SURES	0
7	Thin Oxide	Sequence			
8	Metal Conductors	Sequence			
9	Anisotropic Wet Etch - Backside	Straight Cut			
10	Insulating Oxide Etch	Straight Cut			
11	Anodic Bonding Top Glass	Sequence			
12	Anodic Bonding Bottom Glass	Sequence			

**Figure 4.8:** The simplified process sequence as extracted from the Coventorware™ process design tool.

In identifying the key structural layers required for successful and effective implementation of finite element analysis, it is important to understand the operational aspects of the sensing mechanism. Referring to the mathematical modeling work, the most important studies are the membrane deflection and membrane stress analysis. This is true considering the fact that they determine the maximum measurable pressure and also the linearity of the output signal. For this reason, the realizations of membrane models for each of the designs are performed at this stage. Based on this requirement, it is therefore necessary to identify the layers that make up the actual physical membrane. According to the MultiMEMS design documents (MultiMEMS, 2008), to produce a thick membrane, the layers required are the N-well layer, the epitaxial layers and the oxide layer.

Complementing the previous stage, the layout specifications design stage describes the structural features for every physical layers required in the analysis of the designs. The layout specification must be decided as they determine the final size and shape of the required layers. In executing this task, an application provided by MultiMEMS is used to obtain the key design specification of the sensor, namely, the bulk etch dimension. The application named Bulk Etch Calculator calculates the feature dimension to be drawn on the bulk etch mask for both thin and thick membrane based on the target membrane size input.

The calculation of membrane size,  $W_M$ , based on bulk etch dimension,  $W_{BE}$ , and etch depth,  $Z$ , is based on the work of Jia & Madou (2006) represented by equation (13) where the chemical reaction process that is acting on the silicon crystal surface is characterized. Once this feature

dimensions are obtained, the last stage of silicon modeling process is implemented, namely the determination of mesh design requirement. If  $H$  is wafer thickness, the resulting membrane thickness,  $h$  can be directly determined using equation (14).

$$W_M = W_{BE} - 2Z \cot(54.74^\circ) \quad (13)$$

$$h = H - Z \quad (14)$$

Meshing of a square silicon membrane is bounded by a number of rules due to its physical dimension. While most meshing type is generally producing reliable results, meshing must still be performed carefully so that the finite element analysis result is closer to reality. For a square shaped membrane that is held fixed by a frame as shown in Figure 4.9, a mapped bricks type of meshing is the most suitable option (Coventor, 2006). As mapped bricks meshing requires that the structure to be meshed have six sides, it is a necessity that the whole structure is partitioned into a number of six sided individual segments.

It is important to note that Coventorware treats different layers as different segments, therefore, this must be taken into account in partitioning the sensor. Most of the segments are in the shape of cuboid. However, the trickiest part of the partitioning process is the inner section of the p-substrate frame as shown in Figure 4.9 as a dashed line triangle and rectangle. To satisfy this complicated needs, the partitioning requirement is then modeled and analyzed in this research.

If  $L$  is set to zero, the cross-section of that region will only be of the shape of a triangle. Unluckily, the resulting three dimensional segment will never be having six sides. Therefore,  $L$  shall always be greater than zero and that the cross-section of the region shall always be the combination of the triangle and the rectangle and this combination forms a right angled trapezium instead. In three dimensions, the segment will be of a hexahedron shape. After careful analysis using Figure 4.9, equations (15) to (18) are derived and the meshing requirement is finally identified. That is, the silicon substrate must be drawn so that the edge of the silicon frame is extended outward to a distance governed by equation (17). By selecting suitable structural parameter values, the equation (18) should have been complied.

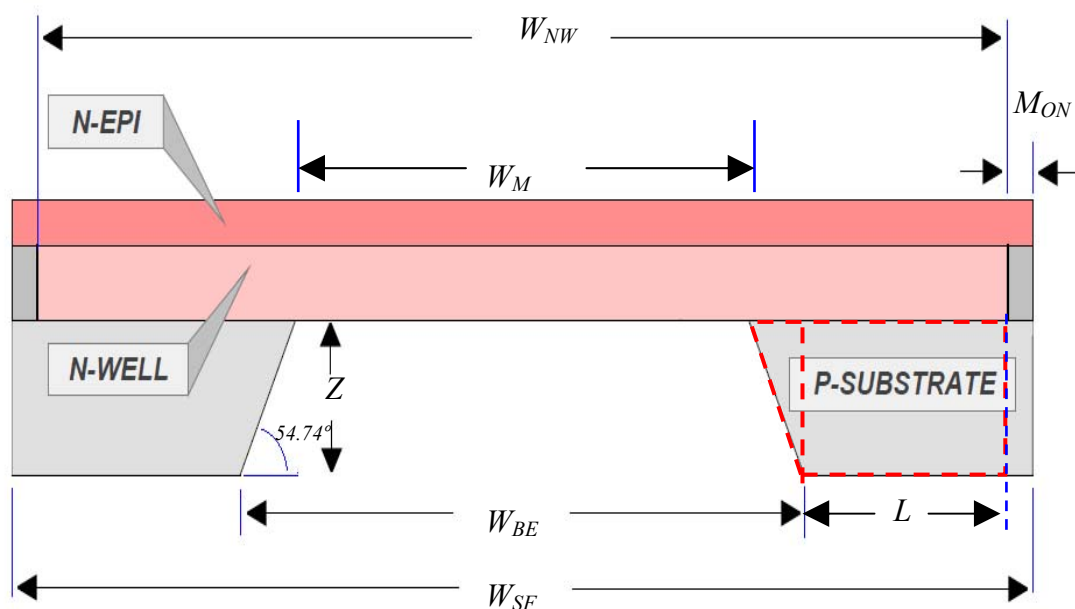


**Figure 4.9:** A cross-sectional view of the key mechanical parts of the sensor structure with definition of various structural dimension parameters.

$$W_{SF} = W_{NW} + 2M_{ON} \quad (15)$$

$$W_{NW} > W_{BE} \quad (16)$$

$$W_{SF} > W_{BE} + 2M_{ON} \quad (17)$$

$$W_{SF} - W_{BE} - 2M_{ON} > 0 \quad (18)$$

The layout of the sensor membrane is as shown in Figure 4.10 showing the key layers that are required to produce the required three dimensional sensor membrane and sensor frame. Only two mask layers are required to be drawn. They are the silicon substrate frame mask which is the outer square feature, and the bulk etch mask, which is the smaller pink coloured square. A point in the middle of the drawn features is the centre of the membrane which is also referring to the reference coordinate.

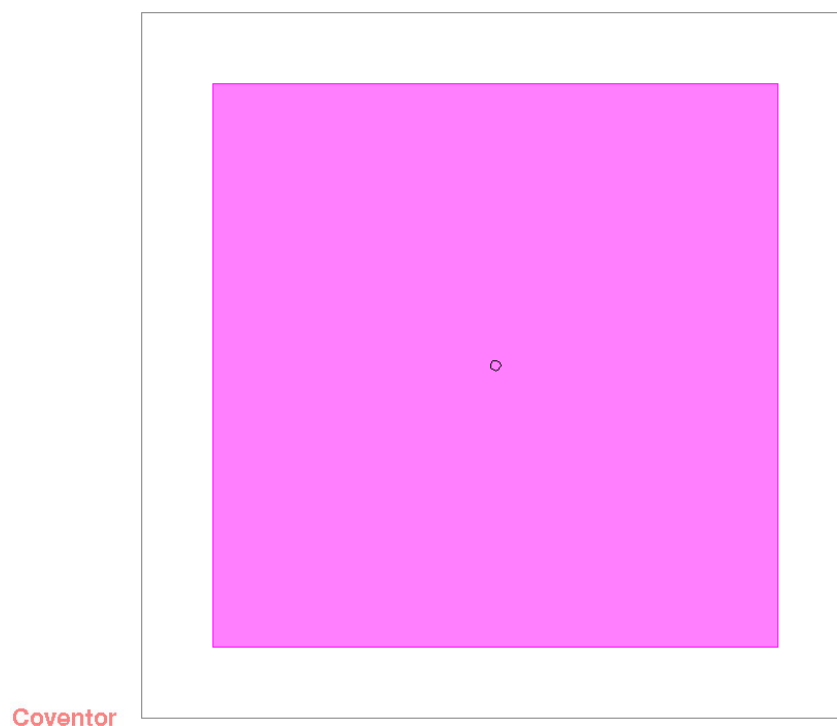


**Figure 4.10:** A layout for the realization of a membrane and its silicon frame.

#### 4.5.2 Result of Process Modelling

The output of the process modeling in three dimensional form is as depicted in Figure 4.11. The creation of the device model, in its three dimensional form is performed in Designer-Solid Modeler module with reference to the process sequence activated in Process Editor.

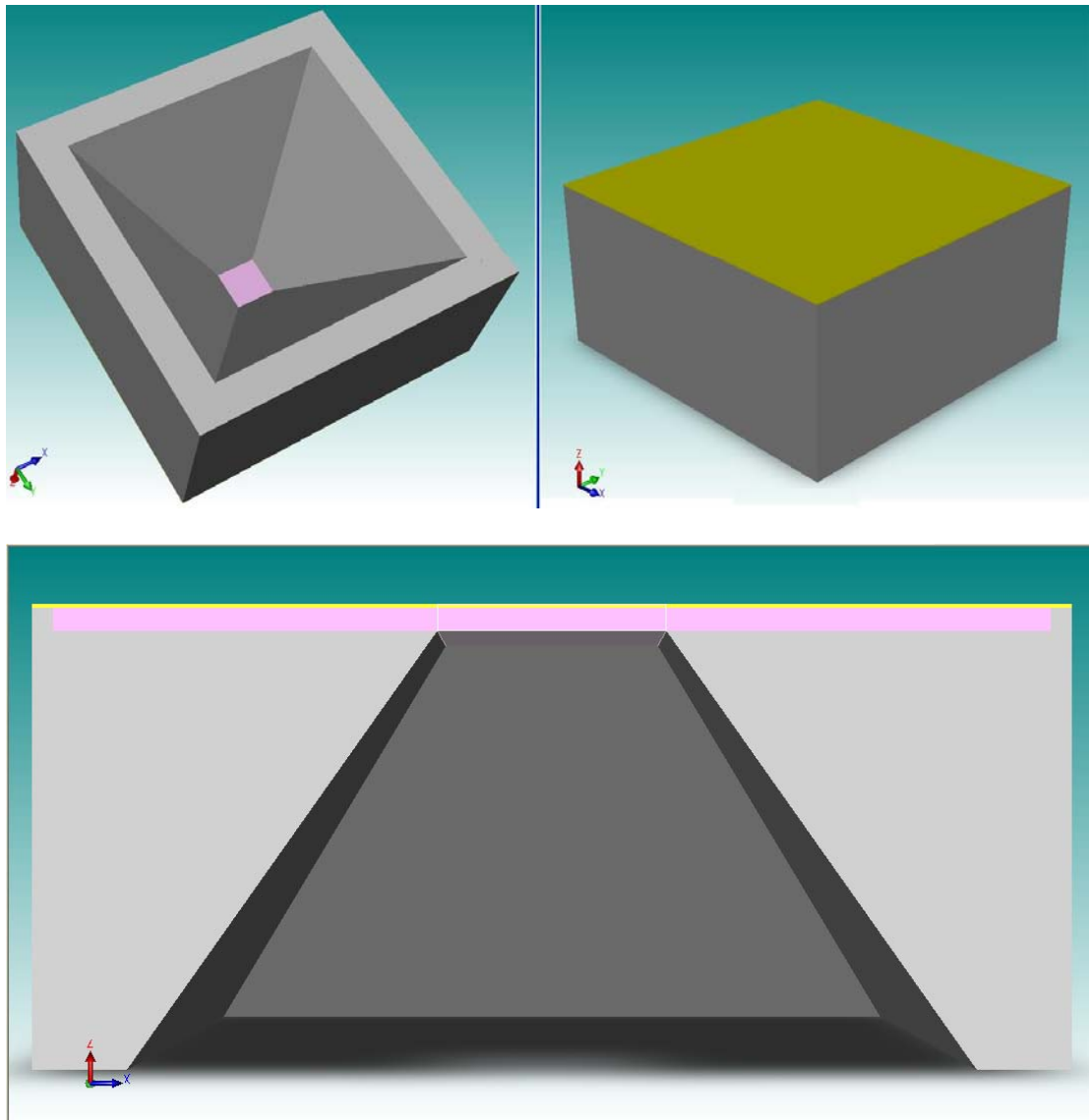


**Figure 4.11:** The yield of silicon process simulation. (Top Left) The square (pink coloured) membrane surface that receives the applied pressure, (Top Right) another view from the other side of the membrane, and (Bottom) is the device cross-section showing various layers.

## 4.6 Sensor Design – FEA Modelling and Simulation

### 4.6.1 Methodology

The model is then analyzed using Finite Element Analysis in the Analyzer module. At this stage, careful segmentation, such as the one shown in Figure 4.12 of the three dimensional sensor model is required. Due to the fact that the whole structure is made of so many layers of various sizes and shapes (as can be seen in Figure 4.11), the segmentation is a very complex task and requires very careful attention. The segmentation, or in Coventorware specific term, partitioning, into various shapes according to meshing rule of the model is critical to produce an efficient mesh throughout the model. A total of 51 segments are produced after extensive partitioning job completed. This is due to the fact that different three dimensional shapes will be suitable for different meshing styles. In Figure 4.12(d) and (e), some segments are hidden for better visualization of the layers and shapes. The product of the meshing step is as shown in Figure 4.13 in cross-section view.

The applied pressure is set in the Analyzer-MemMech settings, which is the boundary condition setting for the Finite Element Analysis (FEA). As gait produces harmonics of a certain frequency range (Urry, 1999), the natural resonant frequency of the membrane must also be identified. It is critical for gait analysis application as the harmonics may cause reading errors (Urry, 1999). The target of at least 200 Hz natural resonance frequency is examined using FEA too.

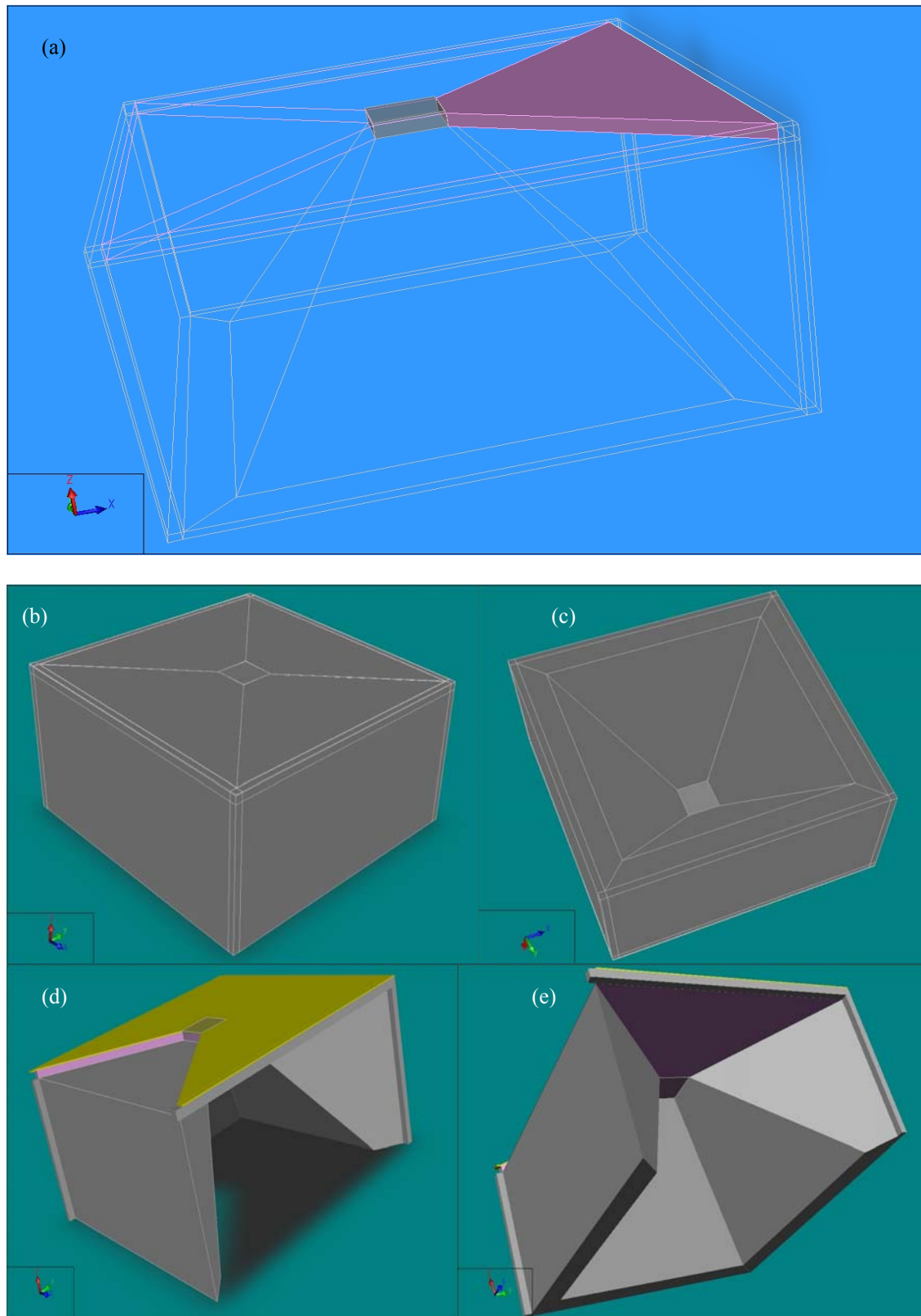


**Figure 4.12:** (a) The partitioning frame view of the developed model. (b)(c) The 3D view with partitioning lines (d)(e) The partitioned 3D model with some segments are made invisible to enable better appreciation of the various layers and segment shapes.

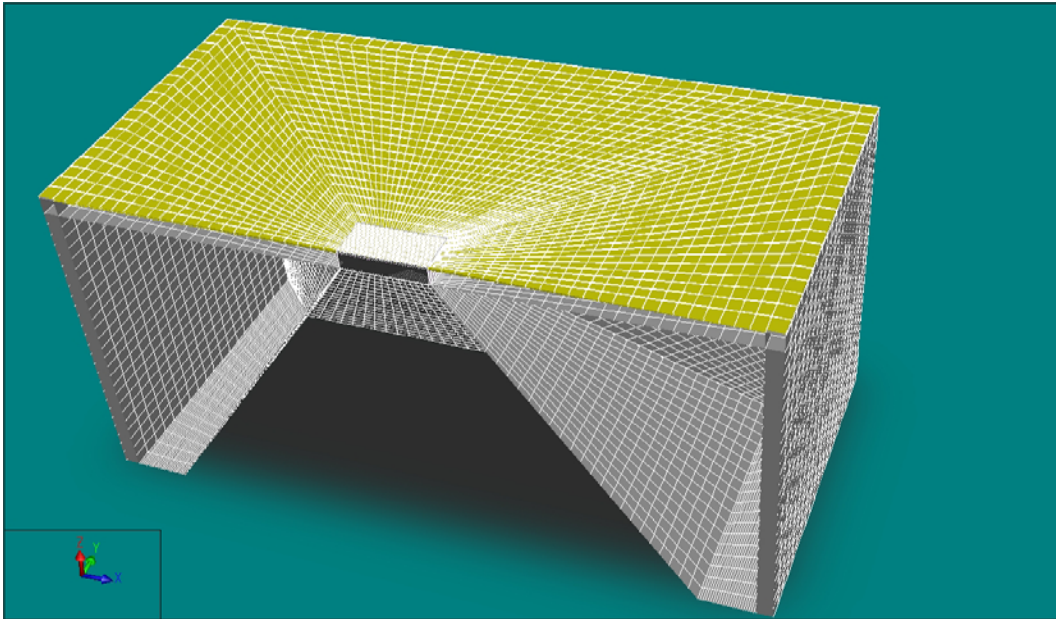


**Figure 4.13:** 3D model and its mesh. In actual design, all four corners of the model are symmetrical.

#### 4.6.2 Results of FEA

Supporting the mathematical modeling results are the more computational intensive computer based Coventorware™ results. The Von Mises stress values are considered a good indicator to determine whether a design is suitable or not (Bistue et al., 1997). As the Von Mises stress is the effective stress acting in the membrane, if the membrane Von Mises stress is more than the fracture stress, the material will break (Cardenas et al., 2007). In Figure 4.14, the stress analysis results are included to enable identification of maximum stress at any particular location on the membrane. As can be seen, the stress map is symmetrical throughout the four corners of the membrane. The Von Mises stress is observed at its maximum at the center of the membrane where deflection is at its peak. However, the value for the 100  $\mu\text{m}$  is merely 13 MPa.

The middle of the four sides of the membrane also show significant stress values of about 6 MPa. This much lower stress value shows that the design is very suitable for the targeted range and it is highly probable that in practical, even if a pressure of more than 3 MPa is applied, the membrane is still far from the risk of rupture. In another observation, the resonance frequencies of the membranes as obtained from modal analysis are in the mega-Hertz zones, putting the device in a very safe operation zone, as far as harmonics related error of gait measurement is concerned. These high resonance frequencies are expected considering the membranes thickness. The Von Mises Stress distribution for the three membrane sizes are shown in Figure 4.14 and the maximum values are given in Table 4.5. As can be seen, the magnitude of stress is very far from the fracture values for all of the sensors and this observation supports the mathematical analysis that is discussed in Section 4.4. The applied pressure is from 0 to 3 MPa and the observed stresses for the 100, 200 and 278  $\mu\text{m}$  membranes are colour coded for easy observation. The results from FEA simulation, encompassing various membrane stresses is kept in the Coventorware design database. This database can be accessed from other Coventorware modules for further analysis too. In the next section, the database is retrieved to perform a sensor system level analysis.

TABLE 4. 5. THE MAXIMUM VON MISES STRESS

SENSORS	100 $\mu\text{m}$	200 $\mu\text{m}$	278 $\mu\text{m}$
<b>VON MISES STRESS</b>	13 MPa	58 MPa	96 MPa

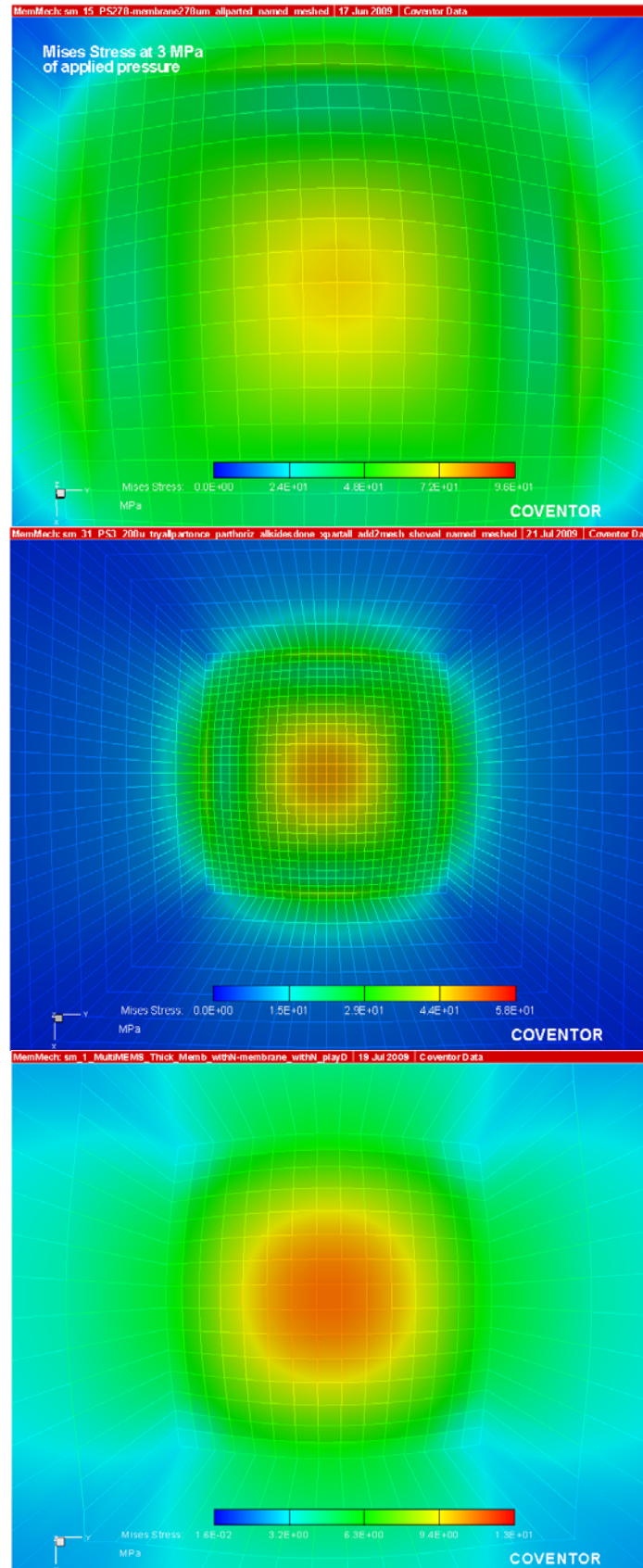


**Figure 4.14:** Mises Stress on the (Top) 278  $\mu\text{m}$  (Middle) 200  $\mu\text{m}$  and (Bottom) 100  $\mu\text{m}$  pressure sensor membranes.

## 4.7 Sensor Design – System Modelling and Simulation

### 4.7.1 Methodology

To retrieve the FEA stress result database from Architect, the set-up for the Database Vector Probe is required and the retrieved information is coupled with the Architect system level simulation. For example, in Figure 4.15, the Finite Element Analysis output of Analyzer, inclusive of the values of membrane stress and deformation due to variations of the applied pressure are retrieved and used by Architect to calculate the change in resistance for each of the piezoresistors PZR1, PZR2, PZR3 and PZR4. With this capability, many simulations can be completed in a shorter period of time and various system level manipulations of the circuit can be efficiently simulated. The larger red rectangle (dashed line) represents the membrane area while the red arrow represents the applied pressure.

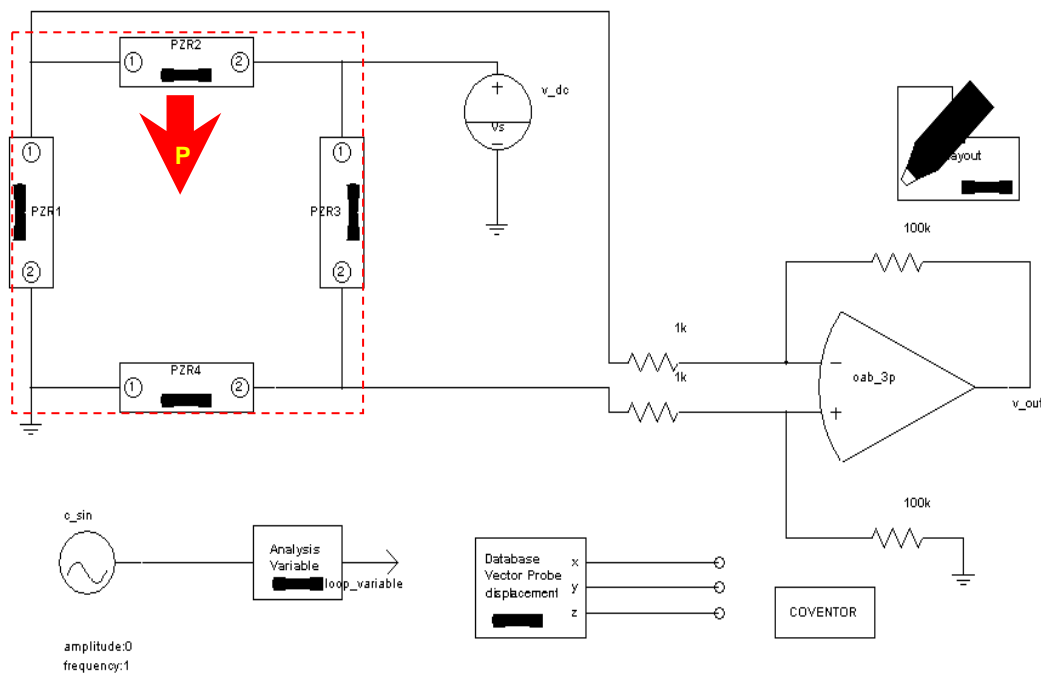


**Figure 4.15:** The system level simulation representation.

The sensing piezoresistors are aligned in the  $\langle 110 \rangle$  direction as the corresponding coefficients are maximum in that direction (Kanda & Yasukawa, 1997). The literature pointed that the regions of high stress were the best options for sensing resistor placement (Gong, 2004, Folkmer, Steiner & Lang, 1996). In this regard, a Wheatstone Bridge structure is used as shown in Figure 4.16 (Karki, 1999). The Wheatstone Bridge configuration is able to increase the output signal as to be explained in subsequent paragraphs.

In this implementation, all piezoresistors are designed in such a way that each of them exhibit equal resistances when no pressure is applied. When an excitation voltage of  $V_{exc}$  is applied between the nodes  $V_{exc}$  and Ground, the voltages at SIG+ and SIG- are theoretically  $1/2 V_{exc}$ . The alignment of the piezoresistors in the branches is determined so that when pressure acts upon the membrane, opposite resistors in the bridge change resistance in opposite direction, either  $+\Delta R$  or  $-\Delta R$ . These stress sensitive resistance varying piezoresistors are also called active resistors. The voltages at nodes of SIG+ and SIG- are then offset from  $1/2 V_{exc}$ . The differential voltage between the nodes, given by (19), is the electrical signal output and it indicates the amount of force or pressure acting upon the sensor.

$$V_{sig} = (SIG+) - (SIG-) \quad (19)$$

In an implementation with four active elements, the output voltage is simply represented by (20). Since  $\Delta R$  is proportional to the applied pressure,

this can be rewritten as (21), where  $P$  is the pressure and  $S$  is the sensitivity, or output voltage, of the sensor in mV per volt of excitation with full scale input.

$$V_{sig} = V_{exc} \times \Delta R/R \quad (20)$$

$$V_{sig} = V_{exc} \cdot P \cdot S \quad (21)$$

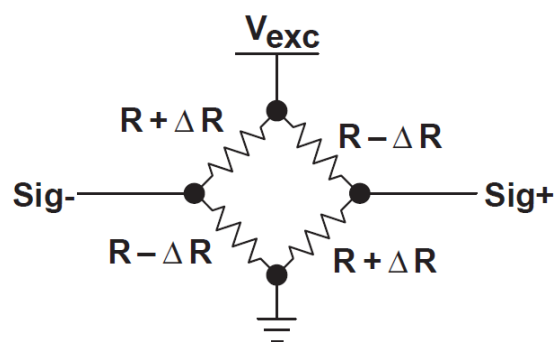


**Figure 4.16:** A resistive Wheatstone bridge circuit (Karki, 1999).

#### 4.7.2 Results of System Simulation

The system level simulation results of the initial design without optimization is shown in Figure 4.17 for piezoresistors of size  $4\mu\text{m} \times 8\mu\text{m}$  placed at the four membrane edges. The superior linearity of the output is so obvious. The relationship of the applied pressure and the output voltage for the other two designs are also depicted in Figure 4.17. As expected, the output is very linear in tandem with the linearity of deflection versus pressure relationship obtained in Section 4.4. The output of the wheatstone bridge piezoresistors are amplified 100 times. It is also obvious that the bigger the membrane size, the higher the output voltage magnitude value results.

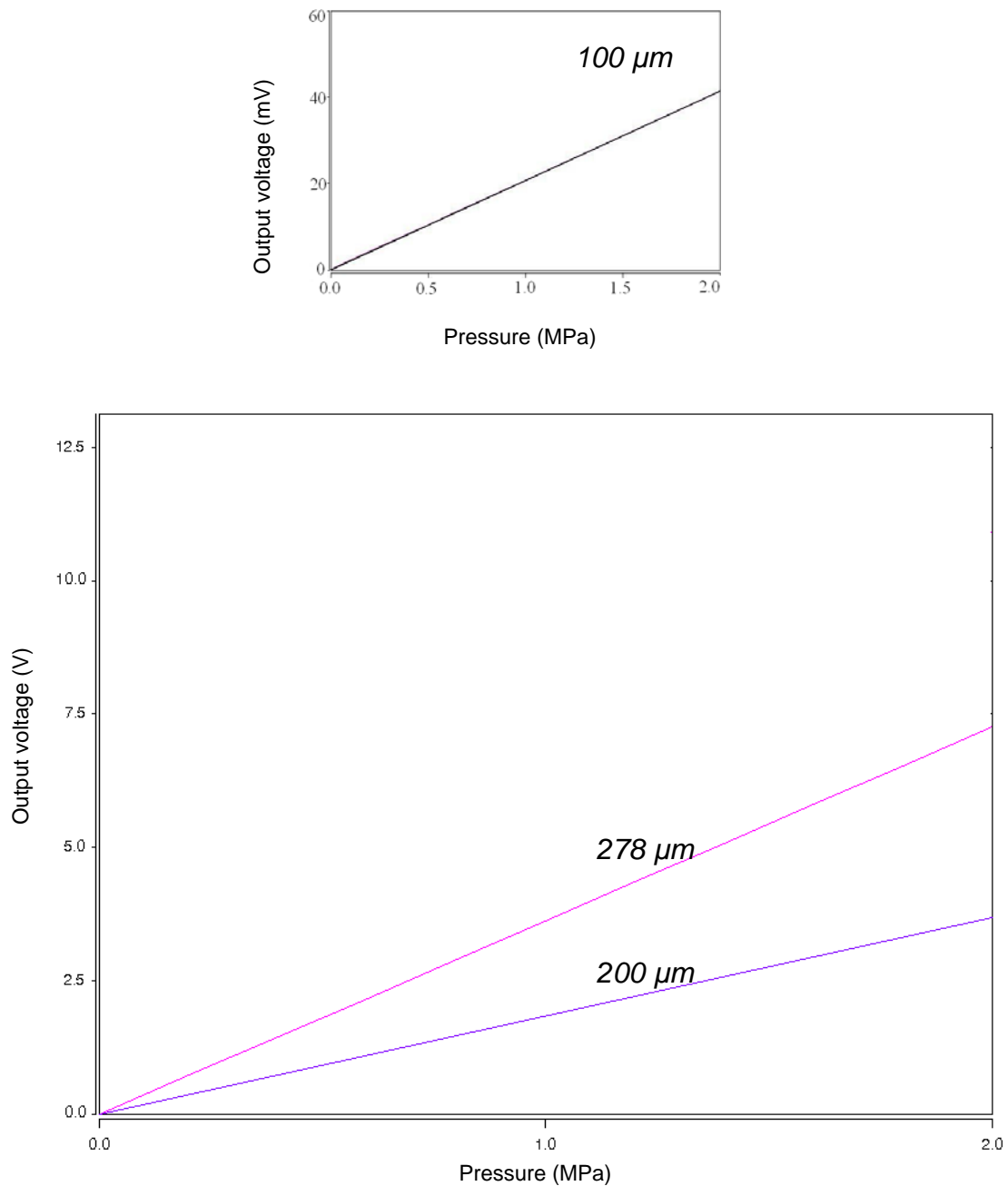


**Figure 4.17:** A highly linear output voltage vs pressure relationship. The relationship between the applied pressure and output voltage of the (Top) 100 , (Bottom) 200 and 278 μm membranes.

Figure 4.17 also shows that there is a need to increase the output voltage values for the 100 μm pressure sensor so that the range is closer to

the other two sensors. For that reason, an extensive performance optimization for that particular sensor is performed in this research. To obtain output voltage in the volts range after amplification, the sensor should be able to increase the current output level to nearly 100 times its current output voltage, which is a very challenging task.

## **4.8 Sensor Design – System Optimization and Simulation**

### *4.8.1 Methodology*

A series of design optimization are performed on the designed 100  $\mu\text{m}$  silicon micromachined pressure sensor. An extensive study is performed with an aim to further increase the output voltage values. As piezo-resistance sensing is used, the design optimization only involves the sensing elements, namely the piezoresistors. In finding ways to increase the output signal, the identification and determination of the best values for the piezoresistor dimensions and placement are the key tasks.

The sensing piezoresistors are aligned in the  $\langle 110 \rangle$  direction to maximize piezo-resistance change, as the corresponding coefficients are maximum in that direction (Kanda & Yasukawa, 1997). The foundry limitation in term of the minimum feature size of the piezoresistor, inclusive of both width and length, is 4  $\mu\text{m}$  (MultiMEMS, 2007). In addition to foundry rule, the choice of piezoresistor size is also constrained by the averaging effect (Shih-Chin & Chengkuo, 2001) and the limitation imposed by the membrane side-length. The placements of piezoresistors are best at places where maximum stress is produced while in operation.

To further optimize the system performance, a study of the effect of piezoresistor placements on the membrane is also conducted. This is realized by use of the powerful analysis options available in the Coventorware's Architect module, especially Vary analysis. With this analysis, the locations of the resistors are made as a two-dimensional variable. In the implementation, variables 'x offset' and 'y offset' are used to vary the resistor's x and y positions. In addition to the change in piezoresistor placement, a study on the effect of changing the piezoresistor size to the output voltage value is also performed. Again, the powerful Vary analysis capability is used whereby the piezoresistor length and width parameters are defined as variables. In actual settings, both Vary analysis are run simultaneously. Figure 4.18 shows the parameters manipulated during optimization process.

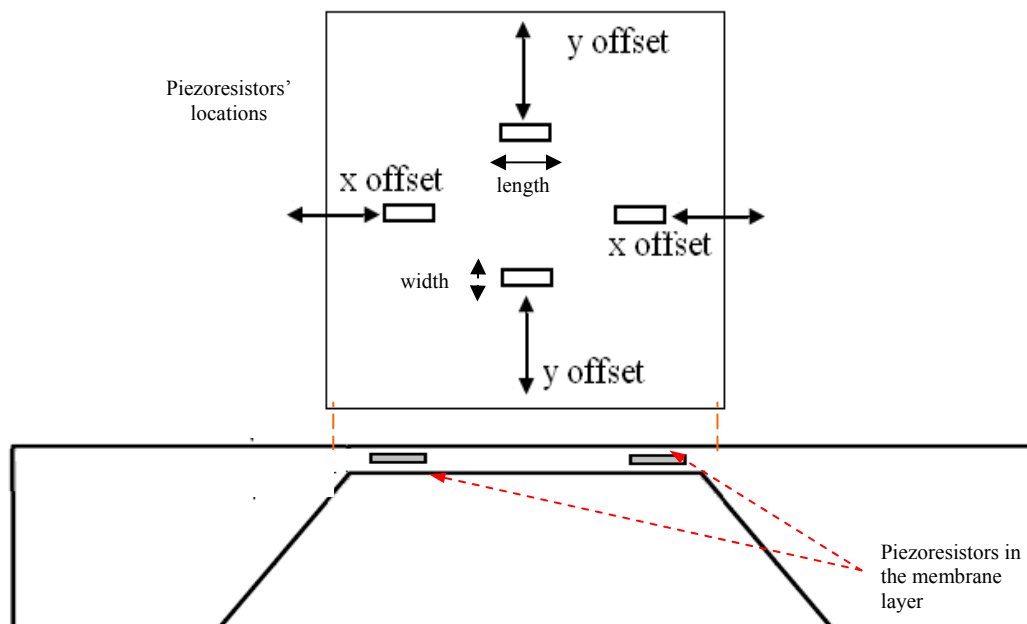


**Figure 4.18:** *The parameters involved in the optimization. (Top) A top view of an enlarged membrane zone. (Bottom) The cross-section of the sensor for reference.*

### a) Analysis and Simulation of Piezoresistor Size Influence

The Wheatstone bridge aligned four sensing piezoresistors are involved in this optimization study. The optimization begins with the effect of sensing piezoresistor size. In this step, the width and length of the sensing piezoresistors are swept across all possible values. The values are limited by the process design rules and the physical dimension of the sensor membrane. In this step, the fact that averaging effect may limit the resistance change is considered. The fabrication process requires that the minimum feature size of the piezoresistor dimension is 4  $\mu\text{m}$  while the separation between adjacent piezoresistors is at least 6  $\mu\text{m}$ . So, in addition to the limitation by averaging effect, the combined effect of membrane side-length value and the foundry requirements will further limit the choices of piezoresistor size. For this reason, an extensive analysis is performed taking into account all the limiting factors.

### b) Analysis and Simulation of Piezoresistor Location Influence

The next analysis was the influence of device location on the maximum output voltage magnitude. The literature pointed that the regions of high stress were the best options for sensing resistor placement as one of the main objective is always to obtain the maximum voltage at the output. In searching for the better locations of the piezoresistors, the locations on the membrane and its surrounding where stress is significant must be identified. Based on FEM result, the stress is significant at the centre of the membrane and also at the

middle of each of the membrane sides. Therefore, those places shown in Figure 4.18 are the areas of interest in this analysis and are the main focus in this study.

The piezoresistors are placed at all key locations during the execution optimization steps. For this reason, the locations of resistors are varied according to the parameter  $y$  offset and  $x$  offset (or  $\text{Offset}_y$  and  $\text{Offset}_x$ , respectively). These offsets represent the distance between the selected location from the membrane edge in the  $x$  or  $y$  direction. Again, the limiting factors that have to be considered are the sensor dimension and process design rules.

#### *4.8.2 Result of Piezoresistor Optimization*

The result of the analysis of the placement optimization is shown in Figure 4.19. In this analysis, the  $\text{Offset}_y$  is varied from  $0\ \mu\text{m}$  to  $33\ \mu\text{m}$ , while the  $\text{Offset}_x$  is swept from  $-10\ \mu\text{m}$  to  $10\ \mu\text{m}$ . The maximum voltage is achieved when  $\text{Offset}_y$  is  $3\ \mu\text{m}$  and  $\text{Offset}_x$  of around  $2\ \mu\text{m}$ , with value of about  $0.57\ \text{V}$ . Further optimization is performed to find an even better location following the indications from the result in Figure 4.19. The result of the extended analysis is given in Figure 4.20. From the final placement optimization results, it is found that the better locations for the piezoresistors are that with  $\text{Offset}_y$  and  $\text{Offset}_x$  of  $4.5\ \mu\text{m}$  and  $2\ \mu\text{m}$  respectively. The value of the output voltage at these locations is very close to  $0.6\ \text{V}$ . This is about  $0.3\ \text{V}$  improvement over the depicted values in Figure 4.19.

As Figure 4.19 indicates the potential of getting higher output voltage if the Offset<sub>y</sub> is further analyzed, the performed study proves its validity.

In terms of piezoresistor dimensions, Figure 4.21 and Figure 4.22 depict the results. The dashed line rectangle in Figure 4.21 is the key finding of this analysis. It is enlarged and reproduced as Figure 4.22. It shows the maximum values of output voltage when the piezoresistors' locations and dimensions are highly optimized.

As can be seen in Figure 4.21, the best value for piezoresistor width is 4  $\mu\text{m}$ . This is obviously the minimum size allowed by the fabrication process (MultiMEMS, 2007). On the other hand, the output voltage is better optimized when the piezoresistor length is chosen to be 15.5  $\mu\text{m}$ , as shown in Figure 4.22. The maximum value for the voltage as recorded at this stage is close to 1.12 V, which is about double the achievement shown in Figure 4.19 and Figure 4.20. This new result shows that the output voltage can be optimized very efficiently using a step by step analysis and optimization.

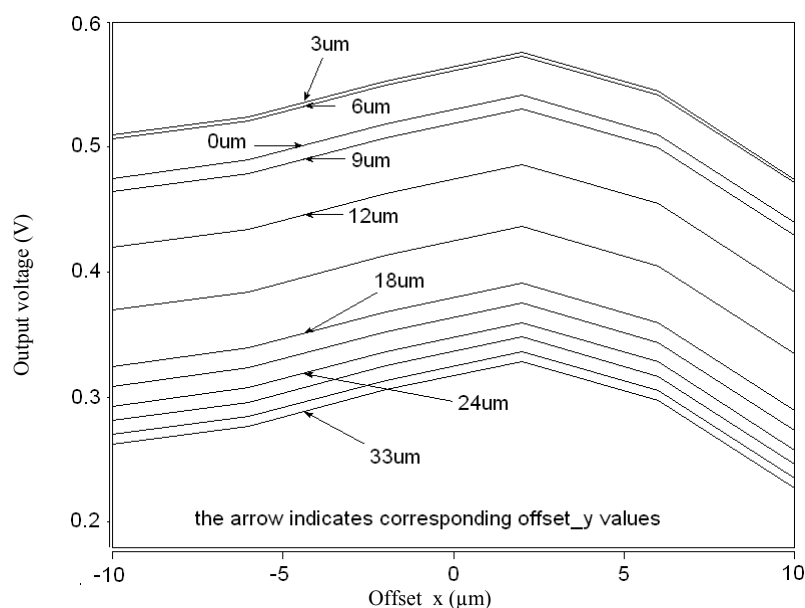


**Figure 4.19:** Output voltage against Offset<sub>x</sub> parameter.

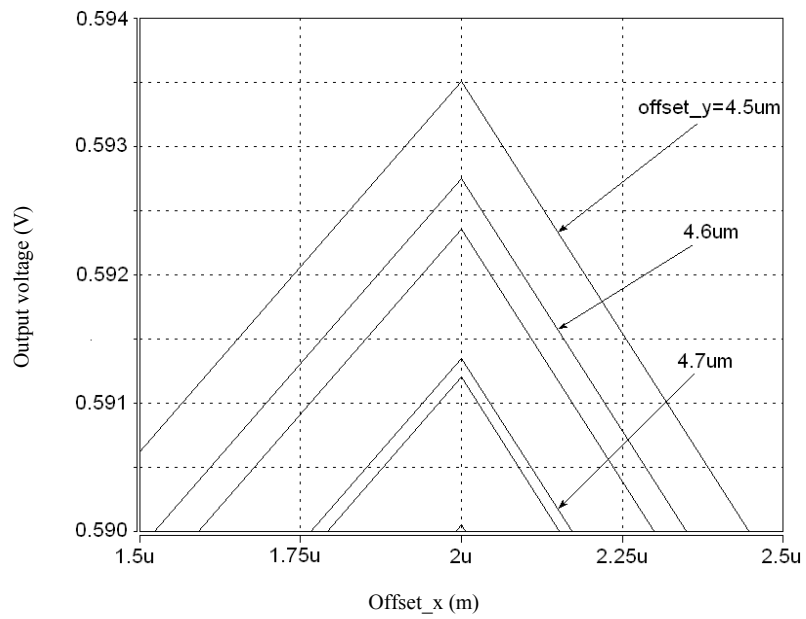


**Figure 4.20:** Output voltage against Offset\_x parameter.

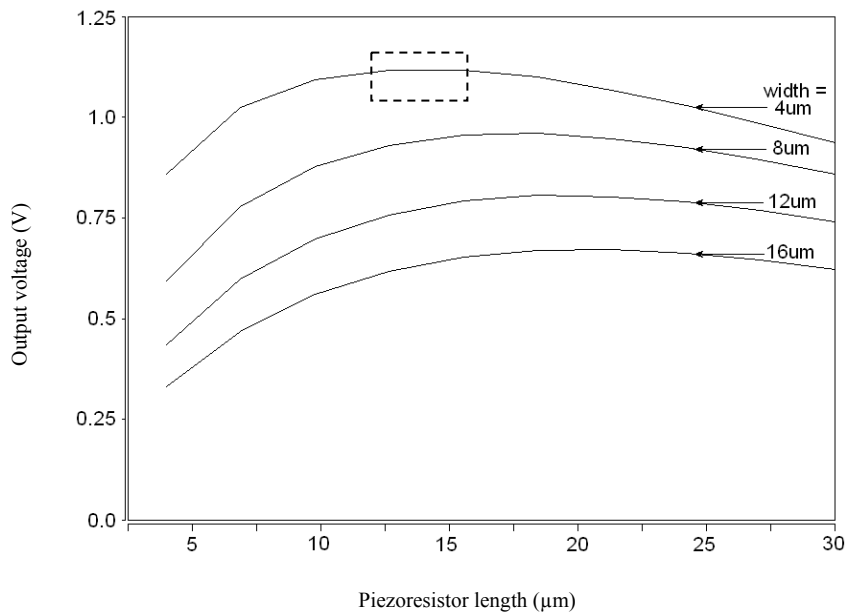


**Figure 4.21:** Output voltage against piezoresistor length.

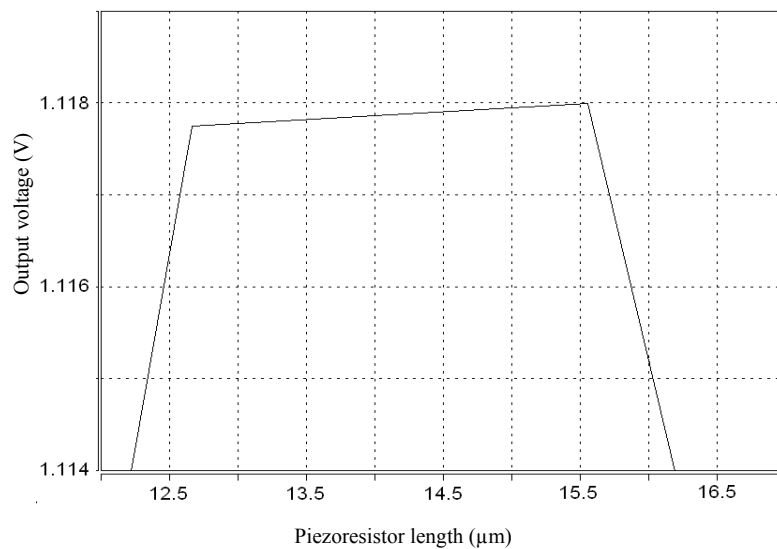


**Figure 4.22:** Output voltage against piezoresistor length.

## 4.9 Sensor Design – Overall Improvement

### 4.9.1 Methodology

Based on both the element dimension and location analysis results, the overall and final optimization is performed. At this stage, only the significant factors that are affecting the output magnitude were considered. The final system simulation is then performed to produce the output voltage to pressure relationship. The most optimum piezoresistor location and dimension are chosen as the input of the simulation.

### 4.9.2 Result of the Final Pressure Sensors Design

Using the optimized locations and dimension, the relationship of the output voltage and the applied pressure is obtained. The overall system simulation

produces plots of output voltage versus applied pressure that is included in Figure 4.23. The optimized relationship of the output voltage and pressure when the applied pressure is varied from 0 Pa to 3 MPa on the membrane is superbly linear. The results as presented in the optimization section are hereby verified. The sensor output is again increased 100 times by use of operational amplifier circuit. Another important observation but not directly shown is that, as predicted in the calculation, the deflection is linearly proportional to the pressure magnitude as proven by Figure 4.23.

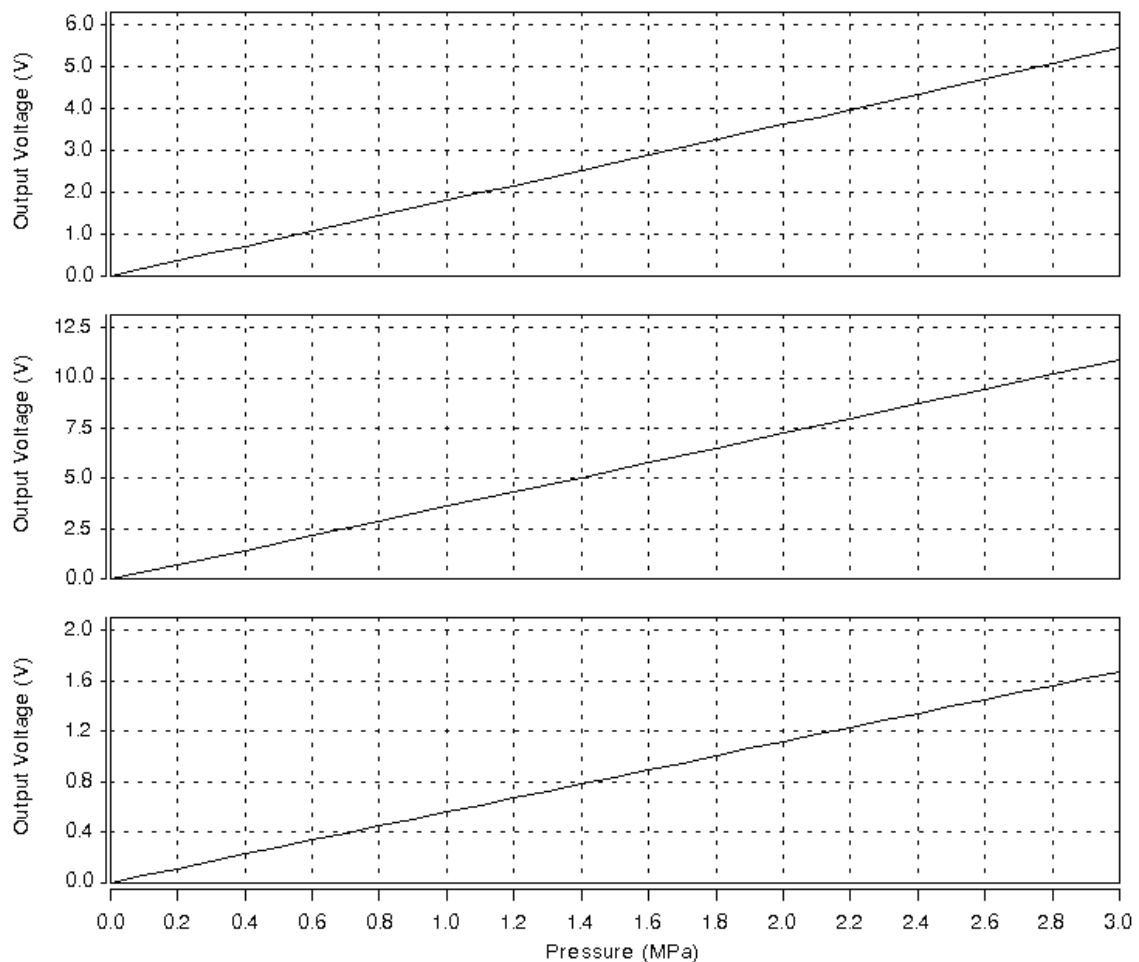


**Figure 4.23:** Graphs showing plots of output voltage versus pressure for (Top) 200  $\mu\text{m}$ , (Middle) 278  $\mu\text{m}$  and (Bottom) 100  $\mu\text{m}$  pressure sensors.

## 4.10 Sensor Design – Silicon Implementation

### 4.10.1 Methodology

In designing and simulating the sensor, the opportunities for experimenting and optimizing are vast and almost limitless. However, when it comes to real silicon implementation, significant number of rules, guidelines and absolute limits really pose great challenges. Since the absolute design limits are already taken care of during the initial design stage documented in Section 4.4, only the remaining key design rules and guidelines will be discussed in this section. Among them, the design rules and guidelines for piezoresistor and interconnection are the two most significant ones. Due to the rules, guidelines and available space, pressure sensor of the sizes 100  $\mu\text{m}$ , 150  $\mu\text{m}$  and 278  $\mu\text{m}$  are chosen to be finalized.

#### A. Membrane Design Space Factors

The key determining factor is the design space related, such as the available area of the membrane. If a membrane of the size of 100  $\mu\text{m}$  X 100  $\mu\text{m}$  is drawn, the piezoresistor lengths are then limited by the this number, and that only fractions of these figures can be used due to minimum item separation requirement of the foundry layout design rule.

#### B. Piezoresistor Design Rules and Guideline

The design of piezoresistors demands that the process's actual limitations are taken into account prior to the preparation of final layout. In actuality, many of the process steps exhibit well characterized deviations, which includes

expansion and shrinking of feature sizes as compared to the drawn sizes.

The piezoresistors are drawn according to the design parameter values that are included in Table 4.6. As stated in Table 4.6, the smallest sensor has very limited area for longer and wider piezoresistor placement. Other key limiting factors for piezoresistor sizing are the design rule and fabrication characteristic. The main rules are: the drawn items' minimum width, minimum length, minimum separation between similar type items and also minimum overlapping of layers for some of the multi-layered items (MultiMEMS, 2007). The minimum feature size of a piezoresistor, for example, is 4  $\mu\text{m}$ . The design rule requires that certain amount of spacing between adjacent features and overlapping of certain layers are implemented. On the other hand, the fabrication characteristic, such as the occurrence of lateral diffusion requires proper sizing of drawn features be made in order to materialize the target design specification of integrated devices.

TABLE 4. 6. THE ELECTRICAL PART DESIGN SHAPES AND PARAMETERS

ITEM \ SENSORS	P1 (100 $\mu\text{m}$ )	P2 (150 $\mu\text{m}$ )	P3 (278 $\mu\text{m}$ )
<b>LONGI-TUDINAL RESISTORS</b>			
<b>TRANS-VERSAL RESISTORS</b>			
<b>RESISTOR LENGTH</b>	19 $\mu\text{m}$	20 $\mu\text{m}$	40 $\mu\text{m}$
<b>RESISTOR WIDTH</b>	4 $\mu\text{m}$	4 $\mu\text{m}$	4 $\mu\text{m}$

Table 4.6 gives the values that are drawn in the layout. These values are different from the simulated values due to the previously mentioned

design constraints. So, it is obvious that layout design also requires optimization so that the layout can best represent the actual target design values as identified from the simulated and finite element analysis results. In order to determine the optimized layout, the calculation of suitable layout features sizes is undoubtedly a necessity. For that reason, the relationship between various silicon layout features and the foundry processing limitation are derived and used extensively to model the final piezoresistor resistance and dimensions.

In deriving the equations for this modelling, the involved layout design parameters are the drawn length,  $L_D$ , the drawn width,  $W_D$ , effective length,  $L_E$ , the effective width,  $W_E$ , the widening compensated length,  $L_{WC}$ , the target length,  $L_T$  and the target width  $W_T$ . In addition, the key process parameters that are required are such as lateral diffusion of contact layers,  $C_{LD}$ , lateral diffusion of piezoresistor layers,  $R_{LD}$ , and finally the sheet resistance,  $S_R$ .

Firstly, the best piezoresistor sizing that is taken from the finite element analysis result is identified. These values correspond to the  $L_T$  and  $W_T$  layout design parameters. The ratio of  $L_T$  to  $W_T$  is then referred as the piezoresistor squares,  $R_S$ . For each of the sensors, the  $R_S$  value is calculated. Following this, the target resistance,  $R_T$  can be obtained by using equation (22) and solving for  $R_T$ .

$$\frac{R_T}{S_R} = R_S \quad (22)$$

As identified through the finite element analysis, the target resistor width is  $W_T$ . In the actual layout drawing, it is drawn as  $W_D$  where  $W_D = W_T$ . The

lateral diffusion of the piezoresistor layer is causing the piezoresistor to be widened by the amount double the  $R_{LD}$ .

$$W_E = W_D + 2R_{LD} \quad (23)$$

Due to this widening effect, the length must be optimized so that the value of  $L_T$  is achievable. Therefore,  $L_{WC}$  must be used according to (24).

$$L_{WC} = W_E R_S \quad (24)$$

Additionally, the effect of another lateral diffusion,  $C_{LD}$ , is taken into account in (25) so that the drawn resistor, which is of the dimension  $L_D * W_D$  matches the intended resistance value of  $R_T$ .

$$L_D = L_{WC} + 2C_{LD} \quad (25)$$

#### 4.10.2 *Result of the Silicon Implementation*

##### A. Piezoresistors

Based on the derived piezoresistor fabrication modelling during the final design analysis, the piezoresistor final specification is produced as shown in Table 4.7. These values are calculated using the piezoresistor model derived earlier in previous step.

TABLE 4. 7. THE PIEZORESISTANCE VALUES

Parameters	Explanation	Values	
$R_{P1}$	Resistance of each of the piezoresistor in the Pressure sensor P1	4.69 k $\Omega$	
$R_{P2}$	Resistance of each of the piezoresistor in the Pressure sensor P2	4.52 k $\Omega$ (Longitudinal)	4.89 k $\Omega$ (Transversal)
$R_{P3}$	Resistance of each of the piezoresistor in the Pressure sensor P3	9.05 k $\Omega$ (Longitudinal)	9.79 k $\Omega$ (Transversal)

After extensive design optimization, the final designs are then determined. These designs require silicon adaptation before its real implementation. At this stage, the designs are translated into the silicon transferable format of GDS II files. In doing this, two major steps involved are the foundry rule and guidelines observations and their adherence in the layout design stage.

### B. Sensor Layouts

The layouts of the three pressure sensors are shown in Figure 4.24. The membranes are defined by the squares in the middle of each of the layout. Interconnections are made possible by use of triple layered conductive materials as offered by the foundry process. In order to minimize the effect of parasitics and electro-migration, the triple stack of metal, surface and buried conductors are used (MultiMEMS, 2007).

### C. GDS II Result for Fabrication

During tape-out, the GDS-II formatted global layout is produced. In this foundry ready format, all the required items are included. Figure 4.24 depicts the drawing in its final form from the top cell view. The MultiMEMS MPW Run 12 is used in the realization of the sensors.

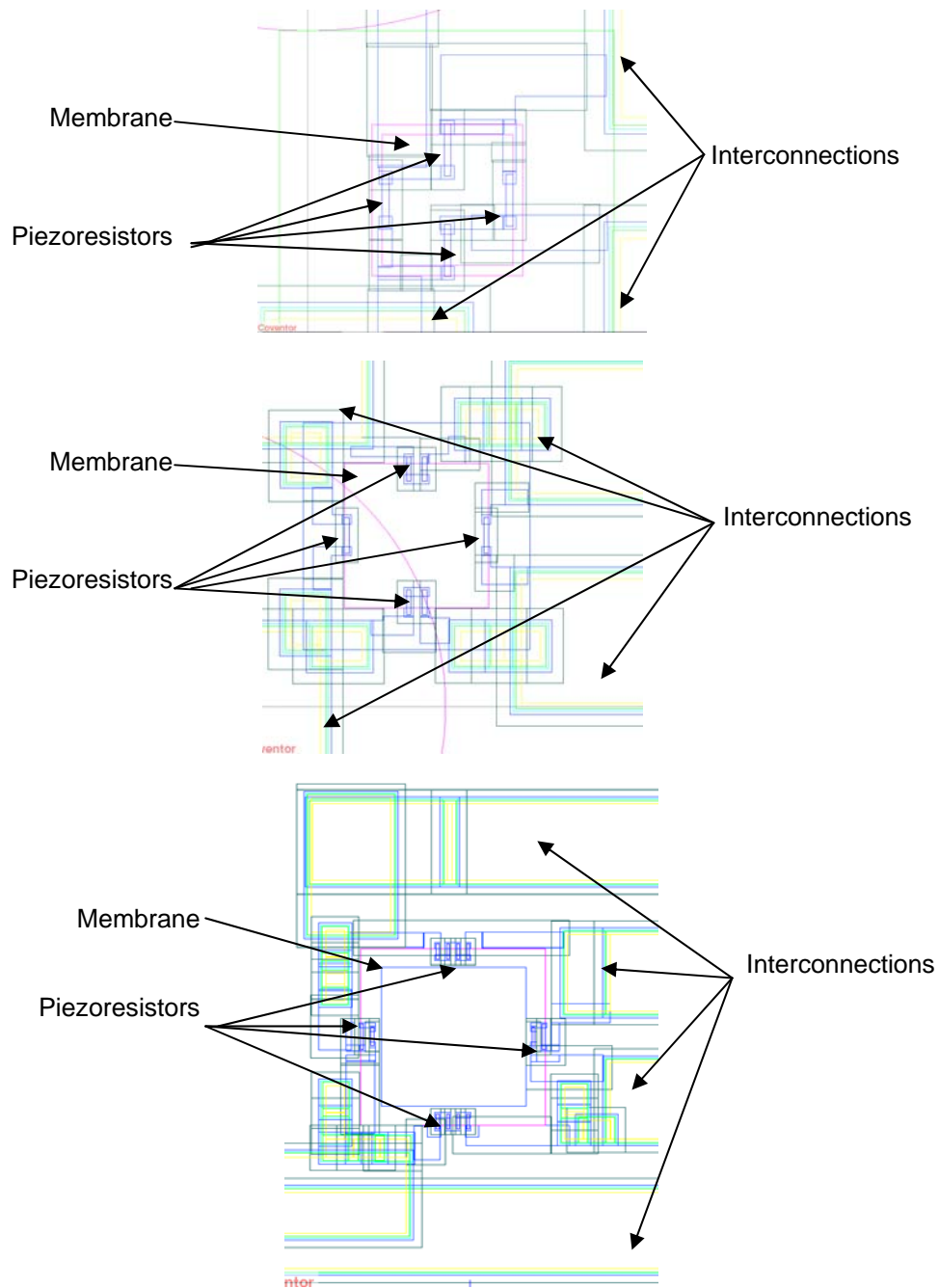


**Figure 4.24:** Layouts of the three sensors. (Top) 100  $\mu\text{m}$  pressure sensor, (Middle) 150  $\mu\text{m}$  pressure sensor and (Bottom) 278  $\mu\text{m}$  pressure sensor.

#### 4.11 Chapter Summary and Discussion

The modeling and implementation of a silicon MEMS pressure sensor for biomedical application is discussed. Every steps of the project is explained, including the requirement study, determination of device specifications, identification of technology for physical realization and its mathematical representation, device design and development using computer aided design tool and also result analysis. It is proven that proper modeling and simulation are critical for a successful product design and development. For this project, it is finally realized that mathematical modeling is essentially important in drafting the sensor development works, especially in determining the key structural parameters. A number of mathematical derivations are successfully performed in order to ensure practically foundry specific silicon-implementable designs. In addition to the original mathematical derivation for modeling work, the success is in part realized through heavy use of a powerful industry standard tool. In addition, the optimization of the pressure sensor is also described. The performance improvement is increased significantly to enable better representation of foot plantar pressure. The high pressure range enables the application of this sensor encompassing wide spectrum of biomechanical activities and clinical diagnosis. The improvement is achieved by thorough analysis of the sensing piezoresistors' placement and sizing. In short, advanced modeling and simulation have enabled precise and efficient device development, in this case, a biomechanical pressure sensor. In short, this work have successfully modeled foundry requirements, simulated using industry standard tool and implemented on silicon using real industry process.

# Pressure Sensor Packaging and Testing

# CHAPTER

# 5

- 5.0 List of Publications Produced
- 5.1 Chapter Overview
- 5.2 Sensor Interconnection
- 5.3 GDS II with Level 0 Packaging
- 5.4 Level 1 Packaging for Testing
- 5.5 Electrical Testing Set-up Design and Result
- 5.6 Mechanical Testing Set-up Design and Result
- 5.7 Chapter Summary and Discussion

## 5.0 List of Refereed Publications Produced From This Chapter

1. *Wahab, Y., Zayegh, A., Begg, R.K. and Sauli, Z., 2009, 'Testing of MEMS Biomedical Pressure Sensor for Gait Analysis,' in **Proceedings of IEEE Regional Symposium on Microelectronics**, IEEE Inc., Kota Bahru, Malaysia.pp 498-501. ISBN 978-967-5048-55-5.*
2. *Wahab, Y., Zayegh, A. and Begg, R.K., 'Comparison and Silicon Realization of Custom Designed MEMS Biomedical Pressure Sensors,' submitted to the **21<sup>st</sup> IEEE International Conference on Microelectronics**, 19-22 December 2009, Marrakech, Morocco.*
3. *Wahab, Y., Zayegh, A. and Begg, R.K., 'Silicon Implementation of Micro Pressure Sensor,' submitted to the **5<sup>th</sup> IEEE International Conference on Intelligent Sensors, Sensor Networks and Information Processing (ISSNIP 2009)**, 7-10 December 2009, Melbourne, Australia.*

## 5.1 Chapter Overview

As discussed in the Chapter 4, the designed pressure sensors are to be fabricated by Infineon Technology SensoNor AS. According to the foundry, the dice of fabricated designs must be sandwiched by two layers of anodically bonded glasses. It is necessary that the GDS II file complies with the guidelines produced by the company to ensure smooth and successful production (MultiMEMS, 2007). Therefore, the designed layouts for the pressure sensors are then extended to include the suitable interconnection and packaging layers, according to the specified guidelines. Furthermore, the testing of the sensors requires special adaptation in the form of another layer of packaging, namely Level 1 Packaging. This is due to the fact that the pads on each die are too small to be probed and interconnected with other off-the-shelf components that are required during testing. The design of system level components such as printed circuit board and pressure chamber which are the prerequisites of the electrical and mechanical testing are also complicated and will be discussed in detail.

This chapter encompasses activities towards silicon implementation that includes the study of gait related design requirement, design and modelling of pressure sensor, the simulation works for the designed sensor, performance optimization and finally silicon implementation. The chapter is divided into twelve sections inclusive of this overview. As their names imply, each of the section presents and discusses specifically the relevant aspects according to the given names. Other than **The List of Refereed Publications Produced From This Chapter** (previous section) and **Chapter Overview** (this section), the other subsections are explained next.

As the name implies, the next section, **GDS II with Level 0 Packaging**, is contained with the discussion on the design of sensor interconnection with the pads. The Level 0 Package design and the whole sensor chip die GDS II finalization are discussed in the subsequent section. Next, the section **Level 1 Packaging for Testing** purposes is discussed in the work. The electrical testing set-up works such as printed circuit board designs, the experimental work and their results are explained in the successive section, namely **Electrical Testing Set-up Design and Result**. Following this, the section named **Mechanical Testing Set-up Design and Result** explains the mechanical works that are performed to design and fabricate mechanical set-up for pressure sensor testing system. Discussions on results of electrical and mechanical testing are included in the two consecutive sections that follow. Lastly, the **Chapter Summary and Discussion** forms the last part of the chapter and it discusses and summarises the whole achievement of the design, packaging and testing implementation of the device level pressure sensor.

## 5.2 Sensor Interconnection

Similar to the interconnections of the sensors' Wheatstone Bridge, the interconnection between the sensors' (Wheatstone Bridge) terminals to the outside pads are also made possible by use of triple layered conductive materials as offered by the foundry process. In order to minimize the effect of parasitics and electro-migration, the triple stack of metal, surface and buried conductors are used (MultiMEMS, 2007).

As each of the pressure sensors has four terminals, corresponding to the power supply terminal, ground terminal, positive output terminal and negative output terminals, the total pads required becomes 12. This is not practical as the space available for the pads placements are limited. In addition, extra pads to bias the p-n junctions are also required to eliminate uncontrollable leakage current phenomenon. However, this problem is finally solved by proper design of the interconnections routing plus implementation of power supply pad sharing among the three sensors. Manual interconnection routing is very time consuming where multiple try and error kind of floor-planning is unavoidable. The produced pads to sensors interconnections are shown in Figure 5.1.

### **5.3 GDS II with Level 0 Packaging**

#### *5.3.1 Design*

Following similar nomenclature in the literature (Krondorfer & Kim, 2007), Level 0 Package is actually the glass sandwich package provided by Infineon Technologies SensoNor AS in its foundry process. The packaging is performed using an anodic bonding process. The requirement to include Level 0 Package in the foundry compatible GDS II design file poses additional challenges to the tape-out process. In addition to the die frame definition mask layers, the mask layers for additional four layers of glasses, two each for physically separated top and bottom glasses, are thus required. For example, to enable pressure measurement, the membrane must be made accessible by the pressurized medium. Therefore, it is necessary to draw suitable holes shapes on the two masks that pattern the glass layer that is

facing the bulk-etched hole of the silicon substrate. Similarly, holes must be defined in the mask that patterns the glass that is facing the opposite membrane surface so that the membrane is allowed to deflect freely according to the pressure magnitude. Actually, there are many other important rules that cover the final tape-out procedure but due to their proprietary nature, only few of the rules are briefly mentioned here. Figure 5.1 shows the overall GDS II file drawing for tape-out. After submission of the design, the foundry performed foundry design compliance using the submitted GDS II file. The design is verified to be complying with the foundry design rules and guidelines (MultiMEMS, 2009a)(see **Appendix B**). The package can be seen in three dimensional in Figure 5.2.

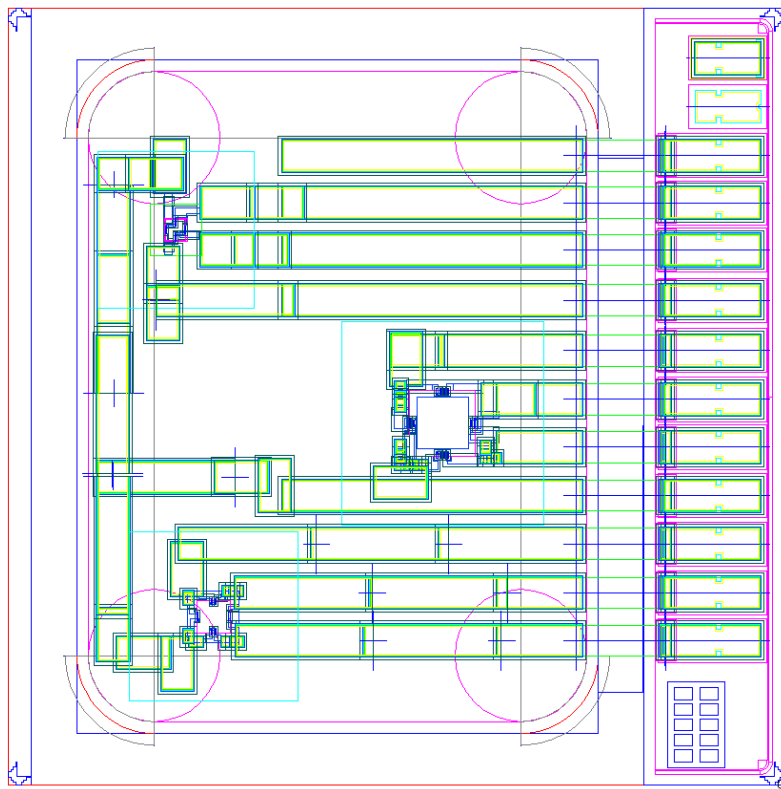


**Figure 5.1:** *The silicon die frame, sensor to pads interconnections and the Level 0 Package definitions all included in this foundry compatible GDS II tape-out file.*

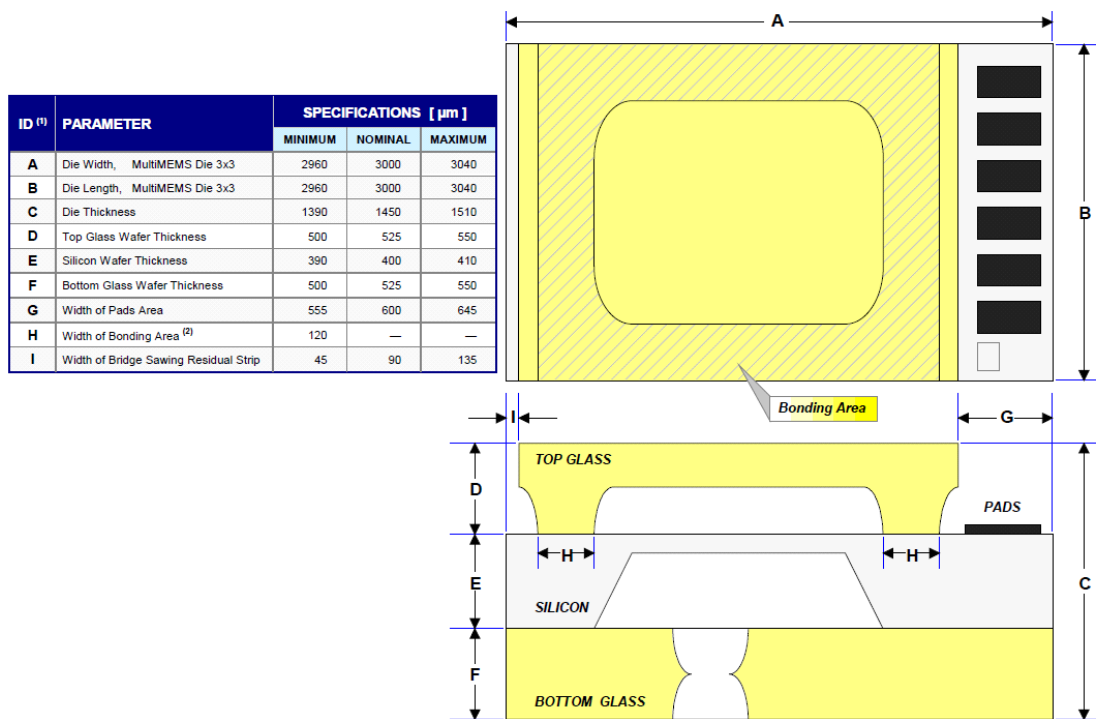
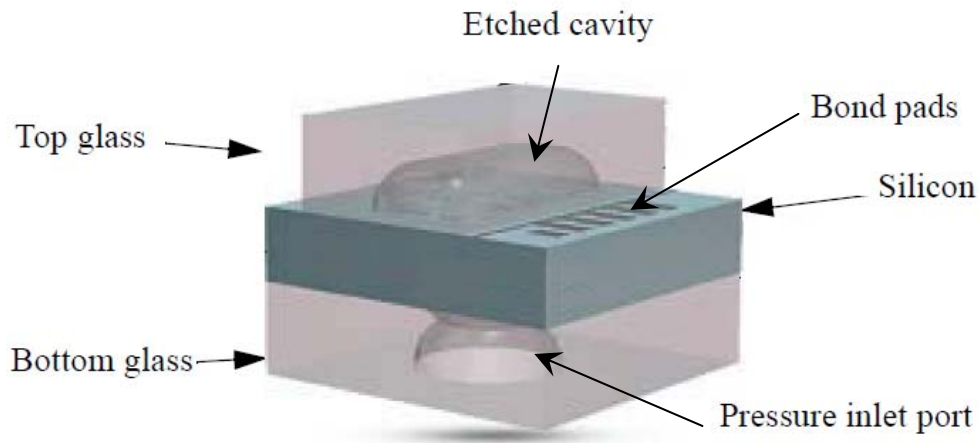


**Figure 5.2:** (Top) A glass waferbonded Level 0 Packaged chip from Infineon Technology SensoNor AS (Krondorfer & Kim, 2007), and (Bottom) the dimensional description (MultiMEMS, 2007).

### 5.4.1 Fabrication Result

The foundry fabrication completes in about six months. Dice in Level 0 Package are shown in a close-up view of the delivered items as shown in Figure 5.3. Dimensions of the dice are roughly 3 mm X 3 mm X 1.5 mm. It is obvious that the scales on the ruler behind the dice indicate 3 mm die side length. As the holes are drawn for each of the sensors, three holes can be seen on one side of the Level 0 Package (the die on the left of the photograph). On the opposite side of the dice, a cavity is seen above the aluminium interconnection lines. The pads are left uncovered by the glass according to the GDS II design for external circuitry connections and are defined in Table 5.1. Process variations that may cause thicker than 23.1  $\mu\text{m}$  membranes and also reduced piezoresistance of the piezoresistors are also reported by the foundry (MultiMEMS, 2009b).

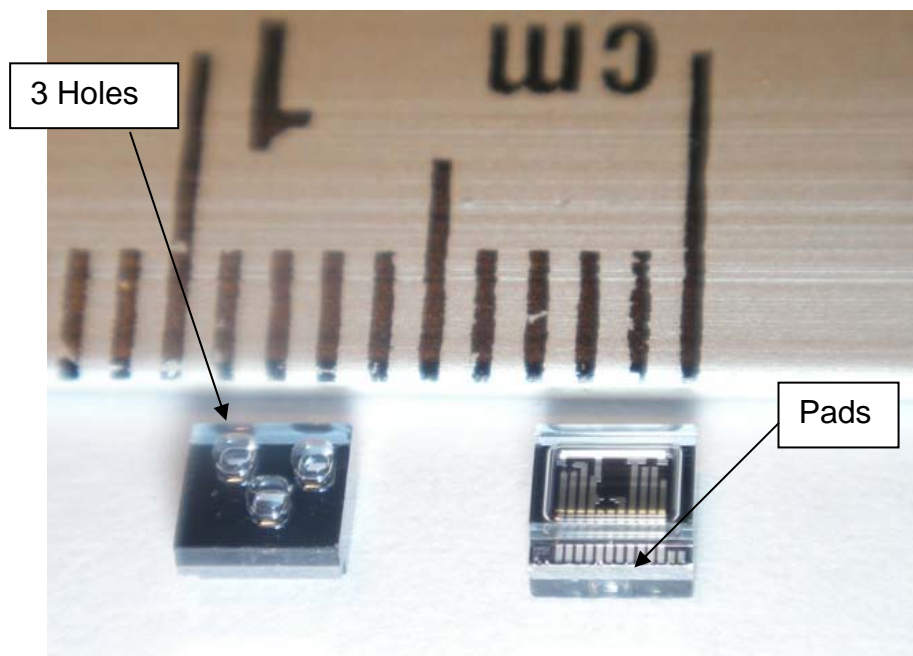


**Figure 5.3:** The produced dice (in Level 0 Package) from the foundry.

TABLE 5.1. THE PADS DESCRIPTIONS

<b>Pads</b>	<b>Function</b>	<b>Device</b>	<b>Estimated Range</b>	<b>Comments</b>
<b>SUB</b>	Direct connection to the SUBSTRATE	Whole chip	Up to +12V	This pad must always be connected to the supply voltage while in operation
<b>EPI</b>	Direct connection to the EPITAXIAL Layer	Whole chip	Up to +12V	This pad must always be connected to the supply voltage while in operation
<b>Vsupply</b>	Supply voltage	All pressure sensors	Up to +12V	A shared power supply pad for all the pressure sensors
<b>Vout2 P1</b>	Branch 2 voltage	Pressure sensor P1	<b>Vsupply</b> dependent	Difference in mV range is expected
<b>Vout1 P1</b>	Branch 1 voltage			
<b>Ground P1</b>	Ground connection for P1		0V	Connected to ground when P1 is in operation
<b>Vout1 P2</b>	Branch 1 voltage	Pressure sensor P2	<b>Vsupply</b> dependent	Difference in mV range is expected
<b>Vout2 P2</b>	Branch 2 voltage			
<b>Ground P2</b>	Ground connection for P2		0V	Connected to ground when P2 is in operation
<b>Vout1 P3</b>	Branch 1 voltage	Pressure sensor P3	<b>Vsupply</b> dependent	Difference in mV range is expected
<b>Vout2 P3</b>	Branch 2 voltage			
<b>Ground P3</b>	Ground connection for P3		0V	Connected to ground when P3 is in operation

## 5.4. Level 1 Packaging for Testing

### 5.4.1 Design

Now that the chip is already materialized, the next step is to package it for testing and characterization of its performance. This way, the simulated specification can be verified at the device level. In this step, the intention is to obtain the device level performance. Even though it is just performed at the device level, it is obviously a very important task. This is so because when the device is properly packaged in a bio-compatible final packaging for biomechanical applications, the final characteristic of the device can be compared with the device level ones, and thus the final bio-compatible packaging effect on the performance of the sensors can be gauged. The two steps that are involved in this process are the wirebonding of the dice to a suitable lead frame, and then the packaging of the device, called Level 1 Package. According to the literature, wirebonding and packaging of similarly shaped dice but for different application is previously reported by Krondorfer (2004) as shown in Figure 5.4. In the implementation of sensor packaging, the key characteristics and consideration of the chosen package are that it satisfies the description below:

1. Package with pressure inlet.
2. Fits the volume of 3 mm X 3 mm X 1.5 mm.

With the use of a package that satisfies the above requirement, the electrical testing and mechanical testing can surely be performed on the device.

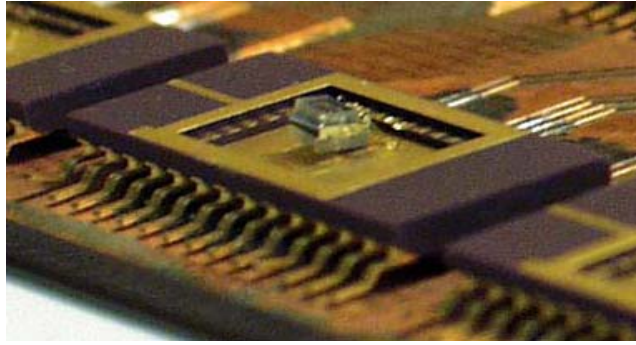


**Figure 5.4:** *The almost similar pressure sensor in an open package (Krondorfer, 2004).*

The wirebonding of the dice to the package involved the use of TPT HB 16 wirebonder produced by TPT. Gold wires of 0.25  $\mu\text{m}$  diameter are used to connect the pads on the dice to the package. The Henkel QiMi adhesive is used in the packaging. SOIC 28L package is chosen for the packaging implementation.

#### 5.4.1 Result

As can be seen in Figure 5.5, SOIC 28L packages are used to encase the chip. Since the pads are all arranged on one side of each die, the wirebonding of the pads to the pins of the package are performed involving only one side of the package. This way of wirebonding makes soldering of the pins to printed circuit boards for electrical characterization is challenging. It is obvious that one side of the die is protruding away from the package cavity surpassing the top side of the package. To solve this problem, a plastic cover is placed on the top side of the package covering the package cavity and the contained die. So as to ensure that the package allows pressure measurement, one side of the plastic cover is then engraved to create an inlet.

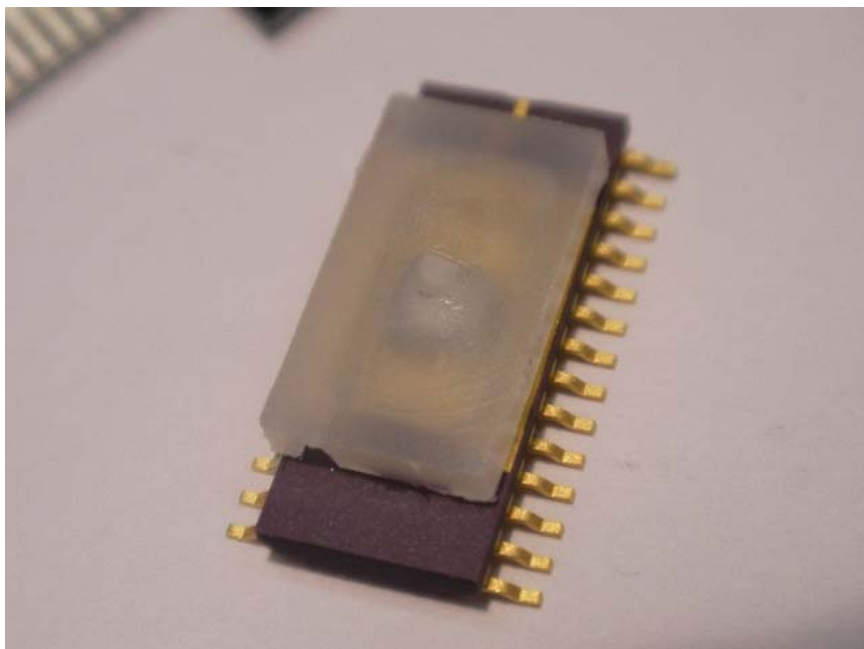
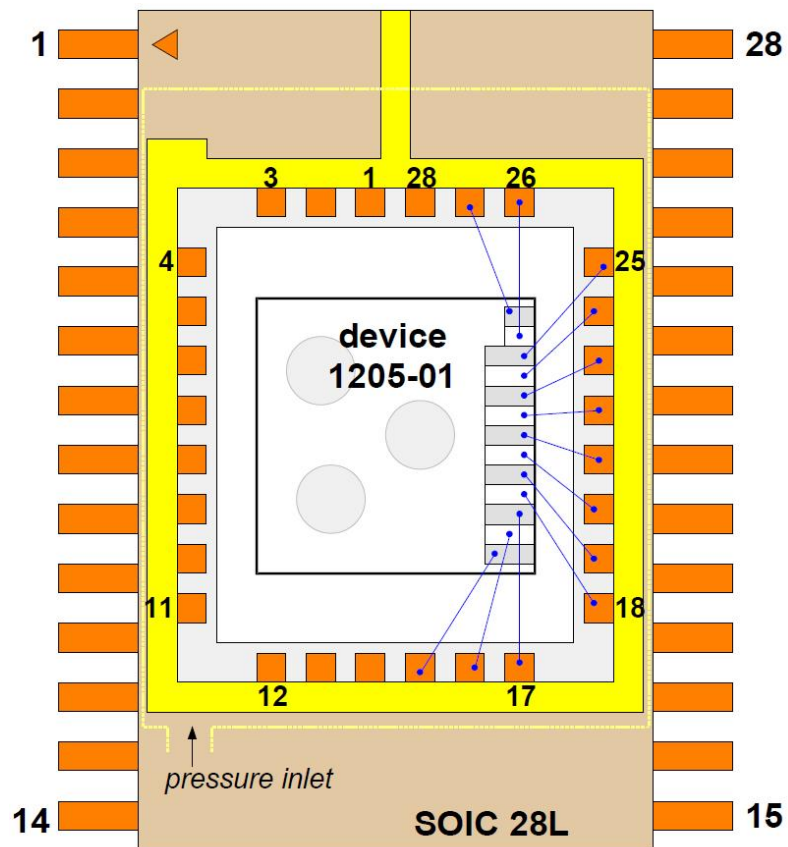


**Figure 5.5:** *The packaged die for device level testing.*

## 5.5 Electrical Testing Set-up Design

### 5.5.1 Methodology

Since the die is packaged in a small package, a veroboard is then patterned to enable easy access to the sensor. The electrical testing that are performed involve the use of an accurate digital multimeter for resistance reading. A digital multimeter produced by Fluke model Fluke 45 Dual Display Multimeter is used to measure the resistances across the corresponding points of the sensor bridge. Figure 5.6 depicts the performed measurement. Specification of the piezoresistor elements according to the calculation results in Section 4.10.2 as shown in Table 5.2 is being referred to ensure appropriate values of electrical parameters are being applied during the characterization and a more straightforward measurement.

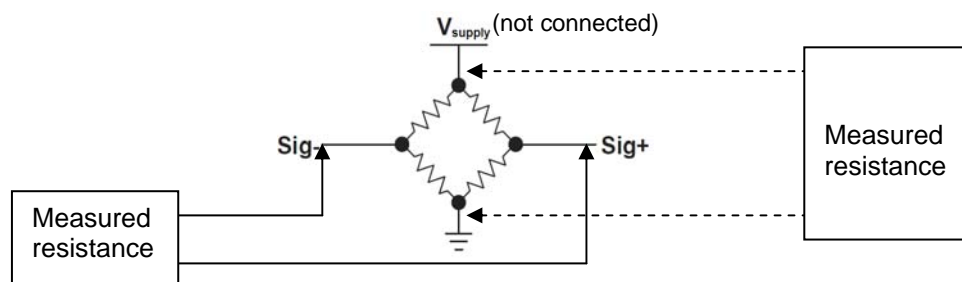


**Figure 5.6 :** *The electrical testing.*

TABLE 5.2. THE SUPPLY VOLTAGE RANGE AND RESISTANCE (CALCULATION)

Parameters	Explanation	Values/Range	
<b>V<sub>supply</sub></b>	Supply voltage	Maximum 12V	
<b>R<sub>P1</sub></b>	Resistance of piezoresistors in P1	4.69 kΩ	
<b>R<sub>P2</sub></b>	Resistance of piezoresistors in P2	4.52 kΩ (Longitudinal)	4.89 kΩ (Transversal)
<b>R<sub>P3</sub></b>	Resistance of piezoresistors in P3	9.05 kΩ (Longitudinal)	9.79 kΩ (Transversal)

### 5.5.2 Result

Due to the way the measurement is performed, the piezoresistance value obtained from the measurement is not giving the exact piezoresistor's resistance. However, it is very helpful in indicating the overall effect of process variations on piezoresistance value. Overall, the fabricated sensors exhibit reduced resistance as compared to the theoretical values as shown in Table 5.3. This is due to the fact that the fabrication process is slightly different in the recent run, particularly the epitaxial layer growth process, as reported by the foundry in its report (MultiMEMS, 2009b). The production report also expects piezoresistance values less than the initial foundry specified minimum piezoresistance for the surface piezoresistors. According to specification, the resistance at its minimum is less than the normal value by close to 10 %, on the other hand, the production report shows about 5.2 % less than the initial foundry specified minimum (see **Appendix C**). Altogether, the piezoresistance change due to fabrication process variations may be at maximum of around 15 %.

As observed during the measurement, the sensor with longer piezoresistor exhibits higher magnitude of resistance reduction, which is around 13.3 %. This reduction is still below the maximum possible total percentage of reduction that is being indirectly portrayed in the production report (i.e. 15%). Therefore, it is highly possible that the process variations have contributed to the resistance difference for all of the sensors. The measurement result also shows that the electrical design work performed during the layout preparations are very helpful and practical in determining the range of piezoresistance value on real silicon after fabrication is completed.

Therefore, it is proven that the produced models are beneficial for any similar designs.

TABLE 5.3. RESISTOR VARIATION

SENSORS OBSERVATION	P1	P2	P3
Resistance between Sig- and Sig+	4.59 k $\Omega$	4.46 k $\Omega$	8.49 k $\Omega$
Resistance between Vexc and Gnd	4.41 k $\Omega$	4.48 k $\Omega$	8.49 k $\Omega$
Difference between branches	0.18 k $\Omega$	0.02 k $\Omega$	Too small
Maximum difference between the fabricated and the FEA result	0.28 k $\Omega$	0.43 k $\Omega$	1.3 k $\Omega$
Maximum % of the resistance reduction	~ 6 %	~ 8.8 %	~ 13.3 %

## 5.6 Mechanical Testing Set-up Design

### 5.6.1 Methodology

The execution of mechanical testing is even more complicated. This is due to the fact that a pressure chamber that can withstand the specified amount of pressure must be designed too. Therefore, consideration of the type of pressurized medium to be used is another key design step. In addition, the size and thickness of the printed circuit board must be considered also. So as to ensure a more straightforward but reliable readings of the electrical signals, instrumentation amplifier circuits and a more custom printed circuit board are designed. With the use of specialized printed circuit board as in Figure 5.7, the enlarged circuitry can be dimensionally minimized. However, the board is designed only for the pressure sensor chip.

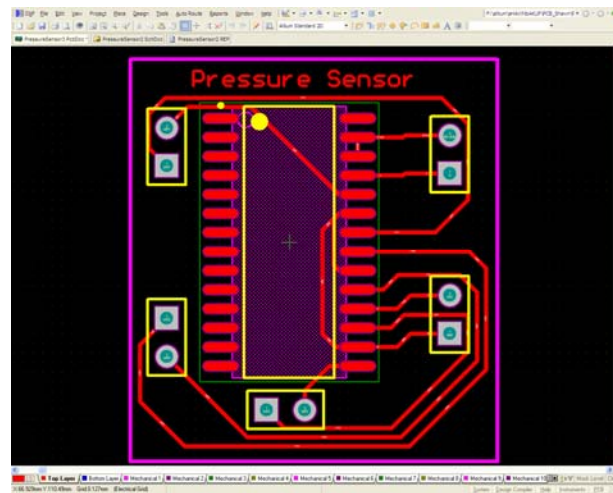


**Figure 5.7:** The designed printed circuit board to reduce the size of the overall circuit and improve the electrical interconnection to the pressure sensor. The design is based on Altium Designer (Altium Inc., 2009).

In addition to the designed board, a veroboard and a small off-the-shelf SOIC 28 to standard DIP 28 adaptor are also used to mount the sensor on and implement complete circuit board. Manual soldering of the SOIC 28L packaged pressure sensor onto the boards and adaptor is a challenging task. A small Weller soldering iron tip of 0.4 mm size is used which is equipped with a precise temperature control and magnification scope. Figure 5.8 shows the sensor package on a veroboard for further interconnections.

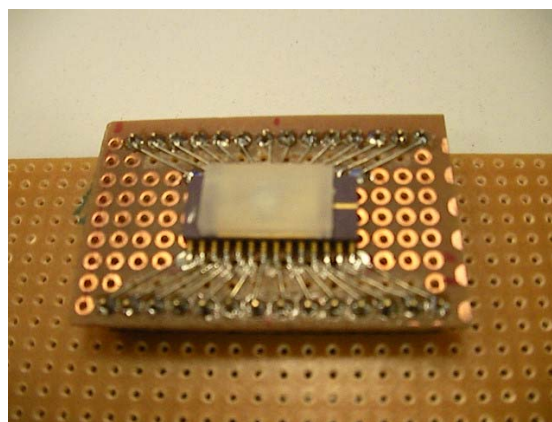


**Figure 5.8:** The completed veroboard for the integrated three pressure sensors.

The development of custom mechanical set-up which is basically consists of a pressure chamber, its stand, a valve, several steel pipe components (threaded end caps, Y connectors etc) and a pressure gauge is also completed prior to the mechanical laboratory testing. The pressure chamber and all other required components are shown in Figure 5.9. Initially, the design uses RF signal transmission but as metal blocks RF signal and to avoid environmental related attenuation, wired solution is later chosen. Wired connection also provides more direct, accurate and highly reliable readings.

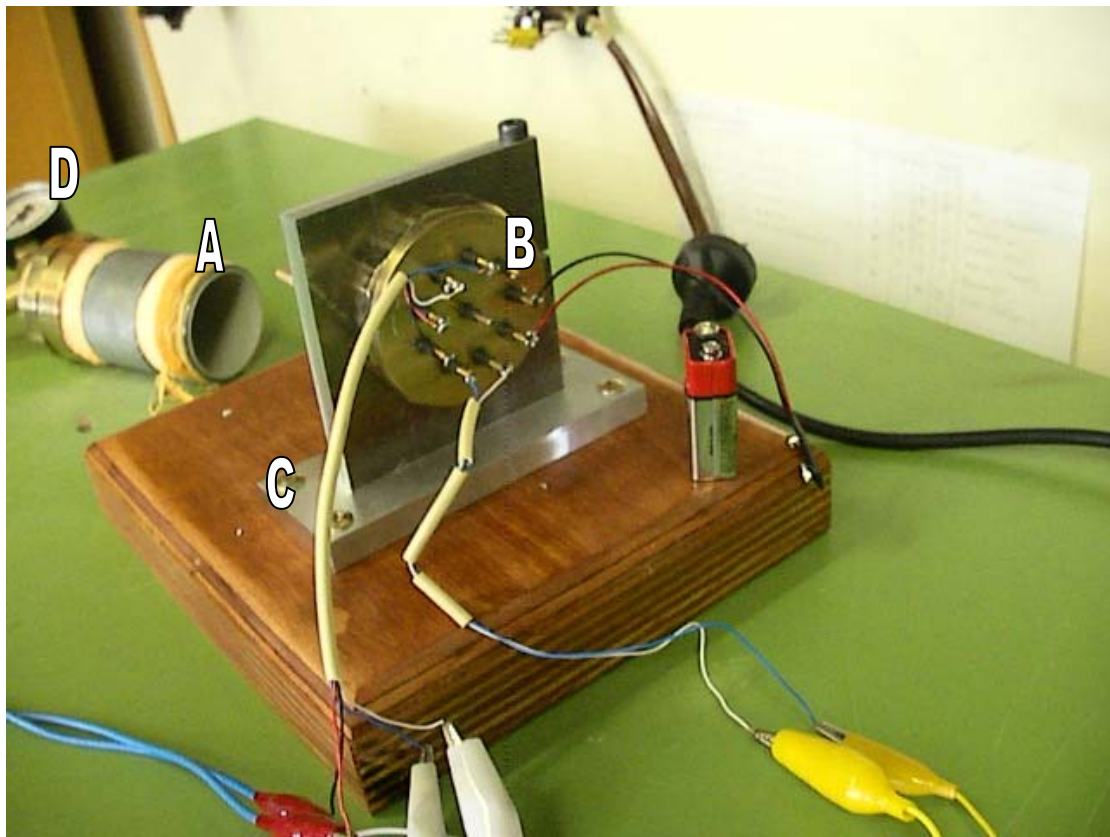


**Figure 5.9:** Pressure chamber with all other required components attached to the main cylinder (A), an end cap (B), the stand (C) and a pressure gauge (D) attached to the other end cap.

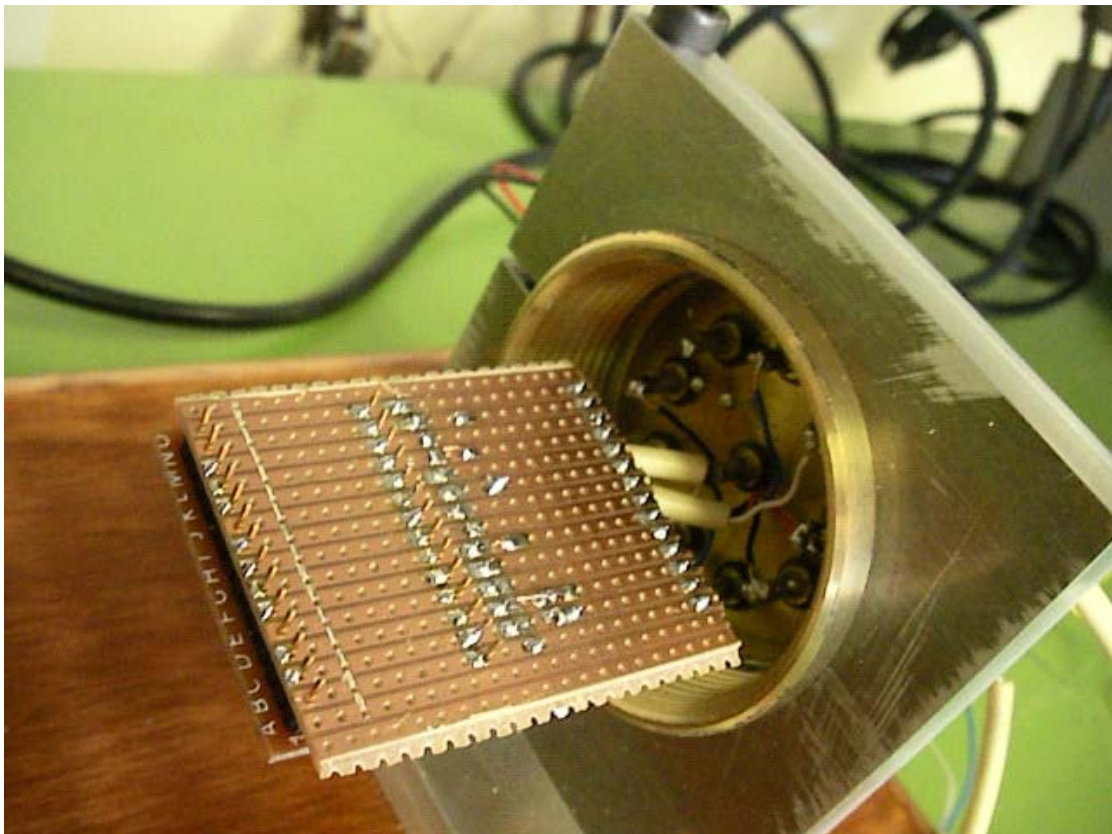
The key dimensional figures of the mechanical set-up components are given in Table 5.4. In ensuring full safety and usability of the designed pressure testing system, the whole set-up is sent for calibration to the licensed calibration vendor, Australian Calibrating Services (Australasia) Pty Ltd, where certification numbered *UAC/188-2B-1* to verify its fitness for use of up to 10 bar (1 MPa) is obtained (Australian Calibrating Services (Australasia) Pty Ltd., 2009) (see **Appendix D**).

Both threaded end caps are drilled to create hole. A hole that acts as the chamber's air inlet on one of the end cap is connected to the air flow control valve through one of the Y connector's branch. A pressure gauge is fitted to the end of another branch of the Y connector. On the other end cap, 10 holes are drilled for placement of 10 feed through capacitors. Feed through capacitors are used to enable sensor signal transmission for measurement outside of the chamber. Figure 5.10 shows the sensor circuit, the capacitive feed through fitted end cap and the stand.

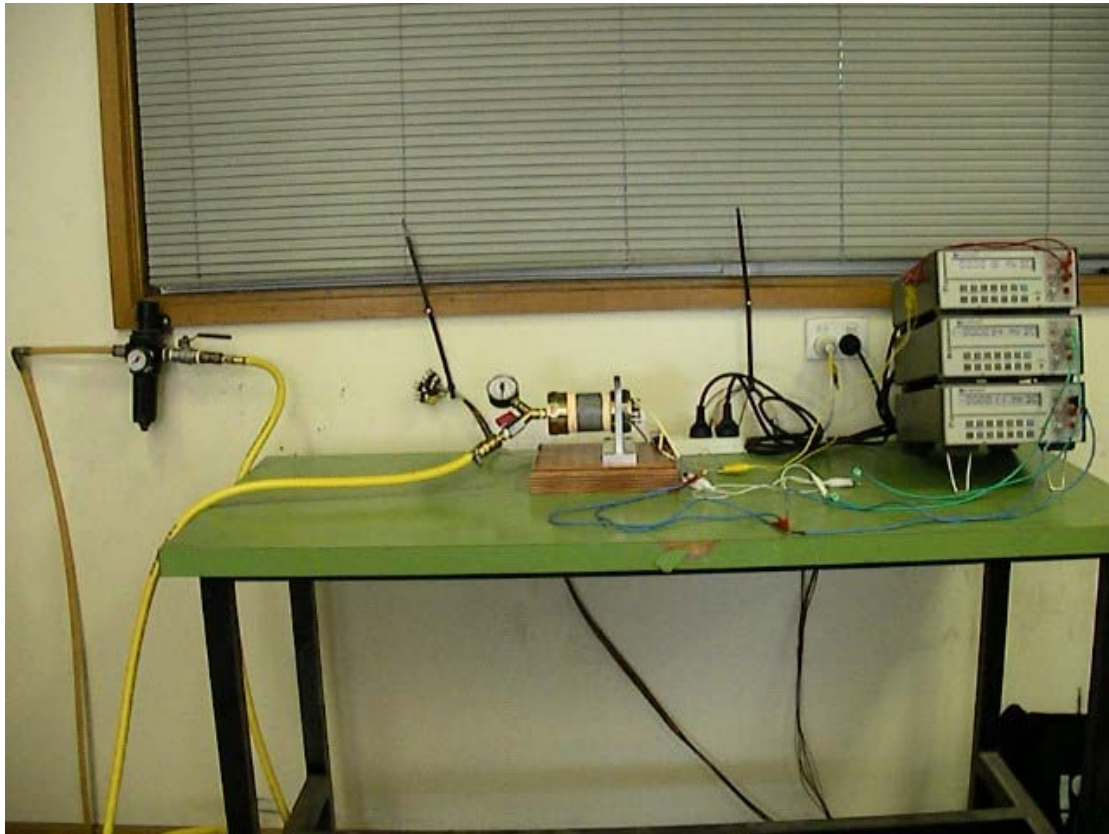
A high pressure industrial grade compressed air system is used to supply pressurized air into the chamber through the valve and the Y connector. To ensure gradual increase of pressure in the chamber, the valve is manually controlled. Air pressure is gauged using the readily fitted pressure gauge as its pressure sensing mechanism is also exposed to the pressurized air in the chamber through the other branch of the Y connector. A photograph showing the complete mechanical testing set-up is given in Figure 5.11.

TABLE 5.4. PHYSICAL DIMENSION OF THE STAINLESS STEEL PRESSURE CHAMBER

PARTS SPECIFICATION	CHAMBER CYLINDER	END CAP
Thickness	2 mm	3 mm
Length	120 mm (Inclusive of threads)	25 mm
Diameter	60 mm	65 mm



**Figure 5.10:** Pressure sensor veroboard attached to one of the end cap. The end cap is clamped to a stand. Visible is the bottom side of the veroboard.



**Figure 5.11:** *The complete mechanical testing set-up.*

Another aspect of the work at this stage is the electronic amplifier circuit design. Since the sensors are producing generally categorized as low voltage signals, it is usually necessary to amplify the signals for more efficient measurement. For that reason, amplifiers that are able to amplify differential signals are designed too as preparation when it is really needed. The designed circuit is based on a high precision instrumentation amplifiers manufactured by Burr Brown Inc (Texas Instruments Inc.), namely INA128. The circuit is shown in Figure 5.12. The gain of the amplification circuit,  $G$ , is dependent of the value of  $R_G$  in a way represented by equation (5.1).

$$G = 1 + \frac{50000}{R_G} \tag{5.1}$$

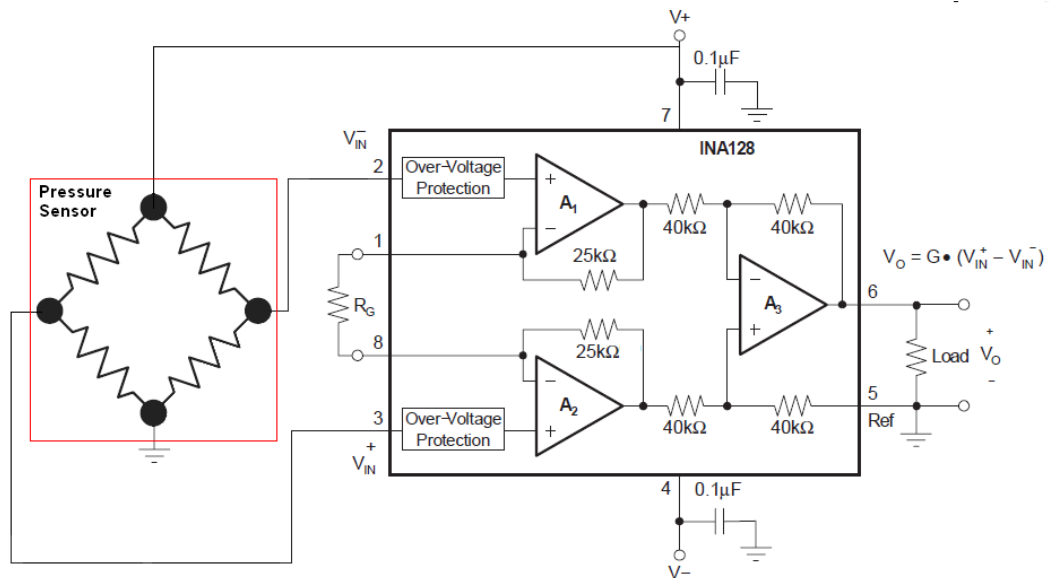
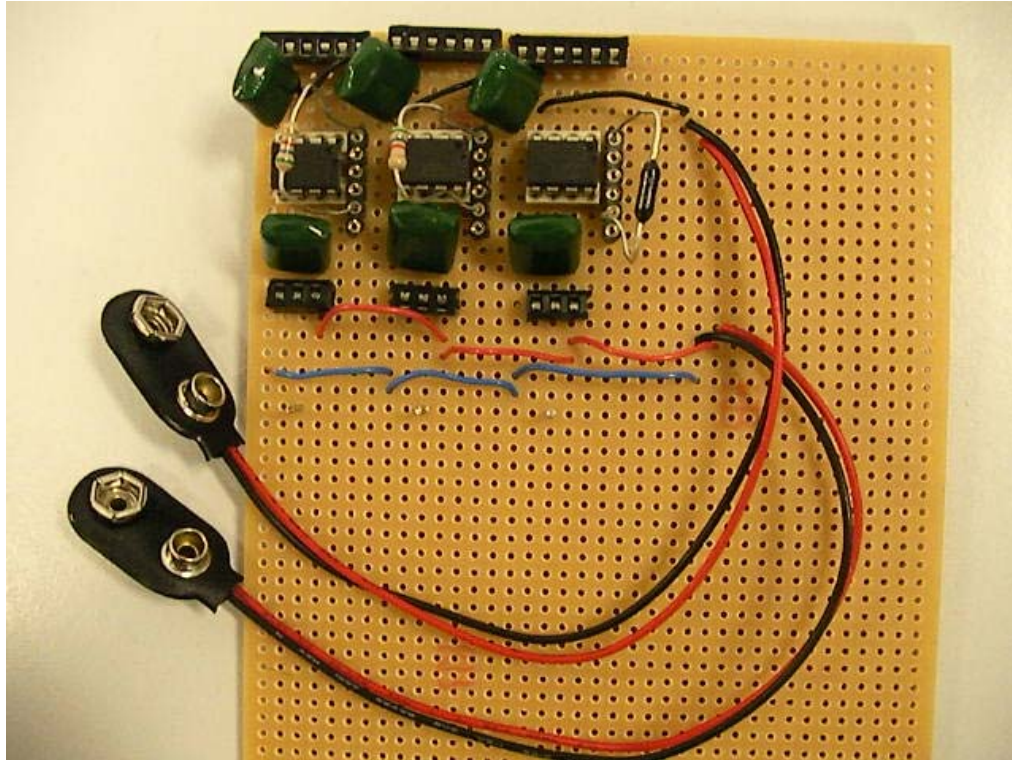


**Figure 5.12:** The amplifier circuit design and its veroboard implementation.

In performing the mechanical testing, it is necessary to ensure safety of all personnel involved. Therefore, this type of procedures requires safety approval that requires risk management and evaluation. Possible key risks and the required actions as extracted from the full risk management assessment (see **Appendix E**) are given in Table 5.5.

TABLE 5.5. RISK MANAGEMENT

TASK	HAZARD	RISK RATING	HAZARD CONTROL	NEW RATING
Pressurizing the chamber	Bursts if over the physical limitation	H	Obtained certificate of fitness up to 300 psi which sets the maximum possible pressure the chamber can withstand. However, for efficiency, 135 psi is the recommended limit.	L
Pressurizing the chamber	Bursts if over the physical limitation	H	Installed industry standard gauge on the system so that the identified calibrated pressure limit can be avoided. A regulator is placed immediately before the valve of the chamber. It is used to efficiently control the pressure from outside of the pressure chamber.	L
Placement of the pressure chamber/cylinder on table	The chamber/cylinder may roll to the edge and fall on the floor	H	A steel based stand is designed so that one of the chamber end cap is clamped to the stand	L

### 5.6.2 Results of Mechanical Testing

The unamplified results of the mechanical testing are given in Table 5.6. Pressure is increased gradually from slightly above the atmospheric pressure up to the maximum pressure allowed by the calibration certificate.

TABLE 5.6. PRESSURE SENSOR RESPONSE TO PRESSURE

PARTS  PRESSURE	100	120	278
	V <sub>OUT</sub> (mV)	V <sub>OUT</sub> (mV)	V <sub>OUT</sub> (mV)
20 psi	28.5	251.4	276.24
40 psi	29.0	259.9	277.7
60 psi	29.7	268.2	279.3
80 psi	30.4	275.5	280.4
100 psi	31.0	284.9	282.3
120 psi	31.7	293.7	284.0
140 psi	33.1	300.0	285.2

Figure 5.12 shows the graphs of the output of the three pressure sensors. The measurements begin with 20 psi level, which is equivalent to 137.9 kPa and ends at 135 psi (930.825 kPa) due to calibration limitation. It is clear that the pressure and output voltage relationship of all the sensors are very linear as expected from simulation result. The system is powered by a 9 V battery. Most interestingly, the results prove the quality of the designed piezoresistive pressure sensors in producing very linear pressure to voltage relationship, which is the key objective of this research.

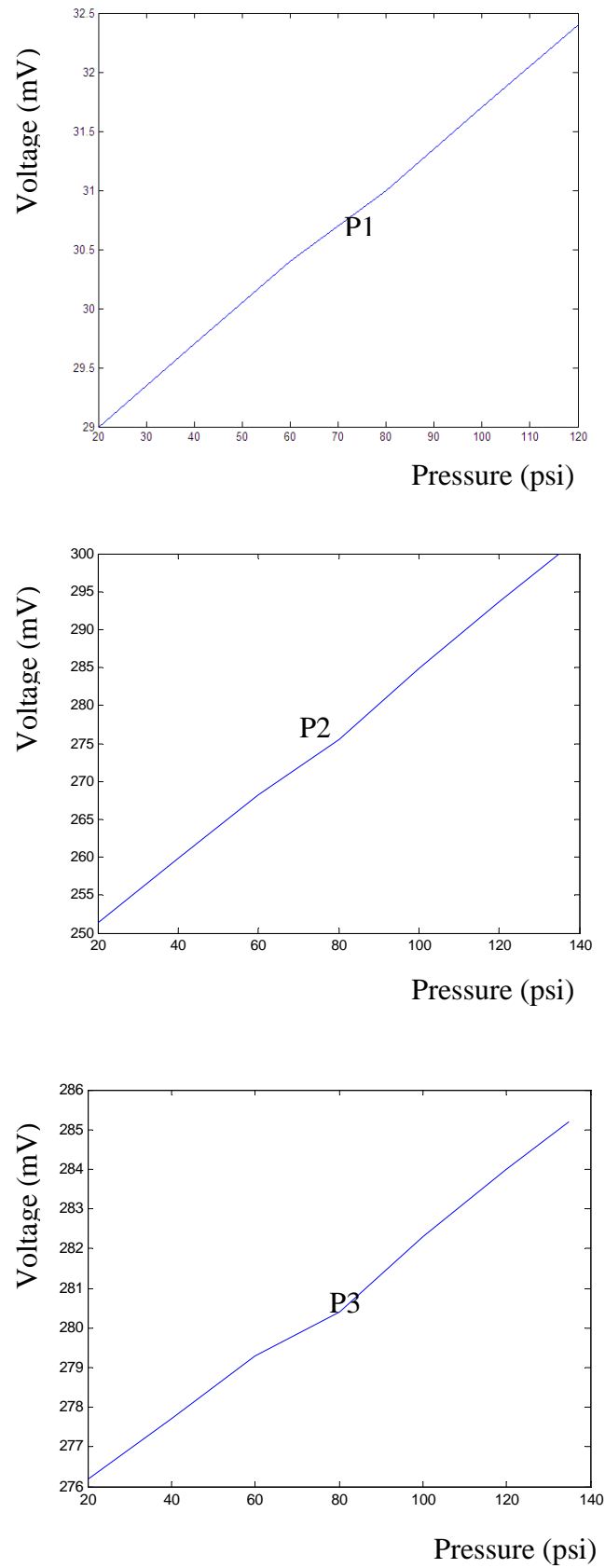


**Figure 5.13:** The graphs produced from the recorded experimental pressure and output voltage relationship. The voltages are not amplified.

## 5.7 Chapter Summary and Discussion

The testing and characterization of a silicon MEMS pressure sensor for biomedical application is described. Every steps of the project is explained, including the internal pads interconnection, Level 0 Package design, GDS II foundry file generation for tape-out, wirebonding from Level 0 Package pads to Level 1 Package pins, Level 1 Packaging, printed circuit board design, amplifier circuit design, complete circuit integration on printed circuit board, electrical testing system design and testing implementation and finally mechanical testing system design and testing implementation. All the steps are successfully performed. The results of each of the steps are recorded, displayed and discussed in detail. The key findings of the work in this chapter cover the electrical and mechanical testing results.

From the electrical design and testing aspects of the fabricated pressure sensor, the resistance of the piezoresistors are of great importance and are thus is discussed in detail. To verify this, the measured results are compared with the calculated values from the design stage. The comparison shows very acceptable resistance variations across three different sensor designs. The source of variation is identified as resulting from foundry process deviation, according to the fabrication report from the foundry (MultiMEMS, 2009b). The result proves that the layout design stage is very important to ensure achievability of the target specification as outlined during the design and optimization stage.

Further work then includes the study of the sensors' response under varying pressure. This is the final part of the research where the sensing capability is studied and discussed. Due to the nature of the measurand, this final job is also very demanding, especially in the aspects of mechanical preparation. A specialized pressure chamber is designed solely for this purpose with the sensor board size and cabling requirements in mind. Finally, the much awaited sensor characterization results are performed and the recorded results prove that the sensors' responses are very linear.

With the completion of the pressure sensor characterization, the research work is now completed successfully. Results from both finite element analysis and experimental works have proven that the sensors are linear and capable of producing high signal values. Therefore, the mission is now accomplished.

## Conclusion and Recommendations

## CHAPTER

# 6

*6.0 Chapter Overview*

*6.1 Summary of Achievements*

*6.2 Recommendation for Future Work*

### 6.0 Chapter Overview

This chapter discusses the accomplishments of this research and how the work has addressed the objectives proposed in Chapter 1 which include:

- The Development of Device Specification for Clearance Measurement.
- Comparative Study of Techniques.
- Development and Characterization of Foot Clearance Device Model.
- The Development of Device Specification for Pressure Measurement.
- Development and Characterization of Pressure Sensor Model.
- Fabrication and Testing of the Physical Pressure Sensor.

Then, the conclusions that are drawn from the findings, as well as the limitations are presented. Also, recommendations for future work are outlined in this chapter.

The findings of this thesis, such as ideas, designs and implementations of the pressure sensor for foot plantar pressure measurement and CMUT based foot clearance measurement sensor have been reported in related publications as shown in the 'List of Publications' section of each chapter.

Section 6.1 of this chapter presents the specific tasks carried out to accomplish the successful completion of this research and describes how the accomplished work has addressed the goals outlined in Chapter 1. Then, Section 6.2 highlights some recommendations for future research directions and possible works that could be applied to the study described in this thesis.

## **6.1 Summary of Achievements**

In Chapter 2, a comprehensive literature review of the present state-of-the-art of gait analysis measurement devices concluded with the limitations in the measurement foot clearance and foot plantar pressure, especially in real world measurement. For instance, the commonly used method for foot clearance measurement involves the use of markers that are not only susceptible to erroneous readings but also requires multiple expensive tools and not suitable for outdoor or real world measurement. Similarly, for foot plantar pressure measurement, commonly reported limitations include limited measurable pressure range, mechanical hysteresis and also creep. Therefore, the proposed sensors could solve this problem by using MEMS based sensors that are proven to be cheap, miniaturized and light for in shoe or on shoe portability and built of reliable mechanical material and design for quality signal output.

Following Chapter 2, are the major works involving the designs and implementations of the foot clearance and plantar pressure sensors for gait analysis which were presented through Chapters 3 to 5. The designs and

implementations of the sensors are realized through the use of industry standard software tools, namely Coventorware™ where real world implementations of the selected silicon MEMS processes are conceptualized and simulated using FEA technique. The silicon realization is achieved by the use of Infineon Technology SensoNor as foundry. Following the success of silicon fabrication, the sensor is then subjected to experimental verification after going through another series of physical processes such as wirebonding, packaging, printed circuit board assembly with electronic instrumentation amplification circuitry and finally electrical and mechanical testings.

Finally, the research carried out in this work has specifically achieved the followings results:

1. So far, the measurement of foot clearance involves the use of camera, markers and sophisticated image processing installed computer system. This approach prohibits real world measurement. For the first time, to the best of my knowledge, mobile ultrasound based measurement system is proposed and modelled for use in this increasingly important biomedical application.
2. Three distance measurement techniques are analytically modelled to identify the one that is most suitable for MEMS realization of foot clearance sensor. The most suitable technique is ultrasound sensing, which is not just proven to be very suitable for MEMS, but also in terms of response performance and silicon area required.

3. While ultrasound is generally optimized for many other applications, to the best of my knowledge, there is no reported work in the literature that includes specific analysis result performed to identify and propose an optimized ultrasound based measurement technique for foot clearance measurement, at least as far as ultrasound signal frequency range and sensor placement are concerned.
4. To the best of my knowledge, this research is the first to come up with the design, modelling and implementation details of a foot clearance measurement sensor based on the trend setting CMUT MEMS technology. This relatively new ultrasound technology is proven to be cheap, SoC CMOS compatible and miniaturized that supports realization of highly mobile on-shoe real world measurement.
5. To the best of my knowledge, this research has proposed, designed, optimized and produced a silicon MEMS pressure sensor, as a device, for foot plantar pressure measurement that exhibits the highest pressure range with great linearity.
6. To the best of my knowledge, this research has been the leader, in terms of timing, in: modelling the minimum membrane size, modelling the suitable silicon area for easy FEA implementation in Coventorware™ Analyzer module and modelling the piezoresistor layout design for a predetermined resistance value; based on the

mature industry standard MEMS process of Infineon Technology SensoNor as for the development of a pressure sensor.

7. This research has also successfully designed and produced a pressure chamber/vessel for testing and calibration of a miniaturized pressure sensor for up to 20 bar (2 MPa) (see **Appendix D**).

In short, the research has been carefully endeavoured and managed that made possible the achievement of the targeted work that encompasses the transformation of conceptual ideas into reality. This is really an interesting journey but undoubtedly, continuous hurdles and bumpy rides have clearly proven that it is a very challenging one too. One of the biggest challenges is to learn and master the use of the industry standard Coventorware™ MEMS design realization tool. The inclusion of silicon prototyping in the project execution has also increased the difficulty level of this research as all design works must be reliably modelled, precisely engineered, real industry technology compatible and financially justified. This includes mastering the real foundry design rules for manual preparation of foundry compatible GDS II tape-out file. As prototyping is successfully performed, the last and foremost frontier, which include die assembly, packaging, printed circuit board design, assembly and finally electrical and mechanical testing set-up design and implementation. After performing all the tasks mentioned here, this research is undoubtedly a life changing experience that enables mastering of wide spectrum of engineering expertise and skills.

## 6.2 Recommendation for Future Work

Due to time and other resources limitation, there are a number of opportunities related to this research that can not be explored in this research. For the sake of knowledge expansion, it is therefore listed here for consideration in future research embarkation.

This research manages to model and prove ultrasound applicability for foot clearance measurement. It is proposed that real gait analysis measurement are performed as further research based on this research's findings. The proposed extended research is obviously of a great commercial value too.

On the pressure sensor design aspect, it is hereby proposed that a specialized biocompatible packaging of the sensor is explored. A research solely dedicated to the design and fabrication of in shoe foot plantar pressure sensor packaging can complement this research and the combination of both is obviously of a valuable social and commercial impact.

## REFERENCES

Abu-Faraj, Z.O., Harris, G.F., Abler, J.H. and Wertsch, J.J. A Holter-type, 1997. 'Microprocessor-based, rehabilitation instrument for acquisition and storage of plantar pressure data', *Journal of Rehabilitation Research and Development*, vol. 34, pp. 187–194.

Abulaffio, D.R., Gelernter, I & Pillar, T., 1996. 'An ultrasonic-operated kinematic measurement system for assessment of stance balance in the clinic', *Clinical Biomechanics*, Vol. 11, pp. 173–175.

Almqvist, M., Holm, A., Persson, H. W. and Lindström, K., 2000. 'Characterization of air-coupled ultrasound transducers in the frequency range 40 kHz–2 MHz using light diffraction tomography', *Ultrasonics*, Vol. 37, No. 8, January, pp. 565-575.

Altium Ltd., *Altium Designer*, ver. Eval. Winter 2009, Altium Ltd., Sydney, Australia.

Aminian, K. and Najafi, B., 2004. 'Capturing human motion using body-fixed sensors: Outdoor measurement and clinical applications', *Computer Animation and Virtual Worlds*, vol. 15, no. 2, pp. 79-94.

Anbalagan, S.A., Uma, G and Umopathy, M., 2006. 'Modeling and simulation of Capacitive Micromachined Ultrasonic Transducer (CMUT)', *Journal of Physics: Conference Series*, vol. 34, pp. 595-600.

Ando, B., 2003. 'Electronic sensory systems for the visually impaired', *IEEE Measurement Magazine*, vol. 6 No. 2, pp. 62- 67.

Arndt, A., 2003. 'Correction for sensor creep in the evaluation of long-term plantar pressure data', *Journal of Biomechanics*, Vol. 36, pp. 1813–1817.

Ashton-Miller, J.A., 1999. 'Effects of age on obstacle avoidance during human locomotion'. in *Proceedings of the International Society of Biomechanics XVIIth Congress*, Calgary, Canada.

Australian Calibrating Services (Australasia) Pty Ltd, 2009. *Calibration Report : An Industrial Pressure Gauge and Pressure Vessel*, Melbourne, Australia: Australian Calibrating Services (Australasia) Pty Ltd, (UAC/188-2B-1).

Baborowski, J. , 2005. 'Microfabrication of Piezoelectric MEMS', in *Electronic Materials: Science and Technology, Electroceramic-Based MEMS*, eds Tuller, H. L. and Setter, N., Vol. 9, Part B, Springer, New York, USA.

Bamberg, S.J.M., Benbasat, A.Y., Scarborough, D.M., Krebs, D.E. and Paradiso, J.A., 2008. 'Gait analysis using a shoe-integrated wireless sensor system', *IEEE Transactions on Information Technology in Biomedicine*, July, vol. 12, no 4, pp. 413-423.

Bamberg, S.J.M., LaStayo, P., Dibble, L., Musselman, J. and Raghavendra, S.K.D., 2006. 'Development of a quantitative in-shoe measurement system for assessing balance: sixteen-sensor insoles', in *Proc. of the IEEE 2006 International Conf. of the Engineering in Medicine and Biology Society*, New York City, NY, Aug. 30-Sept. 3, pp. 6041-6044.

Bank, D., 2002. 'A Novel Ultrasonic Sensing System for Autonomous Mobile Systems', *IEEE Sensors Journal*, vol. 2, no. 6, pp.597-606.

Beeby, S. P., Ensell, G., Kraft, M. and White, N., 2004. *MEMS Mechanical Sensors*, Artech House Publishers, Norwood, MA,USA.

Begg, R. and Sparrow, W.. 2000. 'Gait Characteristics of Young and Older Individuals Negotiating a Raised Surface: Implications for the Prevention of Falls', *Journal of Gerontology, Series A: Biological Sciences & Medical sciences*, Vol. 55A, No 3, pp. M147-M154.

Begg, R.K., Best, R.J., Taylor, S. and Dell'Oro, L., 2007. 'Minimum foot clearance during walking: Strategies for the minimization of trip-related falls', *Gait & Posture*, vol. 25, pp.191-198.

Berg, W.P., Alessio, H.M., Mills, E.M. and Tong, C.,1997. 'Circumstances and consequences of falls in independent community-dwelling older adults', *Age Ageing*, Vol. 26 , No. 4, pp. 261–268.

Berns, A., Buder, U., Obermeier, E., Wolter, A. and Leder, A., 2006. 'AeroMEMS sensor array for high-resolution wall pressure measurements', *Sensors and Actuators A:Physical*,vol. 132,pp. 104-111.

Bernstein, J. J., Finberg, S. L., Houston, K., Niles, L. C., Chen, H. D., Cross, L. E., Li, K. K. and Udayakumar, K., 1997, 'Micromachined high frequency ferroelectric sonar transducers,' *IEEE Transactions on Ultrasonics, Ferroelectrics, and Frequency Control*, vol. 44, no. 5, pp. 960–969.

Best, R. and Begg, R.K., 2006. 'Overview of Measurement Analysis and Gait Features', in *Computational Intelligence for Movement Sciences: Neural Networks and Other Emerging Techniques*, eds Begg, R.K. and Palaniswami, M., Hershey, PA, USA, pp. 1-69.

Bilgin, A., 2003. *A simulation model of indoor environments for ultrasonic sensors*, MSc Thesis,Bilkent University,Turkey.

Billing, D. C., Nagarajah, C. R., Hayes . J. P., Baker, J. ,2006. 'Predicting ground reaction forces in running using micro-sensors and neural networks', *Sports Engineering*, Vol. 9, No. 1, pp. 15- 27.

Bistue, G., Elizalde, J. G., Garcia-Alonso, S., Castano, E., Gracia, F. J. and Garcia-Alonso, A., 1997. 'A design tool for pressure microsensors based on FEM simulations', *Sensors and Actuators A: Physical*, vol. 62, pp. 591-594.

Bohn, D.A. 1988. 'Environmental Effects on the Speed of Sound, *Journal of Audio Engineering Society*, Vol. 36, No. 4, pp. 223-231.

Bontrager, E.L.1998. 'Instrumented gait analysis systems' in *Gait Analysis in the Science of Rehabilitation*, ed. De Lisa, J.A., Chapter 2. Department of Veterans Affairs, Washington, DC, USA. pp. 11-32.

Boulton, A., 2004. 'Pressure and the diabetic foot: clinical science and offloading techniques', *The American Journal of Surgery*, Vol. 187, No. 5, pp. S17-S24.

Bozkurt, A., Ladabaum, I., Atalar, A. and Khuri-Yakub, B.T., 1999. 'Theory and Analysis of Electrode Size Optimization for Capacitive Microfabricated Ultrasonic Transducers', *IEEE Transactions Ultrasonics, Ferroelectrics, and Frequency Control*, vol. 46, no. 6, pp.1364-1375.

Bruinsma, A.J.A, 2006. *Level sensor lithographic apparatus and device manufacturing method*, Paris,France: European Patent Office, EP1674939A1.

Bryzek, J., Roundy, S., Bircumshaw, B., Chung, C. A. C. C., Castellino, K. A. C. K., Stetter, J. R. and Vestel, M. A. V. M., 2006, 'Marvelous MEMS', *Circuits and Devices Magazine, IEEE*, vol. 22, pp. 8-28.

Campbell, E., Davis, LAJ, Hayward, G. and Hutchins, D.A., 2007. 'Cross-coupling in sealed cMUT arrays for immersion applications', in *Proceedings of 2007 IEEE Ultrasonics Symposium*, pp 2135-2138.

Cardenas, M.L., Cardenas-Valencia, A. M., Dlutowski, J., Bumgarner, J. and Langebrake, L., 2007. 'A finite element method modeling approach for the development of metal-silicon nitride MEMS single-use valve arrays', *J. Micromech. Microeng.*, vol. 17, pp 1671-1679.

Carol, M. W., Sarah, M. G. and Sharon, J. D., 1999. 'The shock attenuation characteristics of four different insoles when worn in a military boot during running and marching', *Gait & Posture*, vol. 9, no. 1, pp.31-37.

Carullo, A. and Parvis, M., 2001. 'An Ultrasonic Sensor for Distance Measurement in Automotive Applications', *IEEE Sensors Journal*, vol. 1, no. 2, pp.143-146.

Cavanagh, PR., Ulbrecht, JS. and Caputo, GM., 2000. 'New developments in the biomechanics of the diabetic foot',. Sep-Oct., *Diabetes Metab Res*, Rev. 16, Suppl. 1, pp. S6-S10.

Chebli. R. and Sawan, M., 2004. 'A CMOS high voltage dc-dc up converter dedicated for ultrasonic applications', in *Proceedings of the IEEE International Workshop for Systems-on-Chip*, IEEE , pp. 119–122.

Chen, Z. and Luo, R., 1998. 'Design and implementation of capacitive proximity sensor using microelectromechanical systems technology, *IEEE Trans. Ind. Electron.* Vol. 45, no 6, pp. 886–894.

Chesnin, K. J., Selby-Silverstein, L. and Besser, M. P., 2000. 'Comparison of an in-shoe pressure measurement device to a force plate: concurrent validity of center of pressure measurements', *Gait & Posture*, Vol. 12, No. 2, 1 October, pp. 128-133.

Cittadine, A. 2000. *MEMS Reshapes Ultrasonic Sensing*, Sensors, viewed February 1, 2000, <<http://www.sensorsmag.com/sensors/MEMS/MEMS-Reshapes-Ultrasonic-Sensing/ArticleStandard/Article/detail/360476>>

Coleman, D.J., Silverman, R.H., Chabi, A., Rondeau, M.J., Shung, K.K., Cannata, J., Lincoff, H. 2004. 'High-resolution Ultrasonic imaging of the posterior segment', *Ophthalmology*, Vol. 111, No 7, pp. 1344-1351.

Coventor Inc.,2006. *CoventorWare® 2006:Master Help*, Coventor Inc., Cary, NC, USA.

Coughlin, M. J., 2000. 'Rheumatoid forefoot reconstruction - A long-term follow-up study', *Journal of Bone and Joint Surgery America*, vol. 82, pp. 322–341.

Curran, S. A. and Dananberg, H. J. 2005. 'Future of Gait Analysis: A Podiatric Medical Perspective', *Journal of American Podiatry Medical Association*, vol. 95, no 2, pp 130-142.

De Bruyker, D., Cozma, A. and Puers, R., 1998. 'A combined piezoresistive/capacitive pressure sensor with self-test function based on thermal actuation', *Sensors and Actuators A: Physical*, Vol. 66, No. 1-3, pp. 70-75.

DeHennis, A. and Chae,, J. , 2008. 'Pressure Sensors', in *Comprehensive Microsystems: Fundamentals, Technology and Applications*, Elsevier B.V., 2.04, Vol. 2, eds Gianchandani, Y., Tabata, O. and Zappe, H., Amsterdam, The Netherlands.

DeLong, R. and Booth, C., 2004. *Designing a Non-Contact Appliance Control Panel*, APPLIANCE Magazine, viewed 30 August 2009, <http://www.appliancemagazine.com/editorial.php?article=554&zone=1&first=1>

Dutta, T. and Fernie, G. R., 2005. 'Utilization of ultrasound sensors for anti-collision systems of powered wheelchairs', *IEEE Transaction Neural System Rehabilitation Engineering*, Vol. 13 No 1, pp 24-32.

Eccardt, P-C., Niederer, K. and Fischer, B., 1997, 'Micromachined Transducers for Ultrasound Applications', in *Proceedings of IEEE Ultrasonics Symposium*, IEEE, pp. 1609-1618.

Elble, R.J., Thomas, S.S., Higgins, C. and Colliver, J., 1991. 'Stride-dependent changes in gait of older people', *Journal of Neurology*, vol. 238, no 1, pp 1-5.

Erdemir, A., Petre, M., Budhabhatti, S., Doehring, T., Goske, S., Thangudu, P., Considine, J., Bly, D., Wyllie, J. and Cavanagh, P. R., 2005. 'Therapeutic Footwear Design: A Finite Element Modeling Approach', in *Proceedings of ISB XXth Congress - ASB 29th Annual Meeting*, July 31 - August 5, Cleveland, Ohio, USA.

Ergun, A. S., Yaralioglu, G.G., Oralkan, O. and Khuri-Yakub, B. T., 2006. 'Techniques and Applications of Capacitive Micromachined Ultrasonic Transducers', in *MEMS/NEMS Handbook Techniques and Applications*, ed. Cornelius T. Leondes, vol. 1, Springer, New York, USA, pp. 223-285.

Ergun, A.S., Yaralioglu, G.G. and Khuri-Yakub, B.T., 2003, 'Capacitive Micromachined Ultrasonic Transducers: Theory and Technology', *Journal of Aerospace Engineering*, pp 76-84.

Faivre, A., Dahana, M. , Parratteb B. and Monnier, G., 2004. 'Instrumented shoes for pathological gait assessment', *Mechanics Research Communications*, Vol. 31, no. 5, September-October, pp. 627-632.

Folkmer, B., Steiner, P. and Lang, W., 1996. 'A pressure sensor based on a nitride membrane using single-crystalline piezoresistors', *Sensors and Actuators A: Physical*, Vol. 54, No. 1-3, June, pp.s 488-492.

Freescale, 2006. *Technical Data: Electric Field Imaging Device*, Freescale Semiconductor, Inc., Austin, Texas, USA

Gefen, A.,2002. 'Biomechanical analysis of fatigue-related foot injury mechanisms in athletes and recruits during intensive marching', *Medical and Biological Engineering and Computing*,Vol. 40, No. 3, pp. 302- 310.

Gong, S., 2004. 'Effects of pressure sensor dimensions on process window of membrane thickness', *Sensors and Actuators A*, Vol. 112, pp. 286–290.

Gong, S.-C. and Lee, C., 2001. 'Analysis solutions of sensitivity for pressure microsensors', *IEEE Sensors Journal* , Vol.1, No.4, pp. 340–344.

Grace, R,H., 1991. 'OEM Sensors For The'90's: An Overview Of Enabling Technologies', in *Proceedings of Electro International 1991*, pp. 648-654.

Greve, D.W., Wu, W. and Oppenheim, I.J., 2006. 'Modes and Damping in Cmut Transducers for Acoustic Emission', in *Proceedings of 2006 IEEE Ultrasonics, Ferroelectrics, and Frequency Control*, pp. 661-664.

Gueuning, F. E., Varlan, M., Eugene, C. E. and Dupuis P., 1997. 'Accurate distance measurement by an autonomous ultrasonic system combining time-of-flight and phase-shift methods', *IEEE transactions on instrumentation and measurement*, vol. 46, no 6, pp. 1236-1240.

Hamel, K. A., Okita, N., Higginson, J. S., Cavanagh, P. R., 2005. 'Foot clearance during stair descent: effects of age and illumination', *Gait & Posture*, Vol. 21, No. 2, pp. 135-140.

Hierold, C., 2003. 'Micro- and Nanosystems: Review and Outlook', in *Proceedings of the 14th Micromechanics Europe Workshop (MME03)*, Nov. 2-4, Delft, The Netherlands, pp. 101-104.

Hsiao H, Guan J, Weatherly M., 2002. 'Accuracy and precision of two in-shoe pressure measurement systems', *Ergonomics.*, vol. 45, no. 8, pp 537-555.

Huang, Y., Ergun, A.S., Haeggstrom, E., Badi, M.H. and Khuri-Yakub,B.T., 2003. 'Fabricating capacitive micromachined ultrasonic transducers with wafer-bonding technology', *Journal of Microelectromechanical Systems* , vol. 12, no 2, pp. 128-137.

Infineon Technologies SensoNor AS, 2009. Measurement Report MR-1201-E, Horten, Norway: Infineon Technologies SensoNor AS.

Infineon Technologies SensoNor AS, 2009. Measurement Report MR-1202-E, Horten, Norway: Infineon Technologies SensoNor AS.

Infineon Technologies SensoNor AS, 2007. MultiMEMS Design Handbook Version 4.1, Horten, Norway: Infineon Technologies SensoNor AS.

Jia, G. and Madou, M.J., 2006. 'MEMS Fabrication', in: *The MEMS Handbook: MEMS Design and Fabrication*, 2<sup>nd</sup> Ed., 3, Vol. 2, ed. Gad-el-Hak, CRC Taylor and Francis, Boca Raton, Florida, USA.

Jin, X., Ladabaum, I. and Khuri-Yakub, B.T., 1998. 'The Microfabrication of Capacitive Ultrasonic Transducers', *Journal of Microelectromechanical Systems*, Vol. 7, No. 3, pp. 295-302.

Jones, R., Robertson, T.J., Hutchins, D.A. and Billson, D.R., 2001. 'Novel, Wide Bandwidth, Micromachined Ultrasonic Transducers', *IEEE Transactions on Ultrasonics, Ferroelectrics, and Frequency Control*, vol. 48, no. 6, pp. 1495- 1508.

Jovanov, E., Milenkovic , A., Otto , C , and de Groen , P. C, 2005. A wireless body area network of intelligent motion sensors for computer assisted physical rehabilitation, *Journal of NeuroEngineering and Rehabilitation*, vol. 2, no. 6. March.

Judy, J. W., 2001. 'Microelectromechanical Systems (MEMS) - Their Design, Fabrication, and Broad Range of Application', *Journal of Smart Materials*, vol. 10, no. 6, pp. 1115-1134.

Kajita, S. and Tani, K., 1997. 'Adaptive Gait Control of a Biped Robot Based on Realtime Sensing of the Ground Profile', *Autonomous Robots*, Vol. 4, No. 3, pp. 297-305.

Kanda, Y. and Yasukawa, A., 1997. 'Optimum design considerations for silicon piezoresistive pressure sensors', *Sensors and Actuators A: Physical*, vol. 62, pp. 539-542.

Karki, J.. 1999. *Signal Conditioning Wheatstone Resistive Bridge Sensors, Application Report SLOA034*, Texas Instruments Inc., Dallas, Texas, USA, September.

Ko, H.S., Liu, C.W. and Gau, C., 2007. 'Micropressure sensor fabrication without problem of stiction for a wider range of measurement', *Sensors and Actuators A: Physical*, Vol. 138, No. 1, 20 July, pp. 261-267.

Kong, K. and Tomizuka, M., 2008, 'Estimation of Abnormalities in a Human Gait Using Sensor-Embedded Shoes', in *Proceedings of the 2008 IEEE/ASME Int. Conf. on Adv. Intel. Mechatronics*, July 2-5, Xian, China, pp. 1331-1336.

Kotzar, G., Freas, M., Abel, P., Fleischman, A., Roy, S., Zorman, C., Moran, J.M. and Melzak, J. 2002. 'Evaluation of MEMS materials of construction for implantable medical devices', *Biomaterials*, Vol. 23, no 13, pp.2737–2750.

Krondorfer, R. and Kim, Y., 2007. 'Packaging Effect on MEMS Pressure Sensor Performance', *IEEE Transactions on Components and Packaging Technologies*, Vol. 30, No. 2, June, pp 285-293.

Krondorfer, R. H. , 2004. On Packaging of MEMS. Simulation of Transfer Moulding and Packaging Stress and their Effect on a Family of piezo-resistive Pressure Sensors , PhD Thesis, Norwegian University of Science and Technology, Norway.

Kuratli, C. and Huang, Q., 1998. 'A Fully Integrated Self-Calibrating Transmitter/Receiver IC for an Ultrasound Presence Detector Microsystem', *IEEE Journal of Solid-State Circuits*, Vol. 33, No. 6, June, pp. 832-841.

Kuratli, C., and Huang, Q., 2000, 'A CMOS Ultrasound Range-finder Microsystem', *IEEE Journal of Solid State Circuits*, vol. 35, no. 12, pp.2005-2017.

Ladabaum, I., Jin, X., Soh, H.T., Atalar, A. and Khuri-Yakub, B.T., 1998. 'Surface Micromachined Capacitive Ultrasonic Transducers', *IEEE Transactions on Ultrasonics, Ferroelectrics, and Frequency Control*, vol. 45 no 3, pp.678-690.

Lai, D.T.H., Begg,R.K., Charry, E.,Palaniswami, M. and Hill, K., 2008. 'Measuring toe clearance using a wireless inertial sensing device', in *Proceedings of International Conference on Intelligent Sensors, Sensor Networks and Information Processing*, Sydney, Australia . December 15-18, pp. 375-380.

Lavery, L. A., Armstrong, D. G., Wunderlich, R. P., Tredwell, J. and Boulton, A. J.M., 2003. 'Predictive Value of Foot Pressure Assessment as Part of a Population-Based Diabetes Disease Management Program', *Diabetes Care*, April, Vol. 26, pp.1069-1073.

Lawrence R. C., Helmick C. G., Arnett F. C., Deyo, R. A., Felson, D. T., Giannini, E. H., Heyse, S. P., Hirsch, R., Hochberg, M. C., Hundek, G. G., Liang, M. H., Yillemer, S. R., Steen, V. D. and Wolfe, F., 1998. 'Estimates of the prevalence of arthritis and selected musculoskeletal disorders in the United States', *Arthritis & Rheumatism*, vol. 41, no. 5, pp. 778-799.

Lee, D. and Choi, Y. 2008. 'A novel pressure sensor with a PDMS diaphragm', *Microelectronic Engineering*, Vol. 85, No. 5-6, May-June, pp. 1054-1058.

Lee, H., Chang, S. and Yoon, E., 2006. 'A Capacitive Proximity Sensor in Dual Implementation with Tactile Imaging Capability on a Single Flexible Platform for Robot Assistant Applications', in *Proceedings of IEEE International Conference on MEMS 2006*. Technical Digest, Istanbul, Turkey, pp. 606-409.

Lee, N. K. S., Goonetilleke, R. S., Cheung, Y. S. and So, G. M. Y., 2001. 'A flexible encapsulated MEMS pressure sensor system for biomechanical applications', *Microsystem Technologies*, vol. 7, pp. 55-62.

Liedtke, C., Fokkenrood, S. A.W., Menger, J. T., van der Kooij, H. and Veltink, P. H., 2007. 'Evaluation of instrumented shoes for ambulatory assessment of ground reaction forces', *Gait & Posture*, Vol. 26, No. 1, June, pp. 39-47.

Ling, H., Choi, P., Zheng, Y. and Lau, K., 2007. 'Extraction of mechanical properties of foot plantar tissues using ultrasound indentation associated with genetic algorithm', *Journal of Materials Science: Materials in Medicine*, Vol. 18, No. 8, pp. 1579-1586.

Linlin, Z., Chen, X. and Guangdi, S., 2006. Analysis for load limitation of square-shaped silicon diaphragms', *Solid-State Electronics*, vol. 50, pp. 1579-1583.

Liu, C, 2006, *Foundations of MEMS*, Prentice Hall, Upper Saddle River NJ.

Liu, L.L., Mukdadi, O.M., Herrmann, C.F., Saravanan, R.A., Hertzberg, J.R., George, S. M., Bright, V.M. and Shandas, R., 2004. 'A Novel Method for Fabricating Capacitive Micromachined Ultrasonic Transducers with Ultra-Thin Membranes', in *IEEE Ultrasonics Symposium 2004 Proceedings*, IEEE, pp 497-501.

Luo, Berglund & An, 1998. 'Validation of F-Scan pressure sensor system - A technical note', *Journal of Rehabilitation Research and Development*, Vol. . 35, No . 2, pp 186-191.

Luo, R.C., 1996, 'Sensor Technologies and Microsensor Issues for Mechatronics Systems', *IEEE ASME Transactions On Mechatronics*, Vol. 1, No. 1, pp.39-50.

Maclsaac, D., and Hämäläinen, A., 2002, 'Physics and Technical Characteristics of Ultrasonic Sonar Systems', *The Physics Teacher*, vol. 40 pp. 39-46.

Mackey, J. R., and Davis, B. L., 2006. 'Simultaneous shear and pressure sensor array for assessing pressure and shear at foot/ground interface', *Journal of Biomechanics*, Vol. 39, No. 15, pp. 2893-2897.

Magori, V. 1994. 'Ultrasonic sensors in air', in *Proceedings of IEEE Ultrasonics Symposium 1994*, pp. 471-481.

Magori, V. and Walker, H., 1987. 'Ultrasonic Presence Sensors with Wide Range and High Local Resolution', *IEEE Transactions on Ultrasonics, Ferroelectrics, and Frequency Control*, Vol. UFFC-34, No. 2, pp. 202-222.

Maier-Schneider, D., Maibach, J. and Obermeier, E., 1995. 'A new analytical solution for the load-deflection of square membranes', *Journal of Microelectromechanical Systems*, vol. 4, no. 4, pp 238-241.

Manthey, W., Kroemer, N. and Magori, V., 1992 *Ultrasonic transducers and transducer arrays for applications in air*, *Meas. Sci. Technol.* Vol. 3, No. 3 pp 249-261.

Margolis, D. J., Knauss, J., Bilker, W., Baumgarten, M., 2003. 'Medical conditions as risk factors for pressure ulcers in an outpatient setting', *Age and Ageing*, vol. 32, pp. 259–264.

Martínez-Nova, A., Cuevas-García, J., Pascual-Huerta, J. and Sánchez-Rodríguez, R., 2007. 'BioFoot® in-shoe system: Normal values and assessment of the reliability and repeatability', *The Foot*, Vol. 17, No. 4, pp. 190-196.

Massa, D.P., 1999. *Choosing an ultrasonic sensor for proximity or distance measurement Part 1: acoustic considerations*, *Sensors*, vol. 16, no 2, viewed 30 August 2009  
<<http://www.sensorsmag.com/sensors/article/articleDetail.jsp?id=321383>>.

Matar, B., Rossignol, C., Pizarro, L., Dos Santos, S. and Putat, F., 2000. 'Mapping of Airborne Ultrasonic Fields Using Optical Heterodyne Probing and Tomography Reconstruction', in *Proceedings of 2000 IEEE Ultrasonics Symposium*, pp 1117-1120.

Matilla, P., Tsuzuki, F., Vataaja, H., and Sasaki, K., 1995. 'Electroacoustic Model for Electrostatic Ultrasonic Transducers with V-grooved Backplates', *IEEE Transactions on Ultrasonics, Ferroelectrics, and Frequency Control*, vol. 42, no. 1, pp. 1-7.

MEMSCAP Inc., n.d., *MUMPS*, Research Triangle Park, NC, USA, viewed 30 August 2009, <[http://www.memscap.com/en\\_mumps.html](http://www.memscap.com/en_mumps.html)>

Morris, S.J., 2004, *Shoe-integrated sensor system for wireless gait analysis*, PhD Thesis, MIT, USA.

Mueller, M. J, 1999. 'Application of plantar pressure assessment in footwear and insert design', *Journal of Orthopaedics and Sports Physical Therapy*, vol. 29, no 12, pp. 747-756.

MultiMEMS, 2007, *MultiMEMS Design Handbook*, Horten, Norway: Infineon Technology SensoNor AS.

MultiMEMS, 2009a, *Project Report*, Horten, Norway: Infineon Technology SensoNor AS, (RP 120501).

MultiMEMS, 2009b, *Electrical Measurement*, Report, Horten, Norway: Infineon Technology SensoNor as, (MR 1201).

Muralt, P., 2005. 'Micromachined Ultrasonic Transducers and Acoustic Sensors Based on Piezoelectric Thin Films', in *Electroceramic-Based MEMS: Fabrication-Technology and Applications*, ed. Setter, N., Chapter 3, Springer, New York, USA.

Noble R.A, Jones, A. D. R., Robertson, T. J., Hutchins, D. A. and Billson, D. R., 2001. 'Novel, Wide Bandwidth Micromachined Ultrasonic Transducers', *IEEE Transactions on Ultrasonics, Ferroelectrics, and Frequency Control*, vol. 48, no. 6, November, pp. 1495-1507.

Noble, R.A., Anthony, D., Schindel, D.W., Hutchins, D.A., Zou, L. and Sayer, M, 1995. 'The Design and Characterization of Micromachined Air-coupled Capacitance Transducer', *IEEE Transactions on Ultrasonics, Ferroelectrics, and Frequency Control*, vol. 42, no. 1, pp. 42-50.

Novel Gmbh, n.d.. *Product Info : Pedar Insole Sensors and Pedar Dorsal Pad Sensors*, Munich, Germany, viewed 30 August 2009, <<http://www.novel.de/productinfo/sensors-matrix.htm>>

Octavio, A., Martin, C.J., Martinez, O., Hernando, J., Gomez-Ullate, L. and Montero de Espinosa, F., 2007. 'A Linear CMUT Air-Coupled Array For NDE Based on MUMPS', in *Proceedings of IEEE Ultrasonics Symposium*, 28-31 Oct., pp. 2127-2130.

Ohya, A., Ohno, T. and Yuta, S., 1996. 'Obstacle Detectability of Ultrasonic Ranging System and Sonar Map Understanding', *Robotics and Autonomous Systems*, Vol.18, pp.251-257.

Oralkan, O. Ergun, A.S. Johnson, J.A. Karaman, M., Demirci, U., Kaviani, K. and Lee, T.H., 2002. 'Capacitive Micromachined Ultrasonic Transducers: Next-Generation Arrays for Acoustic Imaging? *IEEE Transactions on Ultrasonics, Ferroelectrics, and Frequency Control*, vol 49, pp. 1596-1610.

Osoinach, B.,2008. *Proximity Capacitive Sensor Technology for Touch Sensing Applications*, Freescale Semiconductor Inc., Tempe, Arizona, USA.

Pappalardo, M., Caliano, G., Savoia, A. S., and Caronti, A., 2008, 'Micromachined Ultrasonic Transducers', in *Piezoelectric and Acoustic Materials for Transducer Applications*, eds A. Safari and E. K. Akdoğan, Chapter 22, Springer USA, New York, USA.

Patel, A., Kothari, M., Webster, J.G., Tompkins, W.J. and Wertsch, J.J. 1989. 'A capacitance pressure sensor using a phase-locked loop', *Journal of Rehabilitation Research and Develeopment*, vol 26, no. 2, pp 55-62.

Patil, K.M., Charanya, G. and Prabhu, K.G., 2002. 'Optical Pedobarography for Assessing Neuropathic Feet in Diabetic Patients—A Review', *The International Journal of Lower Extremity Wounds*, Vol. 1, No. 2, pp. 93-103.

Peters, D., Bolte, H., Marschner, C., Refhuss, S. and Laur, R., 2002. 'Modeling and designing quadratic membrane structures', *Microelectronics Journal*, vol. 33, pp. 11-19.

Qinetiq Ltd.n.d..*Smart Silicon MEMS Prototyping and Manufacture*, London, UK, viewed 30 August 2009, <[http://www.qinetiq.com/home/capabilities/electronics/INTEGRAMplus/Smart\\_Silicon\\_MEMS\\_Prototyping\\_and\\_Manufacture.html](http://www.qinetiq.com/home/capabilities/electronics/INTEGRAMplus/Smart_Silicon_MEMS_Prototyping_and_Manufacture.html)>

Rodgers, M.M., 1988. 'Dynamic biomechanics of the normal foot and ankle during walking and running', *Physical Therapy*, vol. 68, no 12, pp. 1822-1830.

Sabatini, A. M. and Colla, V., 1998. 'A method for sonar based recognition of walking people', *Robotics and Autonomous Systems*, Vol. 24, pp. 117-126, 1998.

Santarmou, E., Dozza, M., Lannocca, M., Chiari, L. and Cappello, A., 2006. 'Insole pressure sensor-based audio-biofeedback for balance improvement', *Gait & Posture*, vol. 24, pp. S30-S31.

Schindel, D. W., Hutchins, D. A., Zou, L. and Sayer, M., 1995. 'The Design and Characterization of Micromachined Air-Coupled Capacitance Transducers', *IEEE Transactions on Ultrasonics, Ferroelectrics, and Frequency Control*, Vol. 42, No. 1, Jan., p42-50.

Schweinzer, H. and Elmer, H., 2005. 'High Resolution Ultrasonic Distance Measurement System Using Pulse Compression and Their Application', *Key Engineering Material*, vol. 295-296, pp. 301-306.

Shih-Chin, G. and Chengkuo, L., 2001. 'Analytical solutions of sensitivity for pressure microsensors,' *IEEE Sensors Journal*, vol. 1, pp. 340-344.

Sieh P. and Steffen M. 2006. *Playing the E-Field: Capacitance Sensors in Action*, Sensors, viewed 11 Dec. 2006, -  
<<http://www.sensormag.com/sensors/content/printContentPopup.jsp?id=369839>>.

Simon, S.R., 2004. 'Quantification of human motion: gait analysis—benefits and limitations to its application to clinical problems', *Journal of Biomechanics*, Vol. 37, No. 12, pp. 1869-1880.

Simpson, R., LoPresti, E., Hayashi, S., Nourbakhsh, I. and Miller, D., 2004. 'The Smart Wheelchair Component System', *Journal of Rehabilitation Research and Development*, Vol. 41, No 3B, May/June, pp. 429 – 442.

Smith, C.S., 1954. 'Piezoresistance Effect in Germanium and Silicon', *Physical Review*, Vol. 94, No. 1, pp 42-49.

Smith, C.V., Jr. and Schoenwald, J.S., 1984. 'A Two Tone Narrow Bandwidth Range-Rate Finding System', in *Proceedings of IEEE 1984 Ultrasonics Symposium*, pp. 465 – 468.

Song, K., Chen, C. and Huang, C. C., 2004. 'Design and experimental study of an ultrasonic sensor system for lateral collision avoidance at low speeds', in *Proceedings of 2004 IEEE Intelligent Vehicles Symposium*, 14-17 June, pp. 647 – 652.

Spearing, S.M., 2000. 'Materials Issues in MEMS', *Acta Materialia*, vol. 48, pp.179-196.

Spoliansky, D., Ladabaum, I., Khuri-Yakub, B.T., 1996, 'Micromachined Ultrasonic Air-Transducers (MUTs)', *Microelectronic Engineering*, Vol. 30, No. 1, pp. 535-538.

Stewart, B., n.d., *Beyond Touch Panels: Appliance Solutions Using Electric Field Sensors*, Freescale Semiconductor Inc., Tempe, Arizona, USA.

Svilainis, L. and Dumbrava, V., 2005. 'Design of a low noise preamplifier for ultrasonic transducer', *ULTRAGARSAS*, vol. 55 no.2, , pp.28-33.

Tanwar, H., Nguyen L. and Stergiou, N., 2007. 'Force Sensitive Resistor (FSR)-based Wireless Gait Analysis Device' , in *Proceedings of Telehealth - 2007*, May 31 – June 1 ,Montreal, QC, Canada.

Tekscan Inc. n.d..F-Scan® *Mobile System untethered in-shoe analysis*, Boston, USA, viewed 30 August 2009, <<http://www.tekscan.com/medical/system-mobile.html>>

Texas Instruments Inc., 2009. *INA128 Precision, Low Power Instrumentation Amplifiers*, Texas Instruments Inc., Dallas, Texas, USA.

Turner, J.D. & Austin, L., 2000. 'Review Article:Sensors for automotive telematics', *Meas. Sci. Technol.* Vol. 11 , pp. R58–R79.

Urry, S., 1999. 'Plantar pressure-measurement sensors', *Measurement Science and Technology*, vol. 10, pp. R16-R32.

van Schie, C. H. M., 2005. A Review of the Biomechanics of the Diabetic Foot., *Lower Extremity Wounds*, Vol. 4, No. 3, pp. 160-170.

Vista Medical Ltd., n.d.. *FSA Foot Assesment: FSA Clinical Foot Assesment System*, Winnipeg, Canada, viewed 30 August 2009,

<<http://www.pressuremapping.com/index.cfm?pageID=13&section=25>>

Vuillerme, N., Pinsault, N., Chenu, O., Fleury, A., Payan, Y., Demongeot, J., 2009, A Wireless Embedded Tongue Tactile Biofeedback System for Balance Control, *Pervasive and Mobile Computing*, Vol. 5, No. 3, June 2009, pp 268-275.

Wahab, Y, Zayegh, A., and Veljanovski, R., and Begg, R.K., 2008. 'Sensitivity optimization of a foot plantar pressure micro-sensor', in *Proc. 20th IEEE International Conf. on Microelectronics 2008*. Sharjah, UAE, 14-17 Dec., pp 104-107.

Wahab, Y, Zayegh, A., and Veljanovski, R., and Begg, R.K., 2008. 'Design of MEMS biomedical pressure sensor for gait analysis', in *Proc. IEEE International Conf. on Semiconductor Electronics 2008*. , 25-27 Nov, Johor Bahru, Malaysia, pp 166-169.

Wahab, Y, Zayegh, A., Begg, R.K. and Veljanovski, R. , 2007b, 'CMUT For Human And Humanoid Locomotion Mesurement', in *Proceedings of Int. Con. on Robotics, Vision, Information and Signal Processing 2007*, Universiti Sains Malaysia, Penang, Malaysia, pp. 359-364.

Wahab, Y, Zayegh, A., Begg, R.K. and Veljanovski, R. 2008. 'A model for the measurement of foot-to-ground clearance and potential realization of micro-electro-mechanical systems', *AMSE Journal: Modelling, Measurement and Control Series C*, vol. 69, no 1, pp 59-74.

Wahab, Y, Zayegh, A., Begg, R.K. and Veljanovski, R., 2007a, 'Analysis of foot to ground clearance measurement techniques for MEMS realization', in *Proceedings of the IEEE International Conference on Computer and Information Technology (ICCIT 2007)*, Dhaka Bangladesh, pp. 1-5.

Wang, Z., Miao, J., Zhu, W. 2008, 'Micromachined ultrasonic transducers and arrays based on piezoelectric thick film', *Applied Physics A: Materials Science and Processing*, vol. 91 no 1, pp. 107-117.

Wang, Z., Zhu, W., Miao, J., Zhu, H., Chao, C. and Tan, O. K., 2006, 'Micromachined thick film piezoelectric ultrasonic transducer array', *Sensors and Actuators A: Physical*, Vol. 130-131, Selected Papers from TRANSDUCERS '05 - The 13th International Conference on Solid-State Sensors, Actuators and Microsystems - Seoul, Korea, 5-9 June 2005, 14 August, pp. 485-490.

Weir, R. F. and Childress, D. S., 1997. 'A new method of characterizing gait using a portable, real-time, ultrasound ranging device', in *Proceedings of the 19th International Conference of the IEEE Engineering in Medicine and Biology Society*, pp.1810-1812.

Wells, L.H., 1968. 'Basic ultrasonics: 2 — The use of compression (longitudinal) waves in ultrasonic testing', *Non-Destructive Testing*, Vol. 1, No. 5, August, pp. 291-296.

Wheeler, J., Rohrer, B., Kholwadwala, D., Buerger, S., Givler, R., Neely, J., Hobart, C. and Galambos, P., 2006. 'In-Sole MEMS Pressure Sensing for a LowerExtremity Exoskeleton', in *Proceedings of The First IEEE/RAS-EMBS International Conference on Biomedical Robotics and Biomechatronics*, pp. 31-34.

Wild, S., Roglic, G., Green, R. Sicree, A. and King, H., 2004. 'Global Prevalence of Diabetes', *Diabetes Care*, Vol. 27, No 5, pp 1047-1053.

Winter, D.A., 1992. 'Foot trajectory in human gait: a precise and multi-factorial motor control task'. *Physical Therapy*, vol. 72, no 1 , pp 45-56.

Wygant, I.O., Zhuang, X., Yeh, D.T., Nikoozadeh, A., Oralkan, O., Ergun, A.S., Karaman, M. and Khuri-Yakub, B.T., 2004, 'Integrated ultrasonic imaging systems based on CMUT arrays: recent progress', in *Proceedings of the IEEE International Ultrasonics Symposium*, vol. 1, IEEE, pp. 391–394.

Wahab, Y., Zayegh, A., Veljanovski, R. and Begg, R.K., 2008. 'Micro-sensor for foot pressure measurement', in *Proc. IEEE Region 10 Conf. TENCON 2008*, Hyderabad, India, 19-21 Nov., pp. 1-5.

Yamaner, F.Y., 2006. *Finite Element and Equivalent Circuit Modeling of Capacitive Micromachined Ultrasonic Transducer (CMUT)*, MSc. Thesis, Sabanci University, Turkey.

Yamashita, K, Chamsomphou, L, Nishimoto, H. and Okuyama M, 2005. 'A new method of position measurement using ultrasonic array sensor without angular scanning', *Sensors and Actuators A: Physical*, Vol. 121, No. 1, 31 May, pp 1-5.

Yano, T., Tone, M., and Akira Fukumoto, A., 1987. 'Range Finding and Surface Characterization Using High Frequency Air Transducers', *IEEE Transactions on Ultrasonics, Ferroelectrics, and Frequency Control*, vol. UFFC 34, no. 2, pp. 232-236.

Yaralioglu, G.G., Ergun, A.S., Huang, Y., and Khuri-Yakub, B.T, 2003. 'Capacitive Micromachined Ultrasonic Transducers for Robotic Sensing Applications'. in *Proceedings of the 2003 IEEE/RSJ Int. Conference on Intelligent Robots and Systems*, IEEE/RSJ, Las Vegas, USA, pp. 2347-2353.

Zamali, M.S.B. and Talghader, J.J., 2006. 'Stress-mapping sensors for high-power adaptive micro-optics', *Applied Optics*, Vol. 45, No. 7, ,March, pp1619-1624.

Zhao, Y. R., Shi, A. P., Chen, G. Q., Chang, Y. Y., Hang, Z. and Liu, B. M., 2006. 'New Type Multielectrode Capacitance Sensor for Liquid Level', *Journal of Physics: Conference Series*, Vol. 48, pp. 223-227.

Zhou, M., Huang, Q. & Qin, M., 2005. 'Modeling, design and fabrication of a triple-layered capacitive pressure sensor', *Sensors and Actuators A: Physical*, Vol. 117, No. 1, 3 January, pp. 71-81.

# APPENDIX

# A

## CoventoreWare™ Datasheet

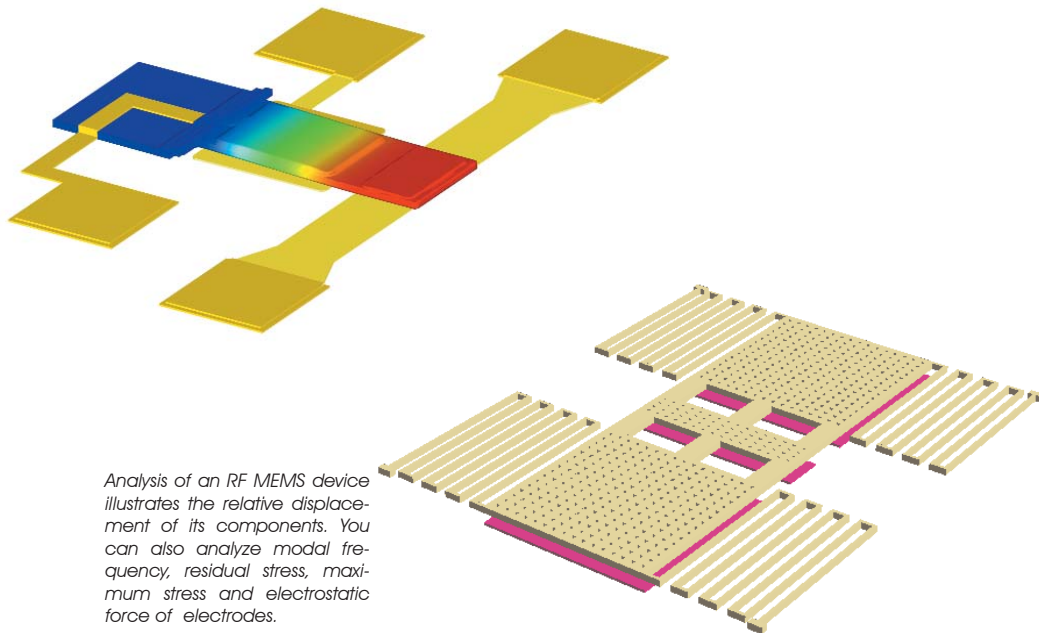
# ANALYZER

from Coventor, Inc.

- Industry-leading suite of MEMS-specific field solvers for electrostatic, structural, thermal, piezoelectric, piezoresistive, damping, electromagnetic, optical, and microfluidic analyses
- Offers best-in-class coupled physics solver for electromechanical analysis
- Includes powerful pre- and post-processing with automatic mesh generation, result queries and 3-D result visualization
- Provides unified access to all solvers in an easy-to-use graphical user interface that reduces training time and automates model and result management and tracking

## ANALYSIS TOOLS FOR MEMS DEVELOPMENT

ANALYZER is Coventor's extensive suite of 3D field solvers designed specifically for MEMS applications. ANALYZER gives you the ability to analyze and simulate the behavior of MEMS devices that are subject to multiple physical effects.



*Analysis of an RF MEMS device illustrates the relative displacement of its components. You can also analyze modal frequency, residual stress, maximum stress and electrostatic force of electrodes.*

### ANALYZER at a Glance

**MEMS Solvers:** Perform complex, fully coupled, multi-domain physics analysis with our comprehensive suite of MEMS-specific solvers. Reveal the interaction between domains using true-coupled electrostatic, mechanical, PZE, and thermal analyses. Offer package-device interaction analysis. Expose time-dependent behaviors of MEMS devices with transient mechanical and thermal analyses. And, perform optical analysis to evaluate beam diffraction in optical MEMS devices.

#### Query, View, and Compare

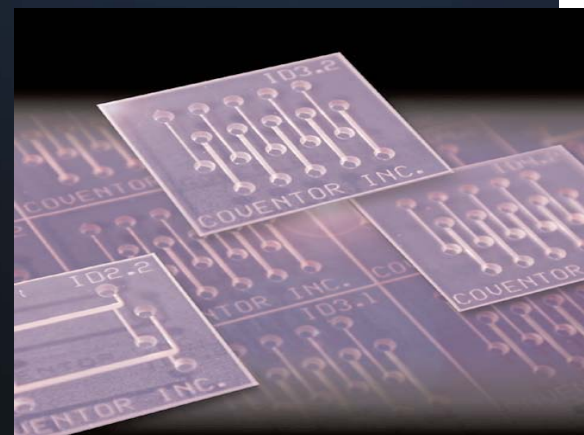
**Results:** Quickly examine results of analyses in selectable presentation formats. The powerful query capability enables you to easily extract a wide variety of results over a wide range of parametric conditions.

#### Automatic Meshing:

Mesh MEMS structures with precision using our automated mesh generator. Mesh volumes using hexahedral or tetrahedral elements. Mesh surfaces using triangular and quad elements. Mesh structures with sloped sidewalls with the mapped brick mesher. Various mesh control techniques, such as boundary refinement and bias, are available.

#### Microfluidic Solvers:

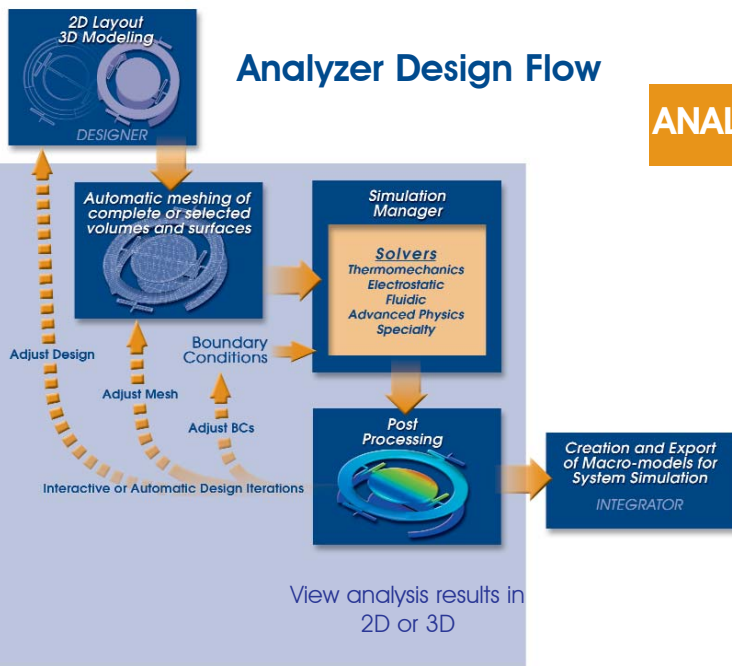
Examine chemical transport and containment physics of lab-on-chip applications in DNA, protein, and chemical analyses. Analyze full 3D electro-phoreses, electro-osmosis, and mixed electro-kinetics. Perform a multi-phase analysis to predict drop or bubble behavior for inkjet or dispensing applications.



COVENTOR™

WHAT'S NEXT. AND NEXT. AND NEXT.™

## Analyzer Design Flow



## ANALYZER - Comprehensive MEMS Physics

- Structural Mechanics**
  - linear and non linear
  - contact
  - static and transient
  - modal and harmonic
  - thermomechanical
  - piezoelectric
  - piezoresistive
  - electro-thermal-mechanics
- Electrical/Electrostatics**
  - capacitance
  - charges
  - dielectrics
  - electroquasistatic
- Coupled Field**
  - combinations of electrostatic/structural/thermal/piezo electric/piezoresistive and fluidic
- Electromagnetics**
  - resistance and inductance
  - full wave EM solver
- Parametric Study**
  - automatic parameter variation of: boundary, material, and dimensions
- Damping**
  - squeeze film, lateral and shear
  - reduced order modeling
  - free space, large angles
- Microfluidics**
  - compressible and incompressible
  - laminar analysis
  - buoancy driven flow
  - newtonian and non-newtonian
  - viscosity models
  - fluid structure interaction
  - steady-state or transient
  - reaction chemistry and enzyme kinetics
  - electrohydrodynamics
  - non-inertial reference frame
  - multi-phase flow
  - electrokinetics flow
  - nucleation and phase transition
  - fluid interaction with rigid bodies
  - multi CPU support for multi phase flow

## ANALYZER SOLVERS

MEMS	STANDARD	<b>MemElectro</b> Analyzes boundary element model electrostatics, for electrostatic force and capacitance calculations of 3-dimensional structures comprised of conductors and dielectrics  <b>MemMech</b> A full Finite Element Analysis tool for structural, thermal, electro-thermal and piezoelectrical physics. Performs modal, harmonic, contact, steady-state and transient computations.  <b>Co-Solve EM</b> Analyzes coupled electromechanics with hysteresis	
	TURBO	<b>ANALYZER Standard, plus:</b>  <b>Enhanced MemElectro Co-Solve &amp; MemMech</b> Advanced capability for analysis of boundary element model electrostatics to enable faster runs, using less memory, with special symmetry options	
ADD ON	<b>MemPZR</b> Computes resistance field, equilibrium potential, and current density fields of resistors under mechanical stress  <b>MemPZE</b> Piezo electric analysis capabilities that couple with mechanical analysis  <b>MemHenry</b> Solves for frequency dependent resistance and inductance  <b>MemOptics</b> Analyzes optical beam propagation and diffraction  <b>MemPackage</b> Analyzes package-induced effects on MEMS devices  <b>INTEGRATOR</b> Add the INTEGRATOR module in order to connect your field solver results to your ASIC design environment in SABER-MAST, CADENCE-Verilog-A or MATLAB-Simulink  <b>DampingMM</b> As part of INTEGRATOR the DampingMM module calculates all types of damping and can be added as a separate module in ANALYZER		
	MICROFLUIDICS	<b>NetFlow</b> Analyzes fluid flow and chemical transport in electro-kinetic, and mixed electro-kinetic systems  <b>MemCFD</b> Solves for general purpose CFD  <b>SwitchSim</b> Computes electro-kinetic response of a species in a fluid subjected to a switched electric field  <b>ReactSim</b> Performs 3D numerical modeling of multiple reacting chemical species, coupled with fluid flow, heat transfer, diffusion, and electro-kinetics  <b>Bubble-DropSim</b> Provides full 3D numerical simulation of the movement of bubbles and surrounding fluids in micro-channels, of droplet formation, transport, and impact. Includes Electro-Hydro-Dynamic capabilities in multi-phase flow  <b>MemFSI</b> Provides detailed 3D analysis of fluid-structure interaction <td> <b>INKJET, DISPENSOR and BIO CHIP DEVELOPER</b> </td>	<b>INKJET, DISPENSOR and BIO CHIP DEVELOPER</b>

## Coventor products

**CoventorWare** is ideal for developing MEMS and microsystems for an unlimited variety of applications including optical communications, RF/wireless communications, biotechnology, automotive, and sensors

- ARCHITECT:** Multi-domain technology simulator for device, component or system level products including physical models, control models and Electronics
- DESIGNER:** MEMS device construction tool; generates 2-D mask layouts and 3-D solid models; includes material property database, process editor and import/export capabilities
- ANALYZER:** Group of field solvers for detailed physical analysis requiring thermoelectromechanics, optics, fluidics, electromagnetics, and more
- INTEGRATOR:** Tools to extract detailed design-specific behavioral models from Finite Element straight into Saber, Cadence or Matlab-Simulink
- MEMulator™:** A versatile virtual prototyping tool used to emulate complex MEMS processes
- Etch3D™:** A 3D simulator for anisotropically etching Silicon in any orientation with etchants such as KOH, TMAH, and others



[www.coventor.com](http://www.coventor.com)

**World Headquarters & Eastern U.S. Sales**  
 4000 CentreGreen Way  
 Suite 190  
 Cary, NC 27513  
 Tel 919.854.7500  
 Fax 919.854.7501

**Western U.S. Sales**  
 951 Mariner's Blvd.  
 Suite 205  
 San Mateo, CA 94404  
 Tel 650.212.6367  
 Fax 650.212.6362

**European Sales**  
 3, avenue du Quebec  
 91951 Courtaboeuf Cedex  
 France  
 Tel +33 (0)1 69 29 84 94  
 Fax +33 (0)1 69 29 84 88

**Worldwide Distribution**  
 Japan: [www.msol.co.jp](http://www.msol.co.jp)  
 Taiwan: [www.apic.com.tw](http://www.apic.com.tw)  
 China: [www.imag.com.cn](http://www.imag.com.cn)  
 Korea: [www.davan.co.kr](http://www.davan.co.kr)  
 Singapore: [www.ftdsolutions.com](http://www.ftdsolutions.com)  
 India: [www.ftdpl.com](http://www.ftdpl.com)

# ARCHITECT from Coventor, Inc.

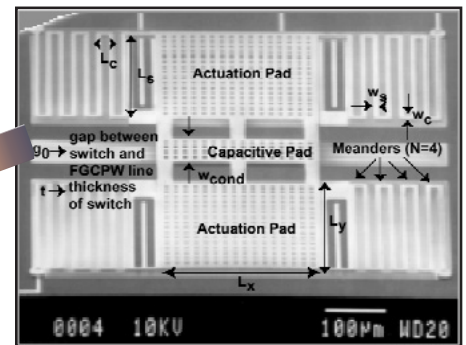
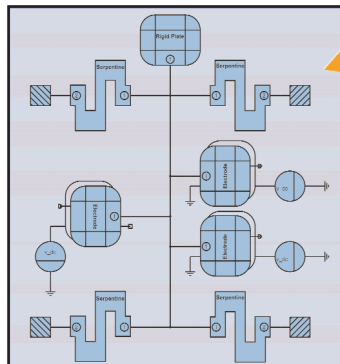
- System simulator that integrates MEMS mixed-domain technologies with coupled multi-physics devices
- Executes accurate 6 degrees-of-freedom simulations up to 100 times faster than traditional FEM techniques
- Enables rapid architectural exploration of design alternatives, saving cost and time-to-market
- Supports device behavioral models and models of surrounding sub-systems
- Provides many customization options with template library components and import of macromodels
- Connects behavioral modeling to FEM results through the CoventorWare database structure

## Behavioral design and simulation environment using parameterized libraries

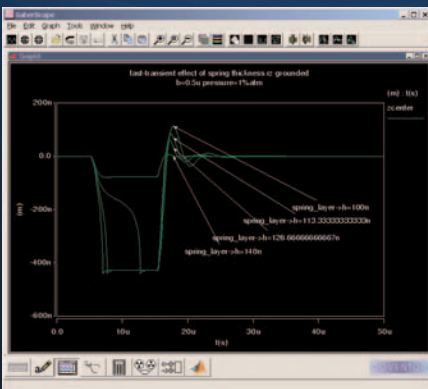
A realistic MEMS simulation requires that 3-D representations of multi-physics devices be created and boundary conditions applied such that the devices can be evaluated in multiple degrees of freedom. The complexity of the modeling and the computation of the equations used to represent the models demand a streamlined approach that enables the design procedure to be both fast and accurate. Coventor's ARCHITECT is a new MEMS paradigm that uses a three-step approach for accurate high-level design and simulation:

- **Capture** a design in circuit form using libraries of parametric elements. The capture process uses placement and interconnect techniques familiar to digital designers.
- **Simulate** device behavior using SPICE-like simulation for mixed-domain technologies. The result is an accurate and rapid solution available in tabular and graphical formats.
- **Optimize** design using advanced techniques such as sensitivity and Monte Carlo analyses. Hundreds of design iterations can be evaluated quickly to produce a device that minimizes the influences of manufacturing tolerances.

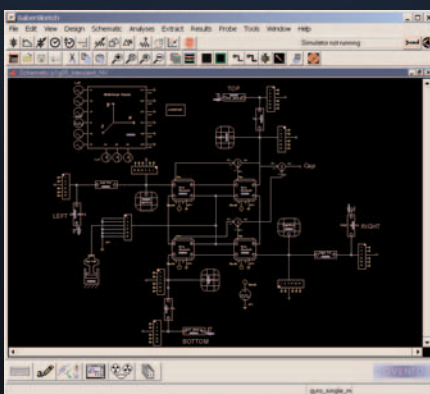
Schematic of complete RF switch including complete meander suspensions, all perforated plates and drive electrodes.



SEM photo of RF switch with beam area shown. S.P. Pacheco, L.P.B. Katehi, and C.T.-C. Nguyen, Design of Low Actuation Voltage RF MEMS Switch, Proceedings of the 2000 IEEE IMS, Boston, MA, June 11-16, 2000



Architect post-processor



Architect schematic editor

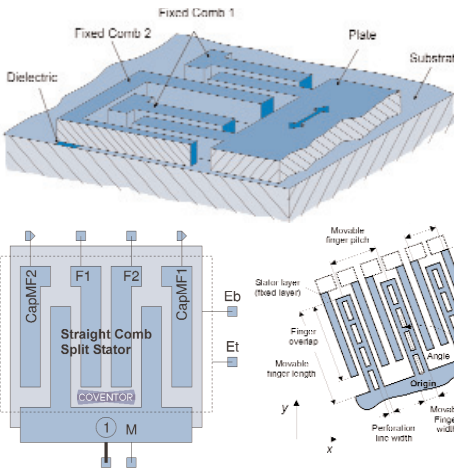
### ARCHITECT includes:

- Graphical schematic capture engine
- Mixed-signal circuit simulator
- Graphical timing and waveform editor
- Schematic driven layout generators: create GDS II from circuit schematic
- Library of standard mechanical and electrical components plus choice of one parameterized MEMS library with template customization

### Optional add-ons:

- Manufacturing analysis software for tolerance performance
- DESIGNER 3-D model creation tool that accepts layout generator output
- Additional multi-physics libraries in the electromechanical, electromagnetic, optical, or fluidics domains

Capture



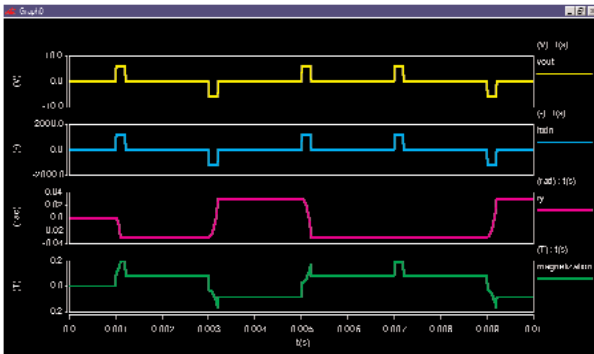
The graphic schematic capture engine uses symbols and customizable parameter tables from electromechanical, electromagnetic, optical, and fluidic library elements. User-defined material property and process parameter values update the parametric libraries automatically. Each electromechanical parameterized model is accurate in 6 degrees of translational and rotational freedom, and up to 5 electrical degrees of freedom. All models allow extensive customization for

changes in geometry and overrides of process parameters. In addition, new fixed custom macromodel elements can be extracted from detailed FEM/BEM simulations and added to the libraries. The finalized schematic is netlisted to create the interconnect file needed for simulation.

changes in geometry and overrides of process parameters. In addition, new fixed custom macromodel elements can be extracted from detailed FEM/BEM simulations and added to the libraries. The finalized schematic is netlisted to create the interconnect file needed for simulation.

Simulate

The mixed technology, mixed-signal circuit simulator simulates the reduced-order parametric models. The fast DC and AC results can be displayed in graphical format (charts, histograms, scatter plots) using a timing and waveform editor. Multiple signals may be displayed or overlaid for comparison, with many display adjustments. Probing capability allows a signal to be displayed at any interconnect point in the original captured schematic.



ARCHITECT postprocessor window showing multiple waveforms for magnetic design

Optimize

A complete add-on manufacturing analysis module allows for parametric, statistical, and stress analysis. Sensitivity analysis assesses critical operating characteristics by varying individual parameters in batch run simulations. Monte Carlo 3 sigma statistical simulation optimizes manufacturability by evaluating component tolerances. The user also can evaluate stresses on components by altering specified operating conditions and assessing results.

(Abbreviated list, visit [www.coventor.com](http://www.coventor.com) for complete list)

ELECTROMECHANICAL

- Generic Masses
- Rigid Plates
- 3D non-linear Elastic Beam theory
- 3D non-linear Elastic Plate theory
- 3D Electrostatic Combs drives
- 3D Electrodes

ELECTROMAGNETIC

- Rectangular Coils
- Magnetic Plate
- Uniform Field Source
- Movable Rectangular Coil

Other MEMS/Microfluidics

- Optical Library
- Damping Library
- Fluidic Library

Mixed-Technology

- Digital
- Analog
- Electro-Mechanical
- Electrical
- Magnetic
- Mechanical
- Thermal
- Hydraulic
- Pneumatic

Coventor products

CoventorWare is ideal for developing MEMS and microsystems for an unlimited variety of applications including optical communications, RF/wireless communications, biotechnology, automotive, and sensors

- **ARCHITECT:** Multi-domain technology simulator for device, component or system level products including physical models, control models and Electronics
- **DESIGNER:** MEMS device construction tool; generates 2-D mask layouts and 3-D solid models; includes material property database, process editor and import/export capabilities
- **ANALYZER:** Group of field solvers for detailed physical analysis requiring thermoelectromechanics, optics, fluidics, electromagnetics, and more
- **INTEGRATOR:** Tools to extract detailed design-specific behavioral models from Finite Element straight into Saber, Cadence or Matlab-Simulink
- **MEMulator™:** A versatile virtual prototyping tool used to emulate complex MEMS processes
- **Etch3D™:** A 3D simulator for anisotropically etching Silicon in any orientation with etchants such as KOH, TMAH, and others



**World Headquarters & Eastern U.S. Sales**  
 4000 CentreGreen Way  
 Suite 190  
 Cary, NC 27513  
 Tel 919.854.7500  
 Fax 919.854.7501

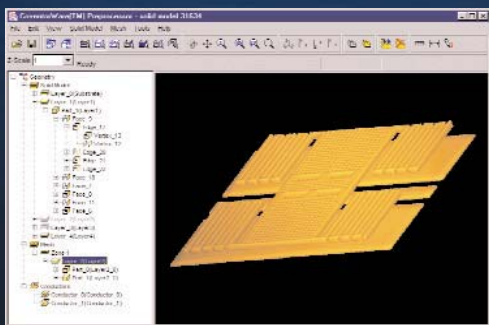
**Western U.S. Sales**  
 951 Mariner's Blvd.  
 Suite 205  
 San Mateo, CA 94404  
 Tel 650.212.6367  
 Fax 650.212.6362

**European Sales**  
 3, avenue du Quebec  
 91951 Courtaboeuf Cedex  
 France  
 Tel +33 (0)1 69 29 84 94  
 Fax +33 (0)1 69 29 84 88

**Worldwide Distribution**  
 Japan: [www.msol.co.jp](http://www.msol.co.jp)  
 Taiwan: [www.apic.com.tw](http://www.apic.com.tw)  
 China: [www.imag.com.cn](http://www.imag.com.cn)  
 Korea: [www.davan.co.kr](http://www.davan.co.kr)  
 Singapore: [www.fdsolutions.com](http://www.fdsolutions.com)  
 India: [www.ftdpl.com](http://www.ftdpl.com)

# DESIGNER from Coventor, Inc.

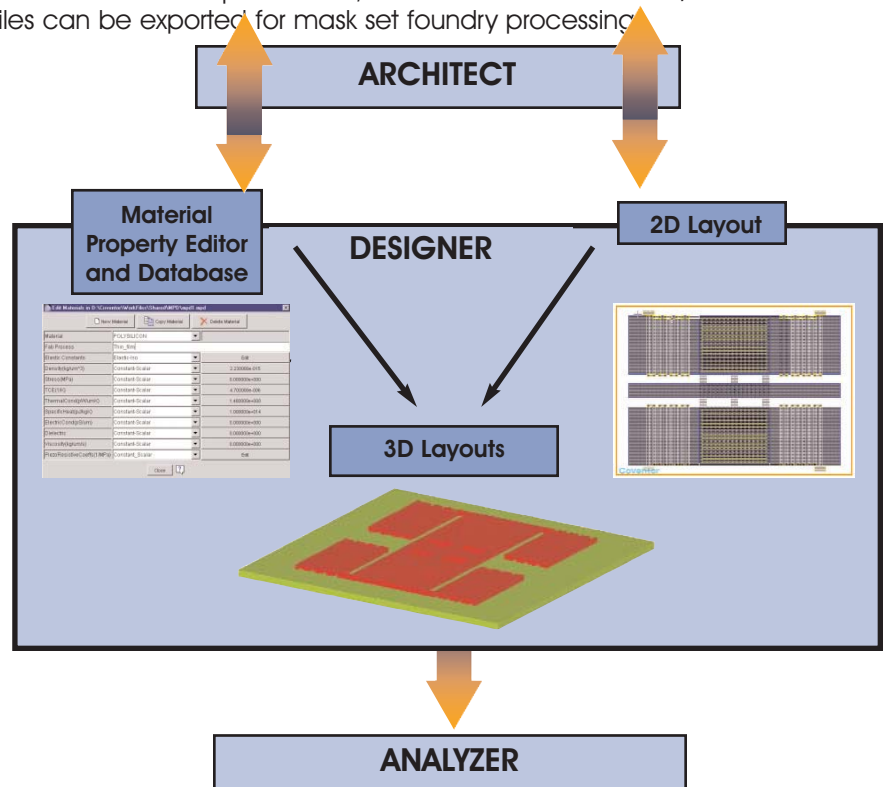
- Creates manufacturable MEMS devices and systems efficiently
- Generates 3-D models automatically
- Supports many import and export formats for compatibility with Coventor and third-party tools
- Works with ARCHITECT and ANALYZER to provide complete design environment: high-level models extracted into layout form can be simulated and verified with FEM/BEM techniques
- Includes process editor and material properties database for complete MEMS definition
- Stores foundry content from design handbooks including example process descriptions of MPW-runs and example DRC and DRC



Preprocessor showing 3-D model and tree view of structure

## 2-D layout and 3-D modeling for MEMS

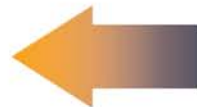
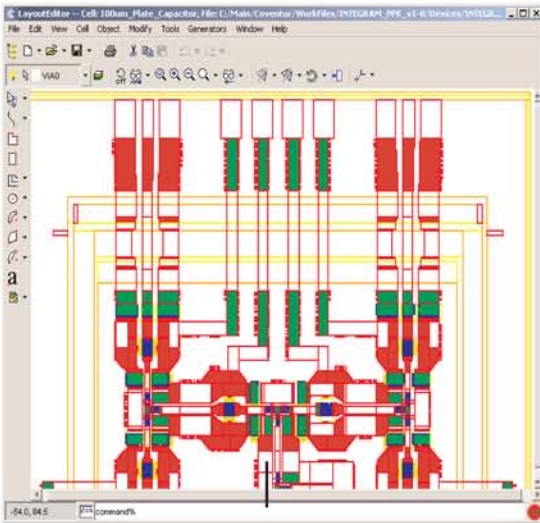
Coventor's DESIGNER is an efficient front-end design tool for creating models of MEMS devices. It combines a fully functional 2-D mask layout program, process editor, materials properties database, and a preprocessor module for 3-D model generation and viewing. The models can be used for export to FEM/BEM simulation verification, while the 2-D files can be exported for mask set foundry processing.



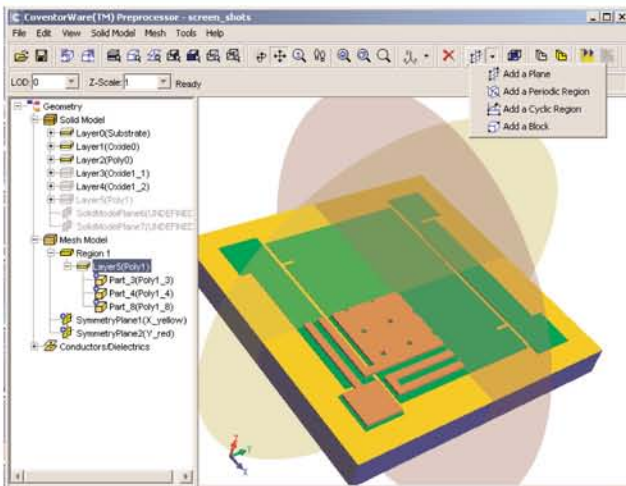
DESIGNER works seamlessly with other Coventor tools to provide a complete MEMS design and simulation verification environment, but is designed to interact with third party layout, solid modeling and finite element tools as well.

DESIGNER assists users in designing MEMS devices in the following ways:

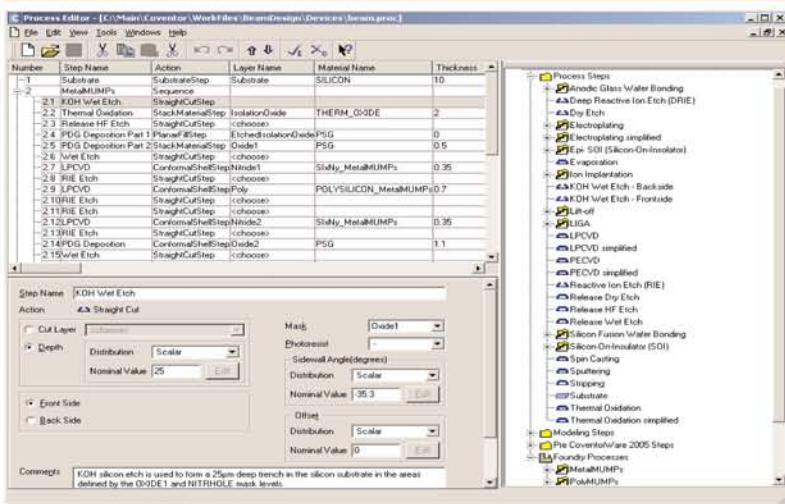
- **2-D layouts** created, imported, generated, or exported
- **Material properties database** to store characteristics of the materials used in the fabrication process. Properties may be specified as scalars, polynomials, or in table format. The database is shared by other Coventor software
- **Process editor** allowing real foundry steps to be emulated, including etching through multiple layers and partial backside etching. The process editor is used in 3-D model creation and in creation of layouts from high-level circuit schematics
- **3-D models** automatically created from a 2-D description and process information and viewed in Preprocessor
- **Optional 3-D meshes** can be created in the Preprocessor using separate meshing software that automatically meshes FEM and BEM volumes and surfaces and interactively names faces and conductors for simulation in ANALYZER or third-party software



Automatic solid model creation and partitioning



Process editor for process definitions



Layout Editor

- Produces analytically defined "true" curves and angle drawings.
- Cell-based hierarchical layout with unlimited layers
- Editor functions include layer, cell and object browsers
- True color viewing
- All-angle Boolean and grow operations
- Design rescaling
- Major and minor grid markers for two levels of display
- Edge, corner, arc, and stretch editing
- Unlimited undo, redo options
- Snap to grid
- Object rotation
- Able to generate forms from an equation
- Imports from GDSII, CIF, or DXF formats
- Full scripting language capabilities
- MEMS Design Rule Checking (DRC)

3D Preprocessor

- Provides easy and convenient model viewing and manipulation
- Patch and conductor names survive re-meshing
- Enables intuitive synchronized "tree view" of the solid model and the mesh
- Applies best mesher for each layer
- Provides immediate feedback on mesh quality
- Meshing options available; extruded, Manhattan, and mapped bricks; tetrahedrons and surface meshing with quads or triangles
- Local mesh refinement and mesh biasing

Coventor products

CoventorWare is ideal for developing MEMS and microsystems for an unlimited variety of applications including optical communications, RF/wireless communications, biotechnology, automotive, and sensors

- **ARCHITECT:** Multi-domain technology simulator for device, component or system level products including physical models, control models and Electronics
- **DESIGNER:** MEMS device construction tool; generates 2-D mask layouts and 3-D solid models; includes material property database, process editor and import/export capabilities
- **ANALYZER:** Group of field solvers for detailed physical analysis requiring thermoelectromechanics, optics, fluidics, electromagnetics, and more
- **INTEGRATOR:** Tools to extract detailed design-specific behavioral models from Finite Element straight into Saber, Cadence or Matlab-Simulink
- **MEMulator™:** A versatile virtual prototyping tool used to emulate complex MEMS processes
- **Etch3D™:** A 3D simulator for anisotropically etching Silicon in any orientation with etchants such as KOH, TMAH, and others



**World Headquarters & Eastern U.S. Sales**  
 4000 CentreGreen Way  
 Suite 190  
 Cary, NC 27513  
 Tel 919.854.7500  
 Fax 919.854.7501

**Western U.S. Sales**  
 951 Mariner's Blvd.  
 Suite 205  
 San Mateo, CA 94404  
 Tel 650.212.6367  
 Fax 650.212.6362

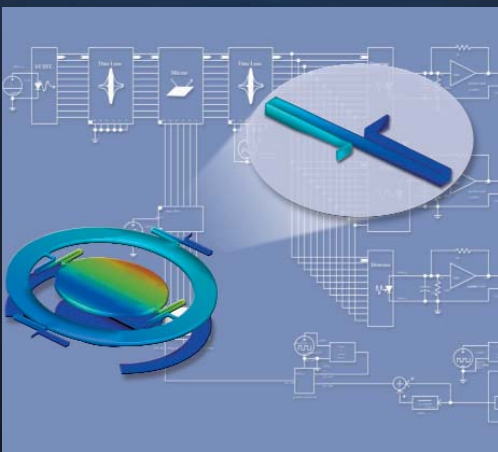
**European Sales**  
 3, avenue du Quebec  
 91951 Courtaboeuf Cedex  
 France  
 Tel +33 (0)1 69 29 84 94  
 Fax +33 (0)1 69 29 84 88

**Worldwide Distribution**  
 Japan: www.msol.co.jp  
 Taiwan: www.apic.com.tw  
 China: www.imag.com.cn  
 Korea: www.davan.co.kr  
 Singapore: www.ftdsolutions.com  
 India: www.ftdpl.com

# INTEGRATOR

from Coventor, Inc.

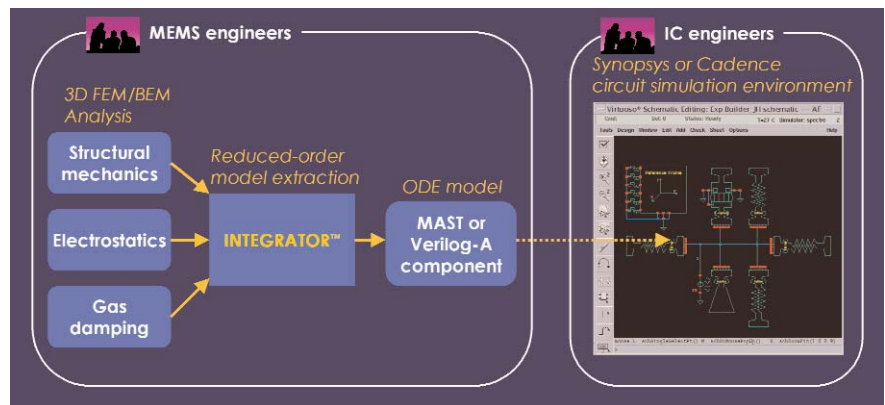
- Extracts reduced-order macromodels from detailed 3-D FEM/BEM simulations
- Each extracted component has 6 mechanical degrees of freedom (DOF) and up to 5 electrical DOF
- Exports macromodels to MAST (for Synopsys Saber), Verilog-A (for Cadence Virtuoso) and MATLAB
- Enables co-simulation of MEMS with surrounding IC early in the design cycle, saving time and reducing risk
- Enables fast transient simulations with fully coupled electromechanics and damping (equivalent FEM simulations are infeasible or prohibitive)
- Creates custom components to supplement Coventor's extensive ARCHITECT library of parameterized MEMS components



A tether on a two-axis, steerable mirror is extracted into a system model containing other mirrors, an electronic control system, and an optical system.

## Custom Macromodel Extraction for SYNOPSIS and CADENCE

MEMS must be tightly integrated with electronic control circuitry, requiring MEMS designers to work closely with IC designers to develop MEMS-based products. Unfortunately, MEMS and IC designers have traditionally used very different design tools. MEMS designers relied on finite-element (FEM) analysis, while IC designers relied on schematic-driven circuit simulators offered by the major EDA vendors, such as Synopsys and Cadence. MEMS designers have been unable to provide suitable system-level behavioral models of MEMS to the IC designers for incorporation into the IC simulations, forcing IC designers to run simulations without including accurate, active models of the MEMS behavior. INTEGRATOR bridges this communication gap by enabling MEMS designers to extract reduced-order macromodels that can be easily incorporated into IC simulations. INTEGRATOR will certainly save time and may eliminate needless fabrication cycles.



INTEGRATOR bridges the gap between MEMS and IC designers

### INTEGRATOR at a Glance:

Enables simulations of electromechanical devices in high-level system modeling environments such as Synopsys Saber and Cadence Virtuoso.

- Add-on to CoventorWare ANALYZER
- Covers all of the physics found in lumped parameter models of dynamic mechanical systems: SpringMM for spring stiffness, DampingMM for damping effects, and InertiaMM for inertial effects
- Intuitive user interface guides user through macromodel extraction steps
- Extracted models include all 6 mechanical DOF (fully coupled translational and rotational displacement) and up to 5 electrical DOF (voltage on conductors)
- Exports custom library components in MAST (for Synopsys Saber), and Verilog-A (for Cadence Virtuoso)

### InertiaMM:

Automatically extracts inertial coefficients for selected sub-sections of a device that can be modeled as rigid bodies.

### SpringMM:

Models flexible structural components, such as tethers, as linear and non-linear springs. Models electrostatic forces between electrodes or combs as electrostatic springs.

- User can specify a separate trajectory for each DOF
- Captures non-linear behavior by multi-dimensional polynomial fit
- User can choose from several polynomial fit algorithms and specify polynomial order

### DampingMM:

Provides multiple 3-D numerical solvers for damping effects which cover the full range of MEMS device and geometry types, including:

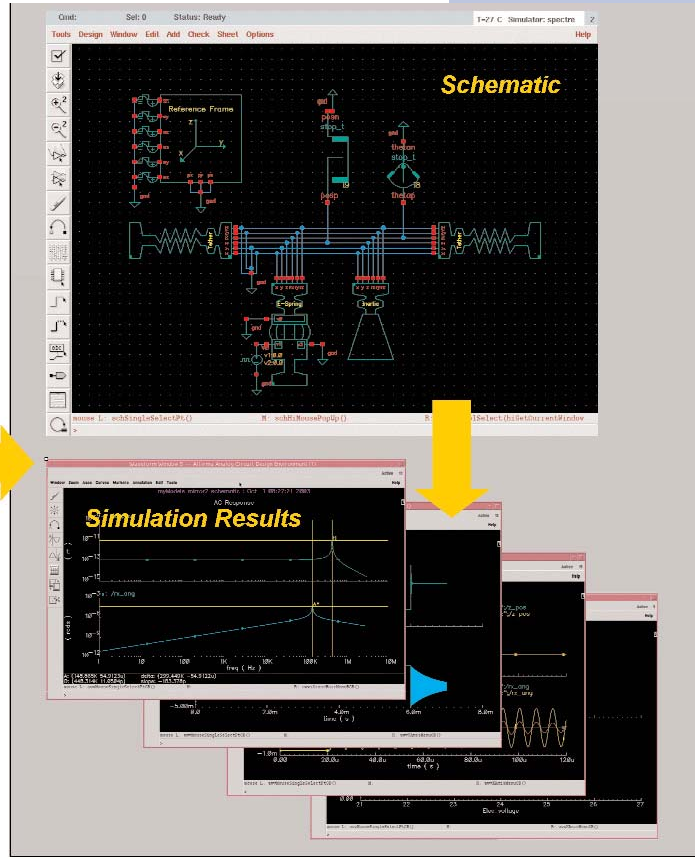
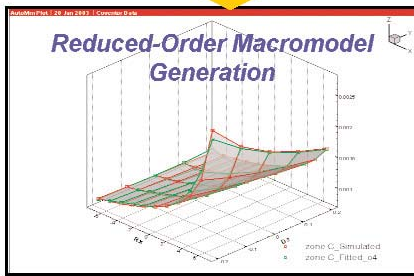
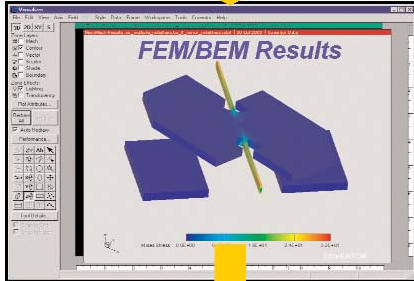
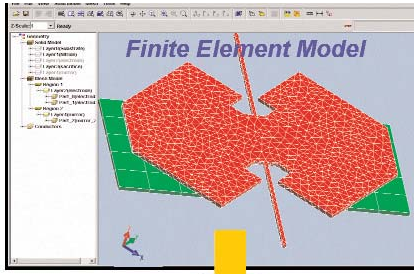
- Reynolds solver for squeeze film, slide film and modal damping in small-gap situations (e.g. accelerometers and gyroscopes);
- Stokes solver for free moving structures in open domains (e.g. torsional mirrors);
- Full Navier-Stokes solver for all devices.

COVENTOR

WHAT'S NEXT. AND NEXT. AND NEXT.™

# INTEGRATOR Design Flow

Reduced-order model extraction from 3-D solvers into Cadence and Synopsys simulators



INTEGRATOR automatically loads the user defined macromodel parameters into Cadence or Synopsys compatible model templates

## Perform co-simulations of MEMS and surrounding control ICs:

The behavior of many classes of MEMS, including accelerometers, gyroscopes, and single- and dual-axis mirrors, can be accurately represented by lumped-parameter models consisting of one or more springs, masses and dampers.

- Decompose the MEMS device into constituent components and extract a set of reduced-order macromodels
- Provide extracted models to IC designers, who incorporate them in an IC schematic and co-simulate the MEMS and IC behavior

## Create custom components to supplement ARCHITECT library:

ARCHITECT includes a comprehensive library of parameterized electromechanical components such as beams, plates, electrodes and comb drives. But some geometric shapes, such as curved tethers, cannot be well represented by the parameterized components.

- Use INTEGRATOR to create custom behavioral models to supplement the ARCHITECT library
- Exported components are fully compatible with the ARCHITECT library, allowing complete flexibility and customization

## Include complex damping for transient analysis

Integrator now includes the most complete set of 3D damping solvers for any MEMS device that generate time and frequency dependent models. We have implemented published theories for correcting the viscosity for pressure and temperature. The user may also choose from a library of pre-defined environment gases.

## Coventor products

CoventorWare is ideal for developing MEMS and microsystems for an unlimited variety of applications including optical communications, RF/wireless communications, biotechnology, automotive, and sensors

- **ARCHITECT:** Multi-domain technology simulator for device, component or system level products including physical models, control models and Electronics
- **DESIGNER:** MEMS device construction tool; generates 2-D mask layouts and 3-D solid models; includes material property database, process editor and import/export capabilities
- **ANALYZER:** Group of field solvers for detailed physical analysis requiring thermoelectromechanics, optics, fluids, electromagnetics, and more
- **INTEGRATOR:** Tools to extract detailed design-specific behavioral models from Finite Element straight into Saber, Cadence or Matlab-Simulink
- **MEMulator™:** A versatile virtual prototyping tool used to emulate complex MEMS processes
- **Etch3D™:** A 3D simulator for anisotropically etching Silicon in any orientation with etchants such as KOH, TMAH, and others



**World Headquarters  
& Eastern U.S. Sales**  
4000 CentreGreen Way  
Suite 190  
Cary, NC 27513  
Tel 919.854.7500  
Fax 919.854.7501

**Western U.S. Sales**  
951 Mariner's Blvd  
Suite 205  
San Mateo, CA 94404  
Tel 650.212.6367  
Fax 650.212.6362

**European Sales**  
3, avenue du Quebec  
91951 Courtaboeuf Cedex  
France  
Tel +33 (0)1 69 29 84 94  
Fax +33 (0)1 69 29 84 88

**Worldwide Distribution**  
Japan: www.msol.co.jp  
Taiwan: www.apic.com.tw  
China: www.imag.com.cn  
Korea: www.davan.co.kr  
Singapore: www.ftdsolutions.com  
India: www.ftdpl.com

# APPENDIX

# B

**Infineon Tech. (MultiMEMS)  
Project Report**

# PROJECT IDENTIFICATION

## DOCUMENT

Based on the received **MPW BOOKING FORM**, Infineon Technologies SensoNor has collected the information listed in this document. In case of any inaccuracy, please contact the MultiMEMS MPW co-ordinator.

Infineon Technologies SensoNor AS respects the privacy of all its customers and is committed to protecting such privacy in accordance with the Privacy Policy available on the MultiMEMS internet site, [www.multimems.com](http://www.multimems.com).



DOCUMENT ID:

**PID-1205**

CLASSIFICATION:

**Confidential**

PAGES:

**2**

ISSUED ON:

**10.12.2008**

## CUSTOMER INFORMATION

SHIPPING DETAILS <sup>(1)</sup>		CONTACT PERSON	
COMPANY / INSTITUTE: <b>Victoria University</b>		NAME: <b>A/Prof. Aladin Zayegh</b>	
DEPARTMENT: <b>School of Engineering and Science</b>		PHONE: <b>+61-3-9919 4858</b>	
ADDRESS: <b>Footscray Park Campus, Building D 721</b> <b>FOOTSCRAY, Victoria 3011</b> <b>Australia</b>		FAX: <b>+61-3-9919 4908</b>	
		E-MAIL: <b>aladin.zayegh@vu.edu.au</b>	
BILLING DETAILS <sup>(2)</sup>		CONTACT PERSON	
COMPANY / INSTITUTE: <b>Victoria University</b>		NAME: <b>Mrs. Christine Dobler</b>	
ENTERPRISE NO.: <b>ABN 83 776 954 731</b>		PHONE: <b>+61-3-9919 5912</b>	
ADDRESS: <b>Footscray Park Campus, Building D 721</b> <b>FOOTSCRAY, Victoria 3011</b> <b>Australia</b>		FAX: <b>+61-3-9919 4908</b>	
		E-MAIL: <b>christine.dobler@vu.edu.au</b>	

(1) The manufactured devices will be shipped to the specified **shipping address**.

(2) The invoice will be sent to the specified **billing address**.

## PROJECT INFORMATION

PROJECT ID	MPW	SITE ID	PRODUCT ID	PRICE
1205-01	Run 12	J1	MultiMEMS Die 3x3	1000.00 €
<b>TOTAL PRICE:</b>				<b>1000.00 €</b>

## PASSWORDS

Certain information concerning the MPW runs and submitted designs will be available to the MPW customers as downloads from the MultiMEMS internet site, [www.multimems.com](http://www.multimems.com). In order to protect the customer's privacy and intellectual propriety, such information will be encrypted. To decrypt these documents/files, use the appropriate password from the list provided below. The passwords are case sensitive.

PASSWORDS	CLASS	VALIDITY	COMMENTS
PER2kys8	Password A	Run 12	Use this password for common files.
YW67mu33	Password B	Run 12	Use this password for user-specific files.

# APPENDIX

# C

## **Infineon Tech. (MultiMEMS) Fabrication Report**

# Electrical Measurements



Doc Type: <b>Report</b>	Classification: <b>Confidential</b>	Pages: <b>2</b>	Issued On: <b>06.05.2009</b>
----------------------------	----------------------------------------	--------------------	---------------------------------

Doc ID: <b>MR-1201</b>
---------------------------

This document reports the results of the in-line electrical measurements carried out on the sample wafers specified below.

Note that the shipped dice are *not* tested. Process control monitoring is performed on test wafers and test structures.

## SAMPLE REFERENCES

MPW	BATCH ID:	SAMPLE SIZE:	BATCH SIZE:	TEST POINTS:
Run 12	32278, 32279	24 wafers	24 wafers	9 / wafer

## MEASUREMENT RESULTS

PRODUCT CHARACTERISTIC	SPECIFICATION	MEASUREMENT RESULTS				
		MIN	MEAN	MAX	STDEV	UNIT
Breakdown Voltage (absolute value)	> 10.0 V	15.9	16.6	16.8	0.1	V
Leakage Current	< 5.0 nA	0.90	3.70	15.0	2.0	nA
Resistance, Test Buried Resistor	3700 ± 300 Ω	5762	5888	6231	70	Ω
Resistance, Test Surface Resistor	6300 ± 600 Ω	5406	5596	5905	91	Ω
Resistance, Test Buried Conductor	105 ± 10 Ω	101.7	103.5	105.2	0.74	Ω
Sheet Resistance, Buried Conductor	31 ± 5 Ω/sq	31.2	31.7	32.0	0.18	Ω/sq
Sheet Resistance, Surface Conductor	53 ± 5 Ω/sq	51.2	51.9	52.5	0.31	Ω/sq
Sheet Resistance, Buried Resistor	550 ± 50 Ω/sq	861	881	820.4	9.3	Ω
Sheet Resistance, Surface Resistor	1210 ± 120 Ω/sq	1126	1141	1158	6.6	Ω/sq

**Note:** Values marked in red are outside the specification range.

# Thickness Measurements



DOC TYPE: <b>Report</b>	CLASSIFICATION: <b>Confidential</b>	PAGES: <b>2</b>	ISSUED ON: <b>06.05.2009</b>	Doc ID: <b>MR-1202</b>
----------------------------	----------------------------------------	--------------------	---------------------------------	---------------------------

This document reports the results of the various thickness measurements carried out on the sample wafers specified below.

Note that the shipped dice are *not* tested. Process control monitoring is performed on test wafers and test structures.

## SAMPLE REFERENCES

MPW	BATCH ID:	SAMPLE SIZE:	BATCH SIZE:	TEST POINTS:
Run 12	32278, 32279	24 wafers	24 wafers	9 / wafer

## MEASUREMENT RESULTS

PRODUCT CHARACTERISTIC	SPECIFICATION	MEASUREMENT RESULTS				
		MIN	MEAN	MAX	STDEV	UNIT
Thickness, Metal Layer	1.20 ± 0.15 µm	1.04	1.12	1.2	0.03	µm
Thickness, Thin Membrane	3.1 ± 0.3 µm	2.85	3.12	3.43	0.23	µm
Thickness, Thick Membrane	23.1 ± 1.0 µm	23.7	24.0	24.3	0.09	µm

**Note:** Values marked in red are *outside* the specification range.

**REPORTED EVENTS**

ID	DEVIATION	CONSEQUENCES <sup>(1)</sup>	STATUS
01	<b>Higher diffusion temperature.</b> <i>First affected layer: N-WELL AREAS.</i> <i>Cause: Thermocouple offset.</i>	Thicker <i>thick</i> membranes.	Verified.
02	<b>Epitaxy process out of range.</b> <i>First affected layer: N-EPI.</i> <i>Cause: Chlorine etch rate too high.</i>	Slightly thinner <i>thick</i> membranes.	Not verified <sup>(2)</sup> .
03	<b>Epitaxy process out of range.</b> <i>First affected layer: N-EPI.</i> <i>Cause: Autodoping.</i>	Slightly thicker <i>thin</i> membranes.	Not verified <sup>(2)</sup> .

<sup>(1)</sup> On delivered devices, concerning reported parameters.

<sup>(2)</sup> Currently under investigation.

**LEGAL DISCALIMER**

The information given in this document shall in no event be regarded as a guarantee of conditions or characteristics. With respect to any examples or hints given herein, any typical values stated herein and/or any information regarding the application of the device, SensoNor Technologies hereby disclaims any and all warranties and liabilities of any kind, including without limitation, warranties of non-infringement of intellectual property rights of any third party.

**CONFIDENTIAL**

Restricted to the owner of the project(s).  
 Proprietary Data. All rights reserved.

# APPENDIX D

## Certificate of Calibration



**AUSTRALIAN  
CALIBRATING  
SERVICES (A/SIA) PTY. LTD.**

4/204 20 000 182 738

126 Oxford Street, Collingwood  
R.O. Box 1174, Collingwood, Vic. 3068, Australia  
Ph: +61 3 9417 5088 Freecall: 1800 334 183  
Fax: +61 3 9417 1578 Email: [acc@auscal.com.au](mailto:acc@auscal.com.au)



4/204 20 000 182 738

JTK:CB:GWH:R51455

Job Number: 53049

27 July 2009

Mr Donald Ermel  
Victoria University / Footscray Park Campus  
Building D/Room D215  
Ballarat Road  
**FOOTSCRAY VIC 3011**

Dear Donald

We have pleasure in enclosing our Report(s) on the Examination and Calibration of your following equipment carried out on 23 July 2009.

Norgren Industrial Pressure Gauge & Pressure Vessel  
Serial Number: V188-2B File Number: V.AC/188-2B-1

Due to our Company currently updating its computer system, kindly note that all Invoices will now be forwarded under separate cover.

*As part of our Quality System and ISO requirements, we invite you to complete our Feed Back Form, which is located on our web site. Please go to [www.auscal.com.au](http://www.auscal.com.au) and click on the 'Feed Back' button.*

Thank you for your continued acceptance of our services.

Yours faithfully



**J.T. KENNON**  
*Managing Director*  
Enc.

Victoria  
Phone: (03) 9417 5088  
Fax: (03) 9417 1578

New South Wales  
Phone: (02) 9542 6588  
Fax: (02) 9742 8454

Queensland  
Phone: (07) 3215 9642  
Fax: (07) 3215 0388

Western Australia  
Phone: 1800 334 183  
Fax: (08) 9417 1578

South Australia  
Phone: (08) 8338 1500  
Fax: (08) 8338 1591

New Zealand  
Phone: +64 9 424 2250  
Fax: +64 9 424 7898

**CALIBRATION - SERVICE - MANUFACTURE - SUPPLY**



43577370

## CALIBRATION REPORT AN INDUSTRIAL PRESSURE GAUGE AND PRESSURE VESSEL

**FOR:** VICTORIA UNIVERSITY  
FOOTSGRAY CAMPUS  
BALLARAT ROAD  
FOOTSGRAY VIC 3011

**LOCATION:** ACS COLLINGWOOD

**TEST DATE:** 23 July 2009

**EQUIPMENT DETAILS:**

	<b>Gauge Details</b>		
Maker:	NORGREN	Capacity:	10 bar
Model:	DIAL	Resolution:	0.5 bar
Serial Number:	V188-2B		
Plant Number:	Nil		

**TEST DETAILS:**

Australian Standard AS1349:1986  
"Bourdon Tube Pressure and Vacuum Gauges"  
Section 4. Performance and Testing

- The pressure gauge was calibrated in a vertical position with increasing & decreasing pressure. The case of the pressure gauge was lightly tapped before each reading.
- The pressure medium was air and nitrogen.
- The Ambient Temperature during calibration was 20 °C
- Reference Equipment: V.AC/100-5B
- Uncertainty Confidence Level = 95%; Coverage Factor k = 2

**COMMENTS:**

The gauge was removed from the pressure vessel for calibration. The pressure vessel was tested to 20 bar to check pressure stability and was found to be satisfactory.

**PERFORMANCE TABLE:**

Applied Pressure (bar)	As Found and Left (bar)	Increasing (bar)		Decreasing (bar)		Uncertainty (bar)
		Reading	Correction	Reading	Correction	
2	2.0	2.0	0.00	2.0	0.00	±0.083
4	4.0	4.0	0.00	4.0	0.00	±0.083
6	6.0	6.0	0.00	6.0	0.00	±0.083
8	8.1	8.1	-0.05	8.1	-0.05	±0.084
10	10.1	10.1	-0.05	10.1	-0.05	±0.085

**OVERLOAD TEST:**

The overload test was not performed.

**CONCLUSION:**

The pressure gauge complied. Note: The pressure vessel test is not NATA endorsed and is not covered by our NATA scope of accreditation.

**RECOMMENDED DATE OF NEXT CALIBRATION:**

23 July 2010

(1 Year)

Signed .....

A M WYNN

Approved Signatory

AUSTRALIAN CALIBRATING SERVICES (A'SIA) PTY LIMITED



NATA Accredited laboratory Number 1209  
This document is issued in accordance with NATA's accreditation requirements. Accredited for compliance with ISO/IEC 17025.  
The results of the tests/calibrations and/or measurements included in this document are traceable to Australian/national standards.  
This report shall not be reproduced except in full.

# APPENDIX E

## Risk Management Assessment Approval



# RISK MANAGEMENT OF PRACTICALS AND FIELD TRIPS

SES019  
School of Engineering and Science

Submitted by: Yufridin Wahab	Date: 13 August 2009	
Signature: 		
Activity No. <u>        </u>	Activity Title: Testing of Sensor in Pressure Chamber	Subject: Postgraduate PhD Research

## HAZARD INFORMATION

TASK	HAZARD	RATING	HAZARD CONTROL	NEW RATING	ONUS
Soldering of electrical components to the end cap	Burn if accidentally come in contact with skin	M	Ensure the soldering station is clear from any winding cables and other objects that blocks movement of hands *Risk assessment for Lead Solder is attached	L	User
Placement of the pressure chamber/cylinder on table	The chamber/cylinder may roll to the edge and fall on the floor	H	A steel based stand is designed so that one of the chamber end cap is clamped to the stand	L	User Supervisor Technical Specialist
Attaching the pressure chamber to the end cap	if the end cap is attached loosely, it may be separated from the stand if pressure is applied internally. It may also fall from the table	H	The pressure chamber/main cylinder is attached securely to the other end cap	L	User Tech
Connecting the compressor hose to the pressure chamber	The hose may block the pathways/walkways or cause tripping	M	Make sure the hose is routed safely by avoiding walkways/pathways	L	User Tech
Pressurizing the chamber	Bursts if over the physical limitation	H	Regulator is used to control the pressure	L	Supervisor and technical Specialist
Pressurizing the chamber	Bursts if over the physical limitation	H	Regulator is used to control the pressure	L	Supervisor and technical Specialist



Risk Assessment		Product Name:	Soldering with Lead resin solder		Date: 15/02/07
		Assessor(s):	Donald Ermel		
Equipment		Soldering Iron			
Compound/Material		Lead resin solder			
Form:		Silver wire with resin core (.71mm)			
Active Ingredient:		Tin/Lead alloy, resin, 20% Ammonium chloride, 70% Zinc Chloride			
Risk & Health Effects:		Irritating if inhaled, Burns			
Exposure Routes:		Inhalation of fumes, expose to lead and possible burns from iron			
Process/Job Description:		Soldering electronic components			
Task	Routes	Controls Already In Place	Risks To Health? Yes/No? Not sure?	Action (Hierarchy of Control)	
Handling and storage of lead resin solder	Exposure to lead	Store in small amounts, wash hands after handling	No		Soap and wash basin in soldering area
	Exposure to resin		No		Soap and wash basin in soldering area
Task 1: Soldering of electronic components	Inhalation	Undertaken only in soldering labs with appropriate fume extraction is installed	Yes	Fume will develop when soldering	Soldering of components should take place under and within 150mm of the extraction intake. If this is not possible use the dilution technique to reduce concentration, i.e. fan to blow fume away
	Skin	Wash hands after handling	No		Soap and wash basin in soldering area
	Eye	Safety Glasses provided in tool box	Yes	Safety Glasses not worn. Hot solder may splatter when soldering	Wear appropriate safety glasses.
	Fire	Fire proof matting in work area	No		
	Burns	Wire stand to hold iron while not in use	Yes	extremely heated tip (over 330C) at the end of soldering iron can result in server burns.	Were possible use pliers/heatsink to handle heated components

Action (Hierarchy of Control): Elimination, Substitution, Isolation, Engineering, Administration, Personal Protective Equipment